INVESTIGATION OF THE INTERFACIAL INSTABILITY BETWEEN A NEWTONIAN FLUID AND A POLYMERIC FLUID UNDER THE INFLUENCE OF AN ELECTRIC FIELD FOR MICROFLUIDICS APPLICATIONS

by

Gülsüm Ersoy

B.S., Chemical Engineering, Yıldız Technical University, 2008

Submitted to the Institute for Graduate Studies in
Science and Engineering in partial fulfillment of
the requirements for the degree of
Master of Science

Graduate Program in Chemical Engineering
Boğaziçi University

2011

to my better half

ACKNOWLEDGEMENTS

First of all, I would like to express my sincere gratitude to my thesis supervisor Assist. Prof. A. Kerem Uğuz for his excellent guidance, continuous encouragement and understanding. It was a pleasure to work with him during my graduate thesis.

I would like to thank Prof. Ramazan Yıldırım and Assoc. Prof. Kunt Atalık for the time they have devoted to reading and commenting on my thesis.

I am extremely thankful to Mehmet İrfan Hösükoğlu for his sincere friendship and for helping and motivating me all the time I needed during the last two years. Likewise, I want to thank to Burcu Yoğurtçu for her friendliness and support in need during we share the KB406 and after. Special thanks to Melek Selcen Başar for her close friendship that is established in a short time and for her helpful advices.

I would like to thank all my friends for their support and encouragement during the time we spent in graduate education. In particular, KB403 members, Aybüke Leba, Caner Ülgüel, Aysun İpek Paksoy, Murat Erol and Okan Yüzüak deserve a great thank for their hospitality and kindness during my visit to their laboratory. I also thank to Aycan Hacıoğlu, my laboratory mate for her friendship and attention.

I wish to express my special thanks to Salih Burak Sezgün for his good fellowship.

I am especially grateful to my family for their endless patience and support during my education life. Above all, very special thanks for my fiancé who encouraged and conduced me to study master of science and was always with me with his patience and care.

Finally, financial support provided by TÜBİTAK through project 109M557 is gratefully acknowledged.

ABSTRACT

INVESTIGATION OF THE INTERFACIAL INSTABILITY BETWEEN A NEWTONIAN FLUID AND A POLYMERIC FLUID UNDER THE INFLUENCE OF AN ELECTRIC FIELD FOR MICROFLUIDICS APPLICATIONS

Microfluidic devices are widely used in various industries as they provide many advantages such as easy control of chemical reactions, heat and mass transfer, short analysis time and consumption of chemicals in small amounts. Reactions are either carried in homogeneous phase in a microchannel or in a batch reactor such as a small crucible or a micro droplet, which is also known as digital microfluidics. In micro length scale, the flow regime is laminar, which makes mixing or formation of mono dispersed micro sized droplets difficult. Electrohydrodynamics is an effective method for efficient mixing when two miscible liquids are used and for generating uniform droplets in microchannels when two immiscible liquids are used. The electric field causes the flat interface to deflect, i.e., to become unstable. The aim of this study is to theoretically and numerically analyze the stability of the interface between a Newtonian fluid and a non-Newtonian fluid under the effect of an electric field applied normal to the interface. The fluids under the effect of pressure-driven flow are assumed to be immiscible, incompressible, and leaky-dielectric. Linear stability analysis is conducted to observe the behavior of the system under the electric field and to show the effects of system parameters such as Reynolds number, applied potential, physical and electrical properties of the fluids, elasticity of the polymer. As a result, it is found that decreasing the permittivity ratio or increasing any of the Weissenberg number, the thickness ratio, the viscosity ratio, the conductivity ratio or the Reynolds number have a stabilizing effect; whereas increasing the dimensionless parameter S, the ratio of fluid to electric time scale does not affect the maximum growth rate but decreases the critical wavenumber. Moreover, increasing the electric number, i.e., increasing the applied voltage could be stabilizing or destabilizing depending on the selected parameters.

ÖZET

MİKROAKIŞKAN UYGULAMALARI İÇİN NEWTONYEN BİR AKIŞKAN İLE POLİMERİK BİR AKIŞKANIN ARAYÜZEY KARARSIZLIĞININ ELEKTRİK ALANI ETKİSİNDE İNCELENMESİ

Mikro akışkan sistemleri reaksiyonların, ısı ve kütle kontrolünün kolay olması, analiz zamanının kısalması ve daha az kimyasala ihtiyaç duyulması gibi avantajlar sağladığı için son yıllarda birçok endüstri uygulamasında sıkça kullanılmaktadır. Fakat, mikrokanallarda boyutlar küçük olduğundan akış laminer rejimde kalır, bu nedenle de reaksiyonlarda istenilen karışma ve katalizör teknolojisi için gerekli olan mikro damlacıkları aynı boyutlarda ve seri bir şekilde oluşturmak çok zordur. Karışan iki sıvıyı mikrokanalda etkin bir şekilde karıştırmak veya karışmayan iki sıvının birinin içerisinde diğerinin eşit büyüklükte damlacıklarını yaratmak için en etkili yöntemlerden biri elektrohidrodinamik uygulamalardır. Bu yöntemle iki sıvı arasındaki başlangıçta düz olan arayüzey elektrik alanı uygulanarak bozulur, yani sistem kararsız hale getirilir. Bu çalışmanın amacı biri Newtonyen, diğeri Newtonyen olmayan iki karışmayan, yarı iletken sıvının elektrik alanı etkisi altındaki arayüzey kararsızlığını teorik ve analitik olarak incelemektir. Sıvılar başlangıçta düz bir arayüzey oluşturarak Poiseuille akışı ile akmaktadırlar ve akış yönüne dik bir elektrik alanı uygulanmaktadır. Sistemin elektrik alanı etkisi altındaki davranışını ve Reynolds sayısı, uygulanan elektrik potansiyeli, sıvıların elektriksel özellikleri ve polimerin elastikliği gibi sistem parametrelerinin sistemin kararsızlığına etkisini gözlemlemek için lineer kararlılık analizi yapılmıştır. Sonuç olarak, elektriksel geçirgenlik oranını azaltmanın veya Weissenberg sayısı, sıvıların kalınlık oranı, viskozite oranı, iletkenlik oranı veya Reynolds sayısından herhangi birini arttırmanın sistemi daha kararlı hale getirdiği; akış zaman boyutunun elektrik zaman boyutuna oranı olan boyutsuz S sayısını arttırmanın maksimum büyüme hızını etkilemediği fakat kritik dalga sayısını küçülttüğü; boyutsuz elektrik sayısını, E_b, arttırmanın ise sisteme girilen parametrelere göre sistemi daha kararlı veya kararsız hale getirici etki edebileceği görülmüştür.

TABLE OF CONTENTS

LIST OF FIGURES

LIST OF TABLES

LIST OF SYMBOLS

Ca	Capillary number
E_b	Dimensionless electric number
$\underline{E}$	Electric field
G	Elasticity modulus
h	Fluid thickness
Hr	Thickness ratio
$\underline{\underline{I}}$	Identity tensor
k	Consistency index for power law (at non-Newtonian models)
k	Wavenumber (at modeling)
M	Viscosity ratio
n	Power law index
$\underline{n}$	Unit normal vector
p	Pressure
P	Density ratio
q	Charge density
q_t	Time derivative of the charge density
Re	Reynolds number
S	The ratio of fluid time scale to electric time scale
t	Time
$\underline{t}$	Unit tangent vector
$\underline{\underline{T}}$	Total stress tensor
$\underline{\underline{T}}^F$	Fluid component of the total stress tensor

$\underline{\underline{T}}^E$	Electric component of the stress tensor
u	Normal speed of the interface
u_0	Base state interface velocity
$\underline{u}$	Interface speed
$\underline{v}$	Velocity
V	Voltage
V_b	Applied voltage
We	Weissenberg number
γ	Surface tension
$\underline{\underline{\dot{\gamma}}}$	Rate of strain tensor
ε	Electrical permittivity
ε_0	Vacuum permittivity
ϵ	Given perturbation
λ_1	Relaxation time
λ_2	Retardation time
μ	Viscosity
μ_a	Apparent viscosity
μ_p	Polymer viscosity
μ_s	Solvent viscosity
μ'	Viscoelasticity
ρ	Density
σ	Electrical conductivity
σ_r	Electrical conductivity ratio

$\underline{\underline{\tau}}$	Viscous stress tensor
$\underline{\underline{\tau}}^{p}$	Polymeric contribution to the stress
$\underline{\underline{\tau}}^{p}_{(1)}$	Convective derivative of the viscous stress tensor
$\underline{\underline{\tau}}^{s}$	Solvent contribution to the stress
τ_y	Yield stress
ω	Growth rate constant
$2\underline{\underline{D}}$	Rate of strain tensor
$2H$	Surface mean curvature
∇	Gradient
∇_s	Surface gradient
x^*	Second fluid property
$\tilde{x}$	Scaled parameter
x_0	Base state parameter
x_1	Perturbed state parameter
$\hat{x}$	Parameter expanded in the normal mode

LIST OF ACRONYMS//ABBREVIATIONS

AC	Alternating current
DC	Direct current
LISA	Lithographically-induced self-assembly
UCM	Upper Convected Maxwell
NSB	Normal stress balance
TSB	Tangential stress balance

1. INTRODUCTION

Microfluidic systems are increasingly used in chemical engineering and biochemical industries as they offer the possibility of performing experiments rapidly and in parallel (Manz *et al.*, 1990). Performing experiments with micro systems offer the advantage to control and enhance chemical reactions and heat transfer, to shorten the analysis time, to control the transfer rates in addition to using tiny amounts of chemical substrates (Jensen, 2001; Squires and Quake, 2005; Ismagilov *et al.*, 2006). As microfluidics gives the opportunity to consume less chemicals, microfluidic systems are especially useful for industries using expensive chemicals such as pharmaceutical industry. However, microfluidic systems have difficulties such as mixing. In small dimensions, as the fluid properties are increasingly controlled by viscous forces rather than inertial forces, Reynolds number is low and the flow in microchannel stays in laminar regime (Stone *et al.*, 2004). Thus, the turbulence could not be employed for mixing in microchannels. Some passive methods such as modifying the channel geometry (Liu *et al.*, 2000; Mengeaud *et al.*, 2002; Wang *et al.*, 2002; Stroock *et al.*, 2002a; Stroock *et al.*, 2002b; Munson and Yager, 2003; Chang and Cho, 2003) and applying pulsing flows (Glasgow and Aubry, 2003) have been used to get rapid and efficient mixing in microchannels.

Recently, to achieve mixing in microchannels, electric field has been applied externally as an active method (El Moctar *et al.*, 2003; Fujii *et al.*, 2003; Lin *et al.*, 2004; Glasgow *et al.*, 2004; Zahn and Reddy, 2006). On the other hand, when two immiscible fluids are injected into a microchannel, micro droplets of one liquid in another are formed by applying an electric field (Ozen *et al.* 2006a). Micro droplet formation is an important step for the catalyst technologies. The catalysts are materials that increase the reaction rate and nano or micro scale catalysts are employed in many reactions such as fuel production from petroleum. Hence, these catalysts have to be manufactured in series and in monodispersed size. It is possible to use a micro droplet as a reaction chamber to produce any chemical reaction. This method is known as digital microfluidics (Ismagilov *et al.*, 2006). There are various means to obtain micro droplets. As in the case of mixing of two miscible liquids, some passive methods such as modifying the channel geometry have been used for droplet formation (Thorsen *et al.*, 2001; Joanicot and Ajdari, 2005; Hsiung *et al.*,

2006). However, it is not easy to fabricate these droplets in the same size due to the formation of satellite droplets. Therefore, it is not possible to control the reactions in the same conditions if these droplets are of non uniform size. Mono sized micro droplet formation is possible by applying electric field to the interface between two immiscible fluids (Ozen *et al.* 2006a). The droplets are generated as a result of an instability of the interface created between the two fluids. The fluids flow very slowly in a microchannel and there is no turbulence to mix the fluids so that the interface between the fluids is flat even at the presence of an electric field provided its magnitude is less than a critical value. This state of the system is called the base state. When the magnitude of the electric field is increased, a given disturbance to the interface can grow in time, i.e. the system is unstable to the given disturbance, or it can decay in time so that the system is back to the base state, i.e. the system is stable. The mechanism for the interfacial instability is explained by Thaokar and Kumaran (2005) in detail. As a result, it can be said that the application of an external electric field can be used for mixing two miscible fluids efficiently or for forming micro droplets of one fluid in another for immiscible fluids.

There are various studies about the interfacial instability between two Newtonian fluids. Although the polymers play crucial role in the chemical industry, there are few works which analyze the instability of the system with Non-Newtonian fluids. After the introduction of the lithographically-induced self-assembly (LISA) process (Chou *et al.*, 1999; Chou and Zhuang, 1999; Chen *et al.*, 2005b), there is a growing theoretical and experimental interest in the interfacial instability of the systems with polymer and air under the effect of an electric field (Schäffer *et al.*, 2000; Schäffer *et al.*, 2001; Lin *et al.*, 2001; Lin *et al.*, 2002a; Lin *et al.*, 2002b; Morariu, *et al.*, 2003; Harkema *et al.*, 2003). However, a system with a Newtonian fluid and a non-Newtonian fluid under the effect of an electric field has not been investigated in detail in the literature so far.

In this work, the instability of the interface between two immiscible fluids (a Newtonian and a non-Newtonian) under the effect of an externally applied electric field is studied theoretically. The Upper Convected Maxwell model is used as a constitutive equation for the non-Newtonian fluid. Linear stability analysis is carried out and the effects of the system parameters such as Reynolds number, applied potential, depth and viscosity ratio of the fluids on the instability is analyzed.

2. LITERATURE SURVEY

2.1. Electrohydrodynamic Instabilities

Electrohydrodynamic instabilities, i.e. the investigation of the interfacial instabilities under the application of an electric field, gained more focus recently because of its scientific promises as well as its practical applications. The method is based on analyzing a specific system, the parameters affecting the instability of the system, and defining the conditions that make the system unstable. There are several experimental works about the interfacial instability of a system subject to an applied electric field. In these works, the aim is to obtain an efficient mixing when miscible liquids are employed (Oddy *et al.,* 2001; El Moctar *et al.,* 2003; Fujii *et al.,* 2003; Tsouris *et al.,* 2003; Glasgow *et al.,* 2004; Park *et al.,* 2005; Shin *et al.,* 2005; Huang *et al.,* 2006; Chang and Yang, 2007), or to form micro droplets when immiscible liquids are employed (Ozen *et al*., 2006a). Theoretical works with Newtonian fluids are discussed in detail in Section 2.1 and experimental and theoretical works about non-Newtonian/polymeric fluids are discussed in Section 2.2.

2.1.1. Theoretical Approaches

There are two different theoretical approaches about the investigation of the interfacial instability of the systems with two flowing or stationary fluids under the influence of an electric field. These are the ‘bulk coupled model’ and the ‘surface coupled model’. The bulk coupled model is used in the electrokinetics which is a branch of the electrohydrodynamics. The bulk coupled model assumes a conductivity gradient at the interface of the fluids. There is not a sharp change in the electrical properties of the fluids and an electrical force occurs in the bulk of the fluids. In the modeling of the system, in addition to the pressure force and the viscous forces, an electrical force is included into the momentum balance equations. Hoburg and Melcher (1976, 1977) and Baygents and Baldessari (1998) studied the interfacial instabilities of the two fluid systems under the effect of an electric field using the bulk coupled model, for the first time. Then, the other authors also analyzed similar systems (Lin *et al.,* 2004; Storey *et al*., 2005; Chen *et al*., 2005a; Posner and Santiago, 2006). The works using the bulk coupled model are

summarized by Lin in a review paper (Lin, 2009) and they are not discussed here. In the surface coupled model, which is the model used in this work, there is a jump between the properties of the electrical and the physical properties of the fluids at the interface. The model assumes that there is no electrical charges in the bulk of the fluids and the charges are assumed to be accumulated at the interface. Thus, the electric forces are not included into the governing equations; they appear only at the interface conditions. The surface coupled model has been used in all the theoretical works mentioned hereafter.

2.1.2. Physical System

In the theoretical works, various systems depending on the finiteness of the boundaries are analyzed. The systems with infinite lengths and infinite thicknesses are used in a few studies and the behaviors of the systems under the application of an electric field are observed (Melcher and Schwarz, 1968; Melcher and Smith, 1969; Abdella and Rasmussen, 1997; Gambhire and Thaokar, 2010). Two stationary fluids with finite thicknesses sandwiched between two infinitely long, rigid and impermeable electrodes are analyzed in the other works (Pease and Russel, 2002; Shankar and Sharma, 2004; Thaokar and Kumaran, 2005; Craster and Matar, 2005; Bandyopadhyay and Sharma, 2007; Li *et al.*, 2007; Uguz *et al.*, 2008; Uguz and Aubry, 2008).

The theoretical works focus on studying the effects of the system parameters such as applied electric field, surface tension, initial thicknesses, viscosities, densities, electrical conductivities, permittivities of the fluids, on the interfacial instability of the system (Pease and Russel, 2002; Shankar and Sharma, 2004; Thaokar and Kumaran, 2005; Craster and Matar, 2005; Ozen *et al.*, 2006b; Ozen *et al.*, 2006c; Bandyopadhyay and Sharma, 2007; Li *et al.*, 2007). The fluids are assumed to be Newtonian and incompressible in these studies. As the fluids are thin, the effect of the gravity is ignored in many works (Pease and Russel, 2002; Shankar and Sharma, 2004; Craster and Matar, 2005; Ozen *et al.*, 2006b; Ozen *et al.*, 2006c), while some of the works takes the gravity into account (Li *et al.*, 2007; Gambhire and Thaokar, 2010). Most of the studies assume the fluids flow in a microchannel so that the momentum equations are solved with Stokes equations, while the effect of the Reynolds number on the stability is studied by Uguz and Aubry (2008). The base states of the systems are also varied. Some of the works assume the fluids to be stationary in the

base state (Shankar and Sharma, 2004; Craster and Matar, 2005), and the others assume the base state flow profiles as the Poiseuille flow (Ozen *et al.*, 2006c; Li *et al.*, 2007) or the Couette flow (Abdella and Rasmussen, 1997; Li *et al.*, 2007). The result of the linear stability analysis showed that the instability of the system does not depend on the base state profiles (Li *et al.*, 2007). Similarly, Uguz and Aubry (2008) analytically showed that the base state flow profile does not affect the stability of the system.

The electrical charge relaxation time scale of the system is assumed to be very small with respect to characteristic flow time scale of the system in most of the works. This is called 'the fast electric time'. So, the ratio of fluid time scale to electric time scale, S, is very large. This assumption simplifies the equations considerably (Pease and Russel, 2002; Thaokar and Kumaran, 2005; Craster and Matar, 2005; Ozen *et al*., 2006b; Ozen *et al*., 2006c; Li *et al.*, 2007) and analytical solutions have been possible for some of the works (Uguz *et al.*, 2008; Uguz and Aubry, 2008). Ozen *et al*. (2006c) investigated the effect of S and showed that when this ratio is very large, according to the conductivity and the permittivity ratios of the fluids, the system could be rendered unstable by the electric field, and they confirmed their results numerically. In addition, it is found that the critical wavenumber decreases with the increasing S, while the maximum growth rate stays constant (Ozen *et al*., 2006c).

The electrical conductivity is another distinction of the analyzed systems. The interfacial instability between two leaky-dielectric fluids is investigated in most of the systems (Shankar and Sharma, 2004; Thaokar and Kumaran, 2005; Craster and Matar, 2005; Ozen *et al*., 2006b; Ozen *et al*., 2006c; Li et al., 2007; Uguz *et al.*, 2008; Uguz and Aubry, 2008). The 'Taylor-Melcher leaky-dielectric model' (Melcher and Taylor, 1969; Saville, 1997) is used in the studies with the leaky-dielectric systems. On the other hand, Thaokar and Kumaran (2005) and Li *et al*. (2007) studied the interfacial instability of the system with two perfect dielectric fluids under the effect of an electric field. Pease and Russel (2002) investigated the instability of the interface between a thin liquid film and air under the application of an electric field, assuming the liquid both perfect dielectric and leaky-dielectric. They found out that the growth rate and the characteristic wavenumber in the leaky-dielectric model (dielectric&leaky-dielectric interface) are much larger than that for the perfect dielectric model (dielectric-dielectric interface). In other words, the

presence of conductivity exerts a destabilizing effect and leads to patterns of smaller wavelength and larger growth rates of instabilities which mean that the system with leaky-dielectrics becomes unstable with a smaller potential difference (Pease and Russel, 2002). Thaokar and Kumaran (2005) have studied the systems with both 'dielectric-dielectric interface' and 'leaky-dielectric and leaky-dielectric interface'. They showed that the critical potential needed to destabilize the system for the leaky-dielectrics is smaller than that for perfect dielectrics. Ozen *et al.* (2006b) observed the effect of a small parallel electric field on the nonlinear dynamics and possible rupture of viscous leaky-dielectric liquid sheet surrounded by a hydrodynamically passive semi infinite medium. Bandyopadhyay and Sharma (2007) analyzed the interfacial instability of the system with two perfect dielectric liquid films and a bounding fluid (non-viscous like air) on top of the liquids under the application of electric field; hence, there are two interfaces (liquid-liquid and liquid air interfaces) in the system. They examined the conditions that make the modes of deformation at the twin interfaces bending or squeezing. In the light of their studies, it is seen that these modes can be switched and the relative amplitudes of deformation at the interfaces could be shifted by varying the thicknesses, permittivities, viscosities and interfacial tensions of the films (Bandyopadhyay and Sharma, 2007). Li *et al.* (2007) performed their analysis for both perfect and leaky-dielectrics. As a result, they found that for perfect dielectrics, the electric field is always destabilizing in such a system, while it can be stabilizing or destabilizing for leaky-dielectrics depending on the ratio of conductivities and permittivities of the fluids.

2.1.3. Alternating or Direct Current

The applied electric field to create interfacial instability could be generated using an alternating current (AC) or a direct current (DC). Although most of the studies used DC electric field in their analyses, there are a few works that prefer AC field (Briskman and Shaidurov, 1968; Robinson *et al.,* 2001; Roberts and Kumar, 2009; Gambhire and Thaokar, 2010). Roberts and Kumar (2009) analyzed the instability of the interface between both two perfect dielectrics and two leaky-dielectric fluids under the effect of AC field using the Floquet theory. They showed that the growth rate of the fastest growing mode, S_{max}, and the wavelength of the fastest growing mode, k_{max}, are smaller for AC field than that for DC field, for perfect dielectrics. For leaky-dielectrics, it is found that the

values of S_{max} and k_{max} decrease as the frequency increases and the behavior of the interfacial instability resembles the perfect dielectrics case at very high frequencies (Roberts and Kumar, 2009). Recently, Gambhire and Thaokar (2010) studied the effect of the alternating normal electric field on the stability of the interface between a perfect dielectric fluid and a leaky-dielectric fluid, two perfect dielectrics, and two leaky-dielectrics which have infinite thicknesses, using Floquet theory. They showed that for the perfect dielectrics system, the AC field does not have any effect on the growth rate of the instabilities compared to the DC field. For perfect-leaky and leaky-leaky-dielectrics systems, the growth rate decreases and the minimum electric field needed to make the system unstable increases with the increasing frequency. At low frequencies, the perfect-leaky and leaky-leaky-dielectrics systems behave like the leaky-leaky-dielectrics DC case, while they behave like the perfect dielectrics system at the higher frequencies (Gambhire and Thaokar, 2010). However, the DC electric field is the most popular way to create an electric field for the electrohydrodynamic instabilities and except for the studies mentioned above, the DC electric field is used in the other studies referred in this work.

2.1.4. Direction of the Applied Electric Field

The electric field could be applied normal or parallel to the interface of the fluids which is initially flat. In most of the studies, the fluid layers are sandwiched between two long electrodes so that an electric field which is normal to the interface and to the flow direction if the fluids flow. Shankar and Sharma (2004), Thaokar and Kumaran (2005), Li *et al*. (2007) analyzed the instability of the interface of the fluids depending on the system parameters such as viscosities, electrical conductivities, permittivities, initial thicknesses, under the effect of a normal electric field. Most of the studies used the normal electric field in their analyses (Abdella and Rasmussen, 1997; Pease and Russel, 2002; Shankar and Sharma, 2004; Craster and Matar, 2005; Ozen et al., 2006c; Bandyopadhyay and Sharma, 2007; Li *et al*, 2007; Gambhire and Thaokar, 2010). On the other hand, Ozen *et al.* (2006c) applied a parallel electric field to their systems with a thin liquid sheet surrounded by a hydrodynamically passive medium. Moreover, Uguz *et al.* (2008) analyzed the instability of the interface of two leaky-dielectric fluids flowing in a microchannel depending on the system parameters under the effect of a parallel electric field and compared their results with the results of normal electric field, analytically. They plotted the permittivity ratio

versus conductivity ratio graph and showed the regions which are unstable for parallel or normal electric field. As a result, it is found that the normal electric field causes instability in the larger range of the parameters than the parallel field. In an another work of Uguz and Aubry (2008), as a continuation of the previous study, the system of two leaky-dielectric fluids flowing in a microchannel subjected to normal or parallel electric field was analyzed quantitatively. The effect of the direction of the applied electric field was determined by solving the equations and plotting the dispersion curves, i.e., the growth rate versus the wavenumber of the disturbance, numerically (Uguz and Aubry, 2008).

2.1.5. Mathematical Analysis Methods

Different mathematical analysis methods are performed in the theoretical analyses of the electrohydrodynamic instabilities. The linear stability analysis for all wavenumbers is the most preferred method (Pease and Russel, 2002; Shankar and Sharma, 2004; Craster and Matar, 2005; Thaokar and Kumaran, 2005; Ozen et al., 2006b; Ozen et al., 2006c; Bandyopadhyay and Sharma, 2007; Li *et al*, 2007; Uguz *et al*., 2008; Uguz and Aubry, 2008). Besides the linear stability analysis, the non-linear stability analysis (Craster and Matar, 2005; Bandyopadhyay and Sharma, 2007; Ozen et al., 2006b) and weakly nonlinear analysis (Thaokar and Kumaran, 2005; Wu *et al.,* 2005) are used in some of the studies. Thaokar and Kumaran (2005) studied their systems analytically using the linear and weakly nonlinear analysis, and numerically using a thin film analysis and a boundary integral method. The thin film analysis assumes that the wavelength of the disturbance is much larger than the fluid thicknesses. Hence, this method is called ‘thin film analysis’, ‘long wave analysis’ or ‘lubrication theory’. Thaokar and Kumaran (2005) used linear stability analysis to show the effects of the system parameters on the critical potential which is the needed potential difference to make the system unstable. They also focused on the nature of the initial bifurcation. And their boundary integral method pointed out that a secondary subcritical bifurcation occurs at a potential which is a little larger than the critical potential when the instability is subcritical. Li *et al.* (2007) performed long wave linear stability analysis and they derived an equation that describes the wave speed which depends on the ratios of conductivities, permittivities, viscosities and initial depths of the fluids. Moreover, they performed a linear stability analysis for all wavenumbers using the Chebyshev spectral method, numerically. By numerical simulations, they plotted the

neutral stability curves for different values of the electrical conductivity and the permittivity ratios of the fluids (Li *et al.*, 2007). Craster and Matar (2005) analyzed the stability of the interface between two thin leaky-dielectric liquid films sandwiched between two infinitely long, rigid and impermeable electrodes in the linear and non-linear regime. Lubrication theory was used to derive the nonlinear partial differential equations to describe development of the interfacial deviation and the surface charge density. As a result, it was shown that decreasing the thickness ratio and the viscosity ratio are destabilizing, leading to the formation of patterns of smaller wavelength. Increasing the difference between permittivities and conductivities of the liquids has a destabilizing effect on both the pattern formation and the surface charge density (Craster and Matar, 2005).

2.2. Non-Newtonian Works

Polymers are used in many industries and scientific researches, recently. The polymeric pattern formation in micro scales without any cavitation or laser application is a significant innovation. After the introduction of lithographically-induced self-assembly (LISA) process (Chou *et al.,* 1999), there is a growing interest in this field. In LISA process, a polymer film is spun onto a flat substrate and is overlaid with a mask which is held apart from the polymer surface by spacers. When the system is heated above the glass transition temperature of the polymer, the polymer rises up against the forces of gravity and surface tension forming periodic structures that are aligned to any pattern on the mask. The formed patterns are very complicated and their shapes depend on many parameters such as the length of the spacers, the physical and the electrical properties of the polymer, and also the molecular weight of the polymer (Chou *et al.,* 1999; Pease and Russel, 2002). This process occurs because of the developed interfacial instability between the polymer and air. The interfacial instability is caused by the electric field that is created between the polymer and the mask (Chou *et al.,* 1999; Chou and Zhuang, 1999; Chen *et al.,* 2005b). On the other hand, Russell, Steiner and their coworkers (Schäffer *et al.,* 2000; Schäffer *et al.,* 2001; Lin *et al.,* 2001; Morariu *et al.*, 2003; Harkema *et al.,* 2003; Lin *et al.,* 2002a; Lin *et al.,* 2002b) applied an external electric field to the polymer-air or polymer-polymer system and they achieved the formation of hierarchical columnar structures, similar to the LISA mechanism. Schäffer *et al.* (2000, 2001) examined the instability of a thin, highly viscous polymer film and air laid between two electrodes, above the glass transition temperature

and under the influence of an applied electric field, experimentally. They used a wedge geometry so that they achieved the varied air height and also the varied electric field, in the same system where the electric field strength is higher for the smaller air gap. They observed the effect of the electric field strength in this way. As a result, they showed that the columnar structures were formed at the higher electric field part of the electrode while only small waves occurred on the polymer surface at the lower electric field part, which can be concluded as the instability increases with the increasing electric field strength. Schäffer *et al.* (2001) conducted linear stability analysis assuming the polymer as dielectric to compare with the experiment results. They used long wave analysis to calculate the wavelength of fastest growing mode and the effects of the applied electric field, permittivities and surface tension on the stability of the interface. Their modeling results were in good agreement with their experimental observations. They showed that the increase in the permittivity ratio results in patterns with smaller diameters. Moreover, they performed experiments with AC electric field and showed that the frequency does not affect the instability since the AC field results are similar to that of DC field. When the upper electrode is designed patterned, the columns formed under the influence of the electric field takes the shape of the upper electrode pattern (Schäffer *et al.,* 2001; Harkema *et al.*, 2003; Deshpande *et al.*, 2004). In contrast to the LISA experiments of Chou *et al*. (Chou et al., 1999; Choua and Zhuang, 1999), no fluctuations/instabilities are observed when the electric field is not applied (Schäffer *et al.*, 2001).

Expanding these observations, Lin *et al.* (2001) analyzed experimentally the behavior of the interface between two liquids (a polymer and an oligomer) under the effect of an electric field. Their experiments showed that the columnar structures formed similar to the polymer-air system but with smaller dimensions and the time of electric field application for instability is shorter than the polymer-air system. In some other works, two polymer and air system with two interfaces is analyzed and the columnar structures of the polymers were observed experimentally (Morariu *et al.*, 2003; Leach et al., 2005).

Although it is known that the polymers are widely used in several industries, because of the modeling is difficult, the theoretical works mentioned in Section 2.1 are for Newtonian fluids. There have been a few studies modeling the non-Newtonian behavior of the polymers. Firstly, Eldabe (1988) investigated the instability of the interface of two

dielectric polymeric fluids flowing with Couette flow between two infinitely long electrodes under the influence of a normal electric field. The power law model is used as a constitutive equation in the modeling of the motion of the fluids. The result of the linear stability analysis showed that the system could be made unstable arranging the electric field strength, which depends on the thicknesses, the viscosities and the power law indexes of the fluids and the speed of the moving plate. In another work, Wu and Chou (2005) studied the stability of a viscoelastic polymer film and air system under a mask under the influence of a normal electric field via a linear stability analysis. They investigated the effects of the polymer elasticity, the initial film thickness, the air gap thickness and the electrical properties of the polymer film on the instability. The leaky-dielectric model is used as the polymer is assumed to be conductive. To describe the rheological behavior of the polymer, Oldroyd-B model is used as a constitutive equation. Under the lubrication approximation, the model reduces to linear Jeffreys model. They neglected the solvent viscosity so that the polymer is modeled as a Maxwell fluid. The air is assumed to be totally stationary and the polymer is assumed to be stationary in the base state. As the Reynolds number is very small, inertial effects are also ignored and Stokes equation is employed. As a result of their study, they found out that the elasticity of the polymer shows a destabilizing effect on the stability. The growth rate increases with the Deborah number, De. However, the elasticity does not affect the most dangerous wavenumber. When De is below a critical value, the elasticity increases the growth rate without affecting the most dangerous wavenumber. When De is above the critical value, infinitely large growth rate (called resonance) occurs. The growth rate approaches infinity at two wavenumbers between which the growth rate is negative. When the resonance appears, only pillars with one resonant wavenumber are observed and the pillar patterns are extremely regular. The resonance is affected by the elasticity and the dimensionless film thickness but not affected by the electrical properties of the polymer (Wu and Chou, 2005). Tomar *et al.* (2007) investigated the same system without long wave assumption and conducted linear stability analysis of the system with and without the solvent viscosity and with and without the inertial effects using the full dispersion relation. They used Taylor-Melcher leaky-dielectric model to demonstrate the electrical contributions and the Jeffreys model as a constitutive equation to describe the rheological behavior of the liquid. The base state velocity is assumed to be zero. They tried to explain the reasons of the singularity in the work of Wu and Chou (2005). In the absence of inertia and solvent viscosity, the similar

results were obtained, so the Lubrication assumption is relevant since it does not affect the results. When the solvent viscosity and the inertial effects were included, they found out that above a critical De, De_c, the growth rate is large but not infinite as it is in the zero inertia case. Inclusion of the solvent viscosity also prohibits the non-bounded growth rate when $De>De_c$ since the solvent viscosity causes an additional dissipation. They concluded that the pillars with similar dimensions formed in the experiments could be explained with this theory (Tomar et al., 2007). El-Sayed and Syam (2007) investigated the stability of a thin cylindrical, dielectric, viscoelastic fluid surrounded by a conductive gas under the effect of a radial electric field. Walters B' and Rivlin-Ericksen models are used as constitutive equations. Linear stability analysis is conducted and the effects of the kinematic viscoelasticity, the applied potential, the kinematic viscosity, the liquid thickness and the surface tension of the fluids on the instability are analyzed. In the light of their studies, it is seen that the kinematic viscoelacticity and the fluid thickness have stabilizing effects while the kinematic viscosity, the applied potential and the surface tension have destabilizing effects (El-Sayed and Syam, 2007).

As a summary, there are various purposes of the application of the electrohydrodynamics: (1) Efficient mixing for miscible fluids, (2) micro droplet formation for immiscible fluids, (3) explanation of the mechanisms of the formation of the hierarchical polymeric structures in the polymer-air systems under the application of the electric field and to arrange the parameters to be able to form structures in needed sizes.

2.3. Non-Newtonian Fluids and Mathematical Models

Non-Newtonian fluids have an important role in the literature. There are different types of non-Newtonian fluids and modeling for each of them is also different.

Non-Newtonian fluids are divided into three groups as time independent non-Newtonian fluids, time dependent non-Newtonian fluids and viscoelastic fluids.

2.3.1. Time Independent Non-Newtonian Fluids

For time independent fluids, the rate of shear at any point depends on only the shearing stress at that point (Wilkinson, 1960; Tanner, 2000).

$$\dot{\gamma}_{yx} = f(\tau_{yx}) \tag{2.1}$$

Time independent fluids are Bingham plastics, pseudoplastic fluids and dilatant fluids. Shear rate-shear stress relation for time independent non-Newtonian fluids is shown in Figure 2.1.

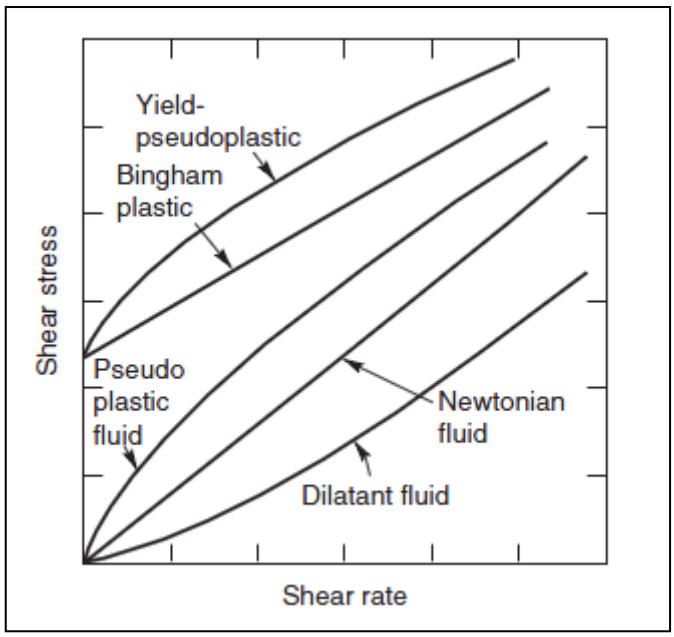

Figure 2.1. Shear rate-shear stress relation for time independent non-Newtonian fluids (This figure was published in 2008, Chhabra, R. P., and J. F. Richardson, Non-Newtonian Flow and Applied Rheology, 2nd ed., pp.6, Copyright Elsevier (2008).).

2.3.1.1. Bingham Plastics. The Bingham fluids exhibit yield stresses. The yield stress τ_y is the magnitude of the stress that must be applied before flow starts. So that the flow curve of Bingham plastics is linear with an intercept on the shear stress axis which is equal to τ_y. Apparent viscosity decreases linearly with increasing shear rate (Figure 2.1). This kind of fluids are called viscoplastic also. Toothpaste, oil paints, ketchup, lava, slurries, drilling mud and sewage sludge are a few examples to Bingham plastics (Wilkinson, 1960; Tanner,

2000). Mathematical models for viscoplastic behavior are as follows (Chhabra and Richardson, 2008):

i. The Bingham plastic model: For $|\tau_{yx}| > |\tau_y|$

$$\tau_{yx} = \tau_y + \mu\, \dot{\gamma}_{yx} \tag{2.2}$$

and for $|\tau_{yx}| < |\tau_y|$

$$\dot{\gamma}_{yx} = 0 \tag{2.3}$$

where μ is viscosity, $\dot{\gamma}_{yx}$ is shear rate, τ_{yx} is shear stress, τ_y is yield stress.

ii. The Herschel-Bulkey fluid model: For $|\tau_{yx}| > |\tau_y|$

$$\tau_{yx} = \tau_y + k\, (\dot{\gamma}_{yx})^n \tag{2.4}$$

and for $|\tau_{yx}| < |\tau_y|$

$$\dot{\gamma}_{yx} = 0 \tag{2.5}$$

where n is power law index and n<1 for Bingham fluids, k is consistency index which depends on the value of n.

iii. The Casson fluid model: For $|\tau_{yx}| > |\tau_y|$

$$|\tau_{yx}|^{\frac{1}{2}} = |\tau_y|^{\frac{1}{2}} + (\mu\, |\dot{\gamma}_{yx}|)^{\frac{1}{2}} \tag{2.6}$$

and for $|\tau_{yx}| < |\tau_y|$

$$\dot{\gamma}_{yx} = 0 \tag{2.7}$$

This model is used generally for biological materials such as blood, yoghurt, tomato puree, molten chocolate, etc. (Chhabra and Richardson, 2008).

2.3.1.2. Pseudoplastic (Shear Thinning) Fluids. Apparent viscosity of this kind of fluids decreases with shear rate and the flow curve becomes linear only at very high rates of shear. Logarithmic plot of the shear rate versus the shear stress is often found to be linear with a slope between zero and unity as shown in Figure 2.2. So, the "power law" equation is mostly used to describe the behavior of pseudoplastic fluids.

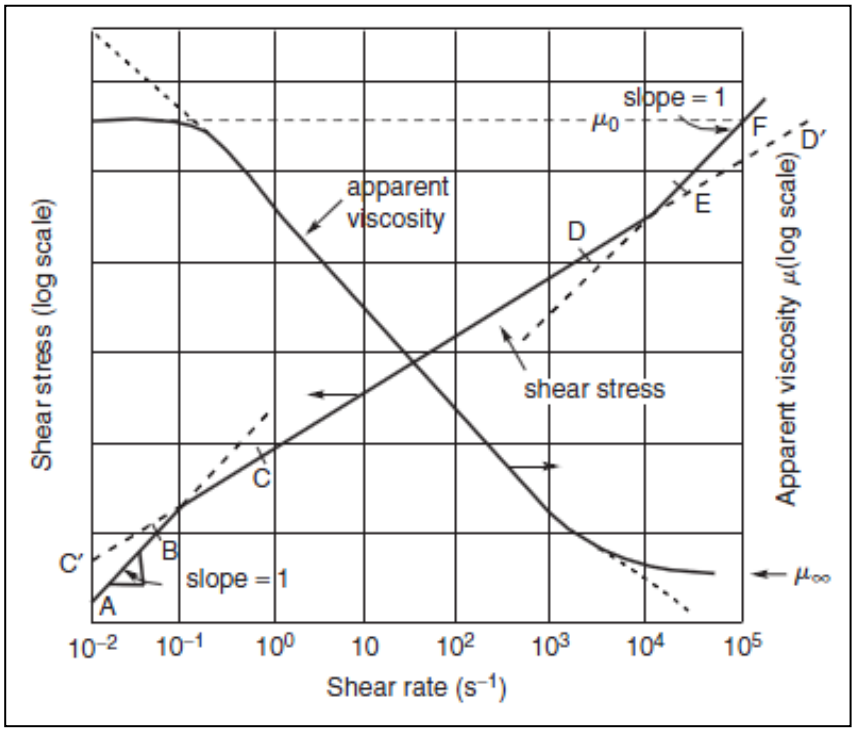

Figure 2.2. Schematic representation of shear thinning behavior (This figure was published in 2008, Chhabra, R. P., and J. F. Richardson, Non-Newtonian Flow and Applied Rheology, 2nd ed., pp.7, Copyright Elsevier (2008).).

Suspensions of asymmetric particles or solutions of high polymers such as cellulose derivatives, soap, grease oil and pulp are some examples of pseudoplastic fluids (Wilkinson, 1960; Bird *et al.*, 1987; Tanner, 2000).

Empirical equations to describe pseudoplastic behavior are as follows:

i. Power law model: This is the most widely used model for describing the pseudoplastic behavior. However, power law model does not predict the zero and infinite shear rate viscosities.

$$\tau_{yx} = k\,(\dot{\gamma}_{yx})^{n} \tag{2.8}$$

where k is higher for more viscous fluids and n is between zero and unity for pseudoplastics. The smaller values of n mean that the fluid exhibits the more shear-thinning behavior. The parameters n and k are temperature dependent that they increase rapidly with increasing temperature (Bird *et al*., 1987). Apparent viscosity is defined as

$$\mu_a = \frac{\tau_{yx}}{\dot{\gamma}_{yx}} \tag{2.9}$$

and

$$\mu_a = k\,(\dot{\gamma}_{yx})^{(n-1)} \tag{2.10}$$

then, the shear stress becomes

$$\tau_{yx} = k\,(\dot{\gamma}_{yx})^{(n-1)}\dot{\gamma}_{yx} \tag{2.11}$$

Since n<1 for pseudoplastics, the apparent viscosity decreases with increasing shear rate.

ii. Prandtl model:

$$\tau_{yx} = A\,\sin^{-1}(\frac{\dot{\gamma}_{yx}}{C}) \tag{2.12}$$

where A, B and C are the specific constants for the fluids.

iii. Eyring model:

$$\tau_{yx} = \frac{\dot{\gamma}_{yx}}{B} + C \sin(\frac{\tau_{yx}}{A}) \tag{2.13}$$

iv. Powell-Eyring model:

$$\tau_{yx} = A\dot{\gamma}_{yx} + B \sinh^{-1}(C\dot{\gamma}_{yx}) \tag{2.14}$$

v. Williamson model:

$$\tau_{yx} = \frac{A\,\dot{\gamma}_{yx}}{(B + |\dot{\gamma}_{yx}|)} + \mu_{\infty}\dot{\gamma}_{yx} \tag{2.15}$$

where μ_{∞} is the apparent viscosity at high shear rate.

vi. Ellis model:

$$\frac{1}{\mu} = \frac{1}{\mu_0} + k^{-\frac{1}{n}}(\tau_{yx}{}^2)^{\frac{(1-n)}{2n}} \tag{2.16}$$

where μ_0 is the apparent viscosity at zero shear rate.

vii. Casson model (solids): For τ_{yx} > A

$$\sqrt{\tau_{yx}} = \sqrt{A} + \sqrt{\mu_a\,\dot{\gamma}_{yx}} \tag{2.17}$$

viii. Carreau-Yasuda Model: This model is used for many concentrated polymer solution and melts (Wilkinson, 1960; Tanner, 2000).

$$\frac{\mu - \mu_\infty}{\mu_o - \mu_\infty} = [(1 + (\lambda\, \dot{\gamma}_{yx})^2]^{\left(\frac{n-1}{2}\right)} \tag{2.18}$$

where λ is the time constant.

ix. The cross viscosity equation (Chhabra and Richardson, 2008):

$$\frac{\mu - \mu_\infty}{\mu_o - \mu_\infty} = \frac{1}{(1 + k\,(\dot{\gamma}_{yx})^n)} \tag{2.19}$$

2.3.1.3. Dilatant (Shear Thickening) Fluids. Apparent viscosity of dilatant fluids increase with increasing rates of shear, since n>1 for this kind of fluids (See Figure 2.1).

The power law model is used for modeling of dilatant fluids. Some examples to dilatants fluids are suspensions of solids at high solids content, starch pastes, wet sand, concentrated suspensions of china clay, titanium dioxide and corn flow in water (Wilkinson, 1960; Chhabra and Richardson, 2008).

2.3.2. Time Dependent Non-Newtonian Fluids

The apparent viscosity depends on not only shear rate, but also on time the shear has been applied for time dependent non-Newtonian fluids. Time dependent fluids can be grouped as thixotropic and rheopectic fluids.

2.3.2.1. Thixotropic Fluids. Apparent viscosity decreases with the time of shearing since the structure of the fluid is broke down by shear (See Figure 2.3). Concentrated suspensions, laponite and bentonite clay suspensions, emulsions, drilling fluids, waxy crude oils, protein solutions and foodstuffs are some examples that exhibit thixotropic behavior (Chhabra and Richardson, 2008).

2.3.2.2. Rheopectic (or negative Thixotropic) Fluids. Apparent viscosity increases with time of shearing as their structure formation occurs by shear (See Figure 2.3).

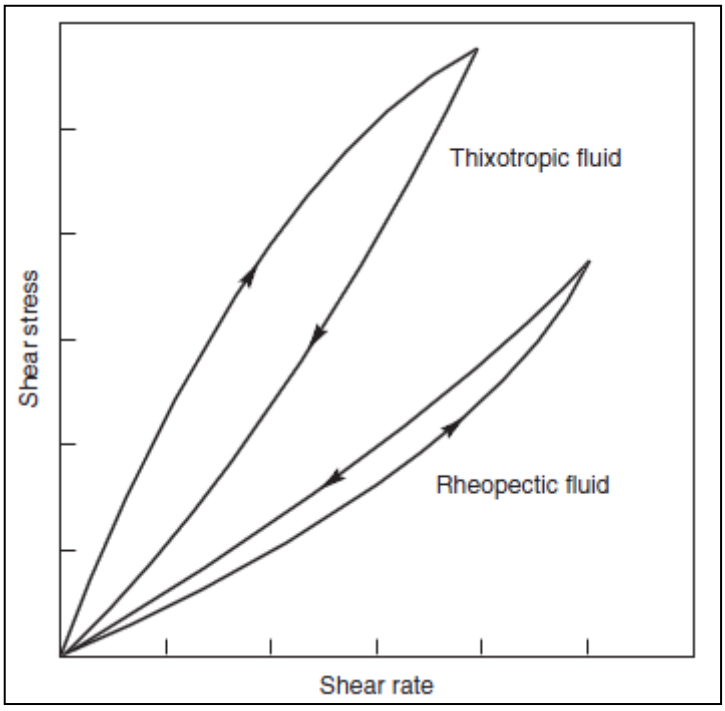

Figure 2.3. Schematic shear stress–shear rate relation for time-dependent fluid behavior (This figure was published in 2008, Chhabra, R. P., and J. F. Richardson, Non-Newtonian Flow and Applied Rheology, 2nd ed., pp.19, Copyright Elsevier (2008).).

The model used for rheopectic fluids is as follows:

$$\tau_{yx} = (\tau_{y0} + \tau_{y1}) + (k_0 + \zeta\ k_1)\dot{\gamma}_{yx}^{n} \tag{2.20}$$

$$\frac{d\zeta}{dt} = a(1-\zeta) - (b\ \zeta\ \dot{\gamma}_{yx}^{\varepsilon}) \tag{2.21}$$

where τ_{y0} and k_0 are permanent yield stress and consistency coefficient, τ_{y1} and k_1 corresponding time-dependent contributions, a, b, ζ and ε are kinetic parameters (Chhabra and Richardson, 2008).

2.3.3. Viscoelastic Fluids

A viscoelastic material is one which possesses both elastic and viscous properties, i.e. although the material might be viscous, it exhibits a certain elasticity of shape.

Elasticity is the ability to recover the original shape after the applied force is removed. And viscous property is the retarded shape deformation of a material under an applied force. A lot of material exhibit both viscous and elastic behavior. Elastic behavior is time independent while viscous behavior is time dependent. So, viscoelastic behavior is assumed as time dependent.

Viscoelastic fluids cannot be expressed with a simple equation such as

$$\dot{\gamma}_{yx} = f(\tau_{yx}) \tag{2.22}$$

Rheological equations of viscoelastic fluids include time derivative of shear stress and shear rate (Wilkinson, 1960), which is shown as

$$f_1\left(\frac{d\tau_{yx}}{dt}\right) = f_2\left(\frac{d\dot{\gamma}_{yx}}{dt}\right) \tag{2.23}$$

The models recommended for viscoelastic behavior generally depend on spring and dash-pod system. In these systems, spring represents the elastic behavior while dash-pod denotes the viscous property. Mathematical models used to describe the viscoelastic behavior are given below.

i. Maxwell model: In this model, spring and dash-pod are modeled as they are connected in series (Wilkinson, 1960; Bird *et al*., 1987).

The equations to describe the system are as below:

$$\dot{\gamma}_{yx} = \frac{\dot{\tau}_{yx}}{G} + \frac{\tau_{yx}}{\mu} \tag{2.24}$$

where

$$\dot{\tau}_{yx} = \frac{d\tau_{yx}}{dt} \tag{2.25}$$

and

$$\dot{\gamma}_{yx} = \frac{d\gamma_{yx}}{dt} \tag{2.26}$$

which becomes

$$\tau_{yx} + \frac{\mu}{G}\frac{\partial \tau_{yx}}{\partial t} = -\mu\dot{\gamma}_{yx} \tag{2.27}$$

integrating, it is found as

$$\tau_{yx} = \exp\left(-\frac{G}{\mu}t\right)\left[\tau_0 + G\int \lambda_1 \exp\left(\frac{G}{\mu}t\right)dt\right] \tag{2.28}$$

where G, and μ are elasticity modulus and viscosity, respectively (Wilkinson, 1960). λ_1 is the relaxation time that is defined as

$$\lambda_1 = \frac{\mu}{G} \tag{2.29}$$

ii. Voigt-Kelvin model: This model assumes spring and dash-pod as connected in parallel (Wilkinson, 1960).

$$\tau_{yx} = G\,\gamma_{yx} + \mu\,\dot{\gamma}_{yx} \tag{2.30}$$

integrating, it is found as

$$\gamma_{yx} = \exp\left(-\frac{G}{\mu}t\right)\left[\gamma_0 + \frac{1}{\mu}\int \tau_{yx} \exp\left(\frac{G}{\mu}t\right)dt\right] \tag{2.31}$$

where γ_0 is the shear at t=0.

iii. Jeffreys model: This model is derived as adding time derivative or shear rate into Maxwell model (Bird *et al*., 1987).

$$\underline{\underline{\tau}} + \lambda_1 \frac{\partial \underline{\underline{\tau}}}{\partial t} = -\mu_0 \left(\underline{\underline{\dot{\gamma}}} + \lambda_2 \frac{\partial \underline{\underline{\dot{\gamma}}}}{\partial t} \right) \tag{2.32}$$

where λ_1 and λ_2 are relaxation and retardation time.

iv. Generalized Maxwell model: This model includes a set of N element of Maxwell system (Wilkinson, 1960).

v. Maxwell and Voigt-Kelvin Models: In order to model the viscoelastic behavior better, different combinations of Maxwell and Voigh-Kelvin systems are designed.

vi. White-Metzner model (Bird *et al.*, 1987):

$$\underline{\underline{\tau}} + \frac{\mu(\dot{\gamma})}{G} \underline{\underline{\tau}}_{(1)} = -\mu(\dot{\gamma}) \underline{\underline{\gamma}}_{(1)} \tag{2.33}$$

$$\underline{\underline{\tau}}_{(1)} = \frac{D}{Dt} \underline{\underline{\tau}} - \left\{ (\nabla v)^T \cdot \underline{\underline{\tau}} + \underline{\underline{\tau}} \cdot \nabla v \right\} \tag{2.34}$$

vii. Convected Jeffreys (Oldroyd-B) model: This model is derived replacing the time derivatives of Jeffreys model with convective derivatives (Bird *et al.*, 1987).

$$\underline{\underline{\tau}} + \lambda_1 \underline{\underline{\tau}}_{(1)} = -\mu (\underline{\underline{\gamma}}_{(1)} + \lambda_2 \underline{\underline{\gamma}}_{(2)}) \tag{2.35}$$

For λ_2, the model reduces to 'convected Maxwell model'; for $\lambda_2 = \lambda_1$, the model reduces to Newtonian fluid model with viscosity, μ.

viii. Giesekus model: This model takes into account the contribution of polymer (μ_s) and solution (μ_p) to viscosity (Bird *et al.*, 1987).

$$\underline{\underline{\tau}} = \underline{\underline{\tau}}_s + \underline{\underline{\tau}}_p \tag{2.36}$$

$$\underline{\underline{\tau_s}} = -\mu_s \underline{\underline{\dot{\gamma}}} \tag{2.37}$$

$$\underline{\underline{\tau_p}} + \lambda_1 \underline{\underline{\tau_{p(1)}}} - \alpha \frac{\lambda_1}{\mu_p} \left\{ \underline{\underline{\tau_p}} \cdot \underline{\underline{\tau_p}} \right\} = -\mu_p \underline{\underline{\dot{\gamma}}} \tag{2.38}$$

where α is dimensionless mobility factor.

ix. Kopaç-Arıkol Model (Kopaç *et al*., 1998):

$$\left(1 + \lambda \mathrm{II}(\underline{\underline{\dot{\gamma}}})\right) \tau = -2m(1 + \lambda \mathrm{II}(\underline{\underline{\dot{\gamma}}})) \underline{\underline{\dot{\gamma}}} \tag{2.39}$$

where m and λ are expressed as

$$m = \frac{\mu_0}{1 + d_1 |II|^{\frac{r}{2}}} \tag{2.40}$$

and

$$\lambda = \frac{1}{\lambda_0 + \lambda_1 |II|^{\frac{r}{2}}} \tag{2.41}$$

where λ_0 , λ_1 , d_1 and r are constants with $\mathrm{II}(\underline{\underline{\dot{\gamma}}})$ being second shear rate constant.

x. Oldroyd 3-constants model (Kopaç *et al*., 1998):

$$(1 + \lambda_1 \Pi) \underline{\underline{\tau}} = -2\mu(1 + \lambda_2 \Pi) \underline{\underline{\dot{\gamma}}} \tag{2.42}$$

xi. Walters-B model: This model is used to model the viscoelastic polymer behavior in porous medium (Sharma *et al.,* 1997).

$$\underline{\underline{\tau}} = 2\left(\mu - \mu' \frac{\partial}{\partial t}\right) \underline{\underline{\dot{\gamma}}} \tag{2.43}$$

where μ' is viscoelasticity.

xii. Rivlin-Ericksen model: This model is also used to describe the viscoelastic behavior in porous medium (El-Sayed and Syam, 2007).

$$\underline{\underline{\tau}} = 2(\mu + \mu' \frac{\partial}{\partial t})\underline{\underline{\dot{\gamma}}} \tag{2.44}$$

In this work, the Oldroyd-B model is preferred as a constitutive equation. The solvent viscosity is ignored and the polymer is assumed to be a Maxwell fluid so that the model reduces to the Upper Convected Maxwell (UCM) model. The studies about the investigation of the instability mechanism of the LISA process generally used the UCM equation to model their polymer behavior. Hence, it is thought that this is a useful model to describe the polymer behavior in LISA process.

3. THE PHYSICAL SYSTEM AND THE MODELING EQUATIONS

Two incompressible, viscous, immiscible, leaky-dielectric, and non-reactive fluids flow side-by-side in a channel due to a pressure gradient. The fluids share a flat interface, located at z=0, whose velocity is u_0 as shown in Figure 3.1.

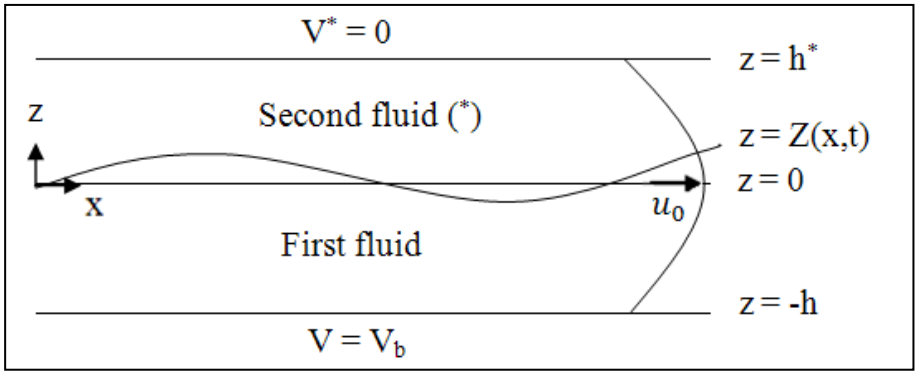

Figure 3.1. The physical system depicting two immiscible fluids in a channel.

The first fluid whose density, ρ, viscosity, μ, electrical permittivity, $\varepsilon_0\varepsilon$, electrical conductivity, σ, is in contact with the second fluid whose parameters are denoted with an asterisk. Here, ε_0 is the vacuum permittivity with the value of $8.85\text{x}10^{-12}$ F/m. An electrical field is applied in the normal direction to the flat interface with a potential V_b at the lower wall located at z=-h. The upper wall, located at $z=h^*$, is grounded, i.e., $V^*=0$.

The stability of the interface of these two fluids is analyzed for four different cases, with Newtonian or non-Newtonian fluids and under the effect of an electric field or without applying an electric field. The modeling equations start with the most general case, i.e., a Newtonian fluid and a non-Newtonian fluid system under the effect of an applied electric field the results of which are presented in Section 4.1. Then, in the subsequent sections, the following special cases are considered. The second case concerns with the stability of two Newtonian fluids under the effect of an electric field. The results are compared with Ozen *et al.* (2006c) (See Section 4.3). For the third case, the electric field is turned off and both fluids are assumed to be Newtonian. The results of this case are

compared with that of Hooper (1989) (See Section 4.1). The last case is where one of the fluids is non-Newtonian but there is no applied electric field. The results of this case are compared with those of the third case (See Section 4.2).

3.1. A Newtonian Fluid and a Non-Newtonian Fluid System under the Influence of an Electric Field

The stability of the interface between a Newtonian fluid and a non-Newtonian fluid flowing in a channel under the effect of an externally applied electric filed is analyzed.

The physical system consists of two immiscible liquids flowing in a long channel sharing a common flat interface. A schematic representation of the system is shown in Figure 3.1 where the first liquid is taken to be non-Newtonian and the second one Newtonian.

The governing equations and the boundary conditions are given as follows.

3.1.1. Governing Equations

As the surface-coupled model (See Section 2.1.1), which assumes electroneutrality in the bulk fluids and accumulation of free charge at the interface, is used (Shankar and Sharma, 2004; Craster and Matar, 2005; Uguz *et al*., 2008), the electric field appears only at the boundary and the interface conditions.

The equation of motion for the first fluid, located at –h < z < Z(x,t), is

$$\rho\left[\frac{\partial \underline{v}}{\partial t} + \underline{v}\cdot\nabla\underline{v}\right] = -\nabla p + \nabla\cdot\underline{\underline{\tau}} \tag{3.1}$$

where $\underline{v}$, p and $\underline{\underline{\tau}}$ represent the velocity, pressure and viscous stress tensor for the first fluid, respectively. For an incompressible liquid, the continuity equation is

$$\nabla\cdot\underline{v} = 0 \tag{3.2}$$

and the Laplace equation for the electric field is given as follows:

$$\nabla^2 V = 0 \tag{3.3}$$

Similar equations for the second fluid occupying Z(x,t) < z < h* are given as

$$\rho^* \left[\frac{\partial \underline{v}^*}{\partial t} + \underline{v}^* \cdot \nabla \underline{v}^*\right] = -\nabla p^* + \nabla \cdot \underline{\underline{\tau}}^* \tag{3.4}$$

$$\nabla \cdot \underline{v}^* = 0 \tag{3.5}$$

$$\nabla^2 V^* = 0 \tag{3.6}$$

For the second fluid, which is assumed to be Newtonian, the viscous stress tensor is defined as

$$\underline{\underline{\tau}}^* = \mu^* 2\underline{\underline{D}}^* \tag{3.7}$$

where $2\underline{\underline{D}}^*$ is the rate of strain tensor and it is given by

$$2\underline{\underline{D}}^* = \left(\nabla \underline{v}^* + \left(\nabla \underline{v}^*\right)^T\right) \tag{3.8}$$

For the Oldroyd-B model the shear stress is defined as

$$\underline{\underline{\tau}} = \underline{\underline{\tau}}^p + \underline{\underline{\tau}}^s \tag{3.9}$$

where $\underline{\underline{\tau}}^p$ is the polymeric contribution and $\underline{\underline{\tau}}^s$ is the viscous solvent contribution to the stress (Bird *et al.*, 1987; Shaqfeh *et al.*, 1989) and their expressions are

$$\underline{\underline{\tau}}^s = \mu_s 2\underline{\underline{D}} \tag{3.10}$$

and

$$\lambda \underline{\underline{\tau}}^{p}_{(1)} + \underline{\underline{\tau}}^{p} = \mu_p 2\underline{\underline{D}} \tag{3.11}$$

where, μ_p is the polymeric contribution, μ_s is the solvent contribution to the shear viscosity, $2\underline{\underline{D}}$ is the shear rate of the fluid given in Equation (3.8), and $\underline{\underline{\tau}}^{p}_{(1)}$ is the convective derivative of the stress tensor which is defined as follows:

$$\underline{\underline{\tau}}^{p}_{(1)} = \frac{D}{Dt}\underline{\underline{\tau}}^{p} - \{(\nabla v)^T \cdot \underline{\underline{\tau}}^{p} + \underline{\underline{\tau}}^{p} \cdot \nabla \underline{v}\} \tag{3.12}$$

Here, the superscript T stands for the transpose. When the definition for the material time derivative D/Dt is inserted, Equation (3.12) becomes

$$\underline{\underline{\tau}}^{p}_{(1)} = \frac{\partial}{\partial t}\underline{\underline{\tau}}^{p} + \underline{v} \cdot \nabla \underline{\underline{\tau}}^{p} - (\nabla v)^T \cdot \underline{\underline{\tau}}^{p} - \underline{\underline{\tau}}^{p} \cdot \nabla \underline{v} \tag{3.13}$$

The component form of Equation (3.13) is

$$\underline{\underline{\tau}}^{p}_{(1)} = \frac{\Delta \tau^{p}_{ij}}{\Delta t} \equiv \frac{\partial \tau^{p}_{ij}}{\partial t} + v_k \frac{\partial \tau^{p}_{ij}}{\partial x_k} - L_{jk}\tau^{p}_{ki} - L_{ik}\tau^{p}_{kj} \tag{3.14}$$

where

$$L_{ij} = \frac{\partial v_i}{\partial x_j} \tag{3.15}$$

For Newtonian fluids, $\mu_p = 0$; and for the Upper Convected Maxwell (UCM) model, $\mu_s = 0$. In this work, the Upper Convected Maxwell model is assumed. Consequently, the viscous stress of the fluid depends only on the polymer viscosity (Bird *et al.*, 1987; Denn, 1990), i.e.,

$$\underline{\underline{\tau}} = \underline{\underline{\tau}}^{p} \tag{3.16}$$

Then, Equation (3.11) is expanded as

$$\lambda\left[\frac{\partial \tau_{ij}}{\partial t} + v_k \frac{\partial \tau_{ij}}{\partial x_k} - \frac{\partial v_j}{\partial x_k}\tau_{ki} - \frac{\partial v_i}{\partial x_k}\tau_{kj}\right] + \tau_{ij} = \mu_p\left[\frac{\partial v_i}{\partial x_j} + \frac{\partial v_j}{\partial x_i}\right] \quad (3.17)$$

These governing equations are solved subject to the following boundary and interface conditions.

3.1.2. Boundary and Interface Conditions

At the bottom wall, z = -h, the no-slip condition yields

$$v_x = 0 \quad (3.18)$$

the no-flow through the wall is

$$v_z = 0 \quad (3.19)$$

and the applied voltage is

$$V = V_b \quad (3.20)$$

At the top wall, z = h^*, the no-slip, no-flow, and the applied voltage conditions are

$$v_x^* = 0 \quad (3.21)$$

$$v_z^* = 0 \quad (3.22)$$

and

$$V^* = 0 \quad (3.23)$$

respectively. At the interface, located at z = Z (x, t), the normal components of the velocities of the fluids are equal to each other and to the normal speed of the interface, u

$$\underline{v} \cdot \underline{n} = \underline{v}^* \cdot \underline{n} = \underline{u} \cdot \underline{n} = u \tag{3.24}$$

The no-slip condition is

$$\underline{v} \cdot \underline{t} = \underline{v}^* \cdot \underline{t} \tag{3.25}$$

and the continuity of the electric field is

$$\underline{E} \cdot \underline{t} = \underline{E}^* \cdot \underline{t} \tag{3.26}$$

where $\underline{n}$, $\underline{t}$ and $\underline{E}$ represent unit normal vector, unit tangential vector and the electric field, respectively. Expressions for $\underline{n}$, $\underline{t}$ and u are as below, and the detailed derivations are given in Appendix A.

$$\underline{n} = \frac{\underline{e_z} - Z_x \underline{e_x}}{\sqrt{1 + (Z_x)^2}} \tag{3.27}$$

$$\underline{t} = \frac{\underline{e_x} + Z_x \underline{e_z}}{\sqrt{1 + (Z_x)^2}} \tag{3.28}$$

$$u = \frac{Z_t}{\sqrt{1 + (Z_x)^2}} \tag{3.29}$$

where $\underline{e_x}$ and $\underline{e_z}$ are the unit base vectors. The Gauss' law for the electric field is expressed as

$$q = \varepsilon_0 \varepsilon^* \underline{E}^* \cdot \underline{n} - \varepsilon_0 \varepsilon \underline{E} \cdot \underline{n} \tag{3.30}$$

where q denotes the surface charge density. The charge distribution at the interface is given as

$$q_t - \underline{u} \cdot \nabla_s q + \nabla_s \cdot (q \underline{u_s}) + q 2H \underline{u} \cdot \underline{n} = (\sigma \underline{E} \cdot \underline{n} - \sigma^* \underline{E}^* \cdot \underline{n}) \tag{3.31}$$

where q_t , ∇_s , $\underline{u_s}$ and 2H represent the time derivative of the charge density, surface gradient, surface velocity and the surface mean curvature, respectively. The definitions of the surface gradient (Castellanos and González, 1998) and the curvature (Johns and Narayanan, 2002) are as follows:

$$\nabla_s = \nabla - \underline{n}(\underline{n} \cdot \nabla) \tag{3.32}$$

$$2H = \frac{Z_{xx}}{\left(\sqrt{1 + (Z_x)^2}\right)^{3/2}} \tag{3.33}$$

The stress balance at the interface is expressed as

$$\underline{\underline{T}}^* \cdot \underline{n} - \underline{\underline{T}} \cdot \underline{n} + \gamma 2H\underline{n} = 0 \tag{3.34}$$

where $\underline{\underline{T}}$ is the total stress tensor, γ is the interfacial tension. The stress balance yields the normal stress balance (NSB) when dotted with the normal vector, and the tangential stress balance (TSB) when dotted with the tangent vector. They are

$$\underline{\underline{T}}^* \cdot \underline{n} \cdot \underline{n} - \underline{\underline{T}} \cdot \underline{n} \cdot \underline{n} + \gamma 2H = 0 \tag{3.35}$$

and

$$\underline{\underline{T}}^* \cdot \underline{n} \cdot \underline{t} - \underline{\underline{T}} \cdot \underline{n} \cdot \underline{t} = 0 \tag{3.36}$$

respectively. The total stress tensor, $\underline{\underline{T}}$, is composed of a fluid component, $\underline{\underline{T}}^F$, and an electrical component (Castellanos and González, 1998), $\underline{\underline{T}}^E$, i.e.,

$$\underline{\underline{T}} = \underline{\underline{T}}^F + \underline{\underline{T}}^E \tag{3.37}$$

and the expressions for those are given as

$$\underline{\underline{T}}^F = -p\underline{\underline{I}} + \underline{\underline{\tau}} \tag{3.38}$$

$$\underline{\underline{\tau}}^E = \varepsilon_0\varepsilon(\underline{E}\underline{E} - \frac{1}{2}|E|^2\underline{\underline{I}}) \tag{3.39}$$

and similar expressions are valid for the * phase. Here, I is the identity tensor. The electric field is the negative of the gradient of the voltage and in Cartesian coordinates, it is given as

$$\underline{E} = -\nabla V = -\left(\frac{\partial V}{\partial x}\underline{e}_x + \frac{\partial V}{\partial z}\underline{e}_z\right) \tag{3.40}$$

and

$$\underline{E}^* = -\nabla V^* = -\left(\frac{\partial V^*}{\partial x}\underline{e}_x + \frac{\partial V^*}{\partial z}\underline{e}_z\right) \tag{3.41}$$

Then, the stress balance equation, i.e. Equation (3.34) can be written as

$$\left\{-p^*\underline{\underline{I}} + \mu^* 2\underline{\underline{D}}^* + \varepsilon_0\varepsilon^*\left(\underline{E}^*\underline{E}^* - \frac{1}{2}|E^*|^2\underline{\underline{I}}\right)\right\}\cdot\underline{n} - \left\{-p\underline{\underline{I}} + \underline{\underline{\tau}} + \varepsilon_0\varepsilon(\underline{E}\underline{E} - \frac{1}{2}|E|^2\underline{\underline{I}})\right\}\cdot\underline{n} = -\gamma 2H\underline{n} \tag{3.42}$$

The NSB becomes

$$\left\{-p^*\underline{\underline{I}} + \mu^* 2\underline{\underline{D}}^* + \varepsilon_0\varepsilon^*\left(\underline{E}^*\underline{E}^* - \frac{1}{2}|E^*|^2\underline{\underline{I}}\right)\right\}\cdot\underline{n}\cdot\underline{n} - \left\{-p\underline{\underline{I}} + \underline{\underline{\tau}} + \varepsilon_0\varepsilon(\underline{E}\underline{E} - \frac{1}{2}|E|^2\underline{\underline{I}})\right\}\cdot\underline{n}\cdot\underline{n} + \gamma 2H = 0 \tag{3.43}$$

The TSB becomes

$$\left\{-p^*\underline{\underline{I}} + \mu^* 2\underline{\underline{D}}^* + \varepsilon_0\varepsilon^*\left(\underline{E}^*\underline{E}^* - \frac{1}{2}|E^*|^2\underline{\underline{I}}\right)\right\}\cdot\underline{n}\cdot\underline{t}$$

$$= \left\{-p\underline{\underline{I}} + \underline{\underline{\tau}} + \varepsilon_0\varepsilon\left(\underline{E}\,\underline{E} - \frac{1}{2}|E|^2\underline{\underline{I}}\right)\right\} \cdot \underline{n} \cdot \underline{t} \tag{3.44}$$

The above equation is simplified to

$$\left(\underline{\underline{\tau}} \cdot \underline{n} \cdot \underline{t}\right) + \left(\varepsilon_0\varepsilon\underline{E}\,\underline{E} \cdot \underline{n} \cdot \underline{t}\right) = \left(\mu^* 2\underline{\underline{D}}^* \cdot \underline{n} \cdot \underline{t}\right) + \left(\varepsilon_0\varepsilon^*\underline{E}^*\underline{E}^* \cdot \underline{n} \cdot \underline{t}\right) \tag{3.45}$$

The next step is to render the equations and the boundary conditions dimensionless.

3.1.3. Scaling

The system variables are scaled with respect to the first fluid's parameters and the physical system in scaled form is shown in Figure 3.2.

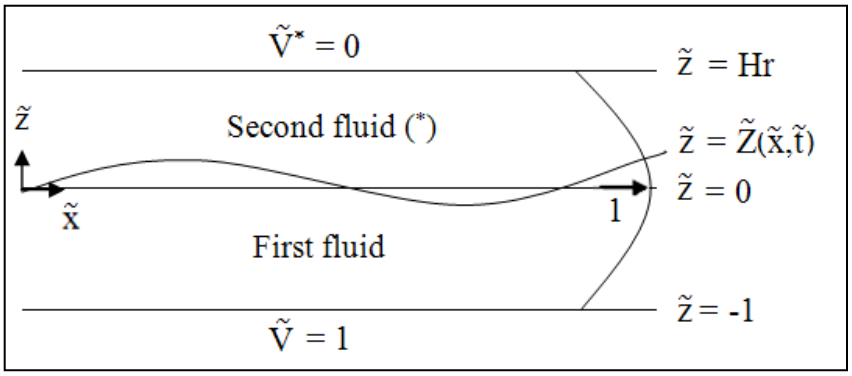

Figure 3.2. The physical system depicting two immiscible fluids in a channel in dimensionless form.

The variables are rendered dimensionless as

$$x = \overline{x}\tilde{x} \tag{3.46}$$

where x can be position, velocity, stress tensor, etc. The variables with a tilde represent the dimensionless quantities, and those with an overbar are the scale factors. The scale factors are given as

$$\overline{v} = u_0;\ \ \overline{t} = \frac{h}{u_0};\ \ \overline{x} = \overline{z} = h;\ \ \overline{p} = \overline{\tau} = \frac{\mu u_0}{h};\ \ \overline{V} = V_b;\ \ \ \overline{q} = \frac{\varepsilon_0 V_b}{h};\ \ \overline{E} = \frac{V_b}{h};$$

$$\overline{D} = \frac{u_0}{h}\ ;\ \overline{\nabla} = \frac{1}{h} \tag{3.47}$$

In the next section, the scaling is introduced into the governing equations.

3.1.3.1. Governing Equations in Dimensionless Form.

The equation of motion for the first fluid is

$$Re\left[\frac{\partial \underline{\tilde{v}}}{\partial \tilde{t}} + \underline{\tilde{v}} \cdot \tilde{\nabla}\underline{\tilde{v}}\right] = -\tilde{\nabla}\tilde{p} + \tilde{\nabla} \cdot \underline{\underline{\tilde{\tau}}} \tag{3.48}$$

where Re is the Reynolds number and is defined as

$$Re = \frac{\rho u_0 h}{\mu} \tag{3.49}$$

The UCM model, i.e. Equation (3.17) is scaled as

$$\lambda \frac{\mu_p {u_0}^2}{h^2}\left[\frac{\partial \tilde{\tau}_{ij}}{\partial \tilde{t}} + \tilde{v}_k \frac{\partial \tilde{\tau}_{ij}}{\partial \tilde{x}_k} - \frac{\partial \tilde{v}_j}{\partial \tilde{x}_k}\tilde{\tau}_{ki} - \frac{\partial \tilde{v}_i}{\partial \tilde{x}_k}\tilde{\tau}_{kj}\right] + \mu_p \frac{u_0}{h}\tilde{\tau}_{ij} = \mu_p \frac{u_0}{h}\left[\frac{\partial \tilde{v}_i}{\partial \tilde{x}_j} + \frac{\partial \tilde{v}_j}{\partial \tilde{x}_i}\right] \tag{3.50}$$

and dividing by $\mu_p \frac{u_0}{h}$,

$$\tilde{\tau}_{ij} + We\left[\frac{\partial \tilde{\tau}_{ij}}{\partial \tilde{t}} + \tilde{v}_k \frac{\partial \tilde{\tau}_{ij}}{\partial \tilde{x}_k} - \frac{\partial \tilde{v}_j}{\partial \tilde{x}_k}\tilde{\tau}_{ki} - \frac{\partial \tilde{v}_i}{\partial \tilde{x}_k}\tilde{\tau}_{kj}\right] = \left[\frac{\partial \tilde{v}_i}{\partial \tilde{x}_j} + \frac{\partial \tilde{v}_j}{\partial \tilde{x}_i}\right] \tag{3.51}$$

is obtained, where We is the Weissenberg number which is the ratio of the relaxation time of the fluid and fluid time scale, and it is defined as

$$We = \frac{\lambda}{\bar{t}} = \lambda \frac{u_0}{h} \tag{3.52}$$

For i=x, and j=x , an implicit equation for $\tilde{\tau}_{xx}$ is obtained as

$$\tilde{\tau}_{xx} + We\left[\frac{\partial \tilde{\tau}_{xx}}{\partial \tilde{t}} + \tilde{v}_x \frac{\partial \tilde{\tau}_{xx}}{\partial \tilde{x}} + \tilde{v}_z \frac{\partial \tilde{\tau}_{xx}}{\partial \tilde{z}} - \frac{\partial \tilde{v}_x}{\partial \tilde{x}} \tilde{\tau}_{xx} - \frac{\partial \tilde{v}_x}{\partial \tilde{z}} \tilde{\tau}_{zx} - \frac{\partial \tilde{v}_x}{\partial \tilde{x}} \tilde{\tau}_{xx} - \frac{\partial \tilde{v}_x}{\partial \tilde{z}} \tilde{\tau}_{zx}\right] = \left[\frac{\partial \tilde{v}_x}{\partial \tilde{x}} + \frac{\partial \tilde{v}_x}{\partial \tilde{x}}\right] \tag{3.53}$$

which reduces to

$$\tilde{\tau}_{xx} + We\left[\frac{\partial \tilde{\tau}_{xx}}{\partial \tilde{t}} + \tilde{v}_x \frac{\partial \tilde{\tau}_{xx}}{\partial \tilde{x}} + \tilde{v}_z \frac{\partial \tilde{\tau}_{xx}}{\partial \tilde{z}} - 2\frac{\partial \tilde{v}_x}{\partial \tilde{x}} \tilde{\tau}_{xx} - 2\frac{\partial \tilde{v}_x}{\partial \tilde{z}} \tilde{\tau}_{zx}\right] = \left[2\frac{\partial \tilde{v}_x}{\partial \tilde{x}}\right] \tag{3.54}$$

Similarly, the equation for $\tilde{\tau}_{xz}$ is

$$\tilde{\tau}_{xz} + We\left[\frac{\partial \tilde{\tau}_{xz}}{\partial \tilde{t}} + \tilde{v}_x \frac{\partial \tilde{\tau}_{xz}}{\partial \tilde{x}} + \tilde{v}_z \frac{\partial \tilde{\tau}_{xz}}{\partial \tilde{z}} - \frac{\partial \tilde{v}_z}{\partial \tilde{x}} \tilde{\tau}_{xx} - \frac{\partial \tilde{v}_z}{\partial \tilde{z}} \tilde{\tau}_{xz} - \frac{\partial \tilde{v}_x}{\partial \tilde{x}} \tilde{\tau}_{xz} - \frac{\partial \tilde{v}_x}{\partial \tilde{z}} \tilde{\tau}_{zz}\right] = \left[\frac{\partial \tilde{v}_x}{\partial \tilde{z}} + \frac{\partial \tilde{v}_z}{\partial \tilde{x}}\right] \tag{3.55}$$

which can be rearranged to

$$\tilde{\tau}_{xz} + We\left[\frac{\partial \tilde{\tau}_{xz}}{\partial \tilde{t}} + \tilde{v}_x \frac{\partial \tilde{\tau}_{xz}}{\partial \tilde{x}} + \tilde{v}_z \frac{\partial \tilde{\tau}_{xz}}{\partial \tilde{z}} - \frac{\partial \tilde{v}_z}{\partial \tilde{x}} \tilde{\tau}_{xx} - \frac{\partial \tilde{v}_x}{\partial \tilde{z}} \tilde{\tau}_{zz} - \tilde{\tau}_{xz} \underbrace{\left(\frac{\partial \tilde{v}_z}{\partial \tilde{z}} + \frac{\partial \tilde{v}_x}{\partial \tilde{x}}\right)}_{0\ from\ continuity}\right] = \left[\frac{\partial \tilde{v}_x}{\partial \tilde{z}} + \frac{\partial \tilde{v}_z}{\partial \tilde{x}}\right] \tag{3.56}$$

Using the continuity equation, Equation (3.56) becomes

$$\tilde{\tau}_{xz} + We\left[\frac{\partial \tilde{\tau}_{xz}}{\partial \tilde{t}} + \tilde{v}_x \frac{\partial \tilde{\tau}_{xz}}{\partial \tilde{x}} + \tilde{v}_z \frac{\partial \tilde{\tau}_{xz}}{\partial \tilde{z}} - \frac{\partial \tilde{v}_z}{\partial \tilde{x}} \tilde{\tau}_{xx} - \frac{\partial \tilde{v}_x}{\partial \tilde{z}} \tilde{\tau}_{zz}\right] = \left[\frac{\partial \tilde{v}_x}{\partial \tilde{z}} + \frac{\partial \tilde{v}_z}{\partial \tilde{x}}\right] \tag{3.57}$$

The equation for $\tilde{\tau}_{zz}$ in dimensionless form is

$$\tilde{\tau}_{zz} + We\left[\frac{\partial\tilde{\tau}_{zz}}{\partial\tilde{t}} + \tilde{v}_x\frac{\partial\tilde{\tau}_{zz}}{\partial\tilde{x}} + \tilde{v}_z\frac{\partial\tilde{\tau}_{zz}}{\partial\tilde{z}} - \frac{\partial\tilde{v}_z}{\partial\tilde{x}}\tilde{\tau}_{xz} - \frac{\partial\tilde{v}_z}{\partial\tilde{z}}\tilde{\tau}_{zz} - \frac{\partial\tilde{v}_z}{\partial\tilde{x}}\tilde{\tau}_{xz} - \frac{\partial\tilde{v}_z}{\partial\tilde{z}}\tilde{\tau}_{zz}\right] = \left[\frac{\partial\tilde{v}_z}{\partial\tilde{z}} + \frac{\partial\tilde{v}_z}{\partial\tilde{z}}\right] \quad (3.58)$$

which simplifies to

$$\tilde{\tau}_{zz} + We\left[\frac{\partial\tilde{\tau}_{zz}}{\partial\tilde{t}} + \tilde{v}_x\frac{\partial\tilde{\tau}_{zz}}{\partial\tilde{x}} + \tilde{v}_z\frac{\partial\tilde{\tau}_{zz}}{\partial\tilde{z}} - 2\frac{\partial\tilde{v}_z}{\partial\tilde{x}}\tilde{\tau}_{xz} - 2\frac{\partial\tilde{v}_z}{\partial\tilde{z}}\tilde{\tau}_{zz}\right] = \left[2\frac{\partial\tilde{v}_z}{\partial\tilde{z}}\right] \quad (3.59)$$

The dimensionless continuity and the Laplace equations for the first fluid are

$$\tilde{\nabla}\cdot\underline{\tilde{v}} = 0 \quad (3.60)$$

$$\tilde{\nabla}^2\tilde{V} = 0 \quad (3.61)$$

respectively.

Similar equations are valid for the second fluid. The only difference is observed for the momentum balance, which is

$$\frac{\rho^*{u_0}^2}{h}\left[\frac{\partial\underline{\tilde{v}}^*}{\partial\tilde{t}} + \underline{\tilde{v}}^*\cdot\tilde{\nabla}\underline{\tilde{v}}^*\right] = -\frac{\mu u_0}{h^2}\tilde{\nabla}\tilde{p}^* + \frac{\mu^* u_0}{h^2}(\tilde{\nabla}\cdot 2\underline{\underline{\tilde{D}}}^*) \quad (3.62)$$

and multiplying by $\frac{h^2\rho}{\mu u_0\rho^*}$, it is found as

$$ReP\left[\frac{\partial\underline{\tilde{v}}^*}{\partial\tilde{t}} + \underline{\tilde{v}}^*\cdot\tilde{\nabla}\underline{\tilde{v}}^*\right] = -\tilde{\nabla}\tilde{p}^* + M\left(\tilde{\nabla}\cdot 2\underline{\underline{\tilde{D}}}^*\right) \quad (3.63)$$

Here, P and M are the density and the viscosity ratios of the fluids which are defined as

$$\mathrm{P} = \frac{\rho^*}{\rho} \quad (3.64)$$

$$M = \frac{\mu^*}{\mu} \tag{3.65}$$

3.1.3.2. Dimensionless Boundary and Interface Conditions.

At the bottom wall, $\tilde{z} = -1$,

$$\tilde{v}_x = 0 \tag{3.66}$$

$$\tilde{v}_z = 0 \tag{3.67}$$

and

$$\tilde{V} = 1 \tag{3.68}$$

at the top wall, $\tilde{z} = Hr$,

$$\tilde{v}_x^* = 0 \tag{3.69}$$

$$\tilde{v}_z^* = 0 \tag{3.70}$$

and

$$\tilde{V}^* = 0 \tag{3.71}$$

conditions are acquired. Here, Hr is the thickness ratio of the fluids which is defined as

$$Hr = \frac{h^*}{h} \tag{3.72}$$

At the interface, $\tilde{z} = \tilde{Z}(\tilde{x}, \tilde{t})$, Equations (3.24)-(3.26) and (30) in dimensionless form become

$$\underline{\tilde{v}} \cdot \underline{n} = \underline{\tilde{u}} \cdot \underline{n} = \underline{\tilde{v}}^* \cdot \underline{n} \tag{3.73}$$

$$\underline{\tilde{v}} \cdot \underline{t} = \underline{\tilde{v}}^* \cdot \underline{t} \tag{3.74}$$

$$\underline{\tilde{E}} \cdot \underline{t} = \underline{\tilde{E}}^* \cdot \underline{t} \tag{3.75}$$

$$\tilde{q} = \varepsilon^* \underline{\tilde{E}}^* \cdot \underline{n} - \varepsilon \underline{\tilde{E}} \cdot \underline{n} \tag{3.76}$$

respectively. The charge balance at the interface, i.e., Equation (3.31), is

$$\begin{aligned} &\frac{\varepsilon_0 V_b}{ht} \tilde{q}_t - \frac{u_0}{h} \frac{\varepsilon_0 V_b}{h} \underline{\tilde{u}} \cdot \tilde{\nabla}_s \tilde{q} + \frac{u_0}{h} \frac{\varepsilon_0 V_b}{h} \tilde{\nabla}_s \cdot \tilde{q} \underline{\tilde{u}}_s + \frac{\varepsilon_0 V_b}{h} \frac{u_0}{h} \tilde{q} 2\tilde{H} \underline{\tilde{u}} \cdot \underline{n} \\ &= \frac{V_b}{h} (\sigma \underline{\tilde{E}} \cdot \underline{n}) - \frac{V_b}{h} (\sigma^* \underline{\tilde{E}}^* \cdot \underline{n}) \end{aligned} \tag{3.77}$$

which can be written as

$$\tilde{q}_t - \underline{\tilde{u}} \cdot \tilde{\nabla}_s \tilde{q} + \tilde{\nabla}_s \cdot \tilde{q} \underline{\tilde{u}}_s + \tilde{q} 2\tilde{H} \underline{\tilde{u}} \cdot \underline{n} = S(\underline{\tilde{E}} \cdot \underline{n} - \sigma_r \underline{\tilde{E}}^* \cdot \underline{n}) \tag{3.78}$$

where σ_r and S are electrical conductivity ratio of the fluids and the ratio of fluid time scale to electric time scale which are defined as

$$\sigma_r = \frac{\sigma^*}{\sigma} \tag{3.79}$$

$$S = \frac{h/u_0}{\varepsilon_0/\sigma} \tag{3.80}$$

The tangential stress balance (TSB), Equation (3.45), is

$$\frac{\mu u_0}{h} \left(\underline{\tilde{\tau}} \cdot \underline{n} \cdot \underline{t} \right) + \varepsilon_0 \varepsilon \frac{{V_b}^2}{h^2} \left(\underline{\tilde{E}} \, \underline{\tilde{E}} \cdot \underline{n} \cdot \underline{t} \right) = \frac{\mu^* u_0}{h} \left(2\underline{\tilde{D}}^* \cdot \underline{n} \cdot \underline{t} \right) + \varepsilon_0 \varepsilon^* \frac{{V_b}^2}{h^2} \left(\underline{\tilde{E}}^* \underline{\tilde{E}}^* \cdot \underline{n} \cdot \underline{t} \right) \tag{3.81}$$

which becomes

$$\left(\underline{\underline{\tilde{\tau}}} \cdot \underline{n} \cdot \underline{t}\right) + \varepsilon\, E_b\left(\underline{\tilde{E}}\,\underline{\tilde{E}} \cdot \underline{n} \cdot \underline{t}\right) = M\left(2\underline{\underline{\tilde{D}}}^* \cdot \underline{n} \cdot \underline{t}\right) + \varepsilon^* E_b\left(\underline{\tilde{E}}^*\,\underline{\tilde{E}}^* \cdot \underline{n} \cdot \underline{t}\right) \tag{3.82}$$

where E_b is the dimensionless electrical number whose definition is given as

$$E_b = \varepsilon_0 \frac{{V_b}^2}{h\mu u_0} \tag{3.83}$$

Finally, NSB Equation (3.43), is

$$\begin{aligned} &\left\{-\frac{\mu u_0}{h}\tilde{p}\underline{\underline{I}} + \frac{\mu u_0}{h}\underline{\underline{\tilde{\tau}}} + \varepsilon\varepsilon_0 \frac{{V_b}^2}{h^2}\left(\underline{\tilde{E}}\,\underline{\tilde{E}} - \frac{1}{2}\left|\underline{\tilde{E}}\right|^2 \underline{\underline{I}}\right)\right\} \cdot \underline{n} \cdot \underline{n} \\ = &\left\{-\frac{\mu u_0}{h}\tilde{p}^*\underline{\underline{I}} + \frac{\mu^* u_0}{h} 2\underline{\underline{\tilde{D}}}^* + \varepsilon^*\varepsilon_0 \frac{{V_b}^2}{h^2}\left(\underline{\tilde{E}}^*\underline{\tilde{E}}^* - \frac{1}{2}\left|\underline{\tilde{E}}^*\right|^2 \underline{\underline{I}}\right)\right\} \cdot \underline{n} \cdot \underline{n} + \frac{\gamma}{h} 2\tilde{H} \end{aligned} \tag{3.84}$$

which becomes

$$\begin{aligned} &\left(-\tilde{p}\underline{\underline{I}} \cdot \underline{n} \cdot \underline{n}\right) + \left(\underline{\underline{\tilde{\tau}}} \cdot \underline{n} \cdot \underline{n}\right) + \varepsilon E_b \left(\underline{\tilde{E}}\,\underline{\tilde{E}} - \frac{1}{2}\left|\underline{\tilde{E}}\right|^2 \underline{\underline{I}}\right) \cdot \underline{n} \cdot \underline{n} \\ = &\left(-\tilde{p}^*\underline{\underline{I}} \cdot \underline{n} \cdot \underline{n}\right) + \left(M 2\underline{\underline{\tilde{D}}}^* \cdot \underline{n} \cdot \underline{n}\right) + \varepsilon^* E_b \left(\underline{\tilde{E}}^*\underline{\tilde{E}}^* - \frac{1}{2}\left|\underline{\tilde{E}}^*\right|^2 \underline{\underline{I}}\right) \cdot \underline{n} \cdot \underline{n} + \frac{1}{Ca} 2\tilde{H} \end{aligned} \tag{3.85}$$

where Ca is the capillary number that is defined as

$$Ca = \frac{\mu u_0}{\gamma} \tag{3.86}$$

As all variables are rendered dimensionless, hereafter (˜) is removed for simplicity. The scaled equations are summarized in Table 3.1 and a summary of the scaled boundary and interface conditions is shown in Table 3.2.

Table 3.1. Summary of the scaled equations for a Newtonian fluid and a non-Newtonian fluid system with electric field.

For the first fluid at $-\mathbf{1} < \mathbf{z} < Z(x,t)$	$Re\left[\frac{\partial v_x}{\partial t} + v_x\frac{\partial v_x}{\partial x} + v_z\frac{\partial v_x}{\partial z}\right] = -\frac{\partial p}{\partial x} + \left(\frac{\partial \tau_{xx}}{\partial x} + \frac{\partial \tau_{xz}}{\partial z}\right)$
	$Re\left[\frac{\partial v_z}{\partial t} + v_x\frac{\partial v_z}{\partial x} + v_z\frac{\partial v_z}{\partial z}\right] = -\frac{\partial p}{\partial \tilde{z}} + \left(\frac{\partial \tau_{xz}}{\partial x} + \frac{\partial \tau_{zz}}{\partial z}\right)$
	$\frac{\partial v_x}{\partial x} + \frac{\partial v_z}{\partial z} = 0$
	$\frac{\partial^2 V}{\partial x^2} + \frac{\partial^2 V}{\partial z^2} = 0$
	$\tau_{xx} + We\left[\frac{\partial \tau_{xx}}{\partial t} + v_x\frac{\partial \tau_{xx}}{\partial x} + v_z\frac{\partial \tau_{xx}}{\partial z} - 2\frac{\partial v_x}{\partial x}\tau_{xx} - 2\frac{\partial v_x}{\partial z}\tau_{zx}\right] = \left[2\frac{\partial v_x}{\partial x}\right]$
	$\tau_{xz} + We\left[\frac{\partial \tau_{xz}}{\partial t} + v_x\frac{\partial \tau_{xz}}{\partial x} + v_z\frac{\partial \tau_{xz}}{\partial z} - \frac{\partial v_z}{\partial x}\tau_{xx} - \frac{\partial v_x}{\partial z}\tau_{zz}\right] = \left[\frac{\partial v_x}{\partial z} + \frac{\partial v_z}{\partial x}\right]$
	$\tau_{zz} + We\left[\frac{\partial \tau_{zz}}{\partial t} + v_x\frac{\partial \tau_{zz}}{\partial x} + v_z\frac{\partial \tau_{zz}}{\partial z} - 2\frac{\partial v_z}{\partial x}\tau_{xz} - 2\frac{\partial v_z}{\partial z}\tau_{zz}\right] = \left[2\frac{\partial v_z}{\partial z}\right]$
For the second fluid at $\mathbf{Z(x,t)} < \mathbf{z} < \boldsymbol{Hr}$	$ReP\left[\frac{\partial v_x^*}{\partial t} + v_x^*\frac{\partial v_x^*}{\partial x} + v_z^*\frac{\partial v_x^*}{\partial z}\right] = -\frac{\partial p^*}{\partial x} + M\left(\frac{\partial^2 v_x^*}{\partial x^2} + \frac{\partial^2 v_x^*}{\partial z^2}\right)$
	$ReP\left[\frac{\partial v_z^*}{\partial t} + v_x^*\frac{\partial v_z^*}{\partial x} + v_z^*\frac{\partial v_z^*}{\partial z}\right] = -\frac{\partial p^*}{\partial z} + M\left(\frac{\partial^2 v_z^*}{\partial x^2} + \frac{\partial^2 v_z^*}{\partial z^2}\right)$
	$\frac{\partial v_x^*}{\partial x} + \frac{\partial v_z^*}{\partial z} = 0$
	$\frac{\partial^2 V^*}{\partial x^2} + \frac{\partial^2 V^*}{\partial z^2} = 0$

Table 3.2. Summary of the scaled boundary and interface conditions for a Newtonian fluid and a non-Newtonian fluid system with electric field.

At z = -1	$v_x = 0$
	$v_z = 0$
	$V = 1$
At z = Hr	$v_x^* = 0$
	$v_z^* = 0$
	$V^* = 0$
At z = Z (x , t)	$\underline{v} \cdot \underline{n} = \underline{u} \cdot \underline{n} = \underline{v}^* \cdot \underline{n}$
	$\underline{v} \cdot \underline{t} = \underline{v}^* \cdot \underline{t}$
	$\underline{E} \cdot \underline{t} = \underline{E}^* \cdot \underline{t}$
	$q = \varepsilon^* \underline{E}^* \cdot \underline{n} - \varepsilon \underline{E} \cdot \underline{n}$
	$q_t - \underline{u} \cdot \nabla_s q + \nabla_s \cdot q\underline{u}_s + q2H\underline{u} \cdot \underline{n} = S(\underline{E} \cdot \underline{n} - \sigma_r \underline{E}^* \cdot \underline{n})$
	$\left(-p\underline{\underline{I}} \cdot \underline{n} \cdot \underline{n}\right) + \left(\underline{\underline{\tau}} \cdot \underline{n} \cdot \underline{n}\right) + \varepsilon E_b \left(\underline{E}\,\underline{E} - \frac{1}{2}\left\|\underline{E}\right\|^2 \underline{\underline{I}}\right) \cdot \underline{n} \cdot \underline{n}$ $= \left(-p^* \underline{\underline{I}} \cdot \underline{n} \cdot \underline{n}\right) + \left(M2\underline{\underline{D}}^* \cdot \underline{n} \cdot \underline{n}\right)$ $+\varepsilon^* E_b \left(\underline{E}^* \underline{E}^* - \frac{1}{2}\left\|\underline{E}^*\right\|^2 \underline{\underline{I}}\right) \cdot \underline{n} \cdot \underline{n} + \frac{1}{Ca} 2H$
	$\left(\underline{\underline{\tau}} \cdot \underline{n} \cdot \underline{t}\right) + \varepsilon\, E_b \left(\underline{E}\,\underline{E} \cdot \underline{n} \cdot \underline{t}\right) = M\left(2\underline{\underline{D}}^* \cdot \underline{n} \cdot \underline{t}\right) + \varepsilon^* E_b \left(\underline{E}^*\,\underline{E}^* \cdot \underline{n} \cdot \underline{t}\right)$

Table 3.3. Dimensionless parameters.

Dimensionless parameter	Definition
Reynolds number	$Re = \frac{\rho u_0 h}{\mu}$
Weissenberg number	$We = \lambda \frac{u_0}{h}$
Density ratio	$\mathrm{P} = \frac{\rho^*}{\rho}$
Viscosity ratio	$M = \frac{\mu^*}{\mu}$
Thickness ratio	$Hr = \frac{h^*}{h}$
Capillary number	$Ca = \frac{\mu u_0}{\gamma}$
Conductivity ratio	$\sigma_r = \frac{\sigma^*}{\sigma}$
Electric number	$E_b = \varepsilon_0 \frac{{V_b}^2}{h \mu u_0}$
Dimensionless parameter S	$S = \frac{h/u_0}{\varepsilon_0/\sigma}$

3.1.4. Linear Stability Analysis

To analyze the stability of the interface, the system is linearized around a base state, where the interface between the fluids is assumed to be flat. All variables are expanded as follows (Johns and Narayanan, 2002):

$$p = p_0 + \epsilon \left(p_1 + z_1 \frac{\partial p_0}{\partial z_0} \right) + O(\epsilon^2) \tag{3.87}$$

Here, ϵ represents the magnitude of the given perturbation, which is assumed to be very small and z_1 denotes the mapping from the reference domain to the current domain, which becomes Z_1 at the interface. The indices 0 and 1 denote the base and the perturbed states,

respectively. The time and the longitudinal position dependences of the variables are separated using normal mode expansion as

$$\mathrm{p}_1(z_0,\, \mathrm{x}_0,\, \mathrm{t}_0) = \hat{\mathrm{p}}_1(z_0)\mathrm{e}^{\omega \mathrm{t}_0}\mathrm{e}^{\mathrm{ikx}_0} \tag{3.88}$$

where 'k' and 'ω' are the wavenumber and the growth/decay rate of the disturbances, respectively (Johns and Narayanan, 2002). As seen from Equation (3.88), the disturbance grows in time if the real part of 'ω' is positive which means the system is unstable to the given disturbance; and the disturbance disappears in time if the real part of 'ω' is negative, i.e., the system is stable to the given disturbance.

3.1.4.1. Base State (ϵ^0). For the pressure driven Poiseuille flow UCM model, the base state flow profile is given as follows

$$v_{x0} = v_{x0}(z_0) \tag{3.89}$$

$$v_{z0} = 0 \tag{3.90}$$

$$\tau_{zz0} = 0 \tag{3.91}$$

$$\frac{d\tau_{xx0}}{dx_0} = 0 \tag{3.92}$$

$$\frac{d\tau_{xz0}}{dx_0} = 0 \tag{3.93}$$

Then, the stress tensor components for the first fluid, i.e., Equations (3.54), (3.57) and (3.59), at the base state can be written as

$$\tau_{xx0} + We\left[-2\frac{dv_{x0}}{dz_0}\tau_{zx0}\right] = 0 \tag{3.94}$$

$$\tau_{xz0} + We\,[0] = \frac{dv_{x0}}{dz_0} \tag{3.95}$$

and

$$0 + We\,[0] = 0 \tag{3.96}$$

Then, τ_{xz0} and τ_{xx0} are found to be

$$\tau_{xz0} = \frac{dv_{x0}}{dz_0} \tag{3.97}$$

and

$$\tau_{xx0} = 2We(\frac{dv_{x0}}{dz_0})^2 \tag{3.98}$$

The continuity equation for the first fluid, Equation (3.60), at the base state is

$$\frac{dv_{x0}}{dx_0} + \frac{dv_{z0}}{dz_0} = 0 \tag{3.99}$$

The x-component of the equation of motion, Equation (3.48), at the base state is

$$\frac{dp_0}{dx_0} = \frac{d}{dz_0}(\frac{dv_{x0}}{dz_0}) = \frac{d^2v_{x0}}{dz_0{}^2} \tag{3.100}$$

and the z-component of the equation of motion, Equation (3.48), is

$$-\frac{dp_0}{dz_0} = 0 \tag{3.101}$$

For the second fluid, the continuity equation, the x and the z-components of the equation of motion, Equation (3.63), at the base state are given as

$$\frac{dv_{x0}^*}{dx_0} + \frac{dv_{z0}^*}{dz_0} = 0 \tag{3.102}$$

$$-\frac{dp_0^*}{dx_0} + M\ \frac{d^2 v_{x0}^*}{dz_0{}^2} = 0 \tag{3.103}$$

and

$$-\frac{dp_0^*}{dz_0} = 0 \tag{3.104}$$

respectively. The velocity profiles are found as

$$v_{x0} = A_0 z_0{}^2 + B_0 z_0 + C_0 \tag{3.105}$$

and

$$v_{x0}^* = A_0^* z_0{}^2 + B_0^* z_0 + C_0^* \tag{3.106}$$

where

$$A_0 = \frac{1}{2}\frac{dp_0}{dx_0} \tag{3.107}$$

and

$$A_0^* = \frac{1}{2M}\frac{dp_0^*}{dx_0} \tag{3.108}$$

Appling the boundary conditions, the base state flow profiles for both fluids are found as in the Equation (3.109) and (3.110) (Yiantsios and Higgins, 1988; Hooper, 1989; Ozen *et al*., 2006c). Detailed solution procedure of the base state is given in Appendix B.

$$v_{x0} = -\frac{Hr + M}{(Hr + Hr^2)}{z_0}^2 + \frac{Hr^2 - M}{Hr + Hr^2} z_0 + 1 \tag{3.109}$$

$$v_{x0}^* = -\frac{Hr + M}{M(Hr + Hr^2)}{z_0}^2 + \frac{(Hr^2 - M)}{M(Hr + Hr^2)} z_0 + 1 \tag{3.110}$$

For the base state, the Laplace equation for the electric field for the first fluid is

$${\nabla_0}^2 V_0 = 0 \tag{3.111}$$

$$\underbrace{\frac{d^2 V_0}{d{x_0}^2}}_{0} + \frac{d^2 V_0}{d{z_0}^2} = 0 \tag{3.112}$$

which yields

$$V_0 = D_0 z_0 + F_0 \tag{3.113}$$

Similarly, one obtains

$$V_0^* = D_0^* z_0 + F_0^* \tag{3.114}$$

Appling the boundary conditions (See Appendix B), the expressions for the base state voltage potentials are found as

$$V_0 = -\frac{\sigma_r}{Hr + \sigma_r} z_0 + \frac{Hr}{Hr + \sigma_r} \tag{3.115}$$

and

$$V_0^* = -\frac{1}{Hr + \sigma_r} z_0 + \frac{Hr}{Hr + \sigma_r} \tag{3.116}$$

Then, the electric field expressions at the base state for the first and the second fluids are found as

$$\underline{E_0} = -\left(\frac{dV_0}{dx_0}\underline{e}_{x0} + \frac{dV_0}{dz_0}\underline{e}_{z0}\right) = \frac{\sigma_r}{Hr + \sigma_r}\underline{e}_{z0} \tag{3.117}$$

and

$$E_0^* = -\left(\frac{dV_0^*}{dx_0}\underline{e}_{x0} + \frac{dV_0^*}{dz_0}\underline{e}_{z0}\right) = \frac{1}{Hr + \sigma_r}\underline{e}_{z0} \tag{3.118}$$

substituting Equations (3.117) and (3.118) into Gauss' law at the base state which is given as

$$q_0 = \varepsilon^* \underline{E_0^*} \cdot \underline{n}_0 - \varepsilon \underline{E_0} \cdot \underline{n}_0 \tag{3.119}$$

the expression for the base state surface charge density is found as

$$q_0 = (\varepsilon^* - \varepsilon\sigma_r)\frac{1}{(Hr + \sigma_r)} \tag{3.120}$$

3.1.4.2. Perturbed State (ϵ^1). For the first fluid, the perturbed x- and z-components of the equation of motion, the continuity equation, and the Laplace equation are

$$Re\left[\frac{\partial v_{x1}}{\partial t_0} + v_{x0}\frac{\partial v_{x1}}{\partial x_0} + v_{z1}\frac{\partial v_{x0}}{\partial z_0}\right] = -\frac{\partial p_1}{\partial x_0} + \left[\frac{\partial \tau_{xx1}}{\partial x_0} + \frac{\partial \tau_{zx1}}{\partial z_0}\right] \tag{3.121}$$

$$Re\left[\frac{\partial v_{z1}}{\partial t_0} + v_{x0}\frac{\partial v_{z1}}{\partial x_0}\right] = -\frac{\partial p_1}{\partial z_0} + \left[\frac{\partial \tau_{xz1}}{\partial x_0} + \frac{\partial \tau_{zz1}}{\partial z_0}\right] \tag{3.122}$$

$$\frac{dv_{x1}}{dx_0} + \frac{dv_{z1}}{dz_0} = 0 \tag{3.123}$$

$$\frac{d^2V_1}{{dx_0}^2} + \frac{d^2V_1}{{dz_0}^2} = 0 \tag{3.124}$$

respectively. The components of the perturbed stress tensor are

$$\tau_{xx1} + We\left[\frac{\partial \tau_{xx1}}{\partial t_0} + v_{x0}\frac{\partial \tau_{xx1}}{\partial x_0} + v_{x1}\frac{\overbrace{\partial \tau_{xx0}}^{0}}{\partial x_0} + \underbrace{v_{z0}}_{0}\frac{\partial \tau_{xx1}}{\partial z_0} + v_{z1}\frac{\partial \tau_{xx0}}{\partial z_0} - 2\frac{\partial v_{x1}}{\partial x_0}\tau_{xx0} - 2\frac{\overbrace{\partial v_{x0}}^{0}}{\partial x_0}\tau_{xx1} - 2\frac{\partial v_{x0}}{\partial z_0}\tau_{zx1} - 2\frac{\partial v_{x1}}{\partial z_0}\tau_{zx0}\right] = \left[2\frac{\partial v_{x1}}{\partial x_0}\right] \tag{3.125}$$

$$\tau_{xz1} + We\left[\frac{\partial \tau_{xz1}}{\partial t_0} + v_{x0}\frac{\partial \tau_{xz1}}{\partial x_0} + v_{x1}\frac{\overbrace{\partial \tau_{xz0}}^{0}}{\partial x_0} + \underbrace{v_{z0}}_{0}\frac{\partial \tau_{xz1}}{\partial z_0} + v_{z1}\frac{\partial \tau_{xz0}}{\partial z_0} - \frac{\partial \overbrace{v_{z0}}^{0}}{\partial x_0}\tau_{xx1} - \frac{\partial v_{z1}}{\partial x_0}\tau_{xx0} - -\frac{\partial v_{x0}}{\partial z_0}\tau_{zz1} - \frac{\partial v_{x1}}{\partial z_0}\overbrace{\tau_{zz0}}^{0}\right] = \left[\frac{\partial v_{x1}}{\partial z_0} + \frac{\partial v_{z1}}{\partial x_0}\right] \tag{3.126}$$

and

$$\tau_{zz1} + We\left[\frac{\partial \tau_{zz1}}{\partial t_0} + v_{x0}\frac{\partial \tau_{zz1}}{\partial x_0} + v_{x1}\frac{\partial \overbrace{\tau_{zz0}}^{0}}{\partial x_0} + \overbrace{v_{z0}}^{0}\frac{\partial \tau_{zz1}}{\partial z_0} + v_{z1}\frac{\partial \overbrace{\tau_{zz0}}^{0}}{\partial z_0} - 2\frac{\partial \overbrace{v_{z0}}^{0}}{\partial x_0}\tau_{xz1} - 2\frac{\partial v_{z1}}{\partial x_0}\tau_{xz0} - 2\frac{\partial \overbrace{v_{z0}}^{0}}{\partial z_0}\tau_{zz1} - 2\frac{\partial v_{z1}}{\partial z_0}\overbrace{\tau_{zz0}}^{0}\right] = \left[2\frac{\partial v_{z1}}{\partial z_0}\right] \tag{3.127}$$

The components of the constitutive equation are simplified to

$$\tau_{xx1} + We\left[\frac{\partial \tau_{xx1}}{\partial t_0} + v_{x0}\frac{\partial \tau_{xx1}}{\partial x_0} + v_{z1}\frac{\partial \tau_{xx0}}{\partial z_0} - 2\frac{\partial v_{x1}}{\partial x_0}\tau_{xx0} - 2\frac{\partial v_{x0}}{\partial z_0}\tau_{zx1} - 2\frac{\partial v_{x1}}{\partial z_0}\tau_{zx0}\right] = \left[2\frac{\partial v_{x1}}{\partial x_0}\right] \tag{3.128}$$

$$\tau_{xz1} + We\left[\frac{\partial \tau_{xz1}}{\partial t_0} + v_{x0}\frac{\partial \tau_{xz1}}{\partial x_0} + v_{z1}\frac{\partial \tau_{xz0}}{\partial z_0} - \frac{\partial v_{z1}}{\partial x_0}\tau_{xx0} - \frac{\partial v_{x0}}{\partial z_0}\tau_{zz1}\right] = \left[\frac{\partial v_{x1}}{\partial z_0} + \frac{\partial v_{z1}}{\partial x_0}\right] \tag{3.129}$$

and

$$\tau_{zz1} + We\left[\frac{\partial \tau_{zz1}}{\partial t_0} + v_{x0}\frac{\partial \tau_{zz1}}{\partial x_0} - 2\frac{\partial v_{z1}}{\partial x_0}\tau_{xz0}\right] = \left[2\frac{\partial v_{z1}}{\partial z_0}\right] \tag{3.130}$$

where, from the base state

$$\frac{d\tau_{xz0}}{dz_0} = \frac{d^2 v_{x0}}{{dz_0}^2} \tag{3.131}$$

and

$$\frac{d\tau_{xx0}}{dz_0} = 4We\frac{dv_{x0}}{dz_0}\frac{d^2 v_{x0}}{{dz_0}^2} \tag{3.132}$$

For the second fluid, the perturbed x- and z-components of the equation of motion, the continuity equation, and the Laplace equation are

$$ReP\left[\frac{\partial v_{x1}^*}{\partial t_0} + v_{x0}^*\frac{\partial v_{x1}^*}{\partial x_0} + v_{z1}^*\frac{\partial v_{x0}^*}{\partial z_0}\right] = -\frac{\partial p_1^*}{\partial x_0} + M\left[\frac{\partial^2 v_{x1}^*}{{\partial x_0}^2} + \frac{\partial^2 v_{x1}^*}{{\partial z_0}^2}\right] \tag{3.133}$$

$$ReP\left[\frac{\partial v_{z1}^*}{\partial t_0} + v_{x0}^*\frac{\partial v_{z1}^*}{\partial x_0}\right] = -\frac{\partial p_1^*}{\partial z_0} + \left[\frac{\partial^2 v_{z1}^*}{{\partial x_0}^2} + \frac{\partial^2 v_{z1}^*}{{\partial z_0}^2}\right] \tag{3.134}$$

$$\frac{dv_{x1}^*}{dx_0} + \frac{dv_{z1}^*}{dz_0} = 0 \tag{3.135}$$

$$\frac{d^2V_1^*}{dx_0{}^2} + \frac{d^2V_1^*}{dz_0{}^2} = 0 \tag{3.136}$$

The perturbed state boundary and interface conditions are shown below where

$$\underline{n}_0 = \underline{e}_{z0} \tag{3.137}$$

$$\underline{t}_0 = \underline{e}_{x0} \tag{3.138}$$

$$Z_{x1} = \frac{\partial Z_1}{\partial x_0} \tag{3.139}$$

$$\underline{n}_1 = -Z_{x1}\underline{e}_{x0} \tag{3.140}$$

$$\underline{t}_1 = Z_{x1}\underline{e}_{z0} \tag{3.141}$$

Derivations of $\underline{n}_1$, $\underline{t}_1$, $\underline{n}_0$, $\underline{t}_0$ and u are given in Appendix A and the detailed derivations of the perturbed state interface conditions are given in Appendix C.

At the bottom wall, $z_0 = -1$, the perturbed boundary conditions are

$$v_{x1} = 0 \tag{3.142}$$

$$v_{z1} = 0 \tag{3.143}$$

and

$$V_1 = 0 \tag{3.144}$$

and at the top wall, $z_0 =$ Hr, they are

$$v_{x1}^{*} = 0 \tag{3.145}$$

$$v_{z1}^{*} = 0 \tag{3.146}$$

and

$$V_{1}^{*} = 0 \tag{3.147}$$

At the interface, $z_0 = 0$, when Equation (3.73) is expanded in Taylor series, the perturbed no-flow through the interface condition at the first order is found as

$$v_{z1} - v_{x0} Z_{x1} = v_{z1}^{*} - v_{x0}^{*} Z_{x1} = \frac{\partial Z_1}{\partial t_0} \tag{3.148}$$

In the same way, the perturbed no-slip condition, i.e. Equation (3.74) at the interface is

$$v_{x1} + Z_1 \frac{\partial v_{x0}}{\partial z_0} = v_{x1}^{*} + Z_1 \frac{\partial v_{x0}^{*}}{\partial z_0} \tag{3.149}$$

The continuity of the electric field at the interface, i.e. Equation (3.75) in perturbed state is found as

$$\frac{\partial V_1}{\partial x_0} + Z_{x1} \frac{\partial V_0}{\partial z_0} = \frac{\partial V_1^{*}}{\partial x_0} + Z_{x1} \frac{\partial V_0^{*}}{\partial z_0} \tag{3.150}$$

The Gauss' law, i.e., Equation (3.76), at the perturbed state is

$$q_1 = \varepsilon^{*} \left(-\frac{\partial V_1^{*}}{\partial z_0} \right) - \varepsilon \left(-\frac{\partial V_1}{\partial z_0} \right) \tag{3.151}$$

Similarly, the charge distribution at the interface, Equation (3.78), at the perturbed state is

$$\frac{\partial q_1}{\partial t_0} - v_{x0}\frac{\partial q_1}{\partial x_0} + q_0\frac{\partial v_{x1}}{\partial x_0} = S\left(\sigma_r\frac{\partial V_1^*}{\partial z_0} - \frac{\partial V_1}{\partial z_0}\right) \tag{3.152}$$

The NSB, Equation (3.85), at the perturbed state becomes

$$-p_1 + \tau_{zz1} - 2Z_{x1}\tau_{xz0} + \varepsilon E_b\left(\frac{\partial V_0}{\partial z_0}\frac{\partial V_1}{\partial z_0}\right) =$$
$$-p_1^* + M\left(-2Z_{x1}\frac{\partial v_{x0}^*}{\partial z_0} + 2\frac{\partial v_{z1}^*}{\partial z_0}\right) + \varepsilon^* E_b\left(\frac{\partial V_0^*}{\partial z_0}\frac{\partial V_1^*}{\partial z_0}\right) + \frac{Z_{xx1}}{Ca} \tag{3.153}$$

Finally, the TSB, Equation (3.82), at the perturbed state is found as

$$\tau_{xz1} + Z_1\frac{\partial \tau_{xz0}}{\partial z_0} - Z_{x1}\tau_{xx0} + \varepsilon E_b\left(\frac{\partial V_0}{\partial z_0}\frac{\partial V_1}{\partial x_0} + Z_{x1}\left(\frac{\partial V_0}{\partial z_0}\right)^2\right) =$$
$$M\left(\frac{\partial v_{x1}^*}{\partial z_0} + Z_1\frac{\partial^2 v_{x0}^*}{\partial {z_0}^2} + \frac{\partial v_{z1}^*}{\partial x_0}\right) + \varepsilon^* E_b\left(\frac{\partial V_0^*}{\partial z_0}\frac{\partial V_1^*}{\partial x_0} + Z_{x1}\left(\frac{\partial V_0^*}{\partial z_0}\right)^2\right) \tag{3.154}$$

Summary of the perturbed equations is given in Table 3.4 and the perturbed boundary and interface conditions are given in Table 3.5.

When all the parameters in the equations and boundary conditions are expanded in normal mode as in Equation (3.88), the equations are given in Table 3.6 and the boundary and interface conditions are given in Table 3.7.

Table 3.4. Summary of the perturbed equations for a Newtonian fluid and a non-Newtonian fluid system with electric field.

For the first fluid at $-1 < z_0 < 0$	$Re\left[\frac{\partial v_{x1}}{\partial t_0} + v_{x0}\frac{\partial v_{x1}}{\partial x_0} + v_{z1}\frac{\partial v_{x0}}{\partial z_0}\right] = -\frac{\partial p_1}{\partial x_0} + \left[\frac{\partial \tau_{xx1}}{\partial x_0} + \frac{\partial \tau_{zx1}}{\partial z_0}\right]$
	$Re\left[\frac{\partial v_{z1}}{\partial t_0} + v_{x0}\frac{\partial v_{z1}}{\partial x_0}\right] = -\frac{\partial p_1}{\partial z_0} + \left[\frac{\partial \tau_{xz1}}{\partial x_0} + \frac{\partial \tau_{zz1}}{\partial z_0}\right]$
	$\frac{dv_{x1}}{dx_0} + \frac{dv_{z1}}{dz_0} = 0$
	$\frac{d^2V_1}{{dx_0}^2} + \frac{d^2V_1}{{dz_0}^2} = 0$
	$\tau_{xx1} + We\left[\frac{\partial \tau_{xx1}}{\partial t_0} + v_{x0}\frac{\partial \tau_{xx1}}{\partial x_0} + v_{z1}\frac{\partial \tau_{xx0}}{\partial z_0} - 2\frac{\partial v_{x1}}{\partial x_0}\tau_{xx0} - 2\frac{\partial v_{x0}}{\partial z_0}\tau_{zx1} - 2\frac{\partial v_{x1}}{\partial z_0}\tau_{zx0}\right] = \left[2\frac{\partial v_{x1}}{\partial x_0}\right]$
	$\tau_{xz1} + We\left[\frac{\partial \tau_{xz1}}{\partial t_0} + v_{x0}\frac{\partial \tau_{xz1}}{\partial x_0} + v_{z1}\frac{\partial \tau_{xz0}}{\partial z_0} - \frac{\partial v_{z1}}{\partial x_0}\tau_{xx0} - \frac{\partial v_{x0}}{\partial z_0}\tau_{zz1}\right] = \left[\frac{\partial v_{x1}}{\partial z_0} + \frac{\partial v_{z1}}{\partial x_0}\right]$
	$\tau_{zz1} + We\left[\frac{\partial \tau_{zz1}}{\partial t_0} + v_{x0}\frac{\partial \tau_{zz1}}{\partial x_0} - 2\frac{\partial v_{z1}}{\partial x_0}\tau_{xz0}\right] = \left[2\frac{\partial v_{z1}}{\partial z_0}\right]$
For the second fluid at $0 < z_0 < Hr$	$ReP\left[\frac{\partial v^*_{x1}}{\partial t_0} + v^*_{x0}\frac{\partial v^*_{x1}}{\partial x_0} + v^*_{z1}\frac{\partial v^*_{x0}}{\partial z_0}\right] = -\frac{\partial p^*_1}{\partial x_0} + M[\frac{\partial^2 v^*_{x1}}{{\partial x_0}^2} + \frac{\partial^2 v^*_{x1}}{{\partial z_0}^2}]$
	$ReP\left[\frac{\partial v^*_{z1}}{\partial t_0} + v^*_{x0}\frac{\partial v^*_{z1}}{\partial x_0}\right] = -\frac{\partial p^*_1}{\partial z_0} + M[\frac{\partial^2 v^*_{z1}}{{\partial x_0}^2} + \frac{\partial^2 v^*_{z1}}{{\partial z_0}^2}]$
	$\frac{dv^*_{x1}}{dx_0} + \frac{dv^*_{z1}}{dz_0} = 0$
	$\frac{d^2V^*_1}{{dx_0}^2} + \frac{d^2V^*_1}{{dz_0}^2} = 0$

Table 3.5. Summary of the perturbed boundary and interface conditions for a Newtonian fluid and a non-Newtonian fluid system with electric field.

At $z_0 = -1$	$v_{x1} = 0$
	$v_{z1} = 0$
	$V_1 = 0$
At z_0 = Hr	$v_{x1}^* = 0$
	$v_{z1}^* = 0$
	$V_1^* = 0$
At $z_0 = 0$	$v_{z1} - v_{x0} Z_{x1} = \frac{\partial Z_1}{\partial t_0}$
	$v_{z1}^* - v_{x0}^* Z_{x1} = \frac{\partial Z_1}{\partial t_0}$
	$v_{x1} + Z_1 \frac{\partial v_{x0}}{\partial z_0} = v_{x1}^* + Z_1 \frac{\partial v_{x0}^*}{\partial z_0}$
	$\frac{\partial V_1}{\partial x_0} + Z_{x1} \frac{\partial V_0}{\partial z_0} = \frac{\partial V_1^*}{\partial x_0} + Z_{x1} \frac{\partial V_0^*}{\partial z_0}$
	$q_1 = \varepsilon^* \left(-\frac{\partial V_1^*}{\partial z_0} \right) - \varepsilon \left(-\frac{\partial V_1}{\partial z_0} \right)$
	$\frac{\partial q_1}{\partial t_0} - v_{x0} \frac{\partial q_1}{\partial x_0} + q_0 \frac{\partial v_{x1}}{\partial x_0} = S \left(\sigma_r \frac{\partial V_1^*}{\partial z_0} - \frac{\partial V_1}{\partial z_0} \right)$
	$-p_1 + \tau_{zz1} - 2 Z_{x1} \tau_{xz0} + \varepsilon E_b \left(\frac{\partial V_0}{\partial z_0} \frac{\partial V_1}{\partial z_0} \right) = -p_1^*$ $+M \left(-2 Z_{x1} \frac{\partial v_{x0}^*}{\partial z_0} + 2 \frac{\partial v_{z1}^*}{\partial z_0} \right) + \varepsilon^* E_b \left(\frac{\partial V_0^*}{\partial z_0} \frac{\partial V_1^*}{\partial z_0} \right) + \frac{Z_{xx1}}{Ca}$
	$\tau_{xz1} + Z_1 \frac{\partial \tau_{xz0}}{\partial z_0} - Z_{x1} \tau_{xx0} + \varepsilon E_b \left(\frac{\partial V_0}{\partial z_0} \frac{\partial V_1}{\partial x_0} + Z_{x1} \left(\frac{\partial V_0}{\partial z_0} \right)^2 \right) =$ $M \left(\frac{\partial v_{x1}^*}{\partial z_0} + Z_1 \frac{\partial^2 v_{x0}^*}{\partial {z_0}^2} + \frac{\partial v_{z1}^*}{\partial x_0} \right) + \varepsilon^* E_b \left(\frac{\partial V_0^*}{\partial z_0} \frac{\partial V_1^*}{\partial x_0} + Z_{x1} \left(\frac{\partial V_0^*}{\partial z_0} \right)^2 \right)$

Table 3.6. Summary of the equations after the normal mode expansion is performed for a Newtonian fluid and a non-Newtonian fluid system with electric field.

For the first fluid at $-1 < z_0 < 0$	$Re\left[\omega\hat{v}_{x1} + v_{x0}(ik)\hat{v}_{x1} + \hat{v}_{z1}\frac{\partial v_{x0}}{\partial z_0}\right] = -(ik)\hat{p}_1 + [(ik)\tau_{xx1} + \frac{\partial\hat{\tau}_{zx1}}{\partial z_0}]$
	$Re[\omega\hat{v}_{z1} + v_{x0}(ik)\hat{v}_{z1}] = -\frac{\partial\hat{p}_1}{\partial z_0} + [(ik)\tau_{xz1} + \frac{\partial\hat{\tau}_{zz1}}{\partial z_0}]$
	$(ik)\hat{v}_{x1} + \frac{d\hat{v}_{z1}}{dz_0} = 0$
	$-k^2\hat{V}_1 + \frac{d^2\hat{V}_1}{dz_0{}^2} = 0$
	$\hat{\tau}_{xx1} + We\left[\omega\hat{\tau}_{xx1} + v_{x0}(ik)\hat{\tau}_{xx1} + \hat{v}_{z1}\frac{\partial\tau_{xx0}}{\partial z_0} - 2(ik)\hat{v}_{x1}\tau_{xx0} - 2\frac{\partial v_{x0}}{\partial z_0}\hat{\tau}_{zx1} - 2\frac{\partial\hat{v}_{x1}}{\partial z_0}\tau_{zx0}\right] = [\,2(ik)\hat{v}_{x1}\,]$
	$\hat{\tau}_{zx1} + We\left[\omega\hat{\tau}_{zx1} + v_{x0}(ik)\hat{\tau}_{zx1} + \hat{v}_{z1}\frac{\partial\tau_{xz0}}{\partial z_0} - (ik)\hat{v}_{z1}\tau_{xx0} - \frac{\partial v_{x0}}{\partial z_0}\hat{\tau}_{zz1}\right] = \left[\frac{\partial\hat{v}_{x1}}{\partial z_0} + (ik)\hat{v}_{z1}\right]$
	$\hat{\tau}_{zz1} + We[\omega\hat{\tau}_{zz1} + v_{x0}(ik)\hat{\tau}_{zz1} - 2(ik)\hat{v}_{z1}\tau_{xz0}] = \left[\,2\frac{\partial\hat{v}_{z1}}{\partial z_0}\,\right]$
For the second fluid at $0 < z_0 < Hr$	$Re\mathrm{P}\left[\omega\hat{v}^*_{x1} + v^*_{x0}(ik)\hat{v}^*_{x1} + \hat{v}^*_{z1}\frac{\partial v^*_{x0}}{\partial z_0}\right] = -(ik)\hat{p}^*_1 + M\left[(-k^2)\hat{v}^*_{x1} + \frac{\partial^2\hat{v}^*_{x1}}{\partial z_0{}^2}\right]$
	$Re\mathrm{P}[\omega\hat{v}^*_{z1} + v^*_{x0}(ik)\hat{v}^*_{z1}] = -\frac{\partial\hat{p}^*_1}{\partial z_0} + M\left[(-k^2)\hat{v}^*_{z1} + \frac{\partial^2\hat{v}^*_{z1}}{\partial z_0{}^2}\right]$
	$(ik)\hat{v}^*_{x1} + \frac{d\hat{v}^*_{z1}}{dz_0} = 0$
	$-k^2\hat{V}^*_1 + \frac{d^2\hat{V}^*_1}{dz_0{}^2} = 0$

Table 3.7. Summary of the boundary and interface conditions after the normal mode expansion is performed for a Newtonian fluid and a non-Newtonian fluid system with electric field.

At $z_0 = -1$	$\hat{v}_{x1} = 0$
	$\hat{v}_{z1} = 0$
	$\hat{V}_1 = 0$
At z_0 **= Hr**	$\hat{v}^*_{x1} = 0$
	$\hat{v}^*_{z1} = 0$
	$\hat{V}^*_1 = 0$
At $z_0 = 0$	$\hat{v}_{z1} - (ik)v_{x0}\hat{Z}_1 = \omega\hat{Z}_1$
	$\hat{v}^*_{z1} - (ik)v^*_{x0}\hat{Z}_1 = \omega\hat{Z}_1$
	$\hat{v}_{x1} + \hat{Z}_1\frac{\partial v_{x0}}{\partial z_0} = \hat{v}^*_{x1} + \hat{Z}_1\frac{\partial v^*_{x0}}{\partial z_0}$
	$(ik)\hat{V}_1 + (ik)\hat{Z}_1\frac{\partial V_0}{\partial z_0} = (ik)\hat{V}^*_1 + (ik)\hat{Z}_1\frac{\partial V^*_0}{\partial z_0}$
	$\hat{q}_1 = \varepsilon^*\left(-\frac{\partial \hat{V}^*_1}{\partial z_0}\right) - \varepsilon\left(-\frac{\partial \hat{V}_1}{\partial z_0}\right)$
	$\omega\hat{q}_1 - v_{x0}(ik)\hat{q}_1 + q_0(ik)\hat{v}_{x1} = S\left(\sigma_r\frac{\partial \hat{V}^*_1}{\partial z_0} - \frac{\partial \hat{V}_1}{\partial z_0}\right)$
	$-\hat{p}_1 + \hat{\tau}_{zz1} - 2(ik)\hat{Z}_1\tau_{xz0} + \varepsilon E_b\left(\frac{\partial V_0}{\partial z_0}\frac{\partial \hat{V}_1}{\partial z_0}\right) = -\hat{p}^*_1$ $+M\left(-2(ik)\hat{Z}_1\frac{\partial v^*_{x0}}{\partial z_0} + 2\frac{\partial \hat{v}^*_{z1}}{\partial z_0}\right) + \varepsilon^* E_b\left(\frac{\partial V^*_0}{\partial z_0}\frac{\partial \hat{V}^*_1}{\partial z_0}\right) + (-k^2)\frac{\hat{Z}_1}{Ca}$
	$\hat{\tau}_{xz1} + \hat{Z}_1\frac{\partial \tau_{xz0}}{\partial z_0} - (ik)\hat{Z}_1\tau_{xx0} + \varepsilon E_b\left(\frac{\partial V_0}{\partial z_0}(ik)\hat{V}_1 + (ik)\hat{Z}_1\left(\frac{\partial V_0}{\partial z_0}\right)^2\right) =$ $M\left(\frac{\partial \hat{v}^*_{x1}}{\partial z_0} + \hat{Z}_1\frac{\partial^2 v^*_{x0}}{\partial {z_0}^2} + \frac{\partial \hat{v}^*_{z1}}{\partial x_0}\right) + \varepsilon^* E_b\left(\frac{\partial V^*_0}{\partial z_0}(ik)\hat{V}^*_1 + (ik)\hat{Z}_1\left(\frac{\partial V^*_0}{\partial z_0}\right)^2\right)$

3.1.5. Solution Procedure Using Chebyshev Spectral Method

The governing equations given in Table 3.6 are solved subject to the boundary conditions given in Table 3.7 using Chebyshev spectral method in MATLAB (Trefethen, 2000). The perturbed equations constitute a generalized eigenvalue problem, which is in the form of $Au = \omega Bu$. The grids are divided using the Chebyshev points which are defined as $x_j = \cos\left(\frac{j\pi}{N}\right)$ where $j = 0,1,\dots,N$. Here, N denotes the cut-off frequency. The eigenvalue with the largest real part is the reported eigenvalue. The convergence of the eigenvalues are checked with N. The equations are rearranged for easy coding; they are given in Appendix D.1. Solving these equations with the boundary conditions, the growth rate 'ω' is acquired as an eigenvalue. Then, the dispersion curve that shows the growth rate of the disturbance as a function of the wavenumber of the disturbance is plotted for various parameters. The effects of the dimensionless numbers, which are Re, We, M, Hr, E_b, S, σ_r, ε_r, are analyzed in the results section.

3.2. Two Newtonian Fluids System under the Influence of an Electric Field

The stability of the interface between two Newtonian fluids flowing in a channel under the effect of an externally applied electric filed is analyzed. The physical system is same as the first case, depicted in Figure 3.1 by assuming that both fluids are Newtonian.

The equations are same as those presented for the first case, presented in Section 3.1, except that the viscous stress for the first fluid is different as the first fluid is now considered to be Newtonian. Substituting

$$\underline{\underline{\tau}} = \mu 2\underline{\underline{D}} \tag{3.155}$$

into the equations and the boundary conditions containing the viscous stress of the first fluid, i.e. Equations (3.1), (3.34), (3.35) and (3.36), the scaled governing equations are obtained as in Table 3.8 and the boundary conditions turn out to be as in Table 3.9.

The base state equations and the boundary conditions are same as in the first case for We=0. Hence, they are not repeated here. The perturbed equations and the boundary conditions are given in Table 3.10 and Table 3.11, respectively.

For the MATLAB code, taking the Weissenberg number zero, We=0, the Newtonian case of the first fluid in the equations and the boundary conditions are acquired. The effects of the thickness ratio, Hr, viscosity ratio, M, dimensionless number S, conductivity ratio, σ_r and permittivity ratio are analyzed in the results section.

Table 3.8. Summary of the scaled equations for two Newtonian fluids system with electric field.

For the first fluid at $-\mathbf{1} < z < Z(x,t)$	$Re\left[\frac{\partial v_x}{\partial t} + v_x\frac{\partial v_x}{\partial x} + v_z\frac{\partial v_x}{\partial z}\right] = -\frac{\partial p}{\partial x} + \left(\frac{\partial^2 v_x}{\partial x^2} + \frac{\partial^2 v_x}{\partial z^2}\right)$
	$Re\left[\frac{\partial v_z}{\partial t} + v_x\frac{\partial v_z}{\partial x} + v_z\frac{\partial v_z}{\partial z}\right] = -\frac{\partial p}{\partial \tilde{z}} + \left(\frac{\partial^2 v_z}{\partial x^2} + \frac{\partial^2 v_z}{\partial z^2}\right)$
	$\frac{\partial v_x}{\partial x} + \frac{\partial v_z}{\partial z} = 0$
	$\frac{\partial^2 V}{\partial x^2} + \frac{\partial^2 V}{\partial z^2} = 0$
For the second fluid at $\mathbf{Z(x,t)} < \mathbf{z} < \boldsymbol{Hr}$	$ReP\left[\frac{\partial v_x^*}{\partial t} + v_x^*\frac{\partial v_x^*}{\partial x} + v_z^*\frac{\partial v_x^*}{\partial z}\right] = -\frac{\partial p^*}{\partial x} + M\left(\frac{\partial^2 v_x^*}{\partial x^2} + \frac{\partial^2 v_x^*}{\partial z^2}\right)$
	$ReP\left[\frac{\partial v_z^*}{\partial t} + v_x^*\frac{\partial v_z^*}{\partial x} + v_z^*\frac{\partial v_z^*}{\partial z}\right] = -\frac{\partial p^*}{\partial z} + M\left(\frac{\partial^2 v_z^*}{\partial x^2} + \frac{\partial^2 v_z^*}{\partial z^2}\right)$
	$\frac{\partial v_x^*}{\partial x} + \frac{\partial v_z^*}{\partial z} = 0$
	$\frac{\partial^2 V^*}{\partial x^2} + \frac{\partial^2 V^*}{\partial z^2} = 0$

Table 3.9. Summary of the scaled boundary and interface conditions for two Newtonian fluids system with electric field.

At z = -1	$v_x = 0$
	$v_z = 0$
	$V = 1$
At z = Hr	$v_x^* = 0$
	$v_z^* = 0$
	$V^* = 0$
At z = Z (x , t)	$\underline{v} \cdot \underline{n} = \underline{u} \cdot \underline{n} = \underline{v}^* \cdot \underline{n}$
	$\underline{v} \cdot \underline{t} = \underline{v}^* \cdot \underline{t}$
	$\underline{E} \cdot \underline{t} = \underline{E}^* \cdot \underline{t}$
	$q = \varepsilon^* \underline{E}^* \cdot \underline{n} - \varepsilon \underline{E} \cdot \underline{n}$
	$q_t - \underline{u} \cdot \nabla_s q + \nabla_s \cdot q\underline{u}_s + q2H\underline{u} \cdot \underline{n} = S(\underline{E} \cdot \underline{n} - \sigma_r \underline{E}^* \cdot \underline{n})$
	$\left(-p\underline{\underline{I}} \cdot \underline{n} \cdot \underline{n}\right) + \left(2\underline{\underline{D}} \cdot \underline{n} \cdot \underline{n}\right) + \varepsilon E_b \left(\underline{E}\,\underline{E} - \frac{1}{2}\left\|\underline{E}\right\|^2 \underline{\underline{I}}\right) \cdot \underline{n} \cdot \underline{n}$ $= \left(-p^* \underline{\underline{I}} \cdot \underline{n} \cdot \underline{n}\right) + \left(M2\underline{\underline{D}}^* \cdot \underline{n} \cdot \underline{n}\right)$ $+\varepsilon^* E_b \left(\underline{E}^* \underline{E}^* - \frac{1}{2}\left\|\underline{E}^*\right\|^2 \underline{\underline{I}}\right) \cdot \underline{n} \cdot \underline{n} + \frac{1}{Ca} 2H$
	$\left(2\underline{\underline{D}} \cdot \underline{n} \cdot \underline{t}\right) + \varepsilon\, E_b \left(\underline{E}\,\underline{E} \cdot \underline{n} \cdot \underline{t}\right)$ $= M\left(2\underline{\underline{D}}^* \cdot \underline{n} \cdot \underline{t}\right) + \varepsilon^* E_b \left(\underline{E}^*\,\underline{E}^* \cdot \underline{n} \cdot \underline{t}\right)$

Table 3.10. Summary of the perturbed equations for two Newtonian fluids system with electric field.

For the first fluid at $-\mathbf{1} < \mathbf{z_0} < 0$	$Re\left(\frac{\partial v_{x1}}{\partial t_0} + v_{x0}\frac{\partial v_{x1}}{\partial x_0} + v_{z1}\frac{\partial v_{x0}}{\partial z_0}\right) = -\frac{\partial p_1}{\partial x_0} + \left(\frac{\partial^2 v_{x1}}{\partial {x_0}^2} + \frac{\partial^2 v_{x1}}{\partial {z_0}^2}\right)$
	$Re\left(\frac{\partial v_{z1}}{\partial t_0} + v_{x0}\frac{\partial v_{z1}}{\partial x_0}\right) = -\frac{\partial p_1}{\partial z_0} + \left(\frac{\partial^2 v_{z1}}{\partial {x_0}^2} + \frac{\partial^2 v_{z1}}{\partial {z_0}^2}\right)$
	$\frac{dv_{x1}}{dx_0} + \frac{dv_{z1}}{dz_0} = 0$
	$\frac{d^2V_1}{d{x_0}^2} + \frac{d^2V_1}{d{z_0}^2} = 0$
For the second fluid at $\mathbf{0} < \mathbf{z_0} < \boldsymbol{Hr}$	$ReP\left(\frac{\partial v^*_{x1}}{\partial t_0} + v^*_{x0}\frac{\partial v^*_{x1}}{\partial x_0} + v^*_{z1}\frac{\partial v^*_{x0}}{\partial z_0}\right) = -\frac{\partial p^*_1}{\partial x_0} + M\left(\frac{\partial^2 v^*_{x1}}{\partial {x_0}^2} + \frac{\partial^2 v^*_{x1}}{\partial {z_0}^2}\right)$
	$ReP\left(\frac{\partial v^*_{z1}}{\partial t_0} + v^*_{x0}\frac{\partial v^*_{z1}}{\partial x_0}\right) = -\frac{\partial p^*_1}{\partial z_0} + M\left(\frac{\partial^2 v^*_{z1}}{\partial {x_0}^2} + \frac{\partial^2 v^*_{z1}}{\partial {z_0}^2}\right)$
	$\frac{dv^*_{x1}}{dx_0} + \frac{dv^*_{z1}}{dz_0} = 0$
	$\frac{d^2V^*_1}{d{x_0}^2} + \frac{d^2V^*_1}{d{z_0}^2} = 0$

Table 3.11. Summary of perturbed boundary and interface conditions for two Newtonian fluids system with electric field.

At z_0 = -1	$v_{x1} = 0$
	$v_{z1} = 0$
	$V_1 = 0$
At z_0 = Hr	$v_{x1}^* = 0$
	$v_{z1}^* = 0$
	$V_1^* = 0$
At $z_0 = 0$	$v_{z1} - v_{x0} Z_{x1} = \frac{\partial Z_1}{\partial t_0}$
	$v_{z1}^* - v_{x0}^* Z_{x1} = \frac{\partial Z_1}{\partial t_0}$
	$v_{x1} + Z_1 \frac{\partial v_{x0}}{\partial z_0} = v_{x1}^* + Z_1 \frac{\partial v_{x0}^*}{\partial z_0}$
	$\frac{\partial V_1}{\partial x_0} + Z_{x1} \frac{\partial V_0}{\partial z_0} = \frac{\partial V_1^*}{\partial x_0} + Z_{x1} \frac{\partial V_0^*}{\partial z_0}$
	$q_1 = \varepsilon^* \left(-\frac{\partial V_1^*}{\partial z_0} \right) - \varepsilon \left(-\frac{\partial V_1}{\partial z_0} \right)$
	$\frac{\partial q_1}{\partial t_0} - v_{x0} \frac{\partial q_1}{\partial x_0} + q_0 \frac{\partial v_{x1}}{\partial x_0} = S \left(\sigma_r \frac{\partial V_1^*}{\partial z_0} - \frac{\partial V_1}{\partial z_0} \right)$
	$-p_1 + \left(-2 Z_{x1} \frac{\partial v_{x0}}{\partial z_0} + 2 \frac{\partial v_{z1}}{\partial z_0} \right) + \varepsilon E_b \left(\frac{\partial V_0}{\partial z_0} \frac{\partial V_1}{\partial z_0} \right) = -p_1^*$ $+M \left(-2 Z_{x1} \frac{\partial v_{x0}^*}{\partial z_0} + 2 \frac{\partial v_{z1}^*}{\partial z_0} \right) + \varepsilon^* E_b \left(\frac{\partial V_0^*}{\partial z_0} \frac{\partial V_1^*}{\partial z_0} \right) + \frac{Z_{xx1}}{Ca}$
	$\left(\frac{\partial v_{x1}}{\partial z_0} + Z_1 \frac{\partial^2 v_{x0}}{\partial {z_0}^2} + \frac{\partial v_{z1}}{\partial x_0} \right) + \varepsilon E_b \left(\frac{\partial V_0}{\partial z_0} \frac{\partial V_1}{\partial x_0} + Z_{x1} \left(\frac{\partial V_0}{\partial z_0} \right)^2 \right) =$ $M \left(\frac{\partial v_{x1}^*}{\partial z_0} + Z_1 \frac{\partial^2 v_{x0}^*}{\partial {z_0}^2} + \frac{\partial v_{z1}^*}{\partial x_0} \right) + \varepsilon^* E_b \left(\frac{\partial V_0^*}{\partial z_0} \frac{\partial V_1^*}{\partial x_0} + Z_{x1} \left(\frac{\partial V_0^*}{\partial z_0} \right)^2 \right)$

3.3. Two Newtonian Fluids System without an Electric Field

In this case, the stability of the interface between two Newtonian fluids flowing with Poiseuille flow in a channel is studied. The physical system is same as the first case depicted in the Figure 3.1. However, there is no electric field in this case, which means V_b=0.

The governing equations are same as the Newtonian-Newtonian system with the electric field, i.e. the second case as the electric field does not appear in the governing equations (See Section 2.1.1). Therefore, for the governing equations, Table 3.8 is also valid for this case with only exception that Laplace equation for the voltage is not anymore needed. However, the boundary conditions are different and are given in Table 3.12.

Table 3.12. Summary of the scaled boundary and interface conditions for two Newtonian fluids system without an electric field.

At z = -1	$v_x = 0$
	$v_z = 0$
At z = Hr	$v_x^* = 0$
	$v_z^* = 0$
At $\mathbf{z = Z(x,t)}$	$\underline{v} \cdot \underline{n} = \underline{u} \cdot \underline{n} = \underline{v}^* \cdot \underline{n}$
	$\underline{v} \cdot \underline{t} = \underline{v}^* \cdot \underline{t}$
	$\left(-p\underline{\underline{I}} \cdot \underline{n} \cdot \underline{n}\right) + \left(2\underline{\underline{D}} \cdot \underline{n} \cdot \underline{n}\right) = \left(-p^*\underline{\underline{I}} \cdot \underline{n} \cdot \underline{n}\right) + \left(M2\underline{\underline{D}}^* \cdot \underline{n} \cdot \underline{n}\right) + \frac{1}{Ca}2H$
	$\left(2\underline{\underline{D}} \cdot \underline{n} \cdot \underline{t}\right) = M\left(2\underline{\underline{D}}^* \cdot \underline{n} \cdot \underline{t}\right)$

The base state flow profiles are same as the second case, which are given in Equations (3.109) and (3.110). The perturbed equations are same as those given in Table 3.10 without the Laplace equation for the electric field. The perturbed boundary conditions are shown in Table 3.13.

Table 3.13. Summary of the perturbed boundary and interface conditions for two Newtonian fluids system without an electric field.

At z_0 = -1	$v_{x1} = 0$
	$v_{z1} = 0$
At z_0 = Hr	$v_{x1}^* = 0$
	$v_{z1}^* = 0$
At $z_0 = 0$	$v_{z1} - v_{x0} Z_{x1} = \frac{\partial Z_1}{\partial t_0}$
	$v_{z1}^* - v_{x0}^* Z_{x1} = \frac{\partial Z_1}{\partial t_0}$
	$v_{x1} + Z_1 \frac{\partial v_{x0}}{\partial z_0} = v_{x1}^* + Z_1 \frac{\partial v_{x0}^*}{\partial z_0}$
	$-p_1 + \left(-2 Z_{x1} \frac{\partial v_{x0}}{\partial z_0} + 2 \frac{\partial v_{z1}}{\partial z_0}\right) = -p_1^* + M \left(-2 Z_{x1} \frac{\partial v_{x0}^*}{\partial z_0} + 2 \frac{\partial v_{z1}^*}{\partial z_0}\right) + \frac{Z_{xx1}}{Ca}$
	$\left(\frac{\partial v_{x1}}{\partial z_0} + Z_1 \frac{\partial^2 v_{x0}}{\partial {z_0}^2} + \frac{\partial v_{z1}}{\partial x_0}\right) = M \left(\frac{\partial v_{x1}^*}{\partial z_0} + Z_1 \frac{\partial^2 v_{x0}^*}{\partial {z_0}^2} + \frac{\partial v_{z1}^*}{\partial x_0}\right)$

To benchmark our code, the system parameters by Hooper (1989) is assumed where the surface is not allowed to deflect, i.e., capillary number approaches infinity. The equations are solved together with the boundary conditions and the dispersion curves are plotted for different Reynolds numbers. The results of the Hooper are reproduced and shown in the results section.

3.4. A Newtonian Fluid and a Non-Newtonian Fluid System without an Electric Field

In this last case, the interfacial instability of the system with a non-Newtonian fluid and a Newtonian fluid flowing with Poiseuille flow in a channel is studied. The schematic representation of the system is given in Figure 3.1; however, here no electric field is applied to the system as in the third case.

The governing equations are same as the first case which is non-Newtonian-Newtonian fluids case, and given in Table 3.1, except for the Laplace equation for the electric field. The boundary conditions are different from the first case as there is no electric field for this the current case; they are shown in Table 3.14.

Table 3.14. Summary of the scaled boundary and interface conditions for a Newtonian fluid and a non-Newtonian fluid system without an electric field.

At z = -1	$v_x = 0$
	$v_z = 0$
At z = Hr	$v_x^* = 0$
	$v_z^* = 0$
At $\mathbf{z = Z(x, t)}$	$\underline{v} \cdot \underline{n} = \underline{u} \cdot \underline{n} = \underline{v}^* \cdot \underline{n}$
	$\underline{v} \cdot \underline{t} = \underline{v}^* \cdot \underline{t}$
	$\left(-p\underline{\underline{I}} \cdot \underline{n} \cdot \underline{n}\right) + \left(\underline{\underline{\tau}} \cdot \underline{n} \cdot \underline{n}\right) = \left(-p^* \underline{\underline{I}} \cdot \underline{n} \cdot \underline{n}\right) + \left(M 2\underline{\underline{D}}^* \cdot \underline{n} \cdot \underline{n}\right) + \frac{1}{Ca} 2H$
	$\left(\underline{\underline{\tau}} \cdot \underline{n} \cdot \underline{t}\right) = M\left(2\underline{\underline{D}}^* \cdot \underline{n} \cdot \underline{t}\right)$

The base state flow profiles are same as the first case, which are given in Equations (3.109) and (3.110). The perturbed equations are same as those in Table 3.4 without the Laplace equation for the electric field. The perturbed boundary conditions are shown in Table 3.15.

These equations are solved with the boundary and interface conditions in MATLAB, and the effects of Reynolds number and Weissenberg number on the stability are observed. The results for the Reynolds number effect are compared with the Newtonian-Newtonian case where the surface tension is ignored to compare the results with Hooper (1989).

Table 3.15. Summary of perturbed boundary and interface conditions for a Newtonian fluid and a non-Newtonian fluid system without an electric field.

At z_0 = -1	$v_{x1} = 0$
	$v_{z1} = 0$
At z_0 = Hr	$v_{x1}^* = 0$
	$v_{z1}^* = 0$
At $z_0 = 0$	$v_{z1} - v_{x0} Z_{x1} = \frac{\partial Z_1}{\partial t_0}$
	$v_{z1}^* - v_{x0}^* Z_{x1} = \frac{\partial Z_1}{\partial t_0}$
	$v_{x1} + Z_1 \frac{\partial v_{x0}}{\partial z_0} = v_{x1}^* + Z_1 \frac{\partial v_{x0}^*}{\partial z_0}$
	$-p_1 + \tau_{zz1} - 2Z_{x1}\tau_{xz0} = -p_1^* + M\left(-2Z_{x1}\frac{\partial v_{x0}^*}{\partial z_0} + 2\frac{\partial v_{z1}^*}{\partial z_0}\right) + \frac{Z_{xx1}}{Ca}$
	$\left(\tau_{xz1} + Z_1 \frac{\partial \tau_{xz0}}{\partial z_0} - Z_{x1}\tau_{xx0}\right) = M\left(\frac{\partial v_{x1}^*}{\partial z_0} + Z_1 \frac{\partial^2 v_{x0}^*}{\partial {z_0}^2} + \frac{\partial v_{z1}^*}{\partial x_0}\right)$

4. RESULTS AND DISCUSSION

In this chapter, the results of the linear stability problems modeled in Chapter 3 are introduced. The results start with the simplest case, i.e., the Newtonian-Newtonian case without an applied electric field (See Section 3.3). Then, the results of the non-Newtonian-Newtonian case without an electric field (See Section 3.4) are given and the results are compared with the results of the Newtonian-Newtonian case. Thirdly, the results of the Newtonian-Newtonian case under the electric field (See Section 3.2) are presented. Finally, the results of the main subject of this thesis, i.e., the non-Newtonian-Newtonian case under the electric field (See Section 3.1) are given and the results are compared with those of the Newtonian-Newtonian case under the electric field.

4.1. Results of the Two Newtonian Fluids System without an Electric Field

The results of the linear stability analysis of the system with two Newtonian fluids without an electric field (See Section 3.3) are given in this section. The effect of the Reynolds number on the stability of the system is analyzed. In the analysis, the system parameters are chosen as: the thickness ratio, Hr is 15, the viscosity ratio, M is 2, and the density ratio, P is 1. The dispersion curves, i.e., the real part of the growth/decay rate constant of the disturbance versus the wavenumber of the disturbance, are plotted for different Reynolds numbers. The neutral stability curves, i.e., plot of Reynolds number versus the wavenumber(s) at which the growth rate vanish(es), are plotted (see Figure 4.1). In this section, the aim is to reproduce the results of Hooper (Hooper A. P., 1989) who concentrates on the neutral stability curves; therefore, only the neutral stability curves are given and the dispersion curves can be found in Appendix E.1.

Figure 4.1 shows the critical wavenumber, i.e. the wavenumber for which the real part of the growth rate is zero, versus Reynolds number. The stable and unstable regions are also marked on the figure.

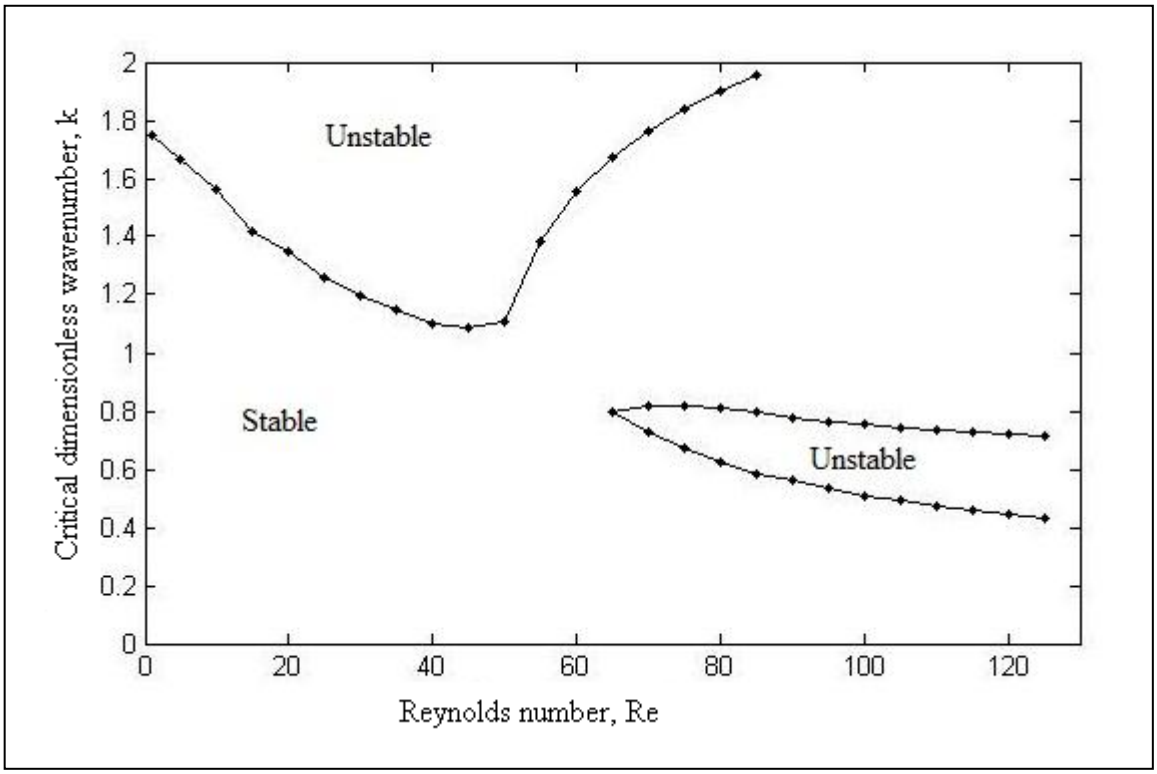

Figure 4.1. Neutral stability curve for two Newtonian fluids system without an electric field (Hr=15, M=2, P=1).

The parameters used to plot the dispersion curves are taken from the work of Hooper (Hooper A. P., 1989) and the surface tension is ignored for a comparison of the results. Figure 4.1 shows that there is only one critical wavenumber for Reynolds numbers in the range of 1-60 while there are three critical points for Reynolds numbers between 65 and 85, and two critical wavenumbers appear when the Reynolds number is above the value of 85 (See Appendix E.1). The acquired neutral stability curve is well-matched with that of the work of Hooper. Figure 4.2 shows the comparison of the results of this work and the work of Hooper.

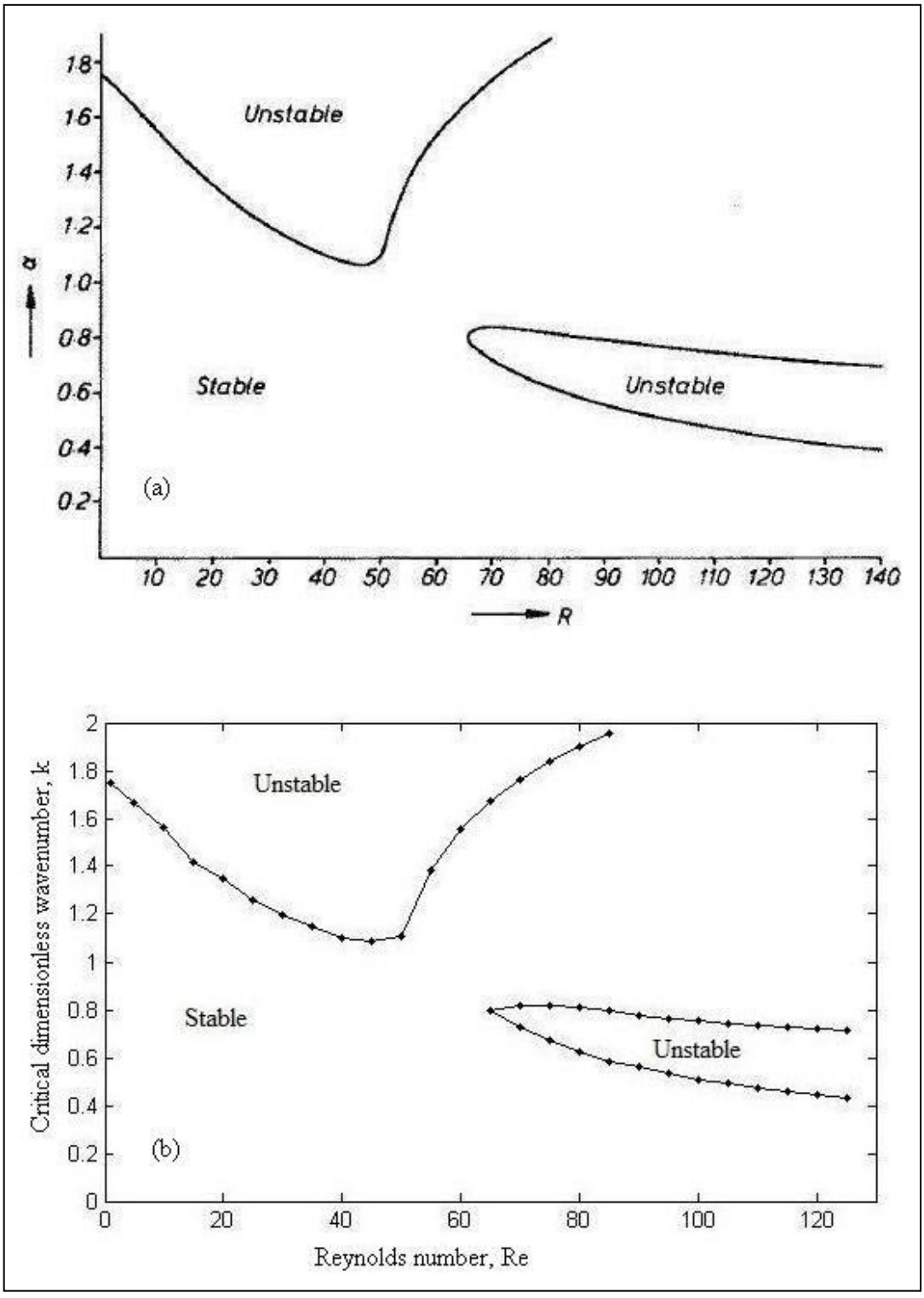

Figure 4.2. Neutral stability curves (a) Results of this work, (b) Results of Hooper (Reprinted with permission from Hooper, A. P., Physics of Fluids, Vol. A1, Page 1133, (1989). Copyright 1989, American Institute of Physics).

4.2. Results of a Newtonian Fluid and a Non-Newtonian Fluid System without Electric Field

In this section, the results of the linear stability analysis of a non-Newtonian fluid and a Newtonian fluid system are presented. Similar to the Newtonian-Newtonian fluids system, the neutral stability curve is plotted to show the effect of the Reynolds number. Moreover, the effect of the Weissenberg number on the stability is also studied.

The neutral stability curve, depicted in Figure 4.3 is plotted using the dispersion curves which are given in Appendix E.2. The system parameters are the same as that of Newtonian-Newtonian case, where the thickness ratio, Hr is 15, the viscosity ratio, M is 2 and the density ratio, P is 1. The Weissenberg number is taken to be 0.5 for the non-Newtonian fluid in the neutral stability curve. Figure 4.4 shows the effect of the Reynolds number on the stability of the system and the stable and unstable regions are shown on the figure.

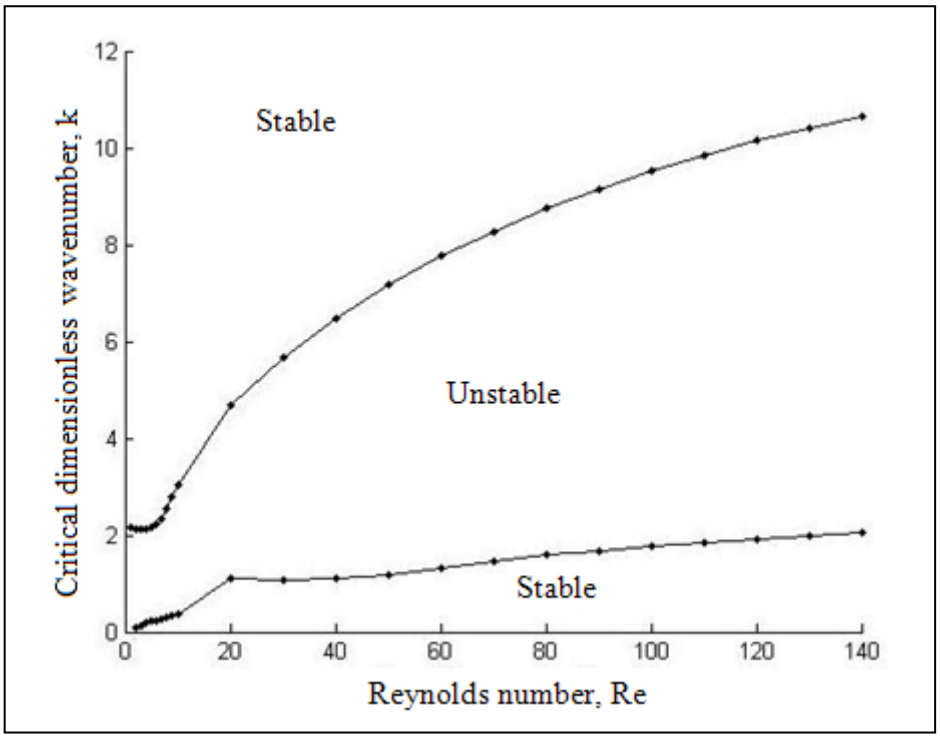

Figure 4.3. Neutral stability curve for a non-Newtonian fluid and a Newtonian fluid system without an electric field (Hr=15, M=2, P=1, We=0.5).

Figure 4.4 represents both the neutral stability curves of the Newtonian-Newtonian system and non-Newtonian-Newtonian system. For the wavenumbers in the range of 0-2, the non-Newtonian case has only one critical wavenumber at which the system becomes unstable after it, for all given Reynolds numbers. However, for the Newtonian-Newtonian case, there are two or three critical wavenumbers that the system is stable first, then unstable and stable again for some of the given Reynolds numbers. Comparing the two plots, it can be said that the system with a non-Newtonian fluid is more unstable to a given disturbance.

In Figure 4.5, the effect of the Weissenberg number on the stability of the system is observed and the dispersion curves are plotted for different Weissenberg numbers. As seen from Figure 4.5, there is not a considerable difference between the Newtonian case (We=0) when the Weissenberg number is below 0.01. However, increasing the Weissenberg number further results in a serious change of the behavior of the system. The system shifts from a stable mode to an unstable mode for the same wavenumber when the Weissenberg number is increased. To show the slight differences between the small Weissenberg numbers a zoomed version of Figure 4.5 is plotted in Figure 4.6. As a result, it is shown that increasing the elasticity of the polymer has a destabilizing effect on the system.

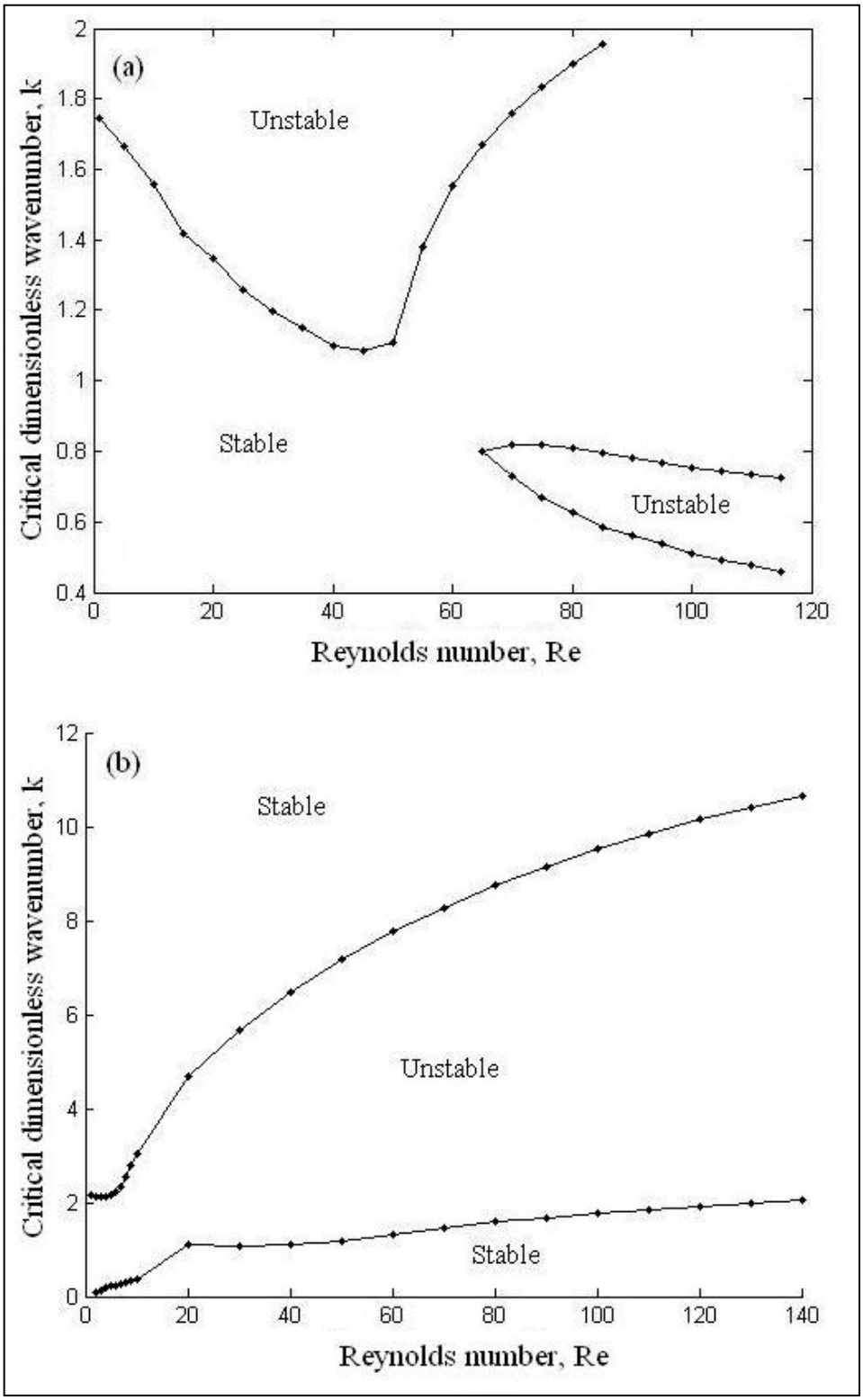

Figure 4.4. Neutral stability curves (Hr=15, M=2, P=1). (a) Newtonian-Newtonian system (We=0), (b) Non-Newtonian-Newtonian system (We=0.5).

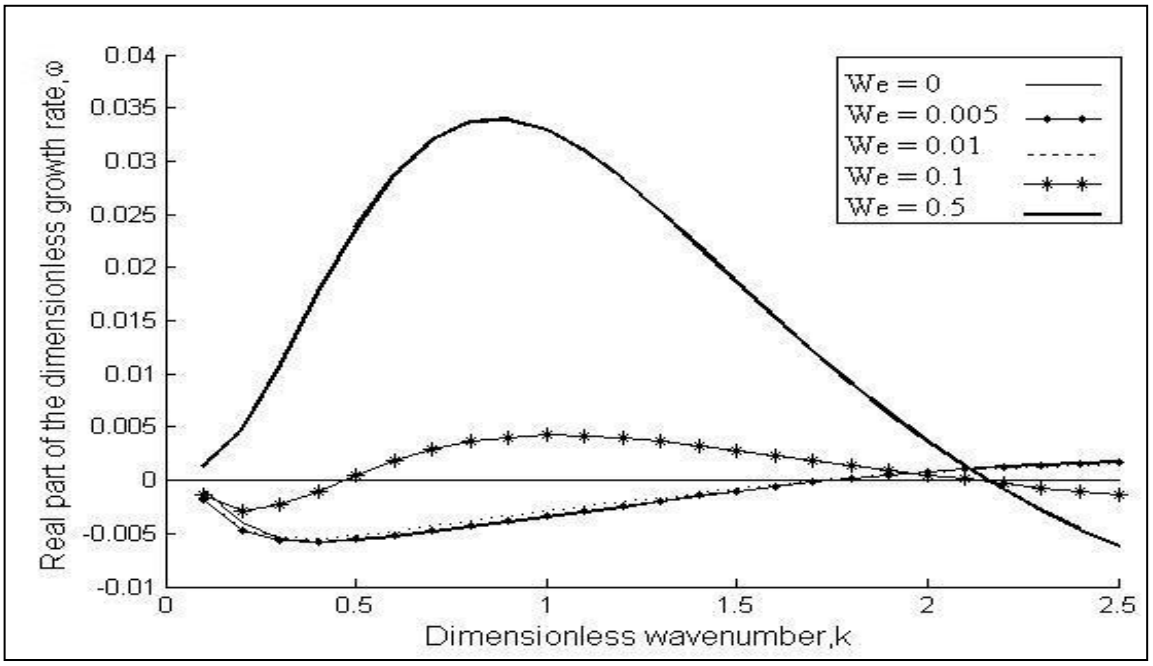

Figure 4.5. Effect of the Weissenberg number on the growth rate and the critical wavenumber without an electric field (Hr=15, M=2, P=1, Re=1).

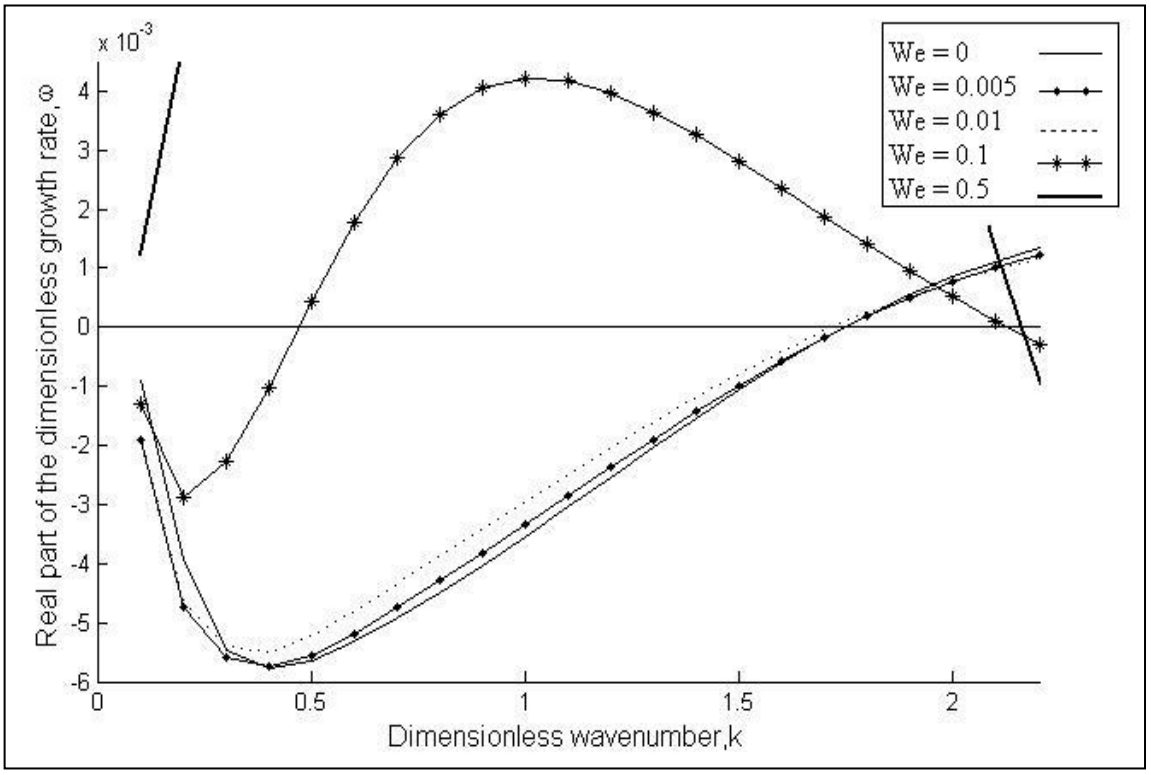

Figure 4.6. Effect of the Weissenberg number on the growth rate and the critical wavenumber without an electric field, zoomed representation (Hr=15, M=2, P=1, Re=1).

4.3. Results of the Two Newtonian Fluids System under the Influence of an Electric Field

In this section, the results of the linear stability analysis of the system with two Newtonian fluids under the effect of an electric field are given. The system parameters are chosen according to the work of Ozen *et al*. (Ozen *et al*., 2006), so that the plots of that work are reproduced to confirm the convergence of our code for the Newtonian case. The Newtonian case is acquired by assigning zero to the Weissenberg number in the MATLAB code for the non-Newtonian case under the effect of an electric field. The effects of the thickness ratio, Hr, the viscosity ratio, M, the dimensionless parameter S, the conductivity ratio, σ_r, and the permittivity ratio, ε_r, on the maximum growth rate and the critical wavenumber are analyzed. The maximum growth rate corresponds to the most unstable mode of instability while the critical wavenumber is the wavenumber for which the real part of the growth rate is zero. The results of Ozen *et al*. (Ozen *et al*., 2006) are recovered with the same input parameters.

Figure 4.7 shows the effect of the thickness ratio of the fluids on the stability. The system parameters are taken as Re=1, M=0.1, P=1, Hr=1, Ca=1, $S=10^3$, $E_b=1$, $\sigma_r=0.1$, $\varepsilon^*=1$, $\varepsilon=2$ and the depth ratio is varied. For this set of parameters, decreasing the thickness ratio results in increasing both the maximum growth rate and the critical wavenumber. The thickness ratio depends on the flow rates of the fluids that means the thickness of one fluid could be increased by increasing its flow rate. A smaller value of the thickness ratio indicates that one of the fluids occupies more of the channel. As seen from Figure 4.7 that an increase in depth ratio of the fluids has a stabilizing effect.

The effect of the viscosity ratio is shown in Figure 4.8. The system parameters are taken as Re=1, P=1, Hr=1, Ca=1, $S=10^3$, $E_b=1$, $\sigma_r=0.1$, $\varepsilon^*=3$, $\varepsilon=4$ and the viscosity ratio ranges from 0.1 to 2. Figure 4.8 shows that increasing the viscosity ratio has a stabilizing effect. The maximum growth rate decreases with increasing viscosity ratio while the critical wavenumber decreases slightly.

In Figure 4.9, the effect of the dimensionless number S, which is the ratio of the fluid time scale to the electrical time scale is shown. The input parameters for the fluids are

chosen as Re=1, M=1, P =1, Hr=1, Ca = 1, E_b =1, σ_r = 0.1, ε* =3, ε=4 and S is varied from 0.01 to 100. As seen from Figure 4.9 that increasing S decreases the critical wavenumber but it does not affect the maximum growth rate considerably for this set of parameters.

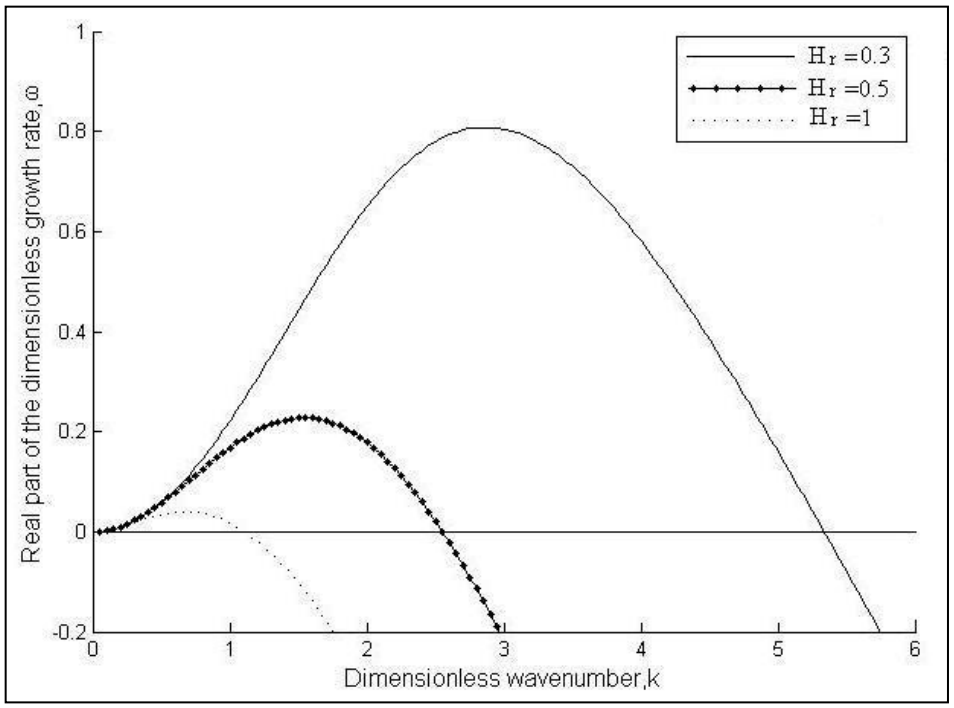

Figure 4.7 Effect of the thickness ratio on the growth rate and the critical wavenumber for two Newtonian fluids system under the influence of an electric field. The input parameters are Re=1, M=0.1, P=1, Ca=1, $S=10^3$, E_b=1, σ_r= 0.1, ε*=1 and ε=2.

The effects of the electrical properties of the fluids are presented in Figures 4.10 and 4.11. The physical properties of the fluids are fixed as Re=1, M=0.1, P =1, Hr=0.5, Ca = 1, $S=10^3$, E_b =1, and the electrical conductivity and the permittivity ratios are analyzed in Figures 4.10 and 4.11, respectively. The variation of the electrical permittivity ratio in Figure 4.11 is obtained by fixing ε*=1 and varying ε from 2 to 10. Figure 4.10 shows that the critical wavenumber and the maximum growth rate are both decreased as the ratio of the conductivities is increased from 0.1 to 0.9. Thus, increasing the conductivity difference between the two fluids has a destabilizing effect. Figure 4.11 shows that increasing the electrical permittivity mismatch in favour of the first fluid also has a stabilizing effect as the maximum growth rate and the critical wavenumber both decrease when the electrical permittivity of the first fluid is increased from 2 to 10.

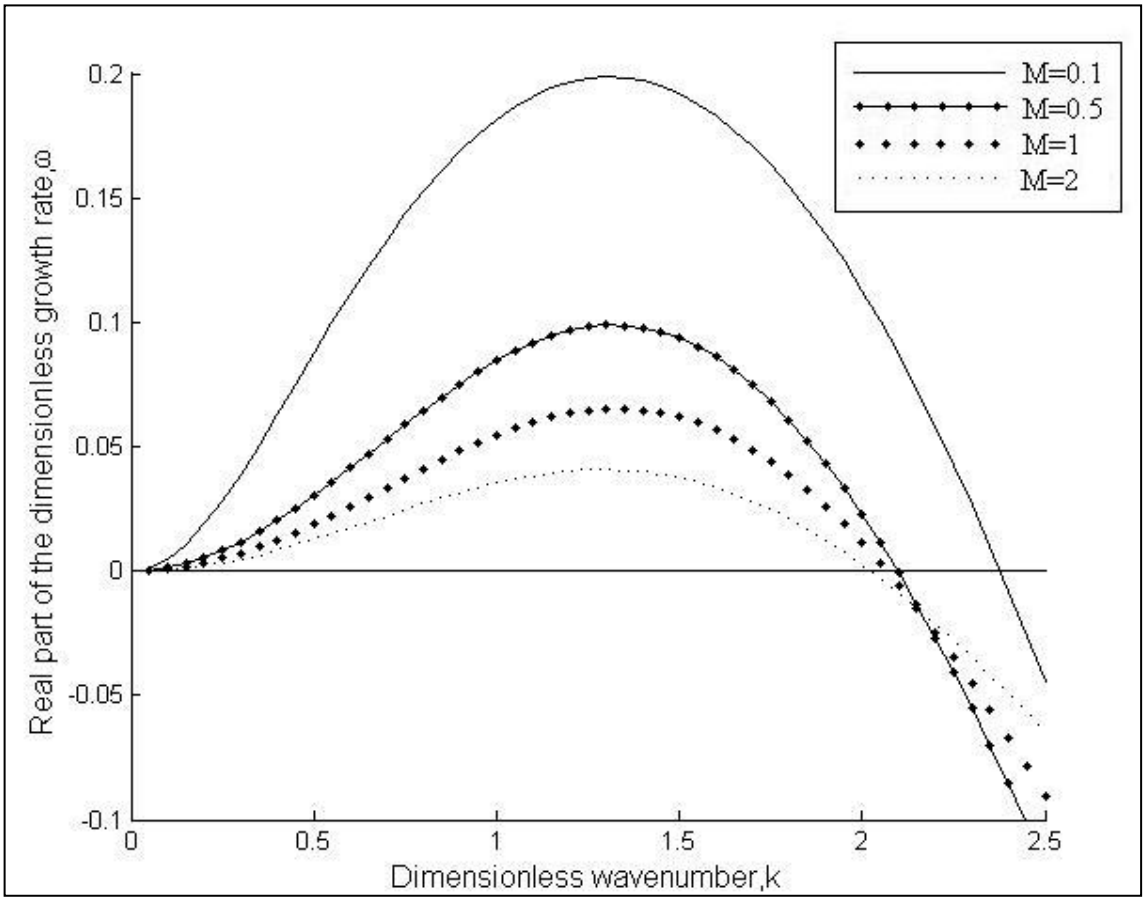

Figure 4.8. Effect of the viscosity ratio on the growth rate and the critical wavenumber for two Newtonian fluids system under the influence of an electric field. The input parameters are Re=1, P =1, Hr=1, Ca = 1, $S=10^3$, E_b =1, σ_r = 0.1, ε* =3 and ε=4.

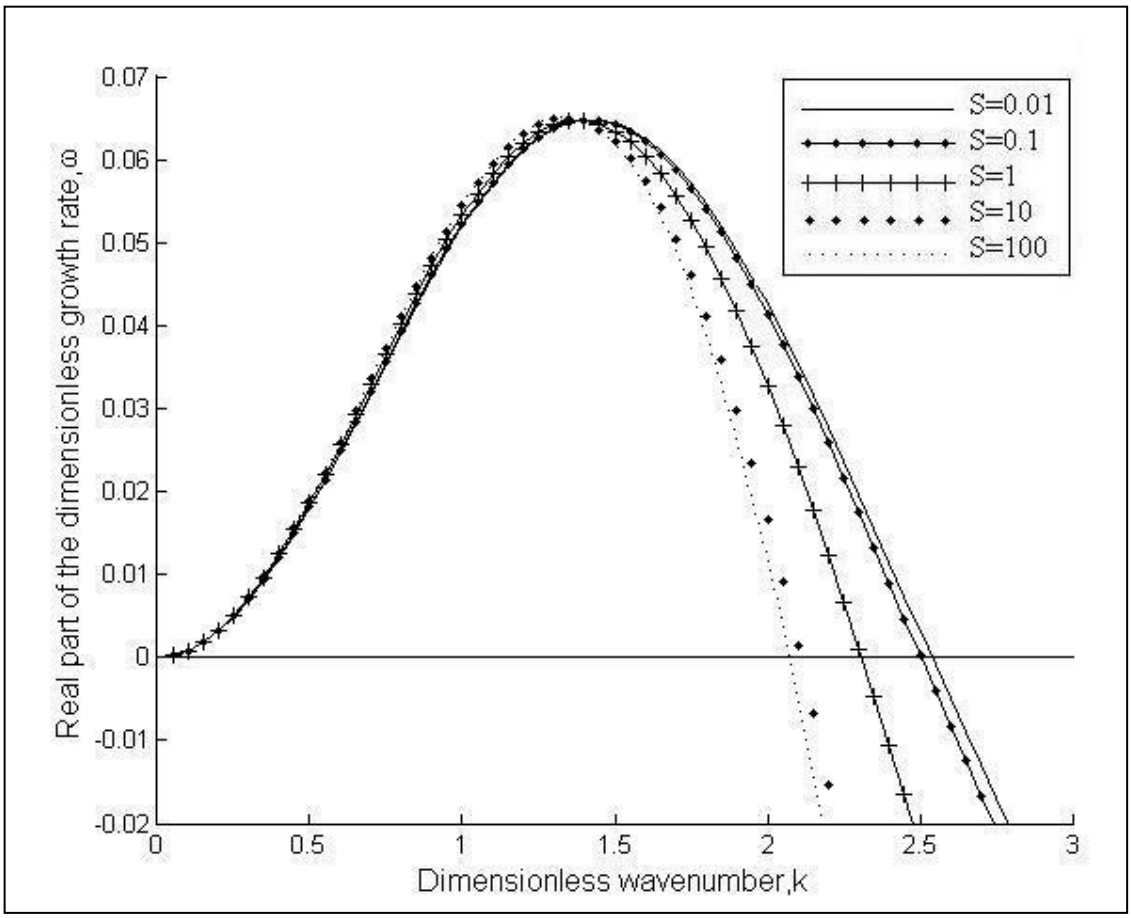

Figure 4.9. Effect of the dimensionless parameter *S* on the growth rate and the critical wavenumber for two Newtonian fluids system under the influence of an electric field. The input parameters are Re=1, M=1, P =1, Hr=1, Ca = 1, E_b =1, σ_r = 0.1, ε* =3 and ε=4.

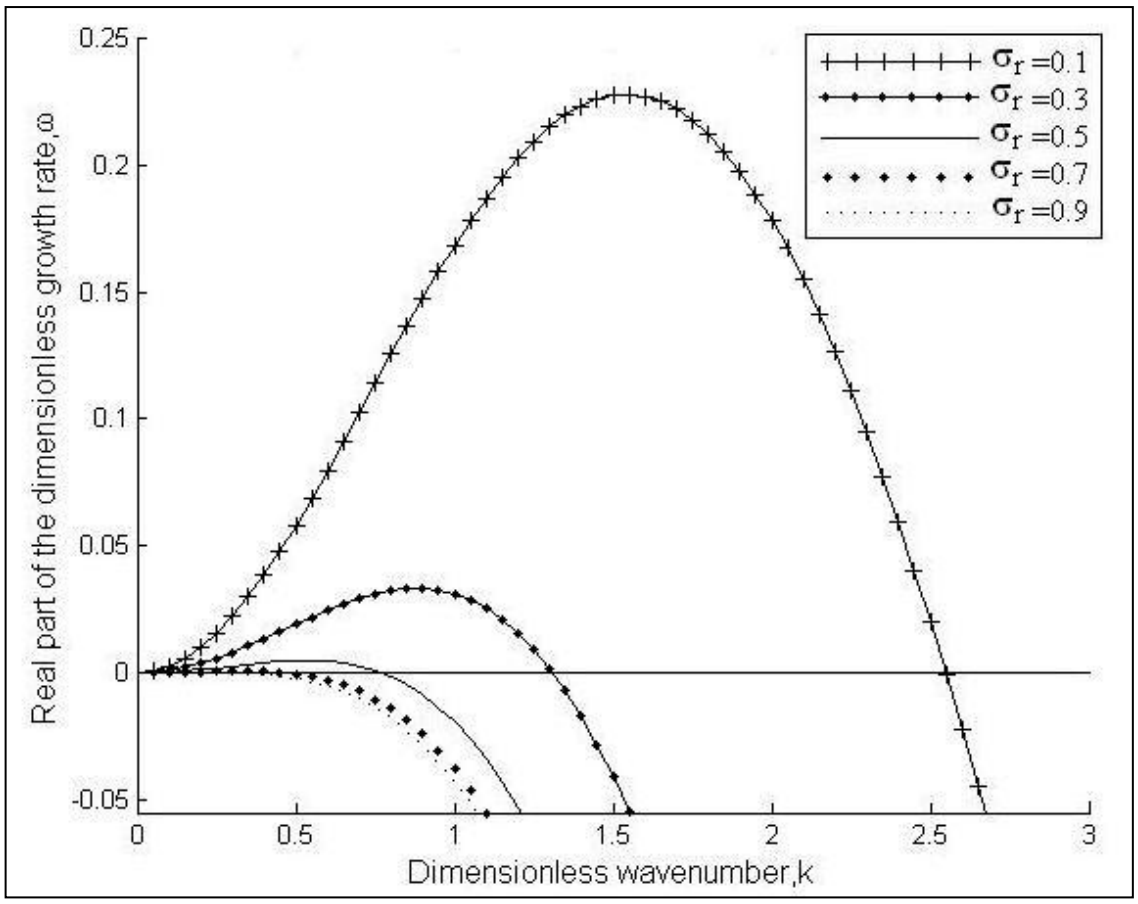

Figure 4.10. Effect of the ratio of the electrical conductivities on the growth rate and the critical wavenumber for two Newtonian fluids system under the influence of an electric field. The input parameters are Re=1, M=0.1, P=1, Hr=0.5, Ca=1, $S=10^3$, E_b=1, ε*=1, ε=2.

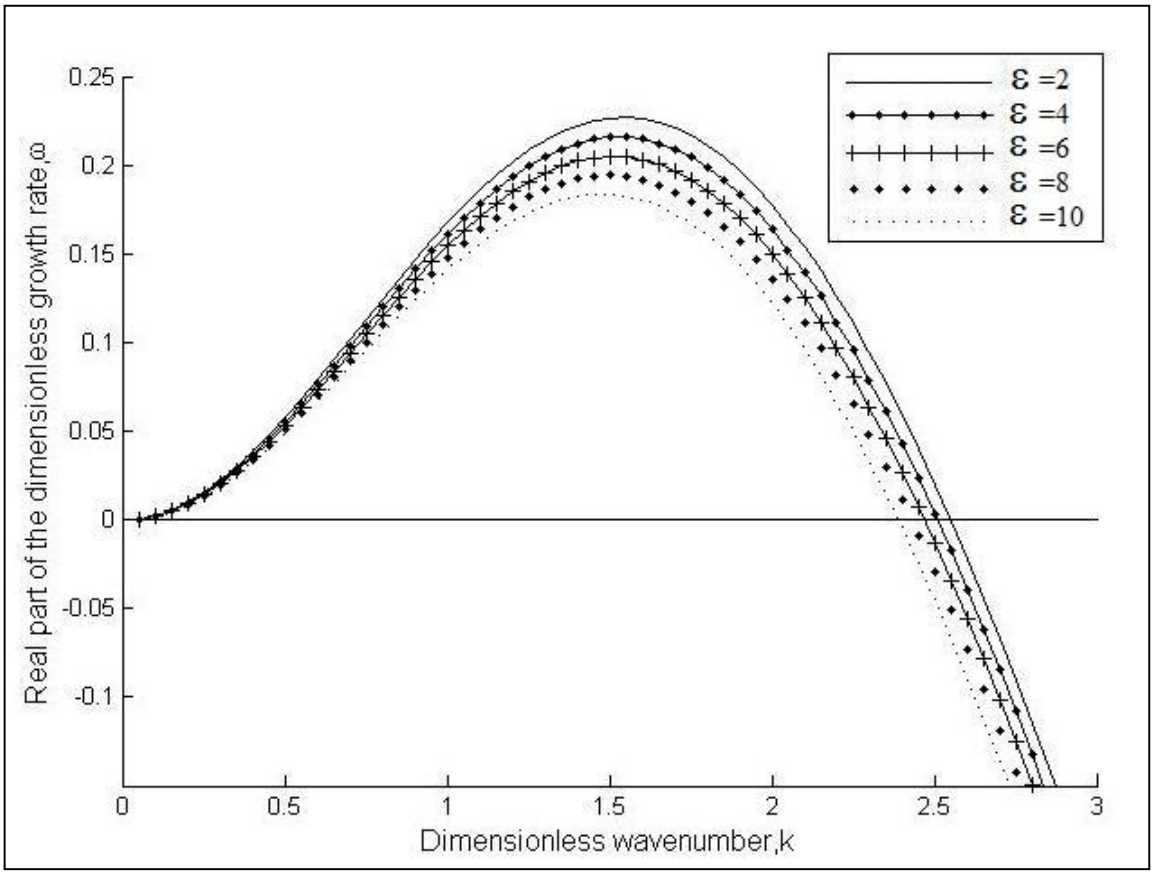

Figure 4.11. Effect of the electrical permittivity ratio on the growth rate and the critical wavenumber for two Newtonian fluids system under the influence of an electric field. The input parameters are Re=1, M=0.1, P =1, Hr=0.5, Ca = 1, $S=10^3$, E_b =1, σ_r = 0.1 and ε^* =1.

4.4. Results of a Newtonian Fluid and a Non-Newtonian Fluid System under the Influence of an Electric Field

The results of the linear stability analysis of the system with a non-Newtonian fluid and a Newtonian fluid under the effect of en electric field (See Section 3.2) are given in this section. The system parameters are chosen as Re=1, M=1, P =1, Hr=1, Ca = 1, $S=10^3$, E_b =1, σ_r = 0.1, ε^* =3, ε =4 and We=1. This set of parameters is used as a default set unless otherwise stated.

Firstly, the effect of the Weissenberg number on the system stability is studied. As mentioned earlier, the Weissenberg number is zero for the Newtonian fluids and it increases as the elasticity of the polymer increases. Figure 4.12 represents the behavior of the stability of the system under an applied electric field with default set of parameters, for

As discussed in Section 3.1.5, the convergence of the results are checked by increasing the cut-off frequency. However, the convergence of the largest eigenvalue is not always satisfied even at larger number of grid points and this determines the upper bound for the Weissenberg number. For example, for the given parameters in Figure 4.12, the largest Weissenberg number that gives converged results is 2.5. As seen from the figure, increasing the Weissenberg number slightly does not affect the stability considerably. The maximum growth rates and the critical wavenumbers are much the same for the Weissenberg number of 0, 0.01 and 0.1. Increasing the Weissenberg number further results in a decrease in the maximum growth rate and an increase in the critical wavenumber. For the no electric field cases (See Sections 4.1 and 4.2), the system with Newtonian fluids has a very different behavior than the system with a non-Newtonian fluid system where the system shifts from a stable to an unstable mode for the same wavenumber when the Weissenberg number is increased. However, under an electric field, for given set of parameters, the only difference between the Newtonian and the non-Newtonian case is the magnitude of the maximum growth rate and the critical wavenumber; there is no shift from a stable to an unstable mode or vice versa.

Figure 4.13 is another representation of the effects of the Weissenberg number on the stability of the interface. The system parameters are chosen according to the experimental parameters of Ozen et al. (Ozen et al., 2006) in which corn oil and glycerine are used as two phases. The figure shows similar results with the Figure 4.12. The maximum growth rate and the critical wavenumber decreases as the Weissenberg number increases. As seen from Figures 4.12 and 4.13, increasing the Weissenberg number of the fluid has a stabilizing effect.

In Figure 4.14, the effect of the thickness ratio of the fluids is given. The thickness ratio is altered from 0.5 to 2 to show its effect on the stability of the system. For the default input parameters, the critical wavenumber and the maximum growth rate decrease as the thickness ratio increases from 0.5 to 2. As mentioned earlier, the thicknesses of the fluids could be arranged altering the volumetric flow rates of the fluids flowing in the channel. Figure 4.14 shows that increasing the thickness ratio of the fluids makes the system more unstable.

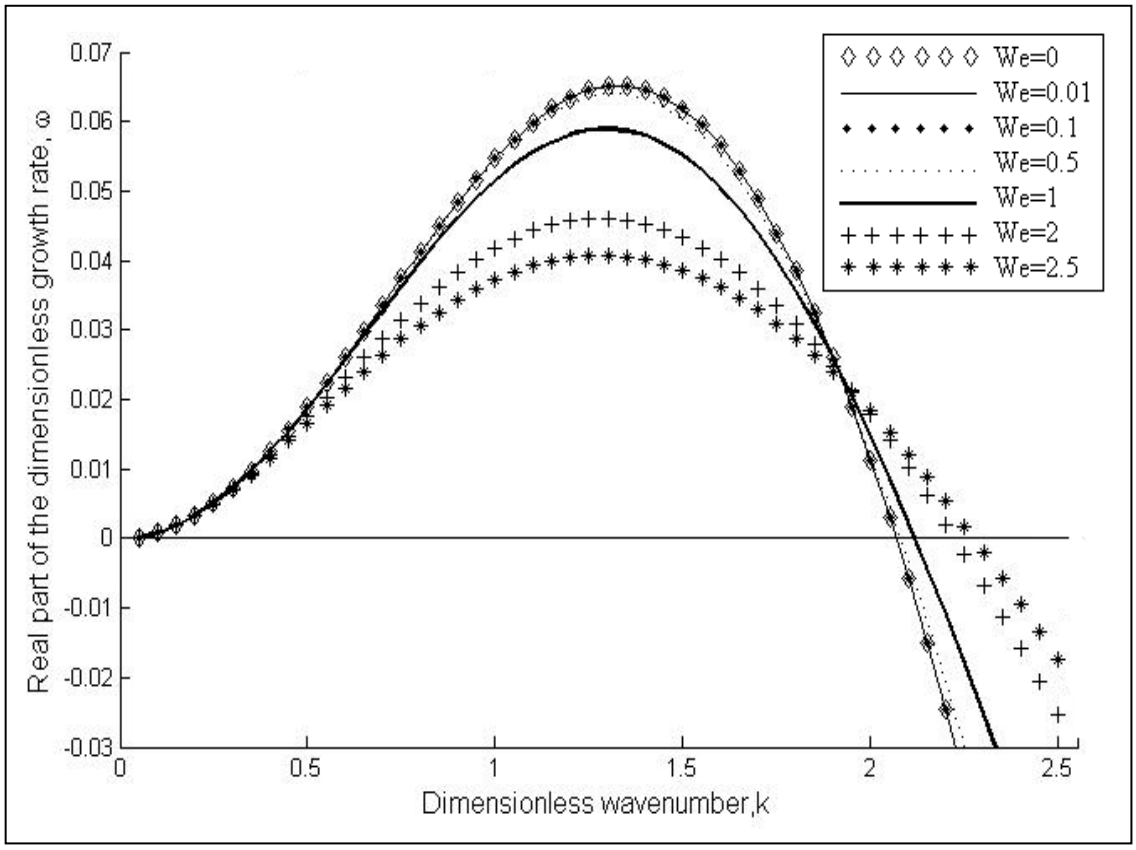

Figure 4.12. Effect of the Weissenberg number on the growth rate and critical the wavenumber for a non-Newtonian fluid and a Newtonian fluid system under the influence of an electric field (Re=1, M=1, P=1, Hr=1, Ca=1, $S=10^3$, $E_b=1$, $\sigma_r=0.1$, $\varepsilon^*=3$ and $\varepsilon=4$).

The effect of the viscosity ratio of the fluids on the system stability is shown in Figure 4.15. For the given set of parameters, increasing viscosity ratio has a stabilizing effect. The maximum growth rate decreases as the viscosity ratio increases. The critical wavenumber decreases with increasing viscosity ratio but it changes very slightly for M=1, 1.5 and 2. The viscosity ratio M is choosen between 0.1 and 2 in order to compare with the Newtonian-Newtonian system; even though the viscosity of a non-Newtonian fluid is expected to be much higher than a Newtonian fluid yielding very small M. However, it is observed that the smaller the value of M the more difficult is the convergence of the results for this set of parameters. So, the effect of viscosity is analyzed for M between 0.1 and 2.

Figure 4.16 presents the effect of the dimensionless parameter S (ratio of fluid time scale to electrical time scale) on the stability of the system. The figure shows that the critical wavenumber decreases as the dimensionless parameter S increases while the

maximum growth rate does not vary much with S. Thus dimensionless parameter S has a stabilizing effect for the selected values of input parameters. Comparing this figure with the effect of S in the Newtonian-Newtonian case (See Figure 4.9), with the same input parameters except for the Weissenberg number, the response of both systems are similar. The only difference is that the maximum growth rates in the non-Newtonian case is smaller and the critical wavenumber has diminished very slightly. This result is in compliance with the Weissenberg effect given in Figure 4.12.

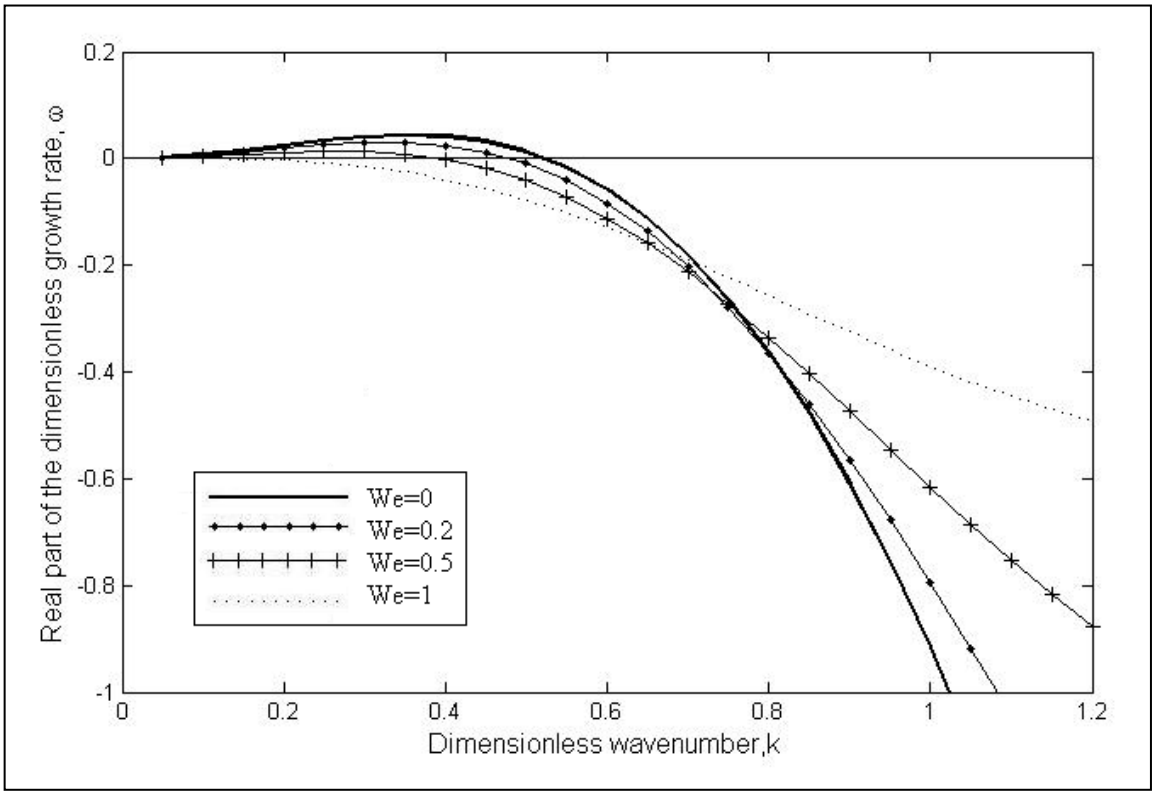

Figure 4.13. Effect of the Weissenberg number on the growth rate and the critical wavenumber with different parameters ($Re=9*10^{-4}$, M= 0.043, P = 0.7873, $Hr= 0.75*10^{-3}$, $Ca = 7.5*10^{-2}$, $S= 4*10^{5}$, E_b =1.6, $\sigma_r=5*10^{-6}$, ε^* =2.1, ε =55.2).

In Figures 4.17 and 4.18, the input parameters for the fluids are chosen to be Re=1, M=0.1, P =1, Hr=0.5, Ca=1, $S=10^3$, E_b =1, ε =2, ε^*=1, σ_r=0.1, We=1, and the effect of the conductivity and the permittivity ratios of the fluids are observed. The input parameters are the same of the Newtonian-Newtonian case for comparison purposes. Figure 4.17 shows the effect of the conductivity ratio in the range of 0.1 to 0.9. It is found that the closer the conductivities of the fluids the more stable the interface is, as also observed in the

Newtonian-Newtonian case. In Figure 4.18, the permittivity of the second fluid is kept constant as ε*=1 and the permittivity of the first fluid is varied from 2 to 10 to alter the permittivity ratio from 0.5 to 0.1. As a result, it is shown that the maximum growth rate and the critical wavenumber decrease as the permittivity of the second fluid increases from 2 to 10. Hence, increasing the permittivity ratio in favour of the first fluid has a destabilizing effect for this set of parameters for both Newtonian-Newtonian case (We=0) and the non-Newtonian case (We=1).

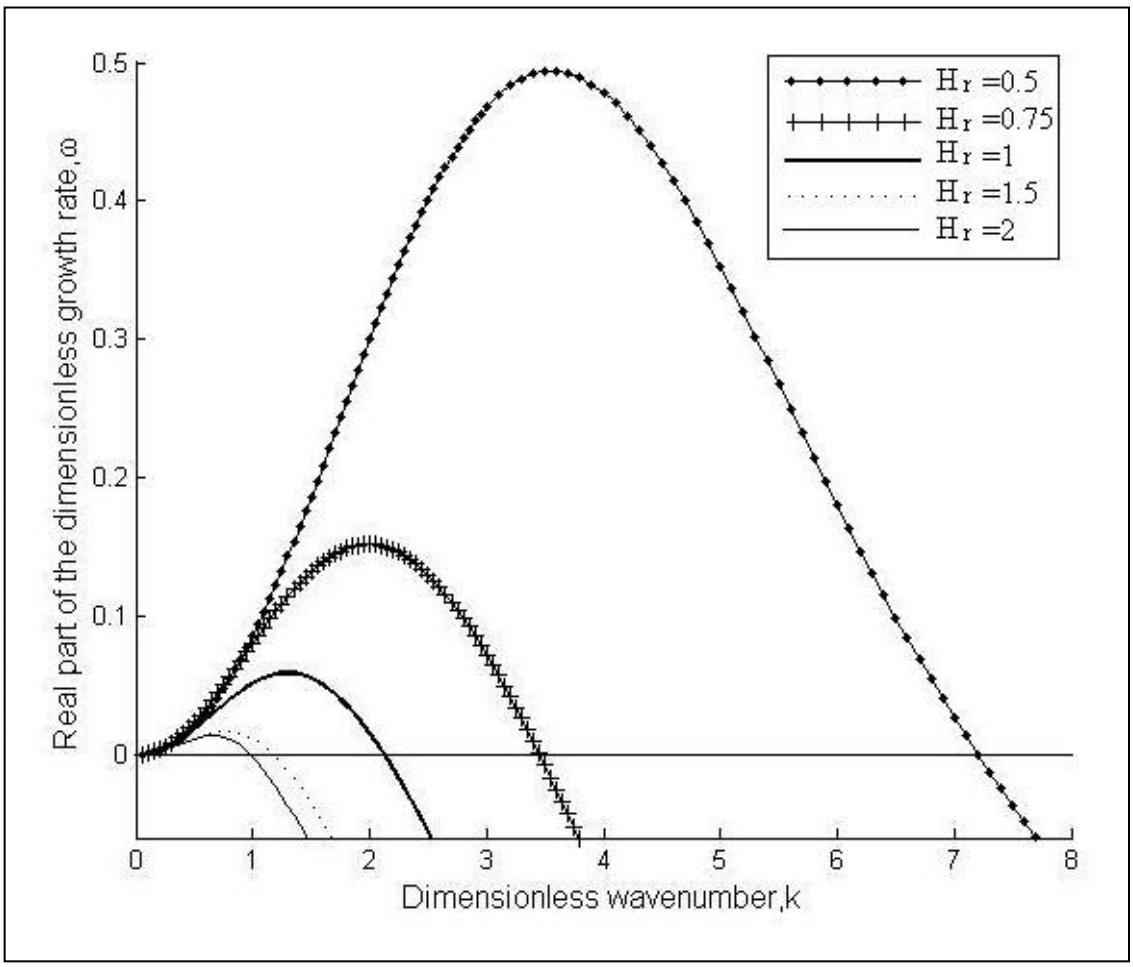

Figure 4.14. Effect of the thickness ratio on the growth rate and the critical wavenumber for a non-Newtonian fluid and a Newtonian fluid system under the influence of an electric field (Re=1, M=1, P=1, Hr=1, $S=10^3$, E_b=1, σ_r = 0.1, ε*=3, ε=4 and We=1).

In addition, the effect of the dimensionless electric number E_b on the stability of the interface is also investigated for two different parameter sets. In Figure 4.19, the effect of E_b is analyzed for the default parameters set and it is found that increasing the electric field

has a destabilizing effect for this set of parameters. The maximum growth rate and the critical wavenumber increase as the electric number increases. However, Figure 4.20 shows that increasing the electric field could be stabilizing according to the selected input parameters and the system is always stable for the input parameters are selected as Re=1, M=1, P =1, Hr=1, Ca=1, $S=10^8$, σ_r =0.5, ε*=2, ε =10, We=1.

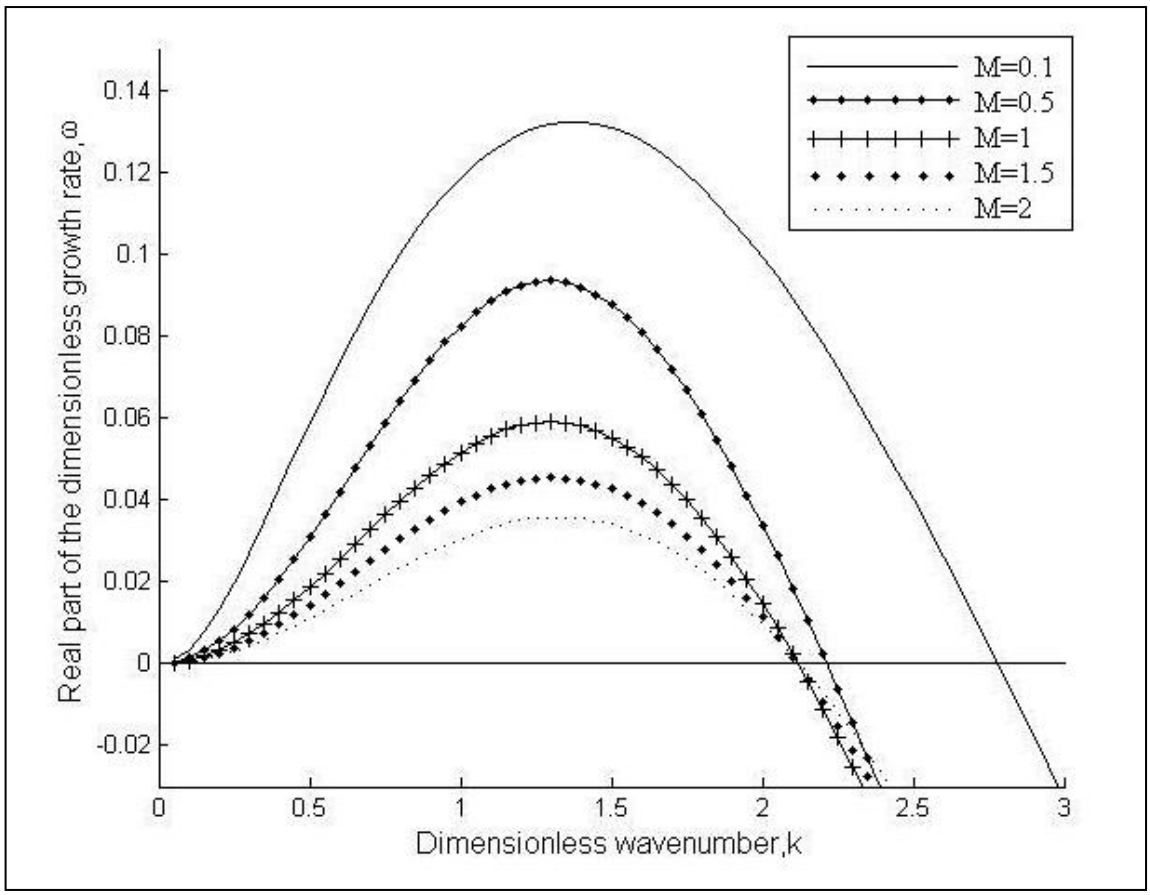

Figure 4.15. Effect of the viscosity ratio on the growth rate and the critical wavenumber for a non-Newtonian fluid and a Newtonian fluid system under the influence of an electric field (Re=1, P=1, Hr=1, Ca=1, $S=10^3$, E_b=1, σ_r=0.1, ε*=3, ε=4 and We=1).

Finally, the effect of the Reynolds number on the stability of the system is analyzed. Figure 4.21 represents the behavior of the system stability with varied Reynolds number. For the default set of parameters, increasing the Reynolds number has a stabilizing effect as the critical wavenumber and the maximum growth rate decrease when the Reynolds number is changed from 10^{-4} to 20.

Comparing the non-Newtonian fluid-Newtonian fluid system with the two Newtonian fluids system for the same input parameters except for the Weissenberg number, the results are similar to each other with a slight difference on the magnitude of the maximum growth rate and the critical wavenumber. The velocity eigenvectors, $\hat{v}_1$ and $\hat{v}_1^*$, are analyzed to understand the difference of the two systems. Figure 4.22 shows the eigenvectors of the Newtonian and the non-Newtonian systems (We=1 and We=2) at their critical wavenumber. The input parameters are Re=1, M=1, P=1, Hr=1, Ca=1, $S=10^3$, E_b=1, σ_r=0.1, ε*=3, ε=4. As seen from the figure, the eigenvectors at the critical point are different for the three cases although the dispersion curves are very similar. The difference between the Newtonian and the non-Newtonian case increases as the Weissenberg number is increased.

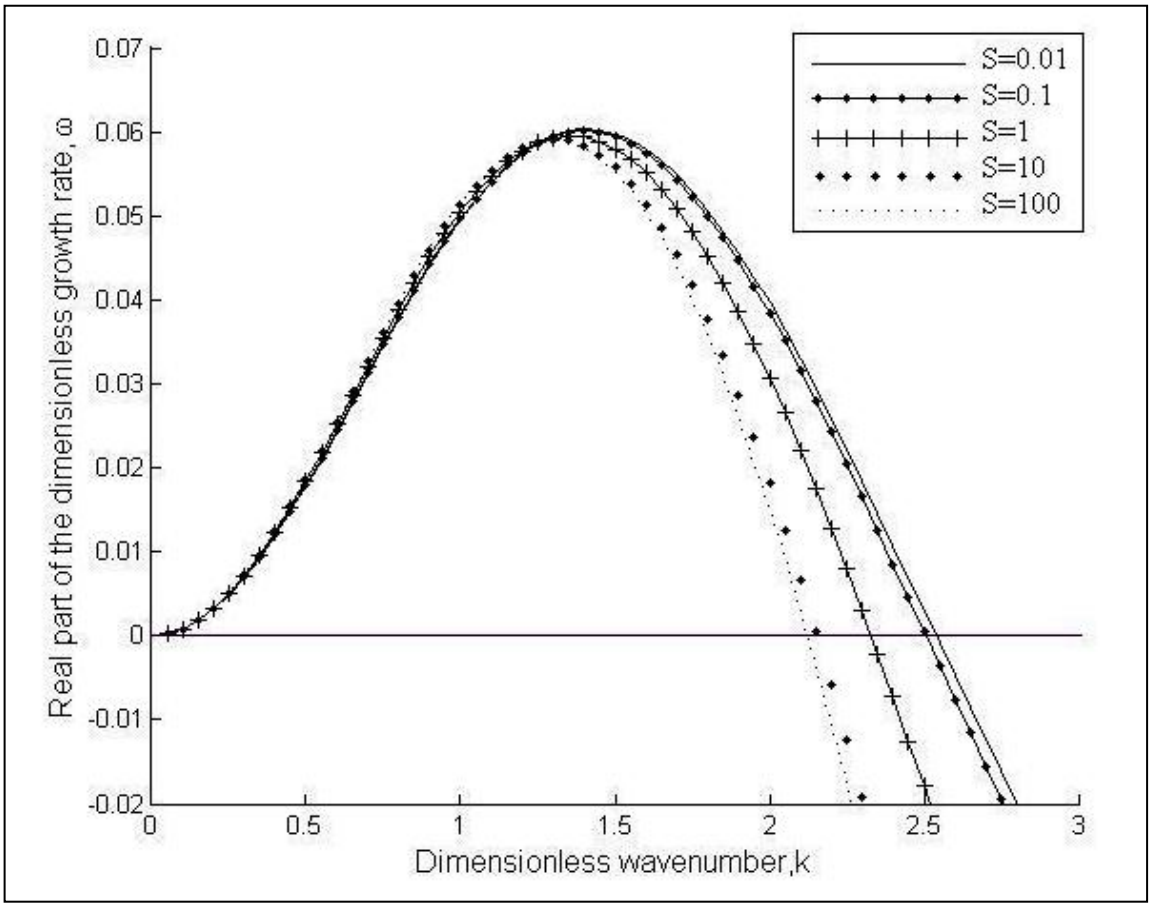

Figure 4.16. Effect of the dimensionless parameter S on the growth rate and the critical wavenumber for a non-Newtonian fluid and a Newtonian fluid system under the influence of an electric field (Re=1, M=1, P=1, Hr=1, Ca=1, E_b=1, σ_r=0.1, ε*=3, ε=4 and We=1).

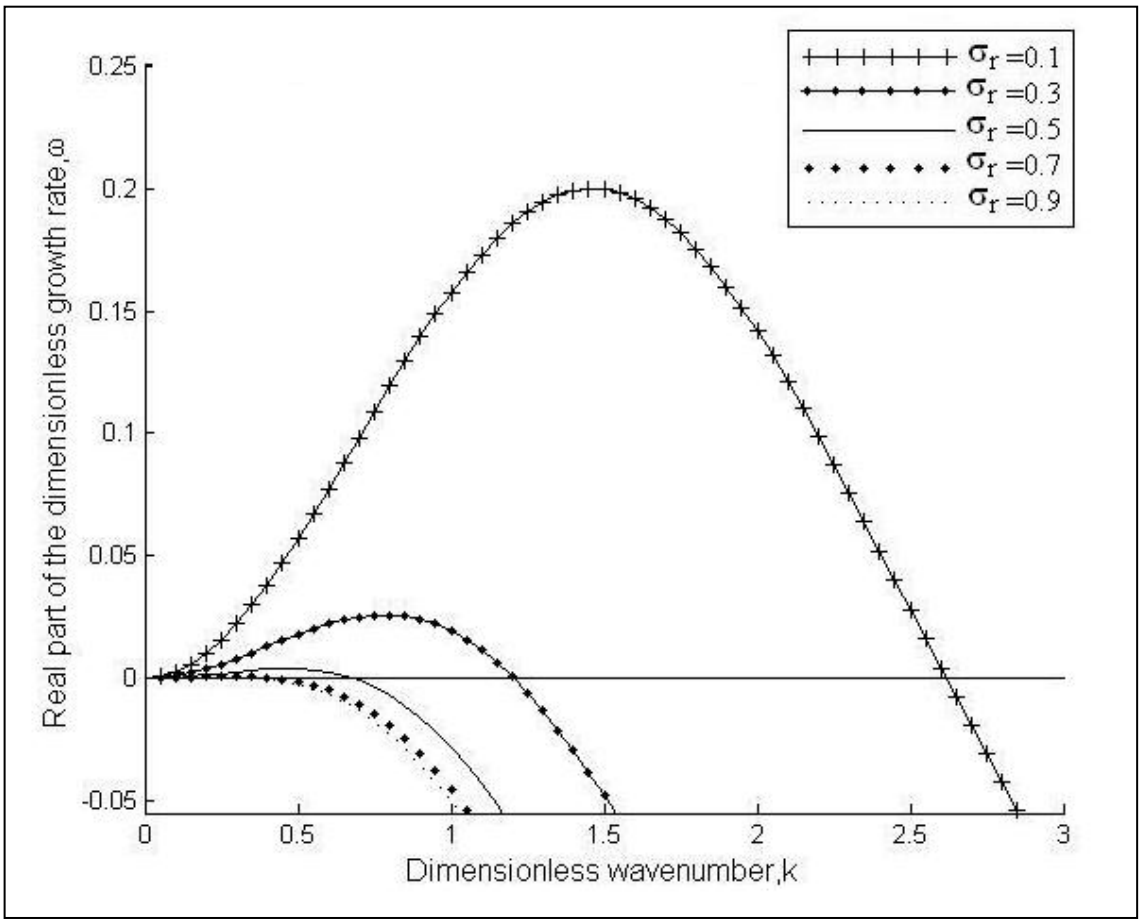

Figure 4.17. Effect of the conductivity ratio on the growth rate and the critical wavenumber for a non-Newtonian fluid and a Newtonian fluid system under the influence of an electric field (Re=1, M=0.1, P =1, Hr=0.5, Ca=1, $S=10^3$, E_b =1, ε*=1, ε=2 and We=1).

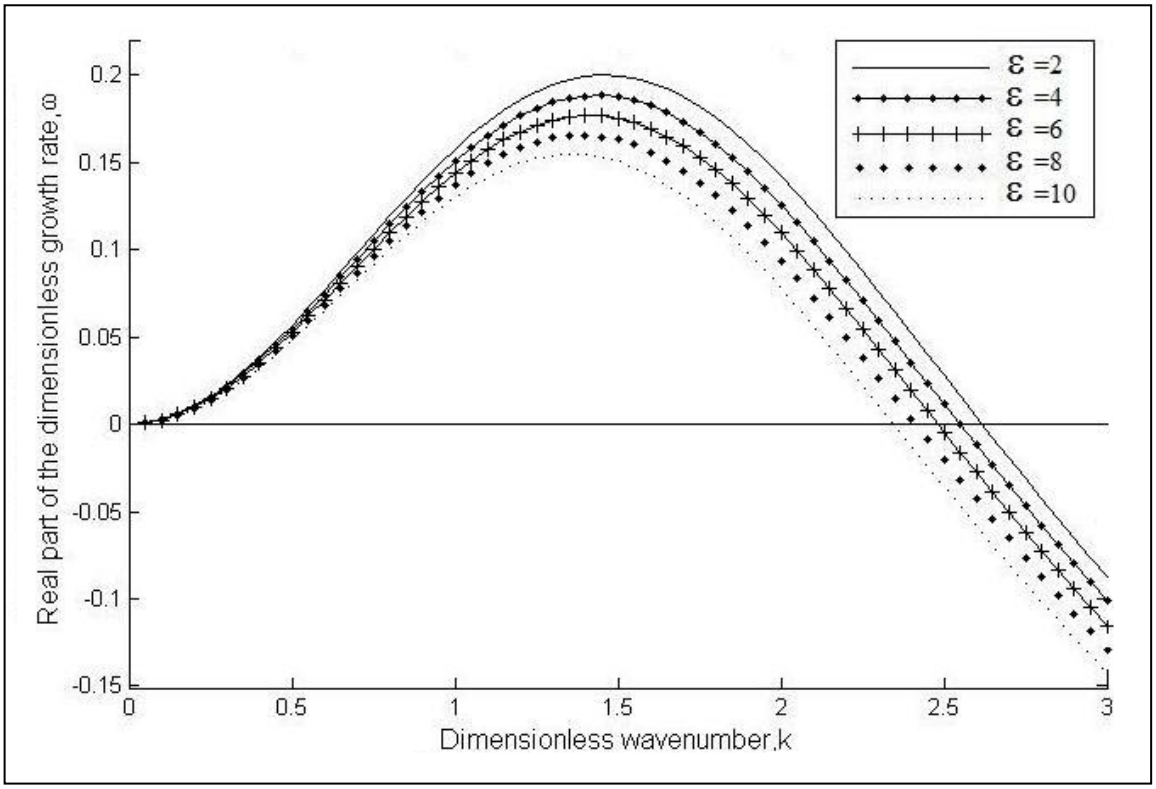

Figure 4.18. Effect of the permittivity ratio on the growth rate and the critical wavenumber for a non-Newtonian fluid and a Newtonian fluid system under the influence of an electric field (Re=1, M=0.1, P =1, Hr=0.5, Ca=1, $S=10^3$, E_b=1, σ_r =0.1, ε*=1 and We=1).

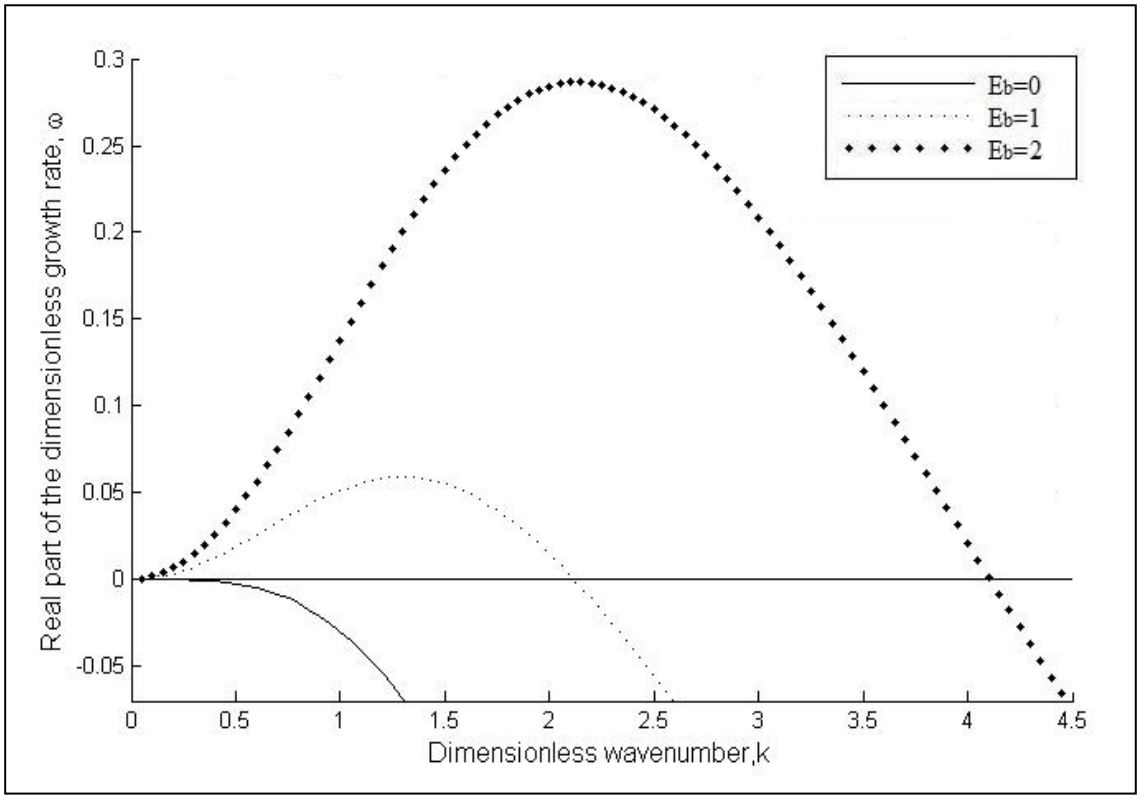

Figure 4.19. Destabilizing effect of the dimensionless electrical number, for a non-Newtonian fluid and a Newtonian fluid system under the influence of an electric field (Re=1, M=1, P=1, Hr=1, Ca=1, $S=10^3$, $\sigma_r=0.1$, $\varepsilon^*=3$, $\varepsilon=4$ and We=1).

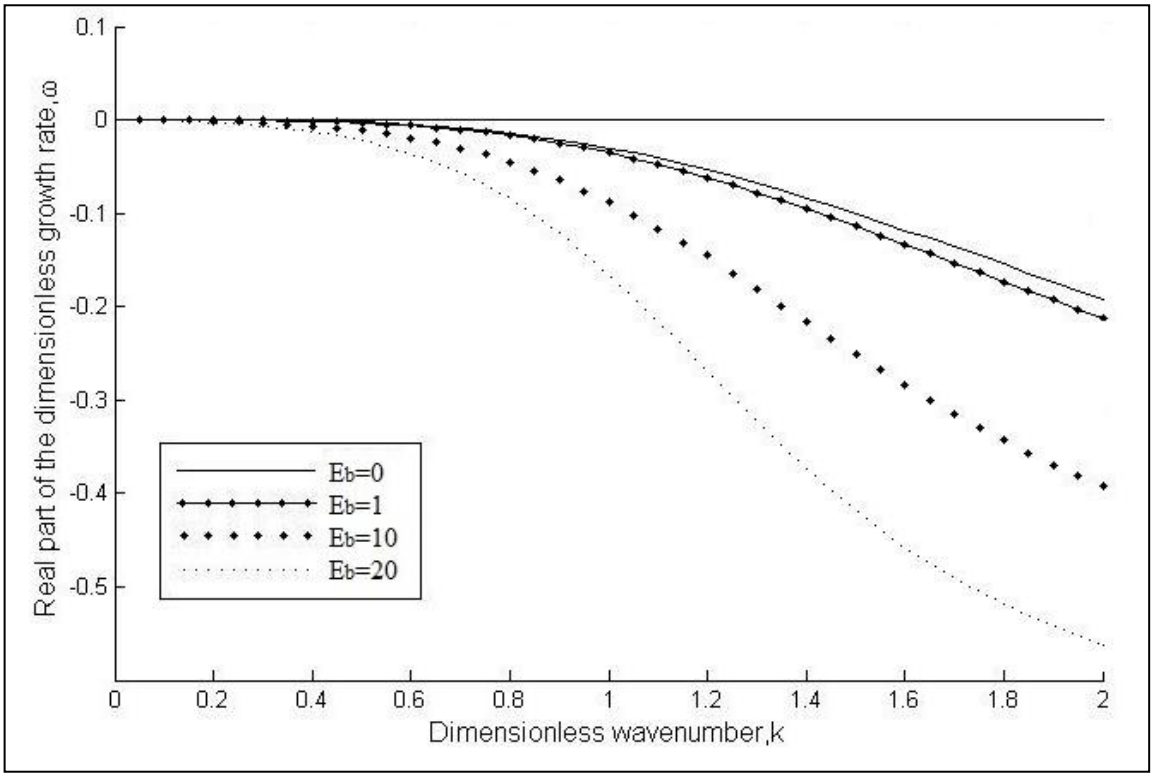

Figure 4.20. Stabilizing effect of the dimensionless electrical number for a non-Newtonian fluid and a Newtonian fluid system under the influence of an electric field (Re=1, M=1, P=1, Hr=1, Ca=1, $S=10^8$, $\sigma_r=0.5$, $\varepsilon^*=2$, $\varepsilon=10$ and We=1).

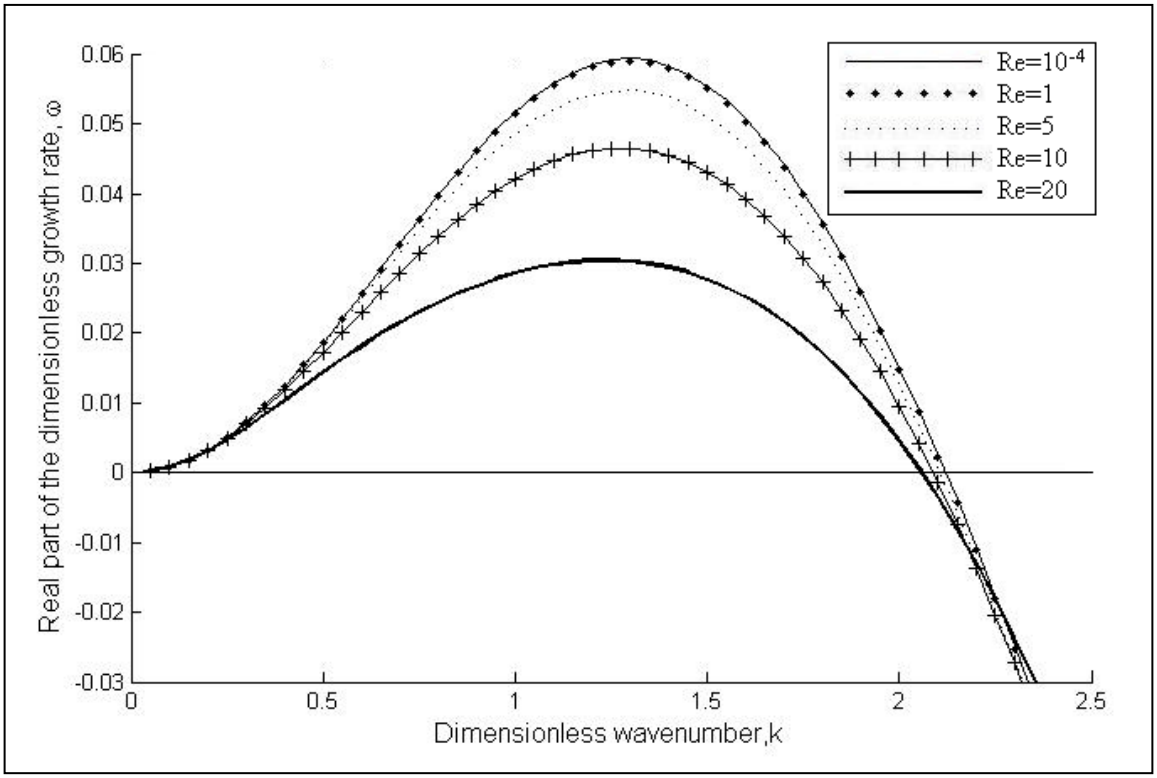

Figure 4.21. Effect of the Reynolds number for a non-Newtonian fluid and a Newtonian fluid system under the influence of an electric field (Re=1, M=1, P =1, Hr=1, Ca = 1, $S=10^3$, E_b =1, σ_r = 0.1, ε^* =3, ε =4 and We=1).

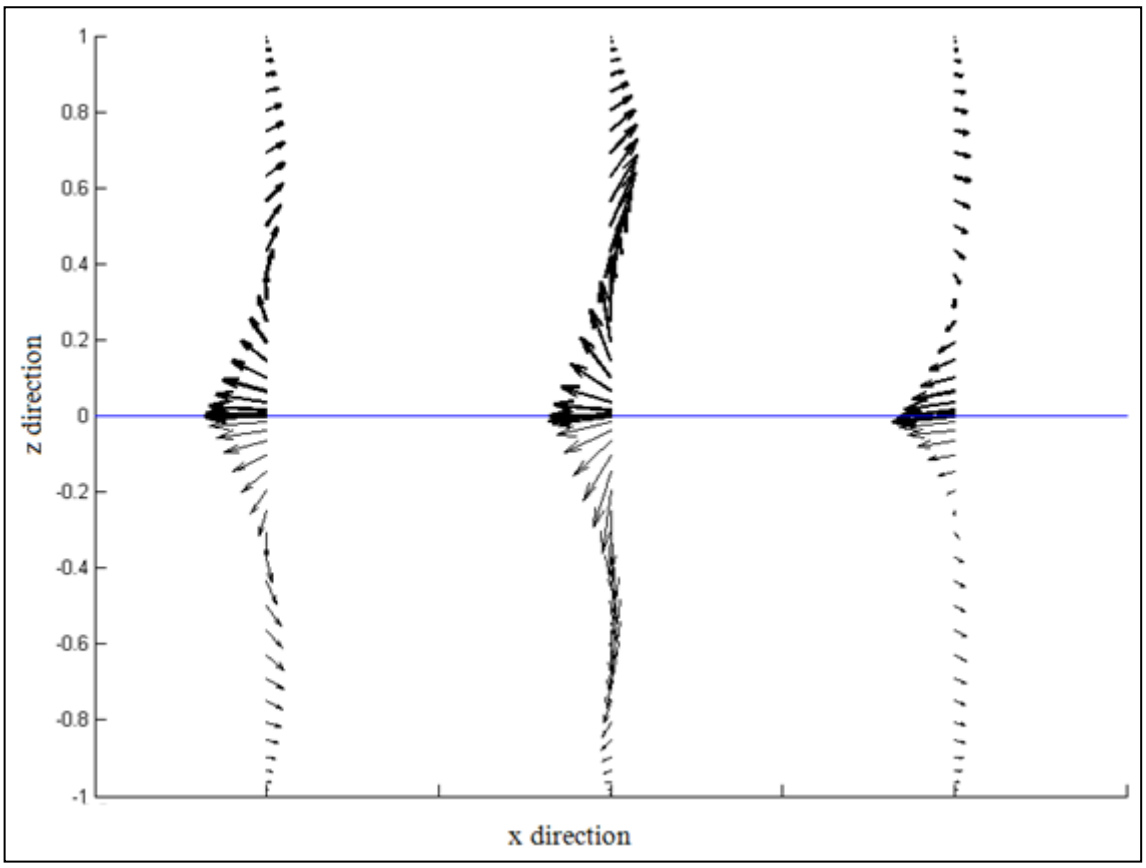

Figure 4.22. Velocity eigenvectors at the critical wavenumbers, We=0 (left, kc=2.0668), We=1 (center, kc=2.1176), and We=2 (right, kc = 2.2235). On the figure, z = 0 represents the interface. Note that the solution is periodic in the x-direction.

5. CONCLUSIONS AND RECOMMENDATIONS

5.1. Conclusions

The linear stability of the interface between two fluids flowing with a Poiseuille flow in a long, rectangular channel is analyzed for four different systems. These systems are the two Newtonian fluids system without an electric field, a Newtonian and a non-Newtonian fluids system without an electric field, two Newtonian fluids system under the influence of an electric field, and a Newtonian and a non-Newtonian fluids system under the influence of an electric field. For all of the systems, the fluids are assumed to be incompressible, viscous, immiscible, non-reactive and leaky-dielectrics with different electrical and physical properties, and identical densities. The gravity is ignored and the interface is assumed to be initially flat.

For the two Newtonian fluids system without an electric field, the effect of the Reynolds number on the stability of the system is studied. The dispersion curves are plotted for different Reynolds numbers and a neutral stability curve is obtained from the critical wavenumbers of the dispersion curves. It is found that there is only one critical wavenumber for Reynolds numbers smaller than 65 while there are more than one critical wavenumbers when the Reynolds number is greater. Having multiple critical wavenumbers means that a stable system becomes unstable at some Reynolds number but a further increase in Reynolds number makes the system again stable.

For a Newtonian and a non-Newtonian fluids system without an electric field, similar to the Newtonian case, the effect of the Reynolds number on the stability of the system is analyzed plotting the dispersion curves and the neutral stability curve. The two neutral stability curves, for Newtonian and non-Newtonian cases, are compared and it is found that the non-Newtonian case with We=0.5 has only one critical wavenumber for all Reynolds numbers while the Newtonian case has more than one critical point for large values of the Reynolds number.

Moreover, the effect of the Weissenberg number is analyzed for a Newtonian and a non-Newtonian fluids system without an electric field. It is observed that the very small values of Weissenberg number (We=0.005 and 0.01) have similar behavior with the Newtonian case; however, increasing the Weissenberg number further results in a shift of the behavior of the system from a stable mode to an unstable mode for the same wavenumbers.

Next, the effects of the system parameters on the stability are analyzed for the two Newtonian fluids system under the influence of an electric field. The analyzed parameters are the thickness ratio Hr, the viscosity ratio M, the ratio of fluid to electric time scale S, the conductivity ratio σ_r, and the permittivity ratio. As a result, it is found that the critical wavenumber and the maximum growth rate decrease as any of the thickness ratio, the viscosity ratio, the conductivity ratio and the permittivity ratio increases; whereas varying the ratio of the fluid to electric time scale, S does not affect the maximum growth rate but it slightly changes the critical wavenumber.

Finally, the interfacial instability of the system with a non-Newtonian and a Newtonian fluid under the influence of an electric field is studied. The effects of the Weissenberg number We, the thickness ratio Hr, the viscosity ratio M, the ratio of the fluid to electric time scale S, the conductivity ratio σ_r, the permittivity ratio, the electric number E_b, and the Reynolds number are analyzed and compared to the Newtonian case. As a result, it is seen that increasing the Weissenberg number slightly, does not affect the stability of the system considerably, but the maximum growth rate decreases and the critical wavenumber increases as the Weissenberg number is increased further. However, when the Weissenberg number is increased, a shift from an unstable to a stable mode, which is seen in the no electric field case, is not observed under the effect of an electric field. The Weissenberg number is varied between 0 and 2.5 as the convergence of the numerical results is not satisfied above We = 2.5 for the given set of parameters.

For the non-Newtonian-Newtonian fluids system, the effects of the parameters are similar to the Newtonian case; the only difference is the magnitude of the maximum growth rates and the critical wavenumbers. In short, it can be concluded that decreasing the permittivity ratio or increasing any of the Weissenberg number, the thickness ratio, the

viscosity ratio, the conductivity ratio or the Reynolds number have a stabilizing effect; whereas increasing the dimensionless parameter S, the ratio of the fluid to electric time scale does not affect the maximum growth rate but decreases the critical wavenumber, and increasing the electric number, i.e., increasing the applied voltage could be stabilizing or destabilizing depending on the selected parameters.

5.2. Recommendations

In this work, the interfacial instability of the systems for given parameter sets are analyzed. Considering the system modeling and the results obtained in this study, the following ideas are suggested for a future work.

- This study contains the effects of the system parameters for a limited set of parameters. A parametric study can be performed as a continuation. The numerical analyses can be enlarged for different parameters, with different physical and electrical properties of the fluids.

- The linear stability analysis could only determine if the system is stable or unstable to the given perturbation, for the given sets of parameters. The fate of the disturbance cannot be determined with a linear analysis. A nonlinear analysis such as long wave analysis can be conducted to find out what will happen to the interface once it becomes unstable. The interface might go to rupture or reach another equilibrium state. Also, the nature of the bifurcation can be obtained using a weakly nonlinear analysis.

- The UCM model is used as a constitutive equation in this work. A different constitutive equation can be used to model the rheological behavior of the polymeric fluid.

- A parallel electric can be applied to the interface of the system and the results can be compared to the normal electric case.

- The fluids can be modeled as perfect dielectric or conductive and the results can be compared to the leaky-dielectric case.

- An experimental system can be set and the stability of the system can be observed using a polymeric fluid and a Newtonian fluid. The results can be compared with the theory.

APPENDIX A: DERIVATION OF THE INTERFACE VARIABLES

In this appendix; the derivations of the interface variables, the normal vector n, the tangent vector T, the surface speed u, and the mean curvature 2H are presented. The expansions of these variables are also presented as they are needed in Chapter 3.

Unit Normal Vector:

The unit normal vector is defined as

$$\underline{n} = \frac{\nabla f}{|\nabla f|} \tag{A.1}$$

where f represents a constant surface and for

$$f = z - Z(x) \tag{A.2}$$

the unit normal in Rectangular Cartesian Coordinate System becomes

$$\underline{n} = \frac{\underline{e}_z - Z_x \underline{e}_x}{\sqrt{1 + (Z_x)^2}} \tag{A.3}$$

The unit normal vector can be expanded in Taylor series as

$$\underline{n} = \underline{n}_0 + \varepsilon \underline{n}_1 \tag{A.4}$$

Using Equation (A.3), the base state unit normal vector is

$$\underline{n}_0 = \frac{\underline{e}_{z0} + \overbrace{Z_{x0}}^{0} \underline{e}_{x0}}{\sqrt{1 + (Z_{x0})^2}} \tag{A.5}$$

which reduces to

$$\underline{n}_0 = \underline{e}_{z0} \tag{A.6}$$

The perturbed unit normal vector is

$$\underline{n}_1 = \frac{\partial \underline{n}}{\partial \varepsilon} \tag{A.7}$$

which gives

$$\underline{n}_1 = \frac{0 - Z_{x1}\underline{e}_{x0}}{\sqrt{1 + (Z_{x0})^2}} \tag{A.8}$$

Equation (A.8) reduces to

$$\underline{n}_1 = -Z_{x1}\underline{e}_{x0} \tag{A.9}$$

Unit Tangent Vector:

The dot product of the unit normal and the unit tangent vectors is zero, i.e.,

$$\underline{n} \cdot \underline{t} = 0 \tag{A.10}$$

Then, the unit tangent vector is found as

$$\underline{t} = \frac{\underline{e}_x + Z_x\underline{e}_z}{\sqrt{1 + (Z_x)^2}} \tag{A.11}$$

The unit tangent vector can be expanded in Taylor series as

$$\underline{t} = \underline{t}_0 + \varepsilon \underline{t}_1 \tag{A.12}$$

The base state unit normal vector becomes

$$\underline{t}_0 = \frac{\underline{e}_{x0} + Z_{x0}\underline{e}_{z0}}{\sqrt{1 + (Z_{x0})^2}} \tag{A.13}$$

Then Equation (A.13) reduces to

$$\underline{t}_0 = \underline{e}_{x0} \tag{A.14}$$

The perturbed unit tangent vector is

$$\underline{t}_1 = \frac{\partial \underline{t}}{\partial \varepsilon} \tag{A.15}$$

which gives

$$\underline{t}_1 = \frac{0 + Z_{x1}\underline{e}_{z0}}{\sqrt{1 + (Z_{x0})^2}} \tag{A.16}$$

Equation (A.16) reduces to

$$\underline{t}_1 = Z_{x1}\underline{e}_{z0} \tag{A.17}$$

Interface Speed:

The normal speed of the interface is expressed as

$$u = \underline{u} \cdot \underline{n} \tag{A.18}$$

where u is defined as

$$u = \mp \frac{\Delta s}{\Delta t} = -\frac{f_t}{\underline{n} \cdot \nabla f} = -\frac{f_t}{|\nabla f|} \tag{A.19}$$

which becomes

$$u = \frac{Z_t}{\sqrt{1 + (Z_x)^2}} \tag{A.20}$$

At the base state, which is steady, the interface speed is

$$u_0 = \frac{\partial Z_0}{\partial t_0} = 0 \tag{A.21}$$

and in the perturbed state it becomes

$$u_1 = \frac{\partial Z_1}{\partial t_0} \tag{A.22}$$

Mean Curvature:

The mean curvature of the surface is expressed as

$$2H = \frac{Z_{xx}}{\left(\sqrt{1 + (Z_x)^2}\right)^{3/2}} \tag{A.23}$$

At the base state, it is found as

$$2H_0 = \frac{\frac{\partial}{\partial x}\frac{\partial}{\partial x}\overset{0}{\widetilde{Z_0}}}{\left(\sqrt{1 + \left(\frac{\partial}{\partial x} Z_0\right)^2}\right)^{3/2}} = 0 \tag{A.24}$$

At the perturbed state, the mean curvature is found as

$$2H_1 = \frac{\frac{\partial}{\partial x}\frac{\partial}{\partial x}Z_1}{\left(\sqrt{1+\left(\frac{\partial}{\partial x}Z_0\right)^2}\right)^{3/2}} \tag{A.25}$$

that is

$$2H_1 = Z_{xx1} \tag{A.26}$$

APPENDIX B: BASE STATE SOLUTION

In this appendix, the base state equations used in Section 3.1.4.1 are derived in detail.

The base state velocity profiles are given in Section 3.1.4.1 as

$$v_{x0} = A_0 {z_0}^2 + B_0 z_0 + C_0 \tag{B.1}$$

and

$$v_{x0}^* = A_0^* {z_0}^2 + B_0^* z_0 + C_0^* \tag{B.2}$$

where

$$A_0 = \frac{1}{2}\frac{dp_0}{dx_0} \tag{B.3}$$

and

$$A_0^* = \frac{1}{2M}\frac{dp_0^*}{dx_0} \tag{B.4}$$

Appling the boundary conditions to the equations,

at $z_0 = -1$,

$$v_{x0} = 0 \tag{B.5}$$

and at $z_0 = \mathrm{Hr}$,

$$v_{x0}^* = 0 \tag{B.6}$$

yield

$$0 = A_0 - B_0 + C_0 \tag{B.7}$$

and

$$0 = A_0^* Hr^2 + B_0^* Hr + C_0^* \tag{B.8}$$

At $z_0 = 0$, the no-slip condition

$$\underline{v}_0 \cdot \underline{t}_0 = \underline{v}_0^* \cdot \underline{t}_0 \tag{B.9}$$

yields

$$v_{x0} = v_{x0}^* \tag{B.10}$$

as $\underline{n}_0 = \underline{e}_{z0}$ and $\underline{t}_0 = \underline{e}_{x0}$ (see Appendix A). Recall that the velocity is rendered dimensionless with the interface speed. Hence, the dimensionless interface velocity is unity at the interface. Equation (B.10) turns out to be

$$v_{x0} = v_{x0}^* = 1 \tag{B.11}$$

Then it is found out that

$$C_0 = C_0^* = 1 \tag{B.12}$$

At $z_0 = 0$, the TSB, Equation (3.82), at the base state is

$$\begin{aligned} &\left(\underline{\tau}_0 \cdot \underline{n}_0 \cdot \underline{t}_0\right) + \varepsilon\, E_b\left(\underline{E}_0\, \underline{E}_0 \cdot \underline{n}_0 \cdot \underline{t}_0\right) \\ &= M\left(2\underline{D}_0^* \cdot \underline{n}_0 \cdot \underline{t}_0\right) + \varepsilon^* E_b\left(\underline{E}_0{}^*\, \underline{E}_0{}^* \cdot \underline{n}_0 \cdot \underline{t}_0\right) \end{aligned} \tag{B.13}$$

which gives

$$\underbrace{\left(\underline{\underline{\tau}}_0 \cdot \underline{n}_0 \cdot \underline{t}_0\right)}_{\tau_{xz0}} + \varepsilon\, E_b \underbrace{\left(\underline{E}_0\, \underline{E}_0 \cdot \underline{n}_0 \cdot \underline{t}_0\right)}_{0}$$

$$= M \underbrace{\left(2\underline{\underline{D}}_0^* \cdot \underline{n}_0 \cdot \underline{t}_0\right)}_{\frac{dv_{x0}^*}{dz_0}} + \varepsilon^* E_b \underbrace{\left(\underline{E}_0{}^*\, \underline{E}_0{}^* \cdot \underline{n}_0 \cdot \underline{t}_0\right)}_{0} \tag{B.14}$$

and finally Equation (B.14) becomes

$$\tau_{xz0} = M\, \frac{dv_{x0}^*}{dz_0} = \frac{dv_{x0}}{dz_0} \tag{B.15}$$

So Equation (B.15) gives

$$B_0 = M\, B_0^* \tag{B.16}$$

and

$$A_0 = M\, A_0^* \tag{B.17}$$

At $z_0 = 0$, the NSB, Equation (3.85), at the base state is

$$-p_0 + \underbrace{\underline{\tau}_{zz0}}_{0} + \varepsilon E_b \left(\underbrace{\underline{E}_0\, \underline{E}_0 \cdot \underline{n}_0 \cdot \underline{n}_0}_{\left(\frac{dV_0}{dz_0}\right)^2} - \frac{1}{2} \underbrace{\left|\underline{E}_0\right|^2}_{\left(\frac{dV_0}{dz_0}\right)^2} \right)$$

$$= -p_0^* + M \underbrace{2\underline{\underline{D}}_0^* \cdot \underline{n}_0 \cdot \underline{n}_0}_{2\underbrace{\frac{dV_{z0}}{dz_0}}_{0}} + \varepsilon^* E_b \left(\underbrace{\underline{E}_0^*\, \underline{E}_0^* \cdot \underline{n}_0 \cdot \underline{n}_0}_{\left(\frac{dV_0^*}{dz_0}\right)^2} - \frac{1}{2} \underbrace{\left|\underline{E}_0^*\right|^2}_{\left(\frac{dV_0^*}{dz_0}\right)^2} \right) + \frac{1}{Ca} \underbrace{2H_0}_{0} \tag{B.18}$$

The Gauss' Law , Equation (3.76), at the base state is

$$q_0 = \varepsilon^* \underline{E}_0^* \cdot \underline{n}_0 - \varepsilon \underline{E}_0 \cdot \underline{n}_0 \tag{B.19}$$

So, it is found as

$$0 = \varepsilon^* \frac{dV_0^*}{dz_0} - \varepsilon \frac{dV_0}{dz_0} \tag{B.20}$$

at the interface, $z_0 = 0$, the base state NSB equation, i.e. Equation (B.18) reduces to

$$-p_0 = -p_0^* \tag{B.21}$$

Solving Equations (B.7), (B.8), (B.12), (B.16) and (B.17) simultaneously, the constants in Equations (B.1) and (B.2) are found as

$$A_0 = -\frac{Hr + M}{(Hr + Hr^2)} \tag{B.22}$$

$$A_0^* = -\frac{Hr + M}{M(Hr + Hr^2)} \tag{B.23}$$

$$B_0 = \frac{Hr^2 - M}{Hr + Hr^2} \tag{B.24}$$

$$B_0^* = \frac{(Hr^2 - M)}{M(Hr + Hr^2)} \tag{B.25}$$

Eventually, the base state flow profiles for both fluids are found as

$$v_{x0} = -\frac{Hr + M}{(Hr + Hr^2)} {z_0}^2 + \frac{Hr^2 - M}{Hr + Hr^2} z_0 + 1 \tag{B.26}$$

$$v_{x0}^* = -\frac{Hr + M}{M(Hr + Hr^2)} {z_0}^2 + \frac{(Hr^2 - M)}{M(Hr + Hr^2)} z_0 + 1 \tag{B.27}$$

The base state voltage potentials are found as

$$V_0 = D_0 z_0 + F_0 \tag{B.28}$$

and

$$V_0^* = D_0^* z_0 + F_0^* \tag{B.29}$$

The boundary conditions are given as follows

At $z_0 = -1$,

$$V_0 = 1 \tag{B.30}$$

which gives

$$1 = -D_0 + F_0 \tag{B.31}$$

at $z_0 = \mathrm{Hr}$,

$$V_0^* = 0 \tag{B.32}$$

which gives

$$0 = D_0 Hr + F_0 \tag{B.33}$$

at $z_0 = 0$,

$$\underline{E_0} \cdot \underline{t_0} = \underline{E_0^*} \cdot \underline{t_0} \tag{B.34}$$

which gives

$$V_0 = V_0^* \tag{B.35}$$

At $z_0 = 0$, the charge balance at the interface is

$$0 = S(\underline{E}_0 \cdot \underline{n}_0 - \sigma_r \underline{E}_0^* \cdot \underline{n}_0) \tag{B.36}$$

where

$$\underline{E}_0 = -(\frac{dV_0}{dx_0}\underline{e}_{x0} + \frac{dV_0}{dz_0}\underline{e}_{z0}) \tag{B.37}$$

Then, Equation (B.36) becomes

$$\frac{\partial V_0}{\partial z_0} = \sigma_r \frac{\partial V_0^*}{\partial z_0} \tag{B.38}$$

which gives

$$-D_0 + \sigma_r D_0^* = 0 \tag{B.39}$$

Solving Equations (B.31), (B.33), (B.35) and (B.39) simultaneously, the unknown constants in Equations (B.28) and (B.29) are found as

$$D_0 = -\frac{\sigma_r}{Hr + \sigma_r} \tag{B.40}$$

$$D_0^* = -\frac{1}{Hr + \sigma_r} \tag{B.41}$$

$$F_0 = \frac{Hr}{Hr + \sigma_r} \tag{B.42}$$

$$F_0^* = \frac{Hr}{Hr + \sigma_r} \tag{B.43}$$

Then, the expressions for the base state voltage potentials take the form

$$V_0 = -\frac{\sigma_r}{Hr + \sigma_r} z_0 + \frac{Hr}{Hr + \sigma_r} \tag{B.44}$$

and

$$V_0^* = -\frac{1}{Hr + \sigma_r} z_0 + \frac{Hr}{Hr + \sigma_r} \tag{B.45}$$

APPENDIX C: DERIVATION OF THE PERTURBED INTERFACE CONDITIONS

In this appendix, the perturbed interface equations used in Section 3.1.4.2 are derived in detail.

At the interface, $z_0 = 0$, when the kinematic condition $\underline{v} \cdot \underline{n} = \underline{u} \cdot \underline{n} = \underline{v}^* \cdot \underline{n}$, i.e. Equation (3.73) is expanded in Taylor series as

$$\left[\underline{v}_0 + \epsilon\left(\underline{v}_1 + Z_1 \frac{\partial \underline{v}_0}{\partial z_0}\right)\right] \cdot \left(\underline{n}_0 + \epsilon \underline{n}_1\right) = \left[\underline{v}_0^* + \epsilon\left(\underline{v}_1^* + Z_1 \frac{\partial \underline{v}_0^*}{\partial z_0}\right)\right] \cdot \left(\underline{n}_0 + \epsilon \underline{n}_1\right) = \frac{\partial (Z_0 + \epsilon Z_1)}{\partial t_0} \tag{C.1}$$

Grouping the terms to the first order in epsilon, the perturbed boundary condition is found as

$$\left(\underline{v}_0 \cdot \underline{n}_1 + \underline{v}_1 \cdot \underline{n}_0 + Z_1 \frac{\partial \underline{v}_0}{\partial z_0} \cdot \underline{n}_0\right) = \left(\underline{v}_0^* \cdot \underline{n}_1 + \underline{v}_1^* \cdot \underline{n}_0 + Z_1 \frac{\partial \underline{v}_0^*}{\partial z_0} \cdot \underline{n}_0\right) = \frac{\partial Z_1}{\partial t_0} \tag{C.2}$$

which becomes

$$-v_{x0} Z_{x1} + v_{z1} + Z_1 \underbrace{\frac{\partial v_{z0}}{\partial z_0}}_{0} = -v_{x0}^* Z_{x1} + v_{z1}^* + Z_1 \underbrace{\frac{\partial v_{z0}^*}{\partial z_0}}_{0} = \frac{\partial Z_1}{\partial t_0} \tag{C.3}$$

Equation (C.3) reduces to

$$v_{z1} - v_{x0} Z_{x1} = v_{z1}^* - v_{x0}^* Z_{x1} = \frac{\partial Z_1}{\partial t_0} \tag{C.4}$$

When the no-slip condition at the interface, $\underline{v} \cdot \underline{t} = \underline{v}^* \cdot \underline{t}$, i.e. Equation (3.74), is expanded in Taylor series as

$$\left[\underline{v}_0 + \epsilon\left(\underline{v}_1 + Z_1\frac{\partial \underline{v}_0}{\partial z_0}\right)\right]\cdot\left(\underline{t}_0 + \epsilon\underline{t}_1\right) = \left[\underline{v}_0^* + \epsilon\left(\underline{v}_1^* + Z_1\frac{\partial \underline{v}_0^*}{\partial z_0}\right)\right]\cdot\left(\underline{t}_0 + \epsilon\underline{t}_1\right) \quad \text{(C.5)}$$

Grouping the first order terms, gives

$$\underline{v}_0\cdot\underline{t}_1 + \underline{v}_1\cdot\underline{t}_0 + Z_1\frac{\partial \underline{v}_0}{\partial z_0}\cdot\underline{t}_0 = \underline{v}_0^*\cdot\underline{t}_1 + \underline{v}_1^*\cdot\underline{t}_0 + Z_1\frac{\partial \underline{v}_0^*}{\partial z_0}\cdot\underline{t}_0 \quad \text{(C.6)}$$

Applying the unit vectors, Equation (C.6) becomes

$$\underbrace{v_{z0}}_{0}Z_{x1} + v_{x1} + Z_1\frac{\partial v_{x0}}{\partial z_0} = \underbrace{v_{z0}^*}_{0}Z_{x1} + v_{x1}^* + Z_1\frac{\partial v_{x0}^*}{\partial z_0} \quad \text{(C.7)}$$

Using the base state solution, Equation (C.7) becomes

$$v_{x1} + Z_1\frac{\partial v_{x0}}{\partial z_0} = v_{x1}^* + Z_1\frac{\partial v_{x0}^*}{\partial z_0} \quad \text{(C.8)}$$

The continuity of the electric field at the interface, $\underline{E}\cdot\underline{t} = \underline{E}^*\cdot\underline{t}$, i.e. Equation (3.75) is expressed as

$$-\left(\frac{\partial V}{\partial x}\underline{e}_x + \frac{\partial V}{\partial z}\underline{e}_z\right)\cdot\left(\frac{\underline{e}_x + Z_x\,\underline{e}_z}{\sqrt{1+(Z_x)^2}}\right) = -\left(\frac{\partial V^*}{\partial x}\underline{e}_x + \frac{\partial V^*}{\partial z}\underline{e}_z\right)\cdot\left(\frac{\underline{e}_x + Z_x\,\underline{e}_z}{\sqrt{1+(Z_x)^2}}\right) \quad \text{(C.9)}$$

giving

$$\frac{\partial V}{\partial x} + \frac{\partial V}{\partial z}Z_x = \frac{\partial V^*}{\partial x} + \frac{\partial V^*}{\partial z}Z_x \quad \text{(C.10)}$$

Expanding this equation and grouping the first order terms give

$$\frac{\partial V_1}{\partial x_0} + Z_1\underbrace{\frac{\partial^2 V_0}{\partial x_0\partial z_0}}_{0} + Z_{x1}\frac{\partial V_0}{\partial z_0} = \frac{\partial V_1^*}{\partial x_0} + Z_1\underbrace{\frac{\partial^2 V_0^*}{\partial x_0\partial z_0}}_{0} + Z_{x1}\frac{\partial V_0^*}{\partial z_0} \quad \text{(C.11)}$$

which becomes

$$\frac{\partial V_1}{\partial x_0} + Z_{x1}\frac{\partial V_0}{\partial z_0} = \frac{\partial V_1^*}{\partial x_0} + Z_{x1}\frac{\partial V_0^*}{\partial z_0} \tag{C.12}$$

For the Gauss' law, $= \varepsilon^* \underline{E}^* \cdot \underline{n} - \varepsilon \underline{E} \cdot \underline{n}$, i.e. Equation (3.76), the perturbed equation can be written as

$$q_1 + Z_1\frac{\partial q_0}{\partial z_0} = \varepsilon^*\left\{\left(\underline{E_1^*} + Z_1\frac{\partial \underline{E_0^*}}{\partial z_0}\right)\cdot \underline{n}_0 + \left(\underline{E_0^*}\cdot \underline{n}_1\right)\right\} - \varepsilon\left\{\left(\underline{E_1} + Z_1\frac{\partial \underline{E_0}}{\partial z_0}\right)\cdot \underline{n}_0 + \left(\underline{E_0}\cdot \underline{n}_1\right)\right\} \tag{C.13}$$

where

$$\underline{E_1} = -\frac{\partial}{\partial x_0}\left(V_1 + Z_1\frac{\partial V_0}{\partial z_0}\right)\underline{e}_{x0} - \frac{\partial}{\partial z_0}\left(V_1 + Z_1\frac{\partial V_0}{\partial z_0}\right)\underline{e}_{z0} \tag{C.14}$$

Substituting $\underline{E_0}$, Equation (B.14), and $\underline{E_1}$, Equation (C.14), into Equation (C.13) gives

$$\begin{aligned} q_1 + Z_1\underbrace{\frac{\partial q_0}{\partial z_0}}_{0} = {} & \varepsilon^*\left\{\left(-\frac{\partial}{\partial x_0}\left(V_1^* + Z_1\frac{\partial V_0^*}{\partial z_0}\right)\underline{e}_{x0} - \frac{\partial}{\partial z_0}\left(V_1^* + Z_1\frac{\partial V_0^*}{\partial z_0}\right)\underline{e}_{z0}\right)\cdot \underline{e}_{z0}\right. \\ & \left. + \left(-\frac{\partial V_0^*}{\partial z_0}\underline{e}_{z0}\cdot -Z_{x1}\,\underline{e}_{x0}\right)\right\} \\ & - \varepsilon\left\{\left(-\frac{\partial}{\partial x_0}\left(V_1 + Z_1\frac{\partial V_0}{\partial z_0}\right)\underline{e}_{x0} - \frac{\partial}{\partial z_0}\left(V_1 + Z_1\frac{\partial V_0}{\partial z_0}\right)\underline{e}_{z0}\right)\cdot \underline{e}_{z0}\right. \\ & \left. + \left(-\frac{\partial V_0}{\partial z_0}\underline{e}_{z0}\cdot -Z_{x1}\,\underline{e}_{x0}\right)\right\} \end{aligned} \tag{C.15}$$

and taking the dot products and using the base sate solution, Equation (C.15) reduces to

$$q_1 = \varepsilon^*\left(-\frac{\partial V_1^*}{\partial z_0}\right) - \varepsilon\left(-\frac{\partial V_1}{\partial z_0}\right) \tag{C.16}$$

The charge distribution at the interface, $q_t - \underline{u}\cdot\nabla_s q + \nabla_s\cdot q\underline{u}_s + q2H\underline{u}\cdot\underline{n} = S(\underline{E}\cdot\underline{n} - \sigma_r\underline{E}^*\cdot\underline{n})$, i.e. Equation (3.78), in perturbed state is

$$\frac{\partial q_1}{\partial t_0} - v_{x0}\frac{\partial q_1}{\partial x_0} + q_0\frac{\partial v_{x1}}{\partial x_0} = S\left(\sigma_r\left(\frac{\partial V_1^*}{\partial z_0} - \frac{\partial V_0^*}{\partial x_0}Z_{x1}\right) - \left(\frac{\partial V_1}{\partial z_0} - \frac{\partial V_0}{\partial x_0}Z_{x1}\right)\right) \quad \text{(C.17)}$$

Substituting the base state solutions for the voltage, i.e., Equations (B.44) and (B.45) into (C.17), the perturbed charge distribution equation reduces to

$$\frac{\partial q_1}{\partial t_0} - v_{x0}\frac{\partial q_1}{\partial x_0} + q_0\frac{\partial v_{x1}}{\partial x_0} = S\left(\sigma_r\frac{\partial V_1^*}{\partial z_0} - \frac{\partial V_1}{\partial z_0}\right) \quad \text{(C.18)}$$

For the NSB, to find the ϵ^1 order perturbation, Equation (3.85) is written in parts as

$$\underbrace{\left(-p\underline{\underline{I}}\cdot\underline{n}\cdot\underline{n}\right)}_{1} + \underbrace{\left(\underline{\underline{\tau}}\cdot\underline{n}\cdot\underline{n}\right)}_{2} + \varepsilon E_b\left(\underbrace{\left(\underline{E}\,\underline{E}\cdot\underline{n}\cdot\underline{n}\right)}_{3} + \underbrace{\left(-\frac{1}{2}\left|\underline{E}\right|^2\underline{\underline{I}}\right)\cdot\underline{n}\cdot\underline{n}}_{4}\right)$$
$$= \left(-p^*\underline{\underline{I}}\cdot\underline{n}\cdot\underline{n}\right) + \underbrace{\left(M2\underline{\underline{D}}^*\cdot\underline{n}\cdot\underline{n}\right)}_{5} + \varepsilon^* E_b\left(\underline{E}^*\underline{E}^* - \frac{1}{2}\left|\underline{E}^*\right|^2\underline{\underline{I}}\right)\cdot\underline{n}\cdot\underline{n} + \underbrace{\frac{1}{Ca}2H}_{6}$$

Part 1: The perturbed expression is

$$-(p_1 + Z_1\frac{\partial p_0}{\partial z_0})\underline{\underline{I}}\cdot\underline{n}_0\cdot\underline{n}_0 + p_0\underbrace{\underline{\underline{I}}\cdot\underline{n}_1\cdot\underline{n}_0}_{0} + p_0\underbrace{\underline{\underline{I}}\cdot\underline{n}_0\cdot\underline{n}_1}_{0}$$
$$= -\left(p_1 + Z_1\frac{\partial p_0}{\partial z_0}\right)$$

Part 2: The perturbed expression is

$$\left(\left(\underline{\underline{\tau}}_1 + Z_1\frac{\partial\underline{\underline{\tau}}_0}{\partial z_0}\right)\cdot\underline{n}_0\cdot\underline{n}_0 + \underline{\underline{\tau}}_0\cdot\underline{n}_1\cdot\underline{n}_0 + \underline{\underline{\tau}}_0\cdot\underline{n}_0\cdot\underline{n}_1\right)$$

$$= \left(\tau_{zz1} + Z_1 \underbrace{\frac{\partial \tau_{zz0}}{\partial z_0}}_{0} \right) + (-Z_{x1}\tau_{xz0}) + (-Z_{x1}\tau_{xz0})$$

$$= \tau_{zz1} - 2Z_{x1}\tau_{xz0}$$

Part 3: The perturbed expression is

$$\underline{E}_0\underline{E}_0 \cdot \underbrace{\underline{n}_0 \cdot \underline{n}_1}_{0} + \underline{E}_0\underline{E}_0 \cdot \underbrace{\underline{n}_1 \cdot \underline{n}_0}_{0} + \left(\underline{E}_1 + Z_1 \frac{\partial \underline{E}_0}{\partial z_0} \right) \underline{E}_0 \cdot \underline{n}_0 \cdot \underline{n}_0 + \underline{E}_0 \left(\underline{E}_1 + Z_1 \frac{\partial \underline{E}_0}{\partial z_0} \right) \cdot \underline{n}_0 \cdot \underline{n}_0$$

which becomes

$$\left(\frac{\partial V_0}{\partial z_0}\frac{\partial V_1}{\partial z_0} + \frac{\partial V_0}{\partial z_0} Z_1 \underbrace{\frac{\partial^2 V_0}{\partial {z_0}^2}}_{0} \right) + \left(\frac{\partial V_0}{\partial z_0}\frac{\partial V_1}{\partial z_0} + \frac{\partial V_0}{\partial z_0} Z_1 \underbrace{\frac{\partial^2 V_0}{\partial {z_0}^2}}_{0} \right)$$

$$= 2\frac{\partial V_0}{\partial z_0}\frac{\partial V_1}{\partial z_0}$$

Part 4: The perturbed expression is

$$-\frac{1}{2}\left(\underbrace{\underline{E}_0 \cdot \underline{n}_0 \cdot \underline{n}_1}_{0} + \underbrace{\underline{E}_0 \cdot \underline{n}_1 \cdot \underline{n}_0}_{0} + \left(\underline{E}_1 + Z_1 \underbrace{\frac{\partial \underline{E}_0}{\partial z_0}}_{0} \right) \cdot \underline{n}_0 \cdot \underline{n}_0 \right)$$

which turns out to be

$$-\frac{1}{2}\left(2\frac{\partial V_0}{\partial z_0}\frac{\partial V_1}{\partial z_0} \right)$$

$$= -\frac{\partial V_0}{\partial z_0}\frac{\partial V_1}{\partial z_0}$$

Part 5: The perturbed expression is

$$M\left(2\underline{\underline{D_0^*}}\cdot\underline{n}_0\cdot\underline{n}_1+2\underline{\underline{D_0^*}}\cdot\underline{n}_1\cdot\underline{n}_0+\left(2\underline{\underline{D_1^*}}+Z_1\frac{\partial 2\underline{\underline{D_0^*}}}{\partial z_0}\right)\cdot\underline{n}_0\cdot\underline{n}_0\right)$$

where

$$2\underline{\underline{D^*}}=2\frac{\partial v_x^*}{\partial x}\underline{e}_x\underline{e}_x+\left(\frac{\partial v_x^*}{\partial z}+\frac{\partial v_z^*}{\partial x}\right)\left(\underline{e}_x\underline{e}_z+\underline{e}_z\underline{e}_x\right)+2\frac{\partial v_z^*}{\partial z}\underline{e}_z\underline{e}_z \tag{C.19}$$

So

$$2\underline{\underline{D_0^*}}=\frac{\partial v_{x0}^*}{\partial z_0}\underline{e}_{x0}\underline{e}_{z0}+\frac{\partial v_{x0}^*}{\partial z_0}\underline{e}_{z0}\underline{e}_{x0} \tag{C.20}$$

and

$$2\underline{\underline{D_1^*}}=$$

$$2\frac{\partial}{\partial x_0}\left(v_{x1}^*+Z_1\frac{\partial v_{x0}^*}{\partial z_0}\right)\underline{e}_{x0}\underline{e}_{x0}+\left(\frac{\partial}{\partial z_0}\left(v_{x1}^*+Z_1\frac{\partial v_{x0}^*}{\partial z_0}\right)+\frac{\partial}{\partial x_0}\left(v_{z1}^*+Z_1\frac{\partial v_{z0}^*}{\partial z_0}\right)\right)\underline{e}_{x0}\underline{e}_{z0}$$

$$+\left(\frac{\partial}{\partial z_0}\left(v_{x1}^*+Z_1\frac{\partial v_{x0}^*}{\partial z_0}\right)+\frac{\partial}{\partial x_0}\left(v_{z1}^*+Z_1\frac{\partial v_{z0}^*}{\partial z_0}\right)\right)\underline{e}_{z0}\underline{e}_{x0}+2\frac{\partial}{\partial z_0}\left(v_{z1}^*+Z_1\frac{\partial v_{z0}^*}{\partial z_0}\right)\underline{e}_{z0}\underline{e}_{z0} \tag{C.21}$$

Then, part 5 becomes

$$M\left(-2Z_{x1}\frac{\partial v_{x0}^*}{\partial z_0}+2\frac{\partial v_{z1}^*}{\partial z_0}\right)$$

Part 6: The perturbed expression is

$$\frac{1}{Ca}\left(2H_1+Z_1\frac{\partial\overset{0}{\widetilde{2H_0}}}{\partial z_0}\right)$$

$$= \frac{2H_1}{Ca} = \frac{Z_{xx1}}{Ca}$$

Finally, the NSB is found to be

$$-\left(p_1 + Z_1 \frac{\partial p_0}{\partial z_0}\right) + \tau_{zz1} - 2Z_{x1}\tau_{xz0} + \varepsilon E_b \left(2\frac{\partial V_0}{\partial z_0}\frac{\partial V_1}{\partial z_0} - \frac{\partial V_0}{\partial z_0}\frac{\partial V_1}{\partial z_0}\right) =$$

$$-\left(p_1^* + Z_1 \frac{\partial p_0^*}{\partial z_0}\right) + M\left(-2Z_{x1}\frac{\partial v_{x0}^*}{\partial z_0} + 2\frac{\partial v_{z1}^*}{\partial z_0}\right) + \varepsilon^* E_b \left(2\frac{\partial V_0^*}{\partial z_0}\frac{\partial V_1^*}{\partial z_0} - \frac{\partial V_0^*}{\partial z_0}\frac{\partial V_1^*}{\partial z_0}\right) + \frac{Z_{xx1}}{Ca} \tag{C.22}$$

As it is known from the base state NSB, Equation (B.24), that the base state pressures of the two fluids are equal, Equation (C.22) reduces to

$$-p_1 + \tau_{zz1} - 2Z_{x1}\tau_{xz0} + \varepsilon E_b \left(\frac{\partial V_0}{\partial z_0}\frac{\partial V_1}{\partial z_0}\right) =$$

$$-p_1^* + M\left(-2Z_{x1}\frac{\partial v_{x0}^*}{\partial z_0} + 2\frac{\partial v_{z1}^*}{\partial z_0}\right) + \varepsilon^* E_b \left(\frac{\partial V_0^*}{\partial z_0}\frac{\partial V_1^*}{\partial z_0}\right) + \frac{Z_{xx1}}{Ca} \tag{C.23}$$

APPENDIX D: REORGANIZED EQUATIONS FOR MATLAB CODING

In this section, the perturbed equations, which are rearranged for the MATLAB program are presented. The order of the equations is as in the MATLAB code.

Equation 1: The x-component of the equation of motion for the first fluid, Equation (3.121), at $-1 < z_0 < 0$,

$$(ikRev_{x0})\hat{v}_{x1} + \left(Re\frac{dv_{x0}}{dz_0}\right)\hat{v}_{z1} + (ik)\hat{P}_1 + (-ik)\hat{\tau}_{xx1} + (-D)\hat{\tau}_{xz1} = \omega\,[\,(-Re)\hat{v}_{x1}\,] \tag{D.1}$$

Here, $D = \frac{d}{dz_0}$,

Equation 2: The z-component of the equation of motion for the first fluid, Equation (3.122), $-1 < z_0 < 0$,

$$(ikRev_{x0})\hat{v}_{z1} + (D)\hat{P}_1 + (-ik)\hat{\tau}_{xz1} + (-D)\hat{\tau}_{zz1} = \omega\,[(-Re)\hat{v}_{z1}\,] \tag{D.2}$$

Equation 3: The continuity equation for the first fluid, Equation (3.123), at $-1 < z_0 < 0$,

$$(ik)\hat{v}_{x1} + (D)\hat{v}_{z1} = 0 \tag{D.3}$$

Equation 4: The x-component of the equation of motion for the second fluid, Equation (3.133), at $0 < z_0 < Hr$,

$$\begin{aligned}(ikRePv^*_{x0} + Mk^2 - MD^2)\hat{v}^*_{x1} + \left(ikReP\frac{dv_{x0}}{dz_0}\right)\hat{v}^*_{z1} + (ik)\hat{P}^*_1 \\ = \omega\,[\,(-ReP)\hat{v}^*_{x1}]\end{aligned} \tag{D.4}$$

Equation 5: The z-component of the equation of motion for the second fluid, Equation (3.134), at $0 < \mathrm{z}_0 < Hr$,

$$(ikRePv_{x0}^{*} + Mk^2 - MD^2)\hat{v}_{z1}^{*} + (D)\hat{P}_1^{*} = \omega\,[\,(-ReP)\hat{v}_{z1}^{*}\,] \tag{D.5}$$

Equation 6: The continuity equation for the second fluid, Equation (3.135), at $0 < \mathrm{z}_0 < Hr$,

$$(ik)\hat{v}_{x1}^{*} + (D)\hat{v}_{z1}^{*} = 0 \tag{D.6}$$

Equation 7: The Laplace equation for the first fluid, Equation (3.124), $-1 < \mathrm{z}_0 < Z(x,t)$,

$$(D^2 - k^2)\hat{V}_1 = 0 \tag{D.7}$$

Equation 8: The Laplace equation for the second fluid, Equation (3.136), at $0 < \mathrm{z}_0 < Hr$,

$$(D^2 - k^2)\hat{V}_1^{*} = 0 \tag{D.8}$$

Equation 9: The normal velocity of the first fluid is equal to normal speed of the interface, Equation (3.148), (An equation for $\hat{Z}_1$) at $\mathrm{z}_0 = 0$,

$$(1)\hat{v}_{z1} + (-ikv_{x0})\hat{Z}_1 = \omega\,[\,(1)\hat{Z}_1\,] \tag{D.9}$$

Equation 10: The charge balance, Equation (3.152), at $\mathrm{z}_0 = 0$,

$$(ikq_0)\hat{v}_{x1} + (SD)\hat{V}_1 + (ikv_{x0})\hat{q}_1 + (-\sigma_r SD)\hat{V}_1^{*} = \omega\,[\,(-1)\hat{q}_1\,] \tag{D.10}$$

Equation 11: The equation for the stress component-1, $\hat{\tau}_{xx}$, Equation(3.128), at $-1 < \mathrm{z}_0 < 0$,

$$(-2Weik\tau_{xx0} - 2We\tau_{xz0}D - 2ik)\hat{v}_{x1} + \left(\frac{d\tau_{xx0}}{d\mathrm{z}_0}We\right)\hat{v}_{z1}$$
$$+(1 + Weikv_{x0})\hat{\tau}_{xx1} + \left(-2We\frac{dv_{x0}}{d\mathrm{z}_0}\right)\hat{\tau}_{xz1} = \omega\,[\,(-We)\hat{\tau}_{xx1}\,] \tag{D.11}$$

Equation 12: The Equation for stress component-2, $\hat{\tau}_{xz}$, Equation (3.129), at $-1 < \mathrm{z}_0 < 0$,

$$(-D)\hat{v}_{x1} + \left(-ik - Weik\tau_{xx0} + \frac{d\tau_{xz0}}{dz_0}We\right)\hat{v}_{z1} + (1 + Weikv_{x0})\hat{\tau}_{xz1} + \left(-We\frac{dv_{x0}}{dz_0}\right)\hat{\tau}_{zz1} = \omega\,[\,(-We)\,\hat{\tau}_{xz1}] \quad \text{(D.12)}$$

Equation 13: The Equation for stress component-3, $\hat{\tau}_{zz}$, Equation (3.130), at -1 < z_0 < 0,

$$(-We2ik\tau_{xz0} - 2D)\hat{v}_{z1} + (1 + Weikv_{x0})\hat{\tau}_{zz1} = \omega\,[\,(-We)\hat{\tau}_{zz1}\,] \quad \text{(D.13)}$$

The boundary and interface conditions rearranged for the MATLAB program as below.

BC1: The no-slip at the bottom wall, Equation (3.142), at $z_0 = -1$,

$$(1)\hat{v}_{x1} = 0 \quad \text{(D.14)}$$

BC2: The no-flow through the wall, Equation (3.143), at $z_0 = -1$,

$$(1)\hat{v}_{z1} = 0 \quad \text{(D.15)}$$

BC3: The constant voltage at the bottom wall, Equation (3.144), at $z_0 = -1$,

$$(1)\hat{V}_1 = 0 \quad \text{(D.16)}$$

BC4: The no-slip at the top wall, Equation (3.145), at $z_0 = \mathrm{Hr}$,

$$(1)\hat{v}^*_{x1} = 0 \quad \text{(D.17)}$$

BC5: The no-flow through the wall, Equation (3.146), at $z_0 = \mathrm{Hr}$,

$$(1)\hat{v}^*_{z1} = 0 \quad \text{(D.18)}$$

BC6: The voltage at the top wall, Equation (3.147), at $z_0 = \mathrm{Hr}$,

$$(1)\hat{V}_1^* = 0 \tag{D.19}$$

BC7: The normal stress balance, Equation (3.153), at z_0=0,

$$\left(\varepsilon E_b \frac{dV_0}{dz_0} D\right)\hat{V}_1 + (-1)\hat{P}_1 + (1)\hat{\tau}_{zz1} + (-2MD)\hat{v}_{z1}^* + (1)\hat{P}_1^* + \left(-\varepsilon^* E_b \frac{dV_0^*}{dz_0} D\right)\hat{V}_1^* + \left(-2ik\tau_{xz0} + 2Mik\frac{dv_{x0}^*}{dz_0} + \frac{k^2}{Ca}\right)\hat{Z}_1 = 0 \tag{D.20}$$

BC8: The normal velocity of the second fluid is equal to the normal speed of the interface, Equation (3.148), at z_0=0,

$$(1)\hat{v}_{z1}^* + (-ikv_{x0}^*)\hat{Z}_1 = \omega\,[(1)\hat{Z}_1] \tag{D.21}$$

BC9: The tangential velocities of the fluids equal, Equation (3.149), at z_0=0,

$$(1)\hat{v}_{x1} + (-1)\hat{v}_{x1}^* + \left(\frac{\partial v_{x0}}{\partial z_0} - \frac{\partial v_{x0}^*}{\partial z_0}\right)\hat{Z}_1 = 0 \tag{D.22}$$

BC10: The tangential stress balance, Equation (3.154), at z_0=0,

$$\left(ik\varepsilon E_b \frac{dV_0}{dz_0}\right)\hat{V}_1 + (1)\hat{\tau}_{xz1} + (-MD)\hat{v}_{x1}^* + (-ikM)\hat{v}_{z1}^* + \left(-ik\varepsilon^* E_b \frac{dV_0^*}{dz_0}\right)\hat{V}_1^* + \left(-ik\tau_{xx0} + \frac{d\tau_{xz0}}{dz_0} - M\frac{d^2 v_{x0}^*}{{dz_0}^2} + ik\varepsilon E_b\left(\frac{dV_0}{dz_0}\right)^2 - ik\varepsilon^* E_b\left(\frac{dV_0^*}{dz_0}\right)^2\right)\hat{Z}_1 = 0 \tag{D.23}$$

BC11: The continuity of the electric field at the interface, Equation (3.150), at z_0=0,

$$(1)\hat{V}_1 + (-1)\hat{V}_1^* + \left(\frac{dV_0}{dz_0} - \frac{dV_0^*}{dz_0}\right)\hat{Z}_1 = 0 \tag{D.24}$$

BC12: The Gauss' law, Equation (3.151), at z_0=0,

$$(-\varepsilon D)\hat{V}_1 + (\varepsilon^* D)\hat{V}_1^* + (1)\hat{q}_1 = 0 \tag{D.25}$$

APPENDIX E: DISPERSION CURVES

E.1. Dispersion Curves for Two Newtonian Fluids System

In this appendix, the dispersion curves are plotted to show the effect of the Reynolds number on the stability of the system with two Newtonian fluids without an electric field. The critical wavenumber, which is the wavenumber at which the real part of the growth rate vanishes, is collected from each plot and this procedure is repeated for all Reynolds numbers. Then, these critical points are gathered to plot the neutral stability curves (See Section 4.1).

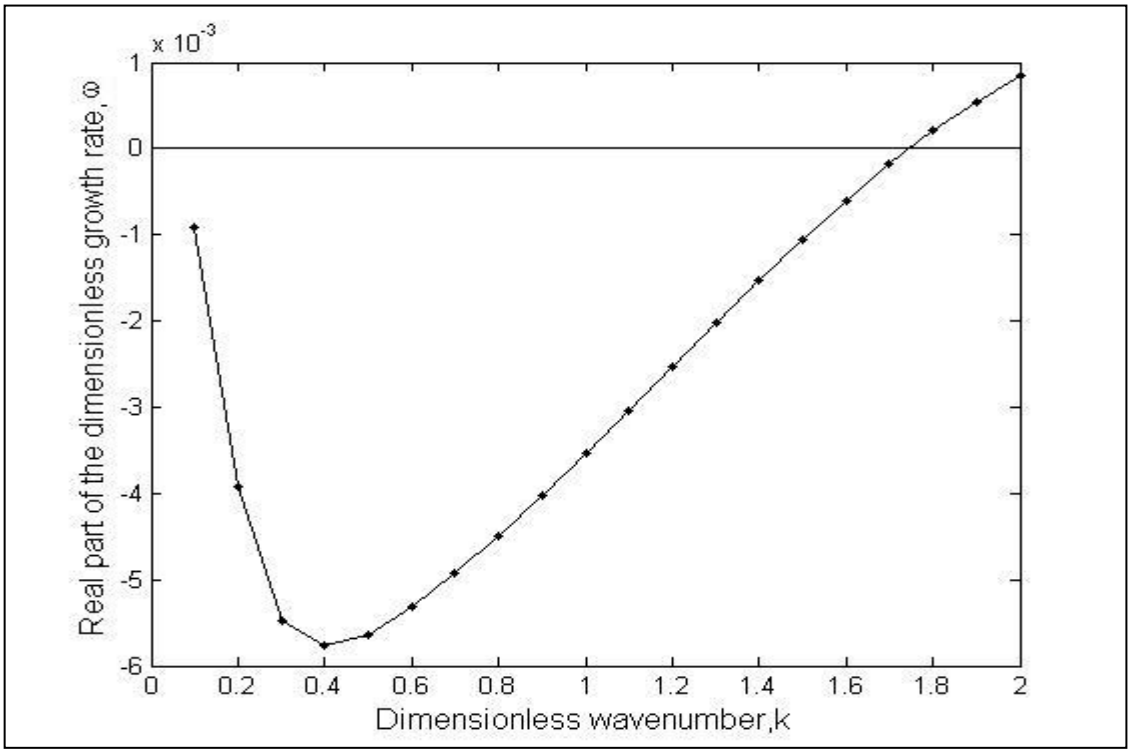

Figure E.1. Dispersion curve for Re=1.

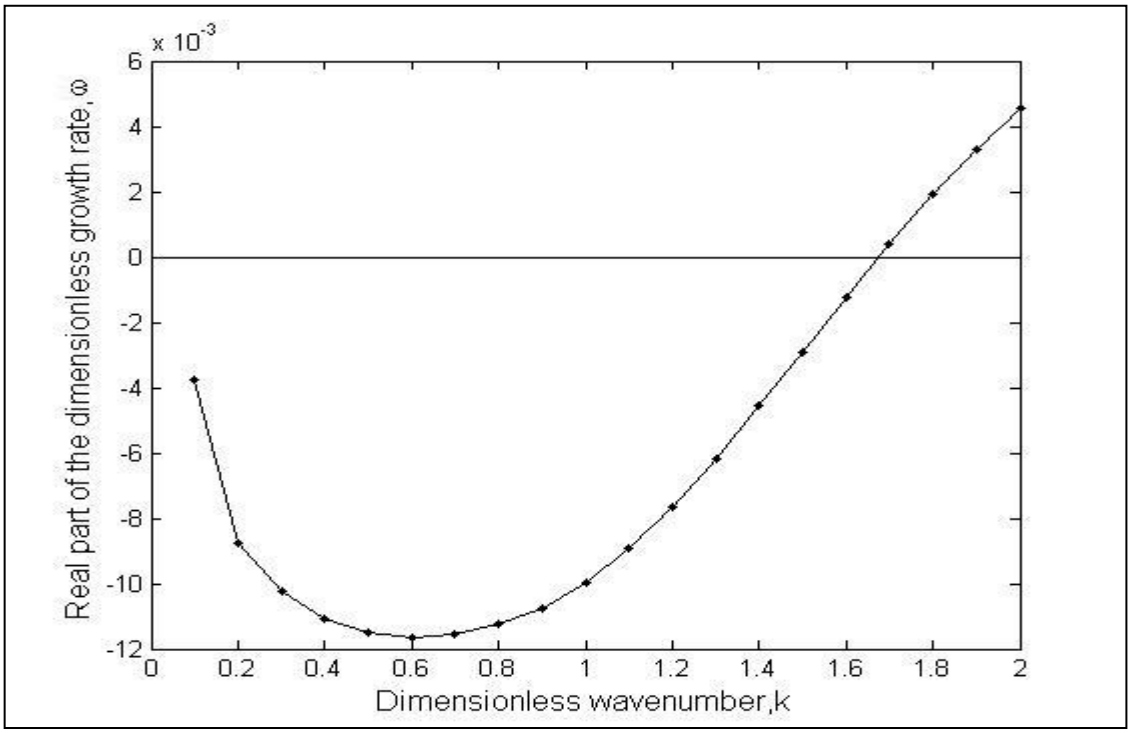

Figure E.2. Dispersion curve for Re=5.

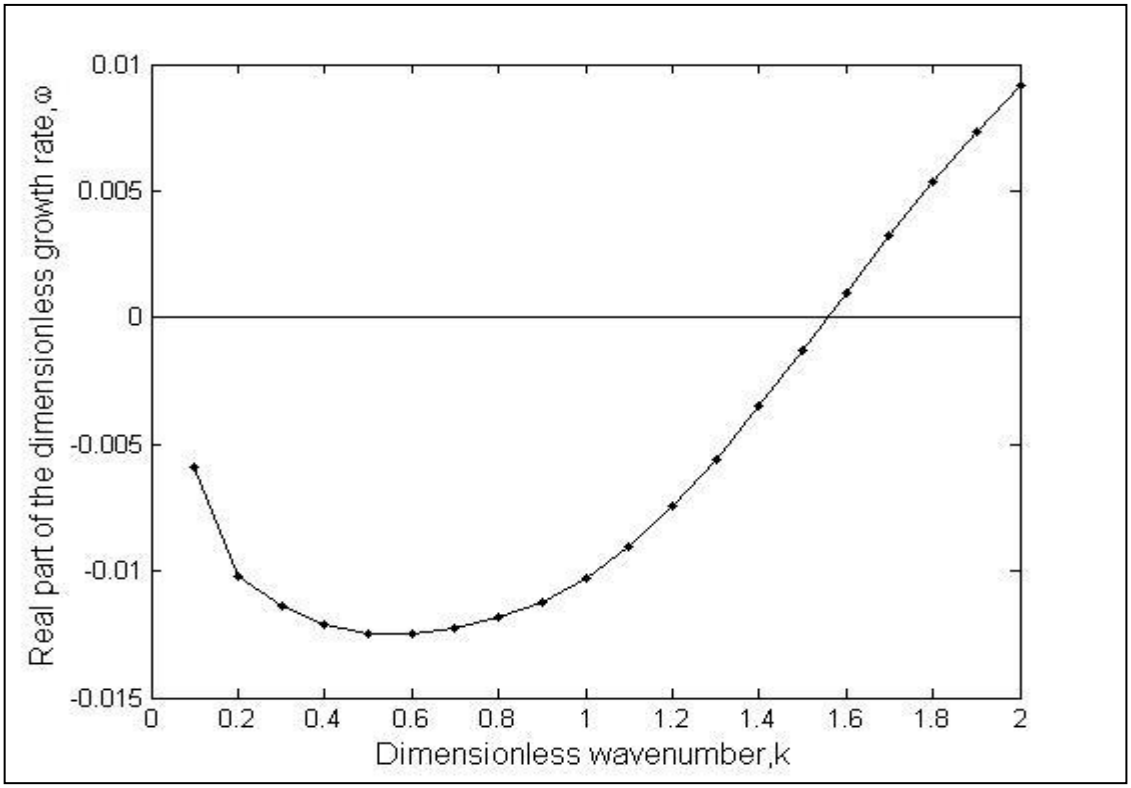

Figure E.3. Dispersion curve for Re=10.

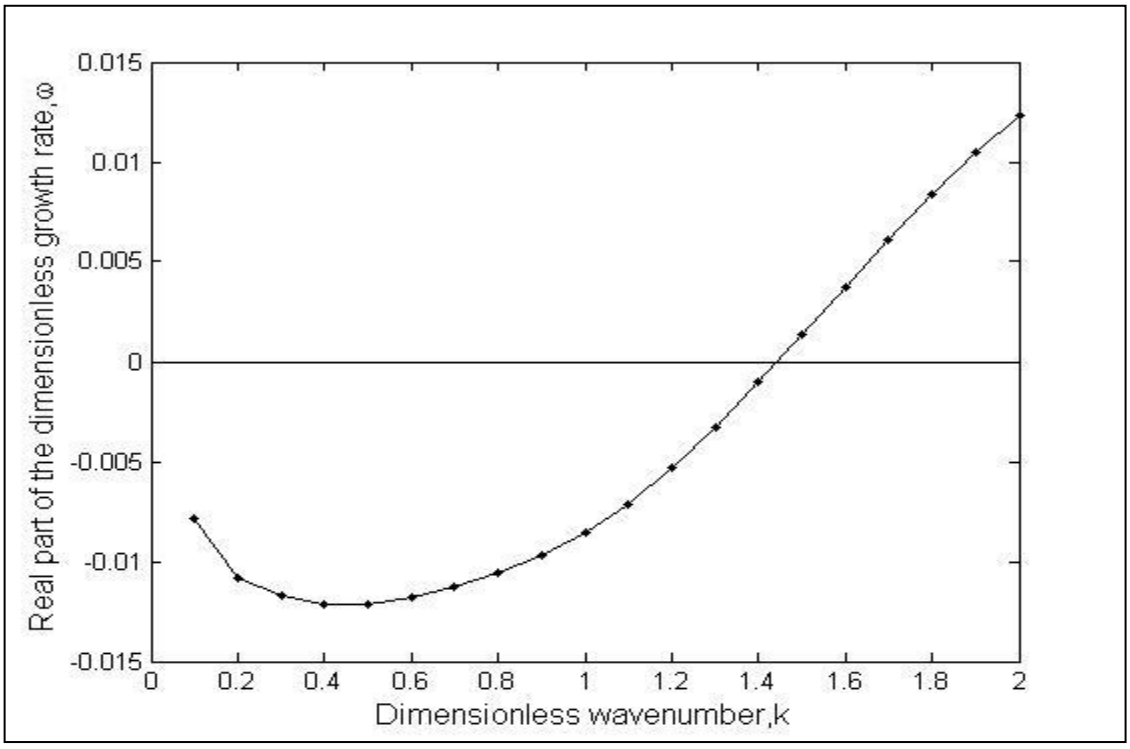

Figure E.4. Dispersion curve for Re=15.

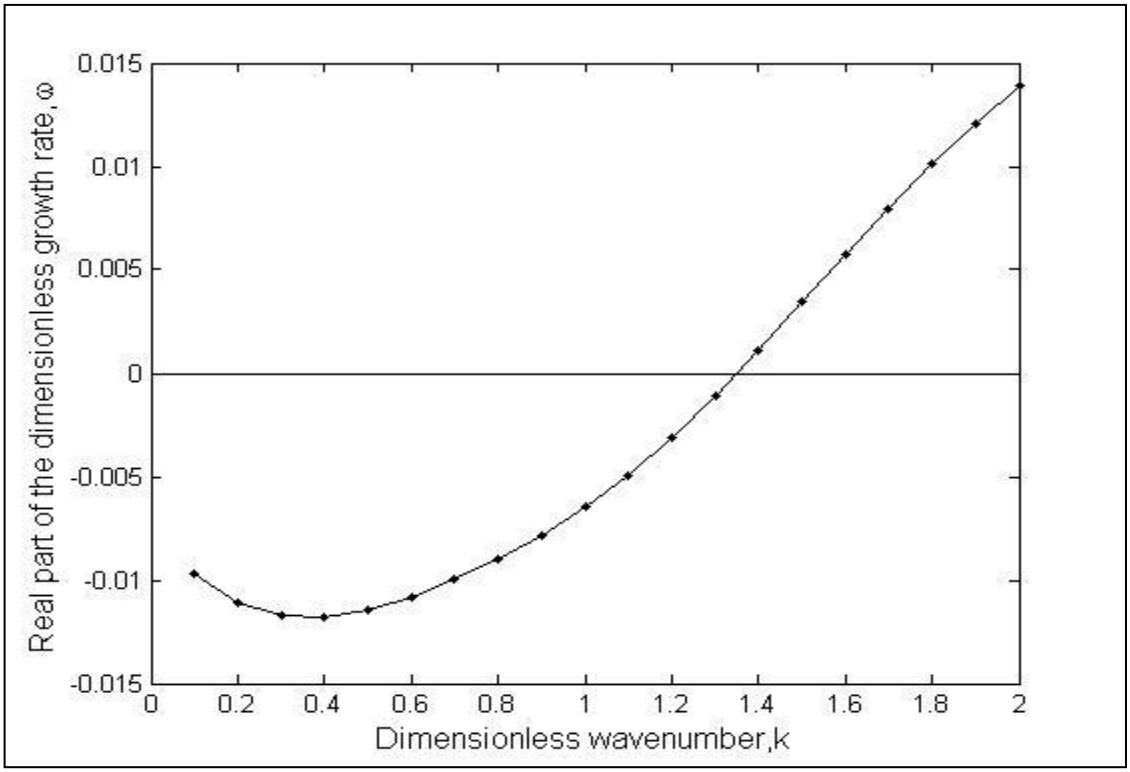

Figure E.5. Dispersion curve for Re=20.

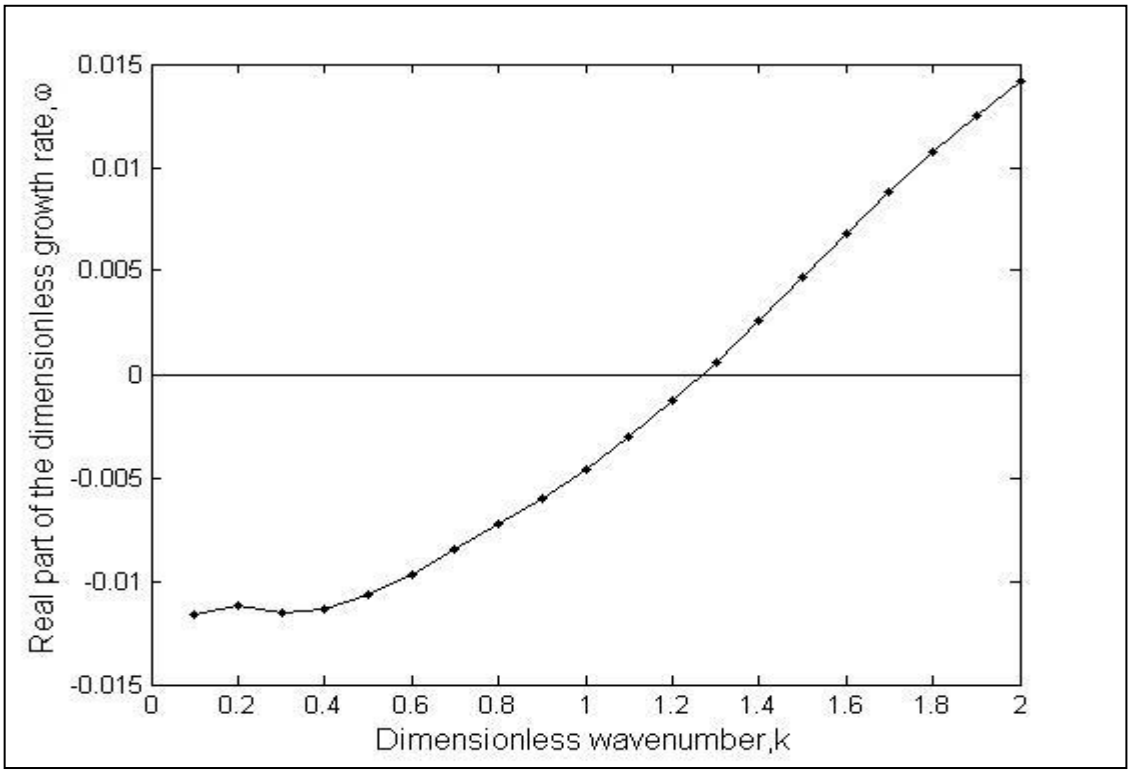

Figure E.6. Dispersion curve for Re=25.

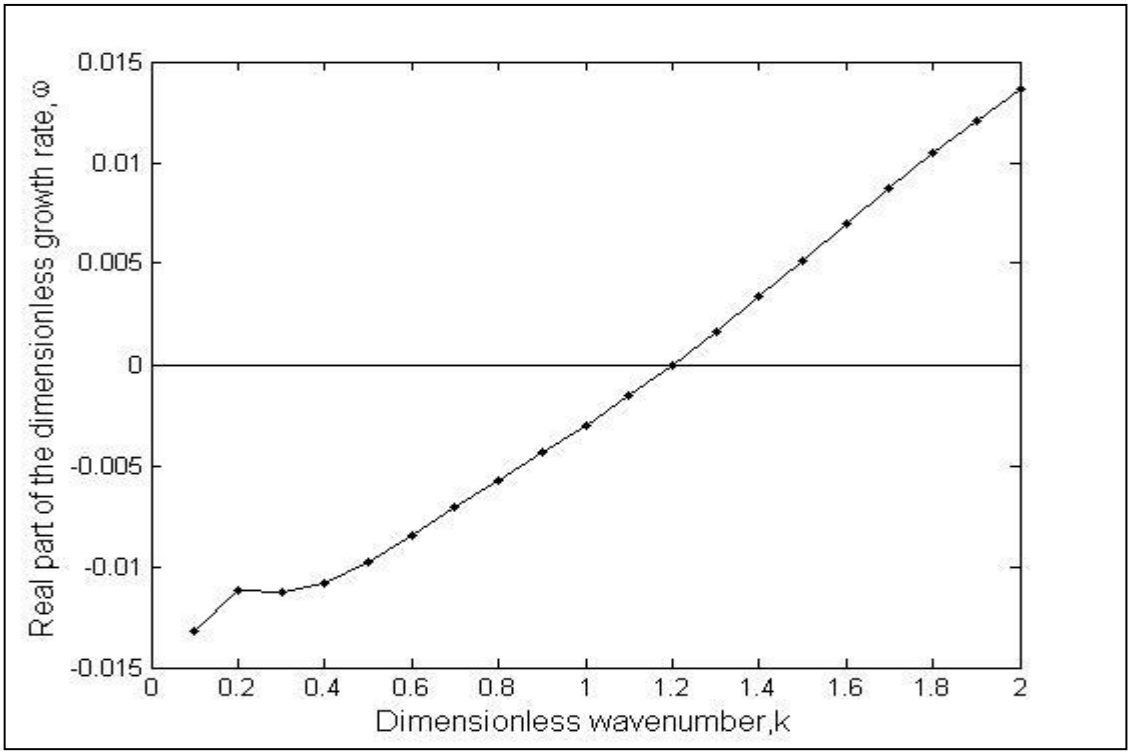

Figure E.7. Dispersion curve for Re=30.

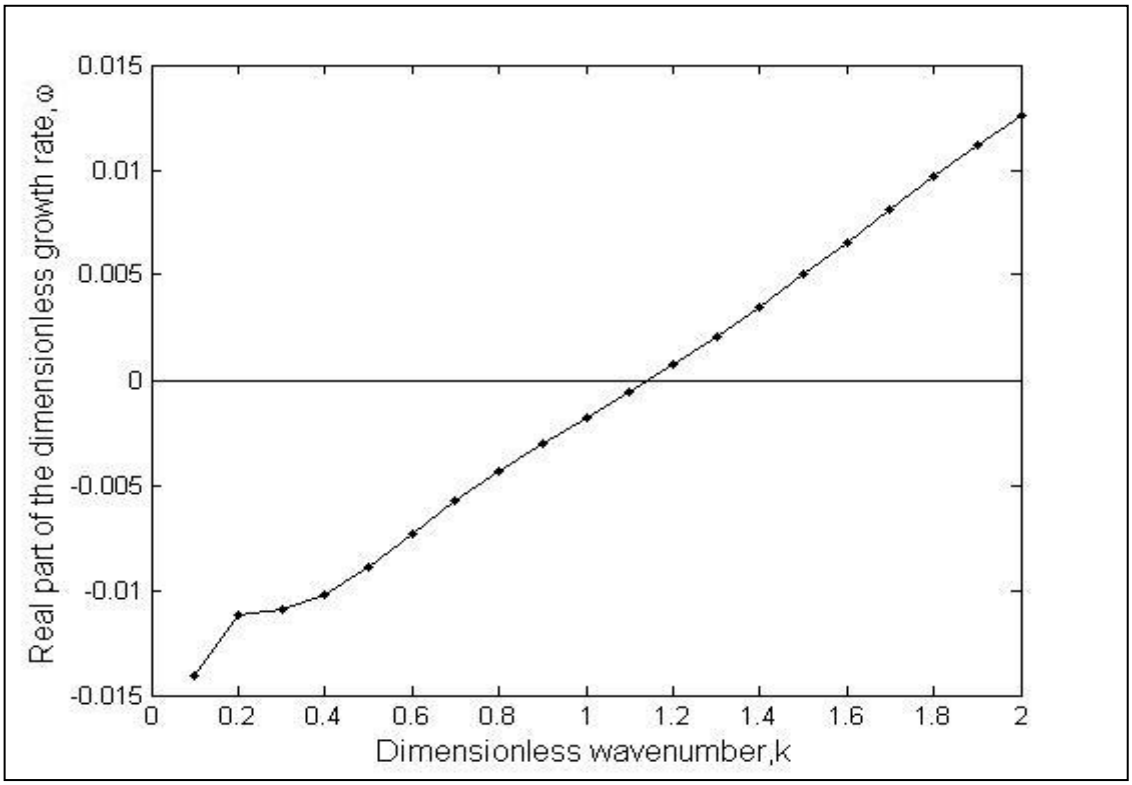

Figure E.8. Dispersion curve for Re=35.

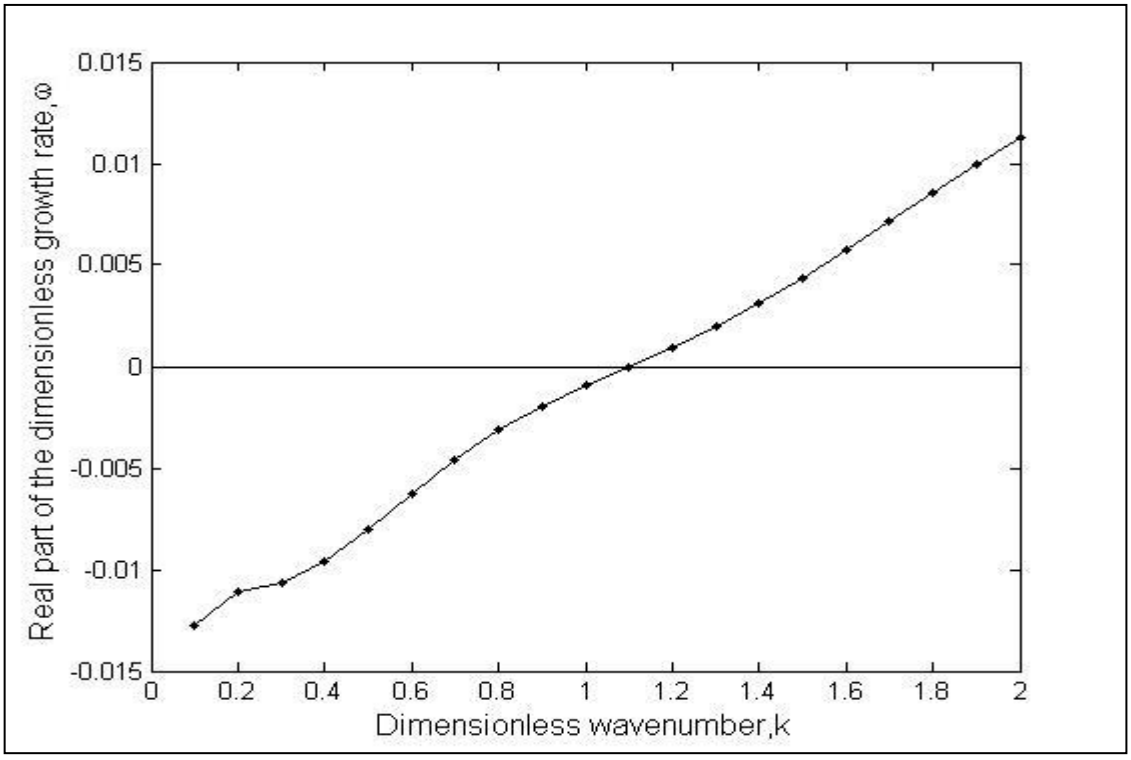

Figure E.9. Dispersion curve for Re=40.

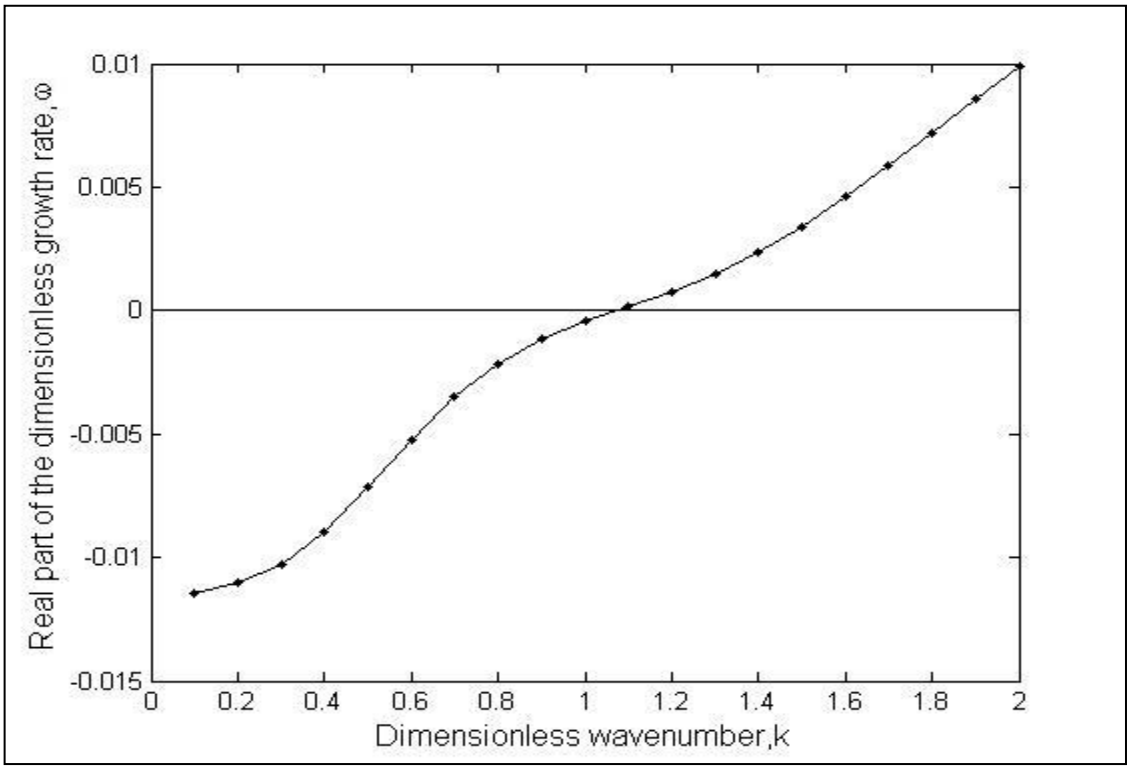

Figure E.10. Dispersion curve for Re=45.

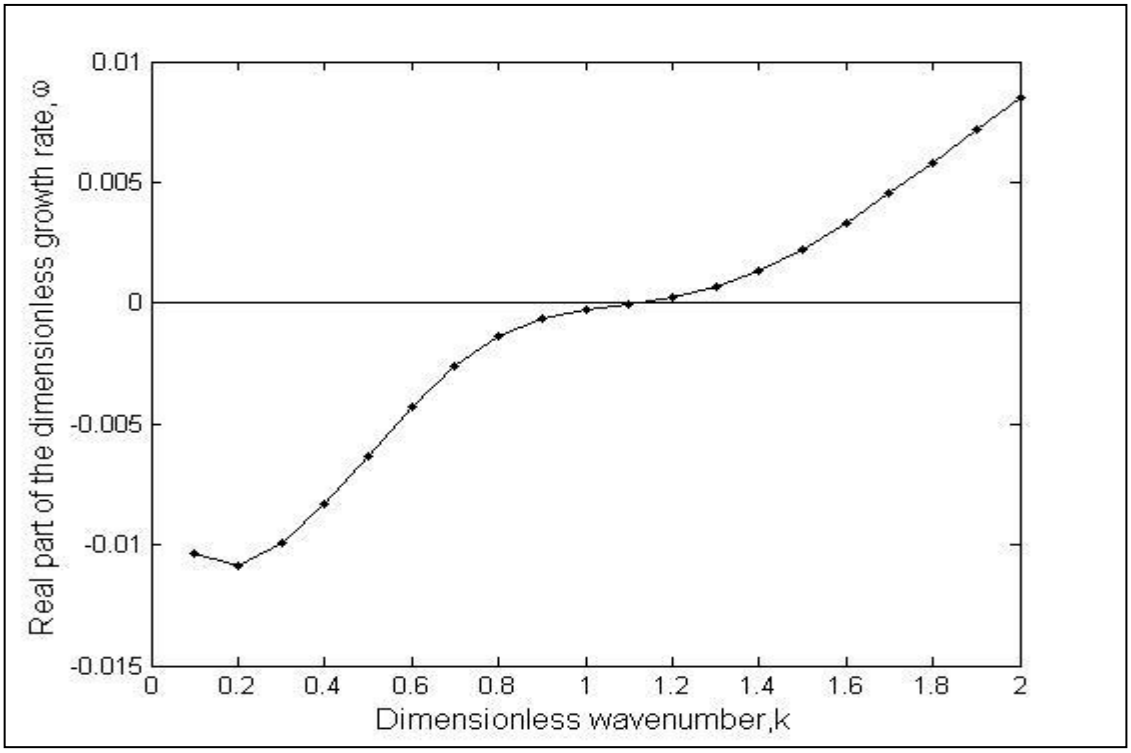

Figure E.11. Dispersion curve for Re=50.

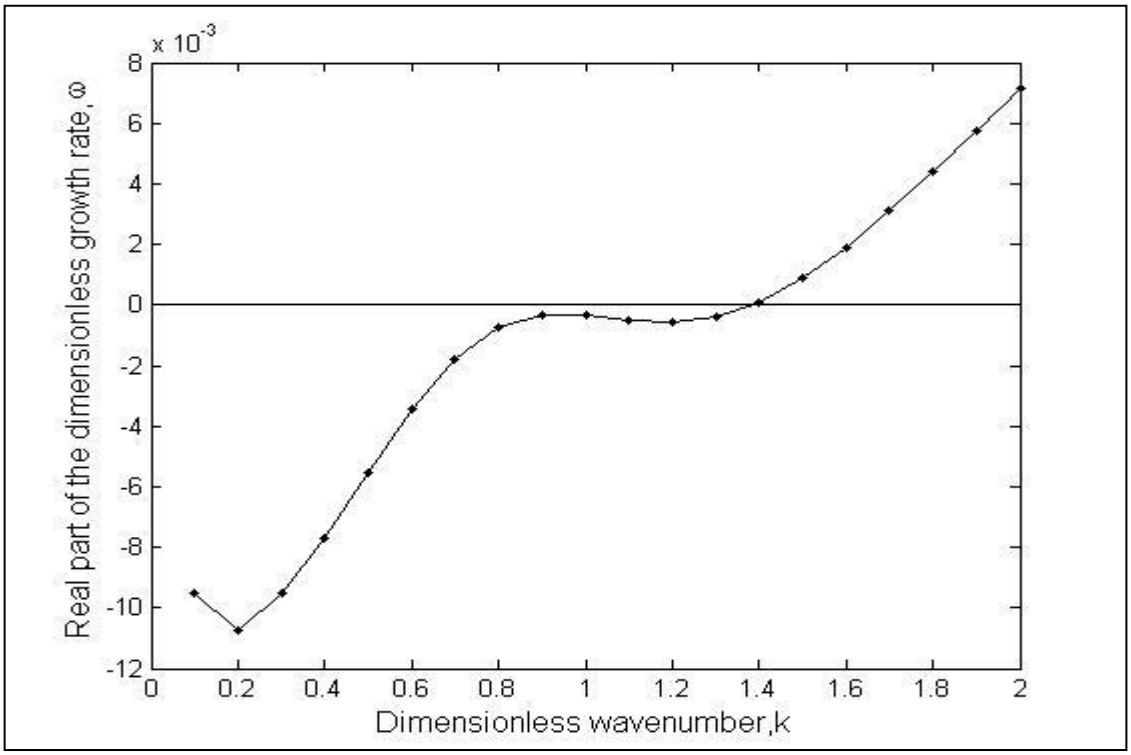

Figure E.12. Dispersion curve for Re=55.

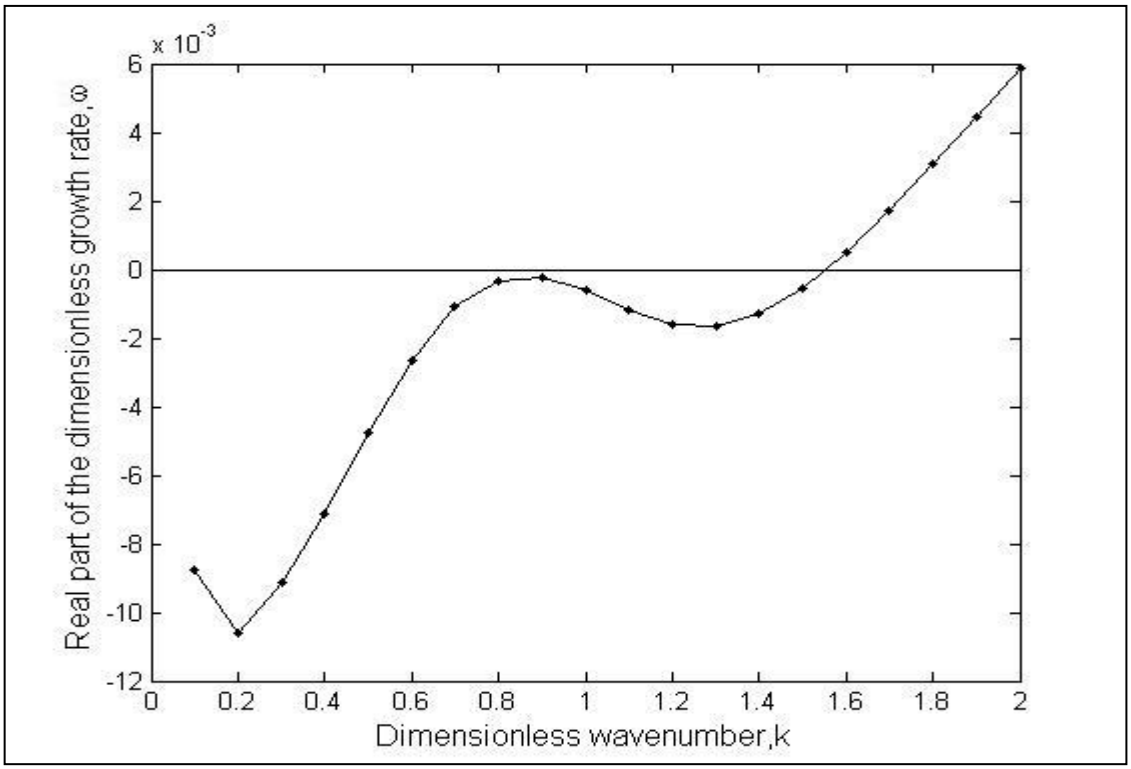

Figure E.13. Dispersion curve for Re=60.

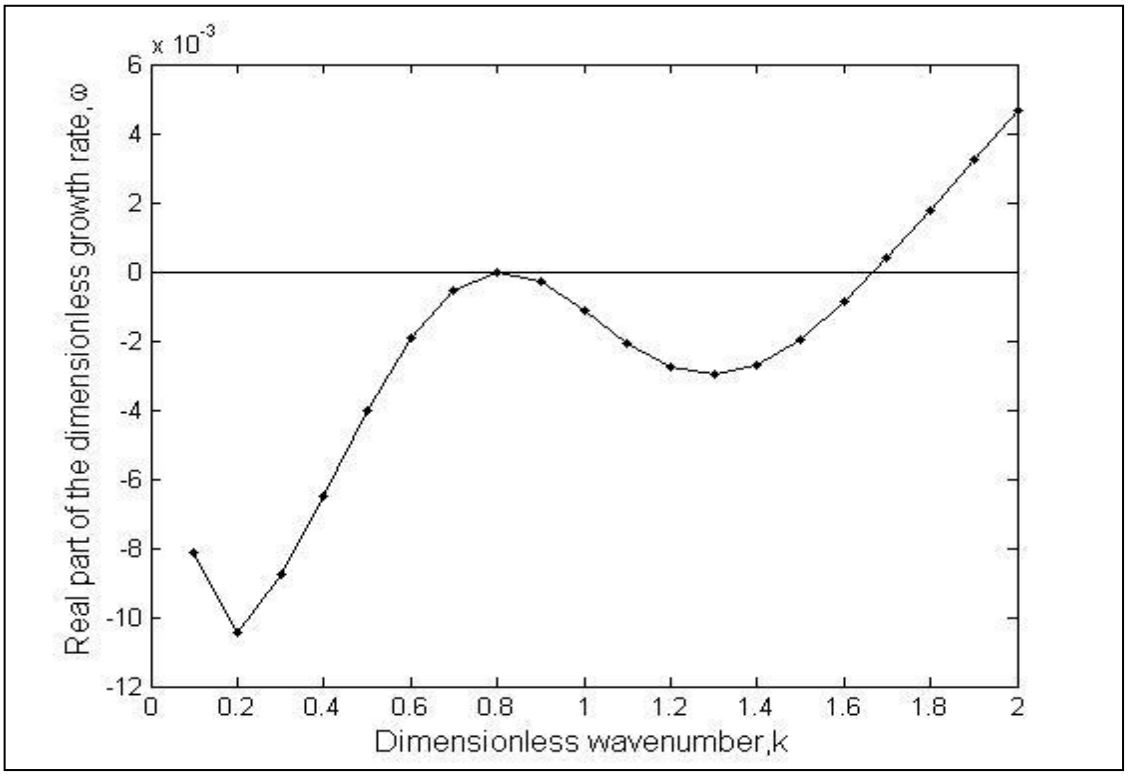

Figure E.14. Dispersion curve for Re=65.

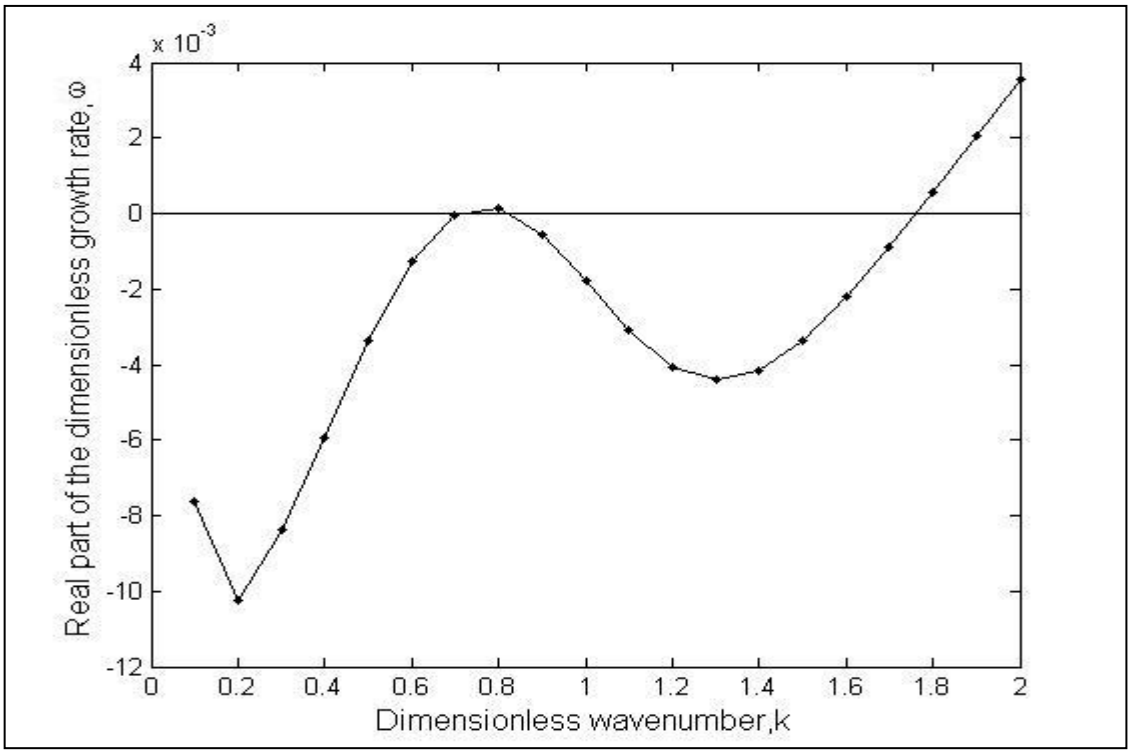

Figure E.15. Dispersion curve for Re=70.

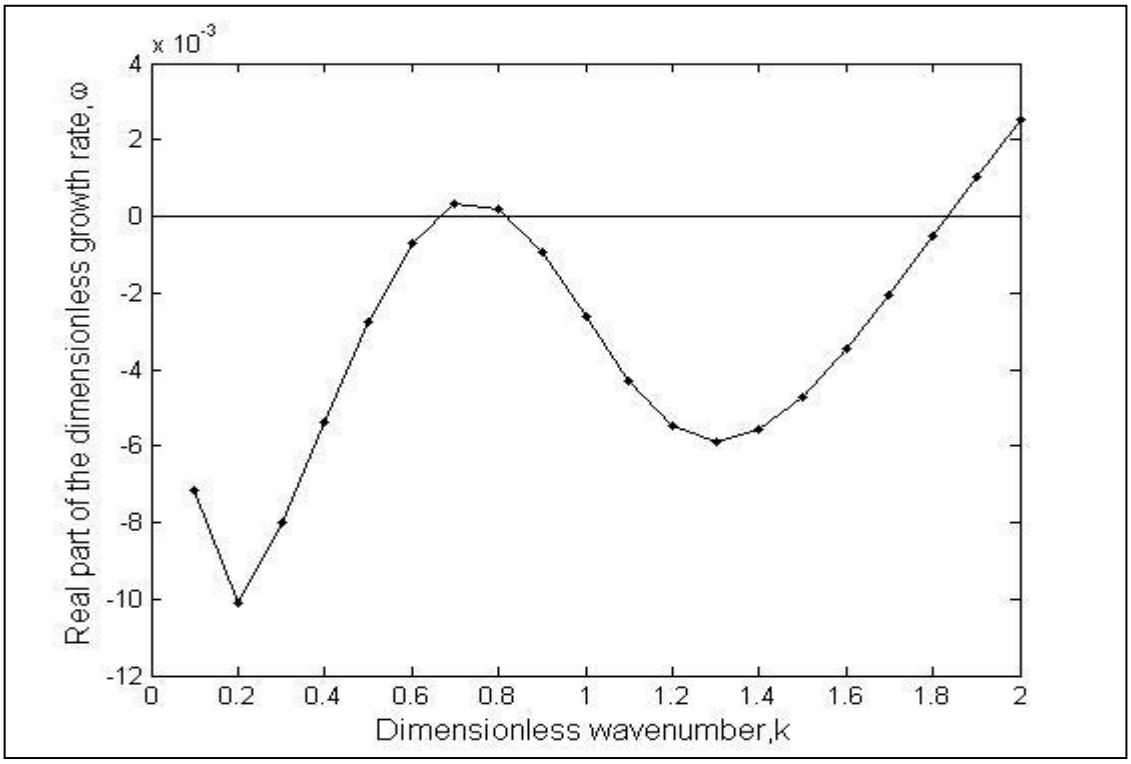

Figure E.16. Dispersion curve for Re=75.

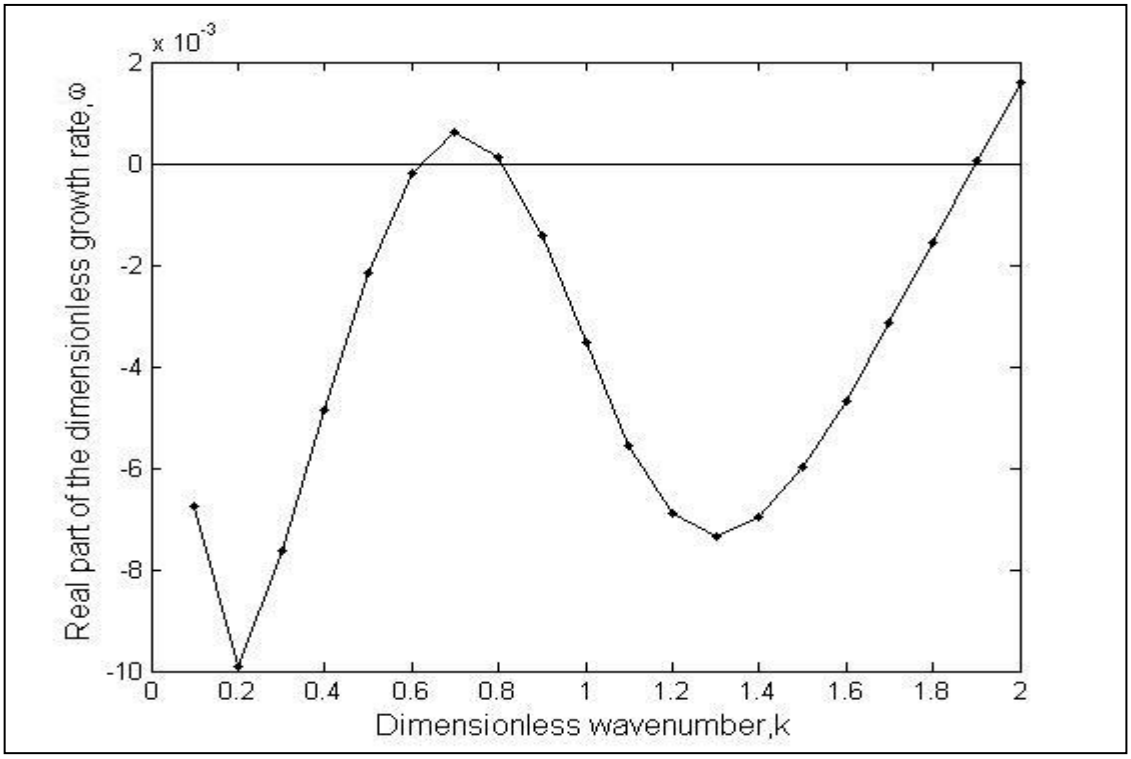

Figure E.17. Dispersion curve for Re=80.

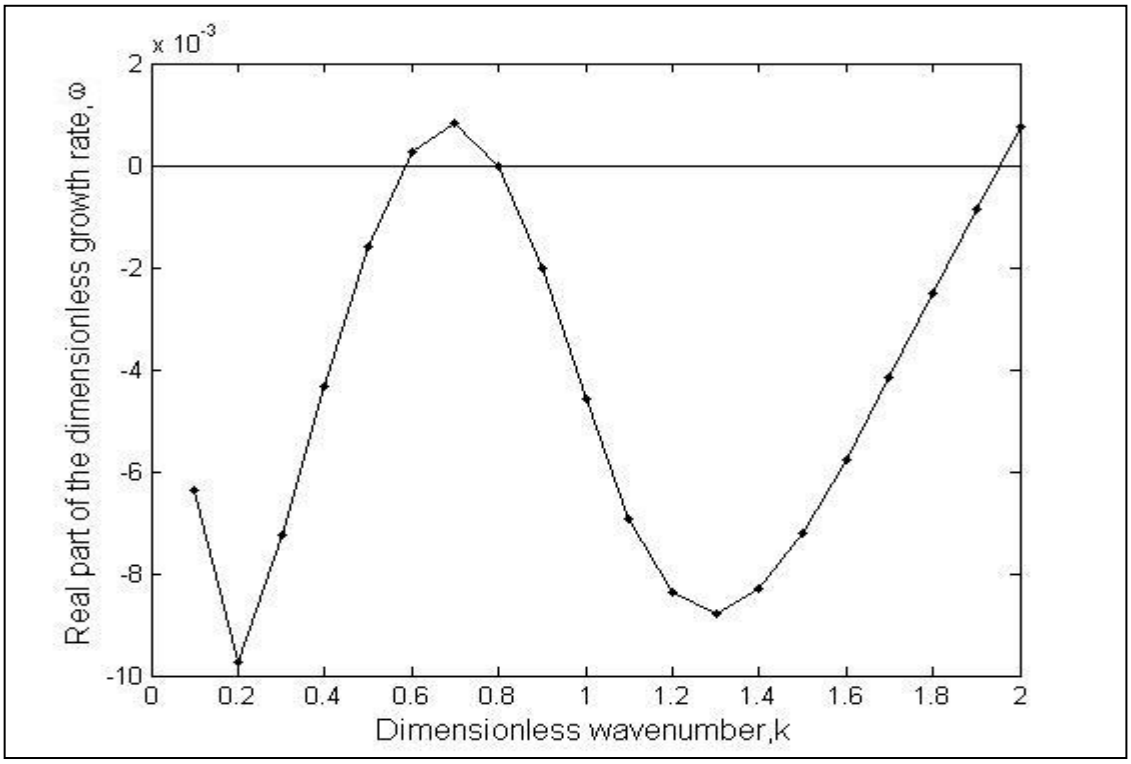

Figure E.18. Dispersion curve for Re=85.

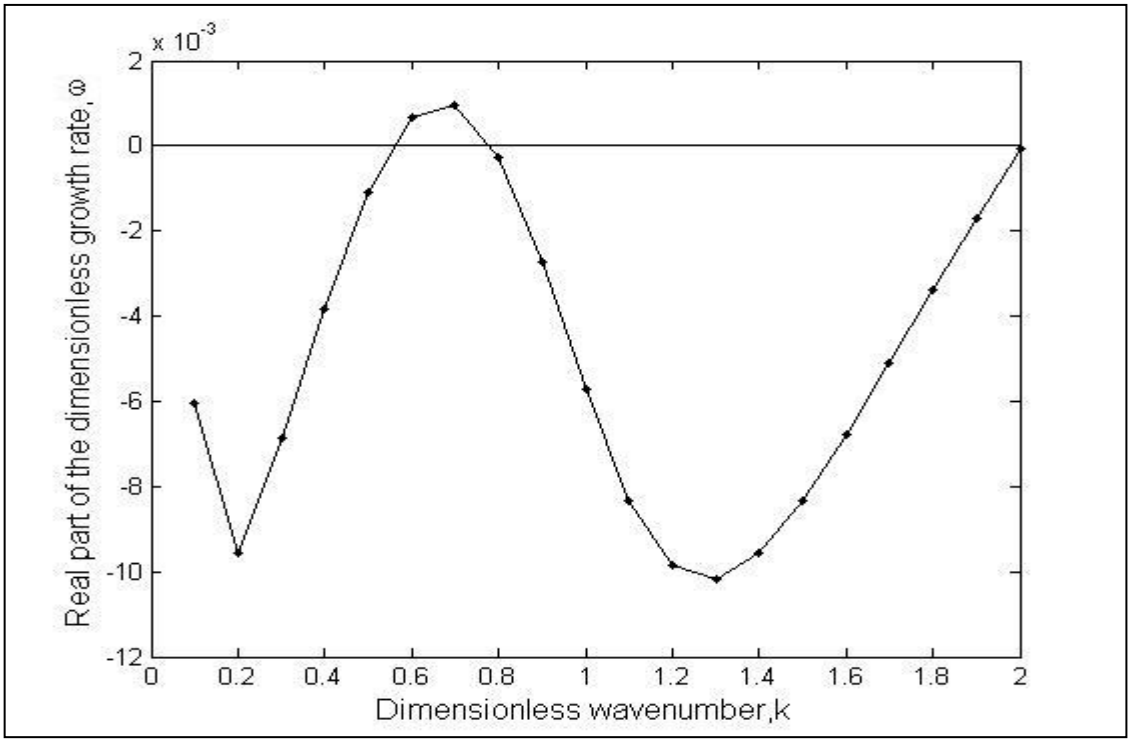

Figure E.19. Dispersion curve for Re=90.

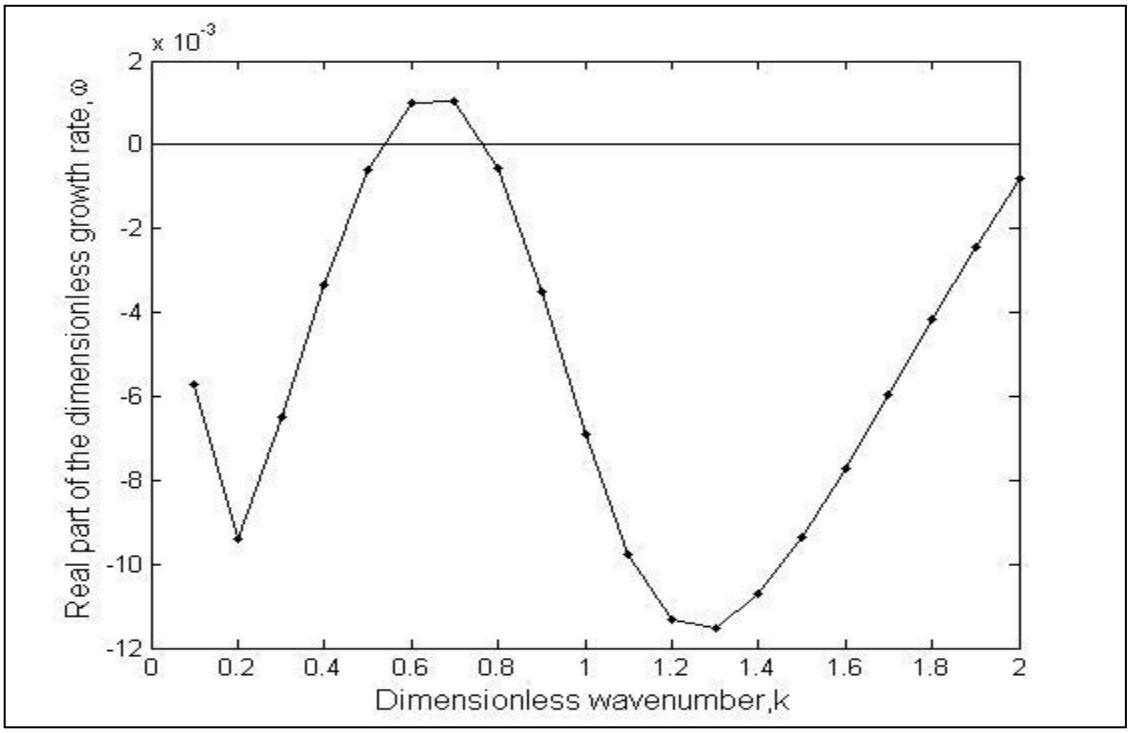

Figure E.20. Dispersion curve for Re=95.

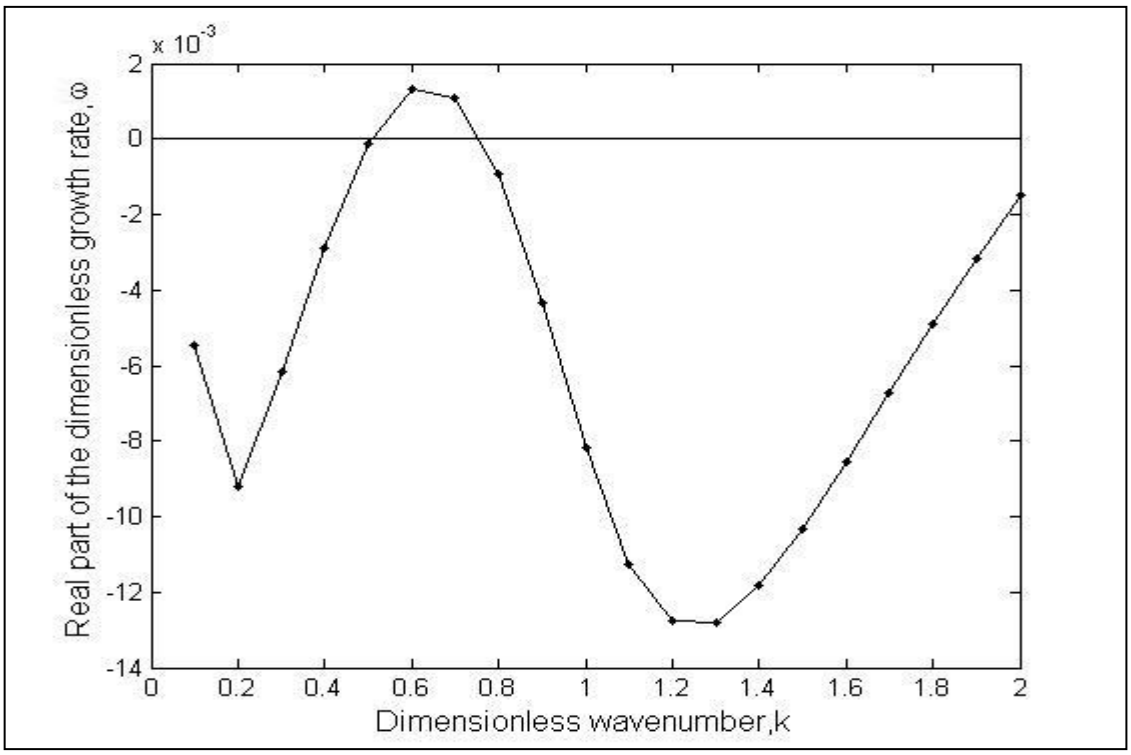

Figure E.21. Dispersion curve for Re=100.

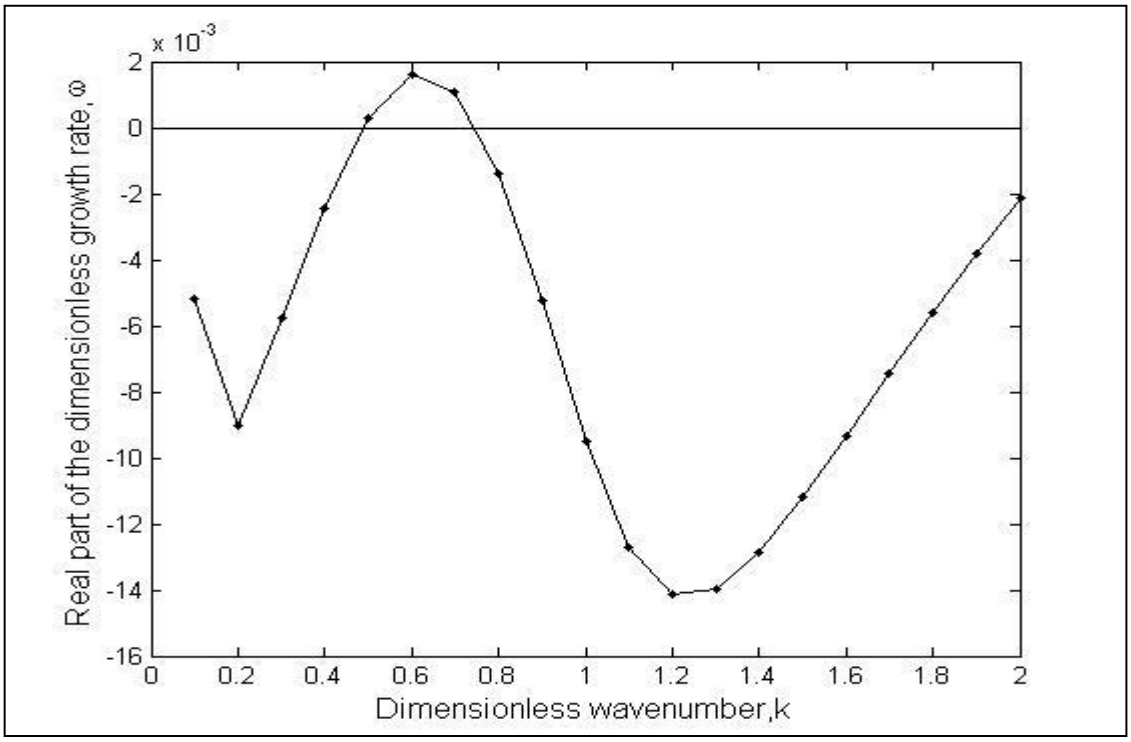

Figure E.22. Dispersion curve for Re=105.

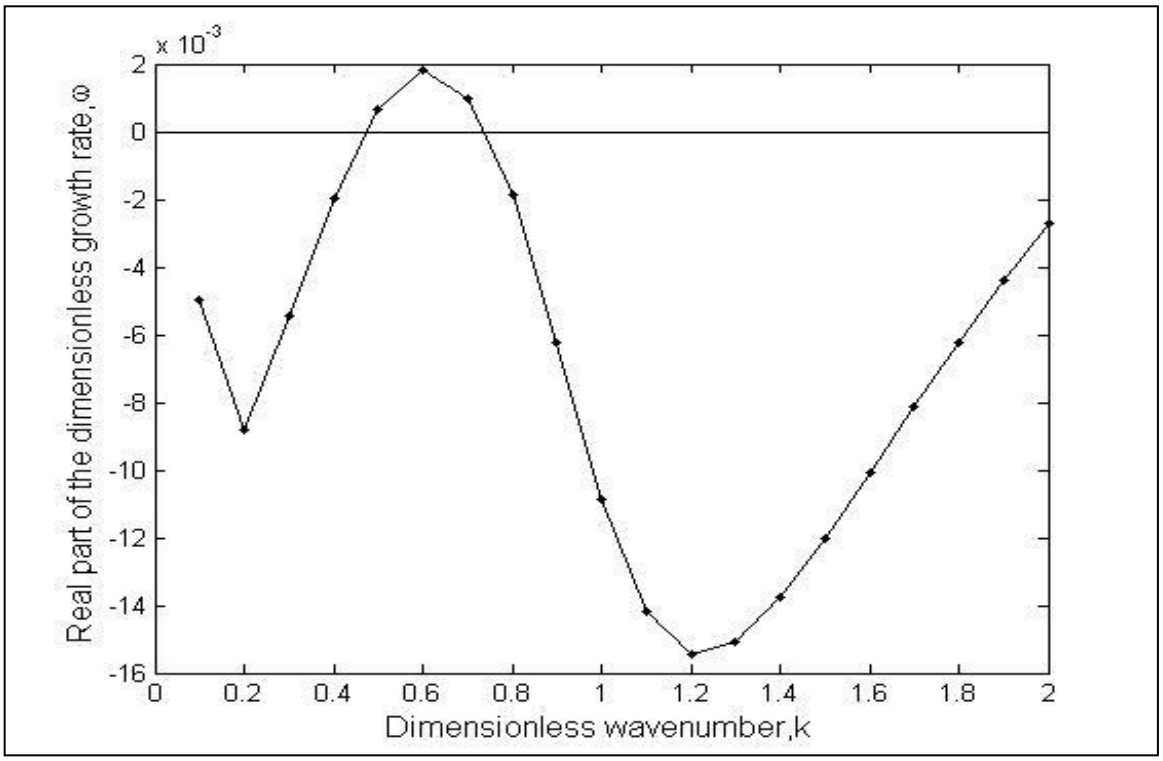

Figure E.23. Dispersion curve for Re=110.

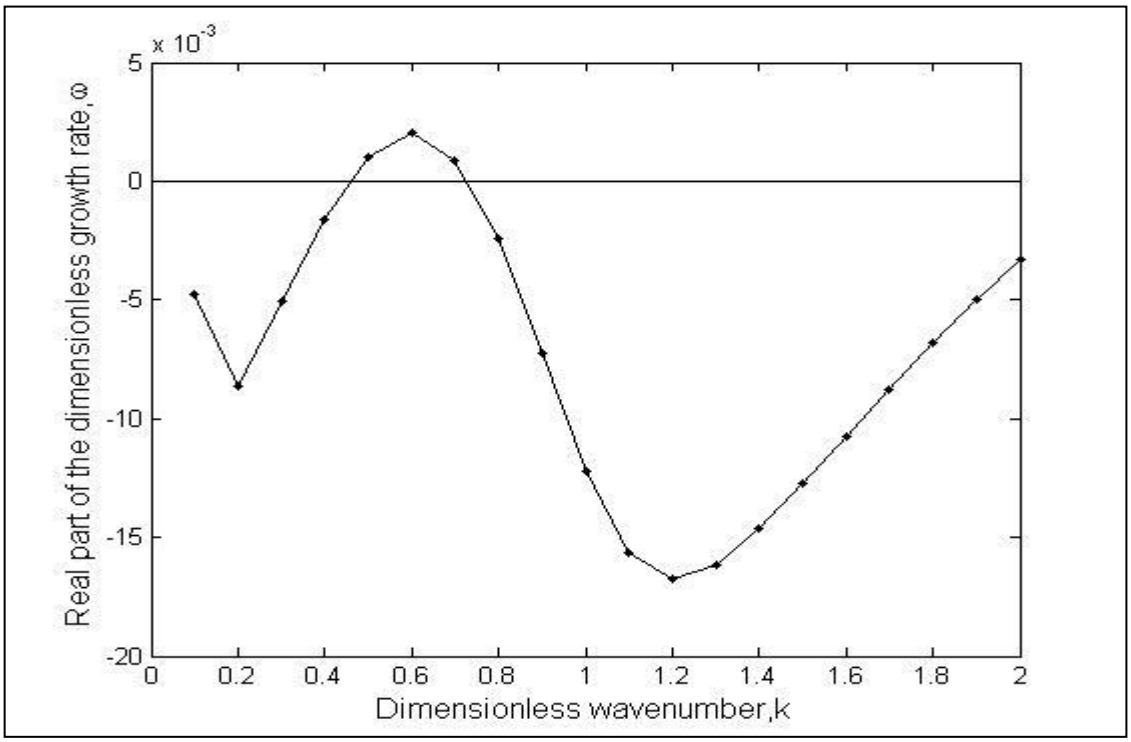

Figure E.24. Dispersion curve for Re=115.

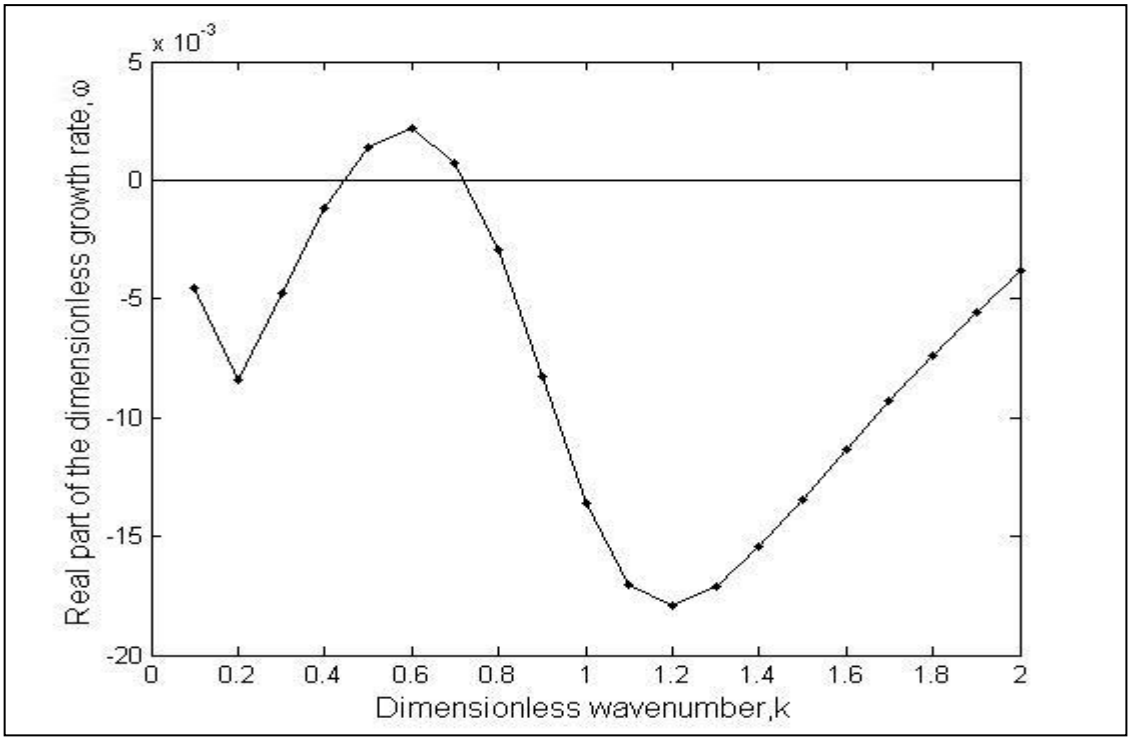

Figure E.25. Dispersion curve for Re=120.

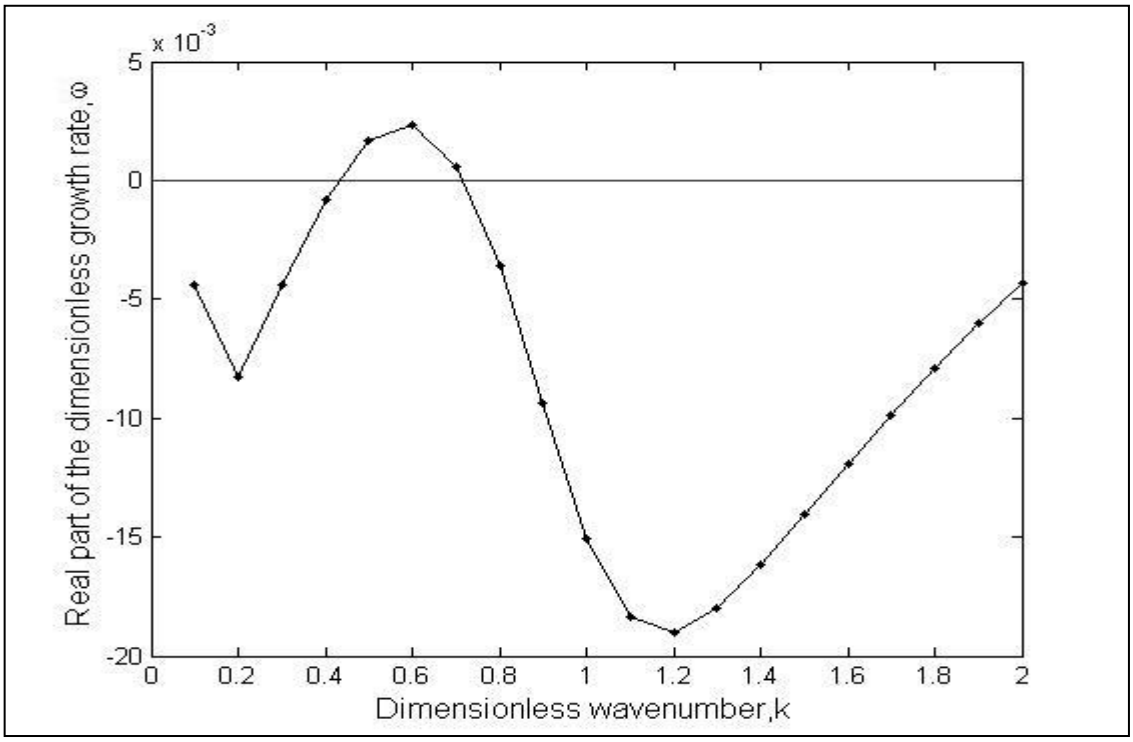

Figure E.26. Dispersion curve for Re=125.

E.2. Dispersion Curves for Non-Newtonian-Newtonian Fluids System

In this appendix, the dispersion curves are plotted to show the effect of the Reynolds number on the stability of the system with a non-Newtonian fluid and a Newtonian fluid without an applied electric field for the system described in Section 4.2.

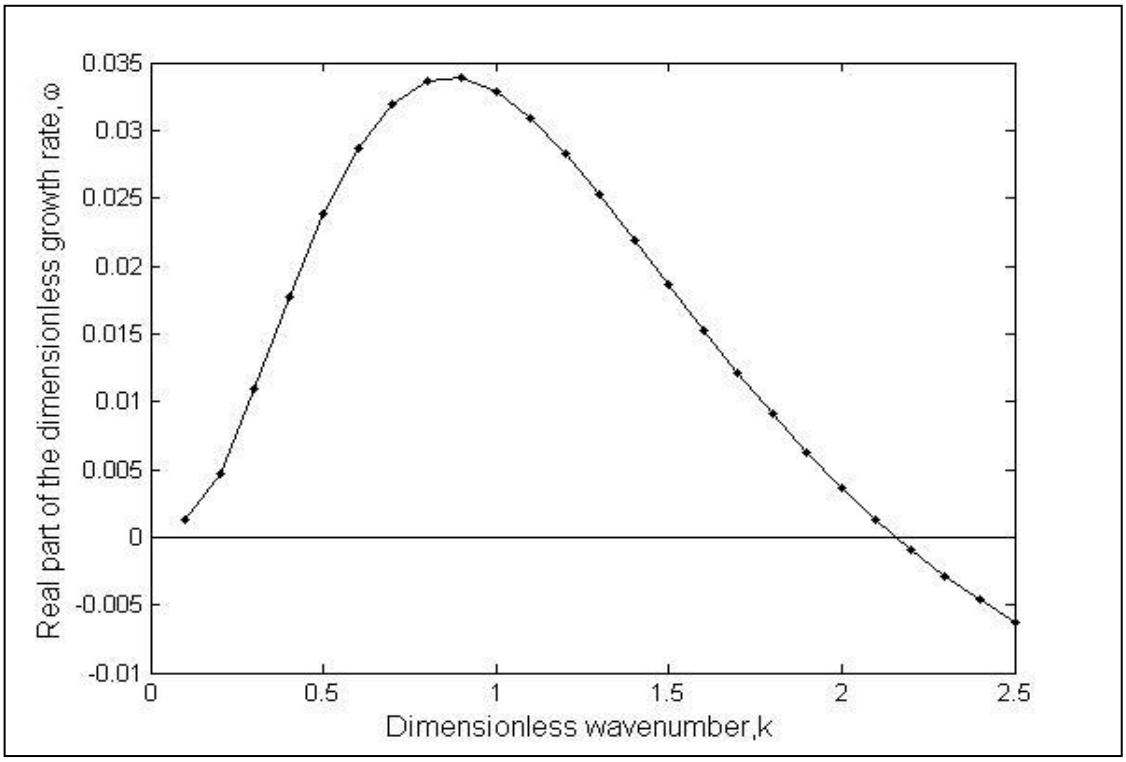

Figure E.27. Dispersion curve for We=0.5, Re=1.

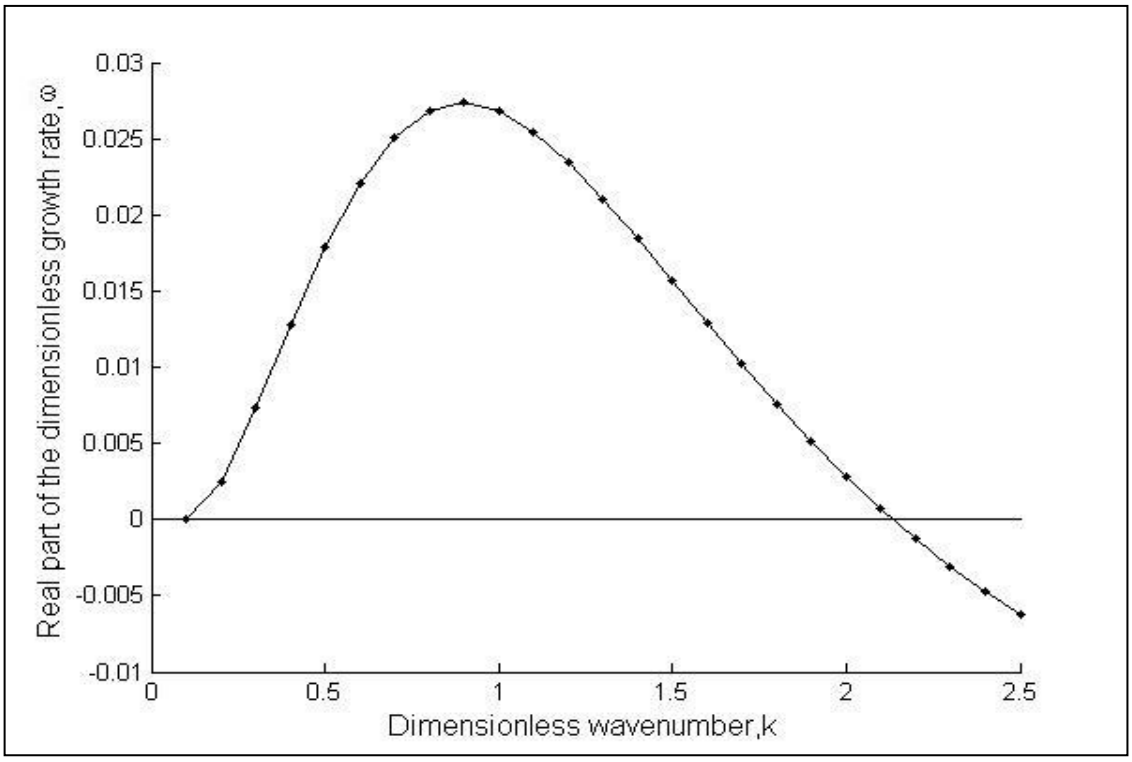

Figure E.28. Dispersion curve for We=0.5, Re=2.

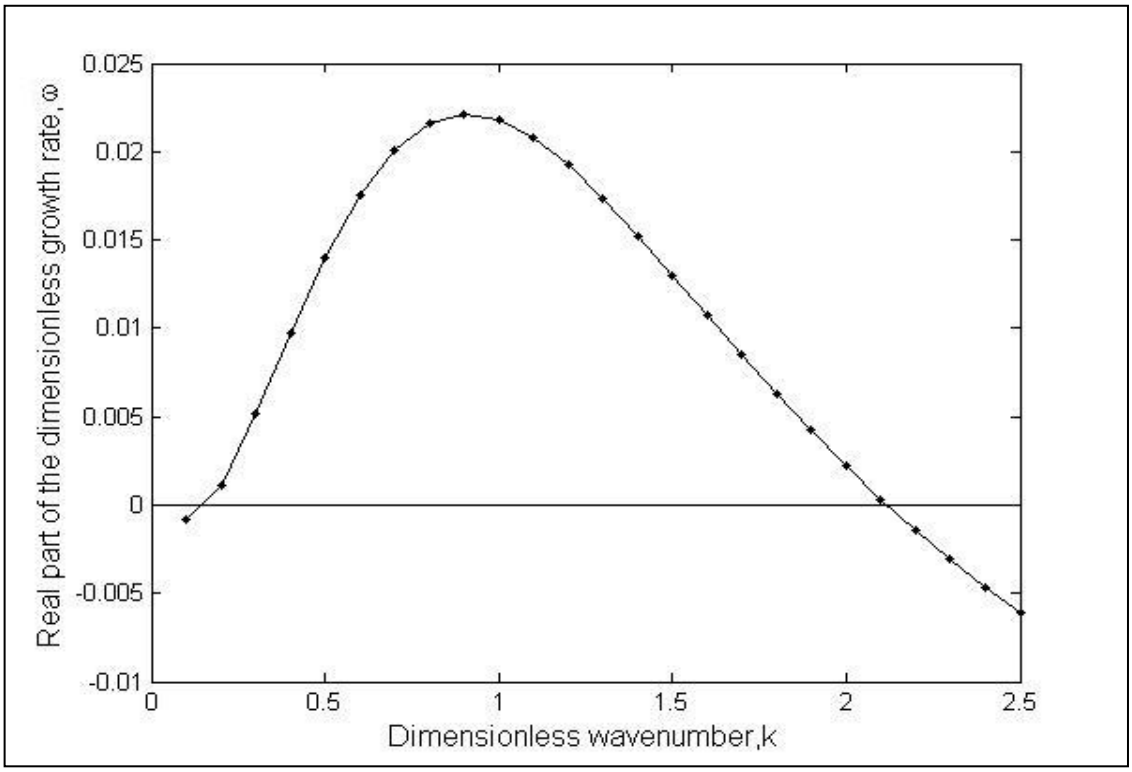

Figure E.29. Dispersion curve for We=0.5, Re=3.

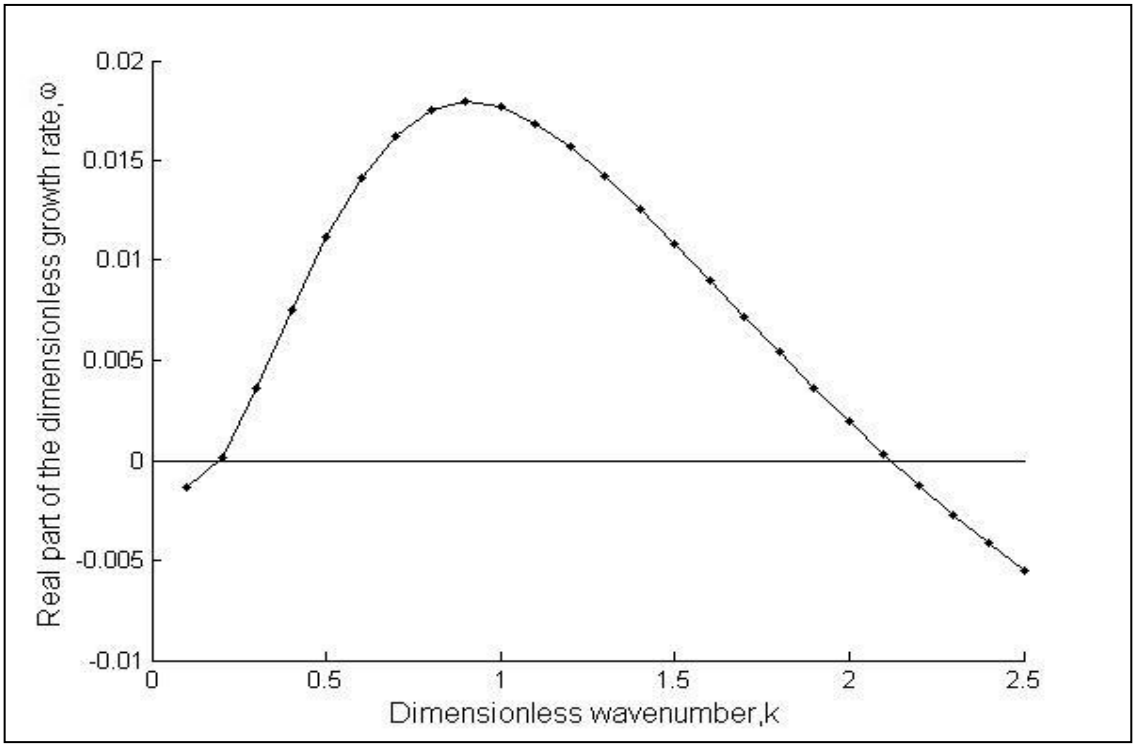

Figure E.30. Dispersion curve for We=0.5, Re=4.

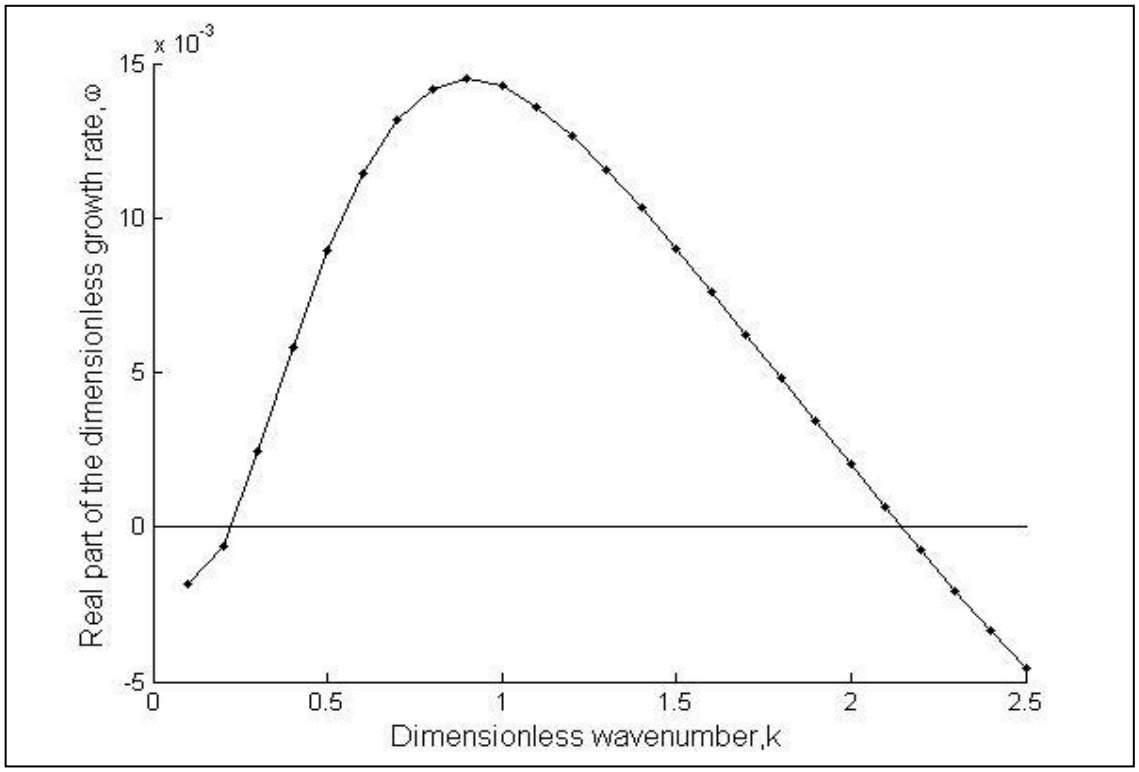

Figure E.31. Dispersion curve for We=0.5, Re=5.

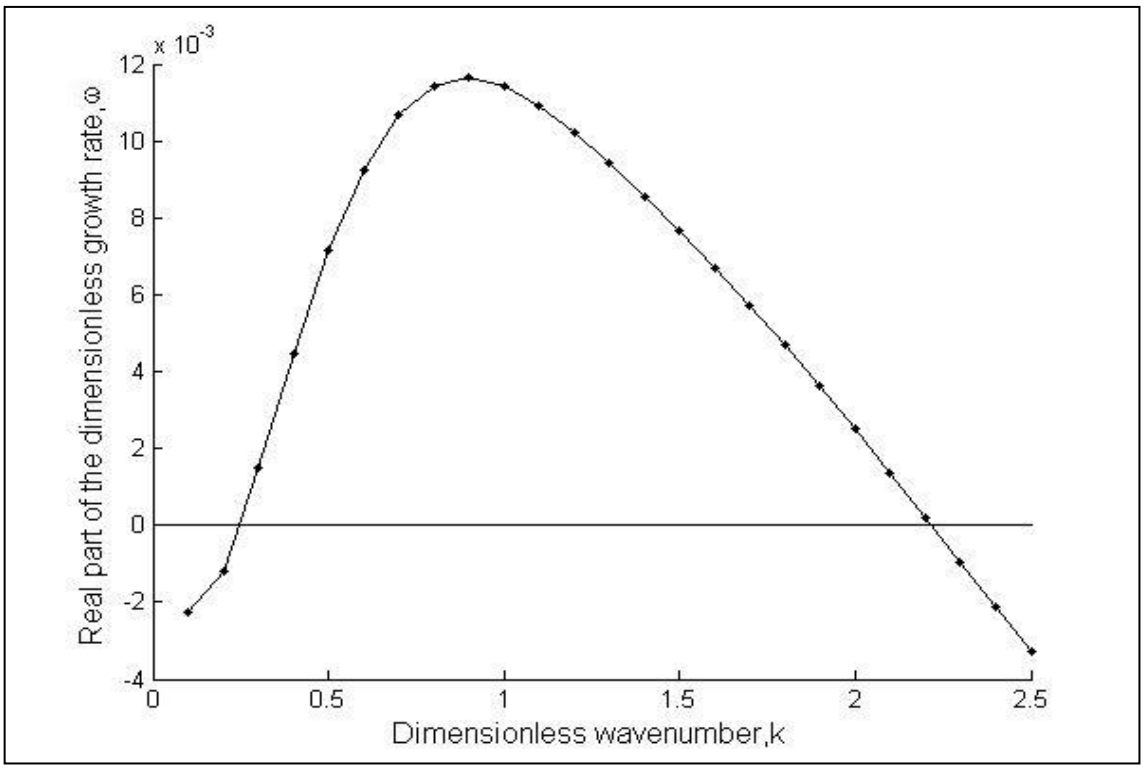

Figure E.32. Dispersion curve for We=0.5, Re=6.

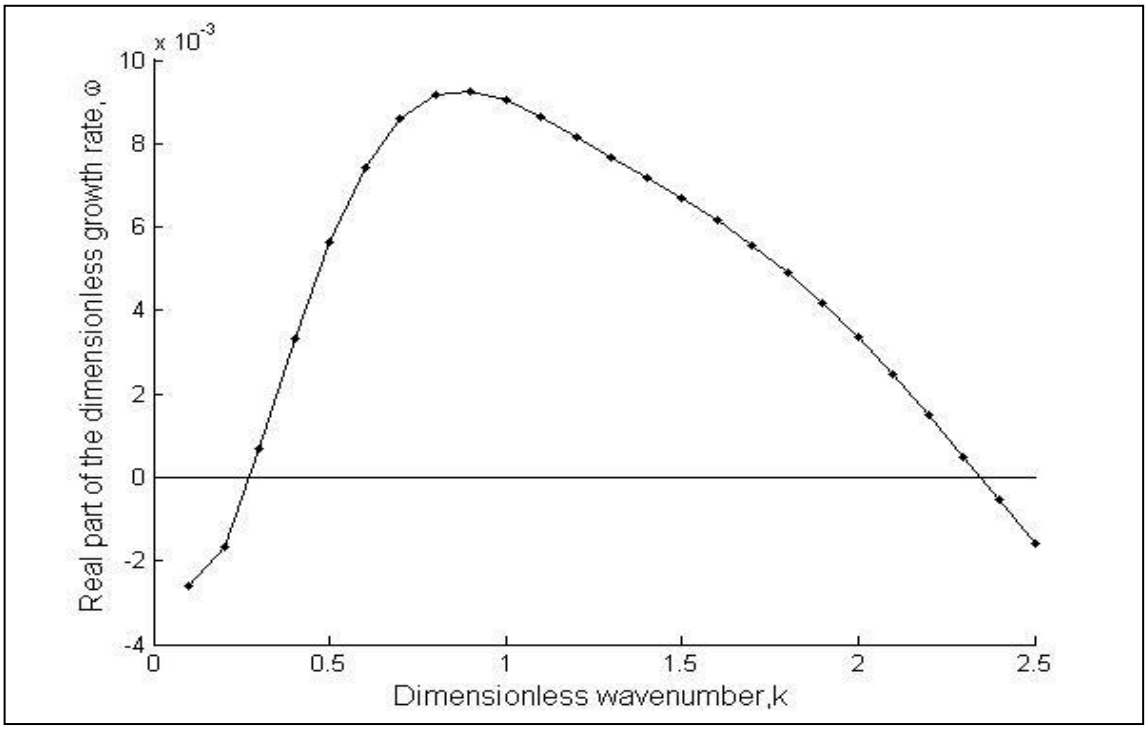

Figure E.33. Dispersion curve for We=0.5, Re=7.

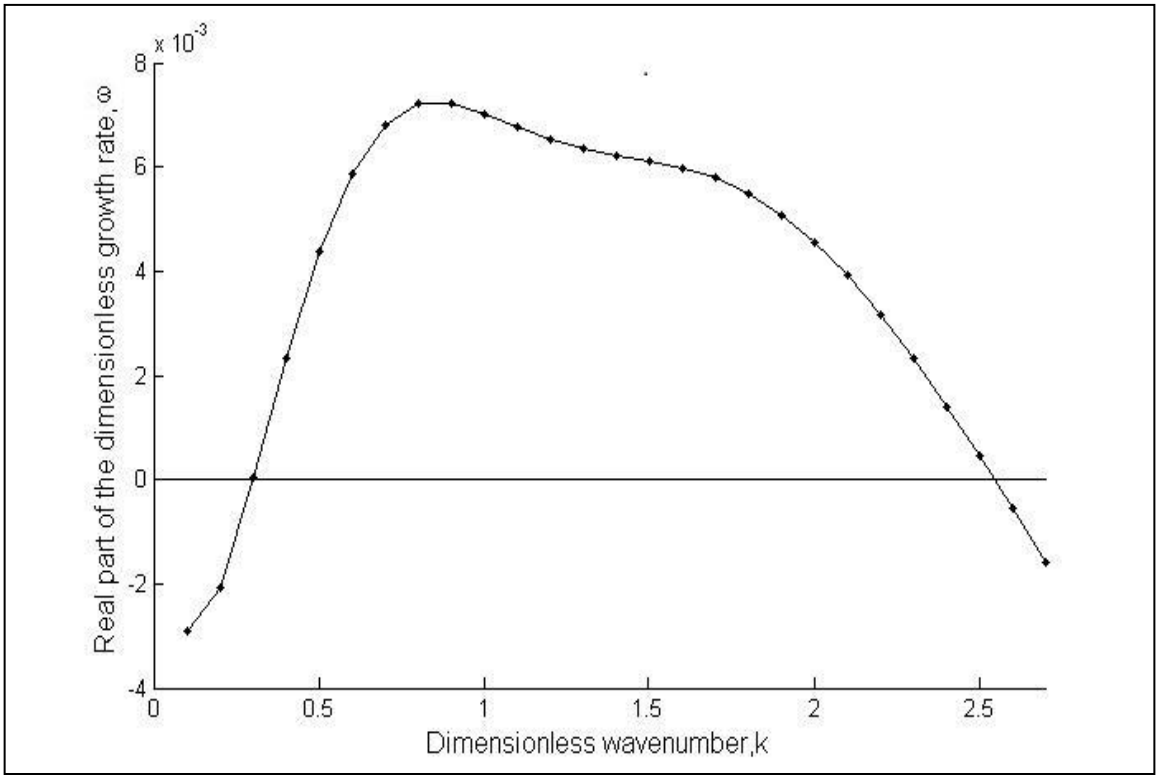

Figure E.34. Dispersion curve for We=0.5, Re=8.

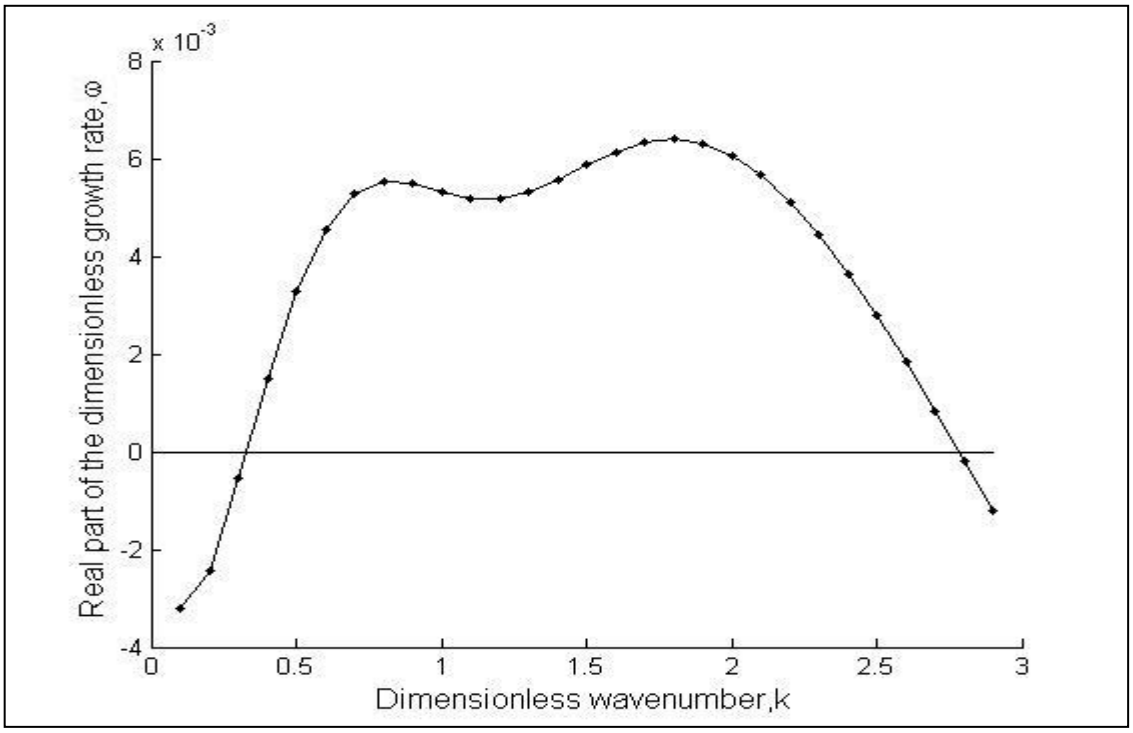

Figure E.35. Dispersion curve for We=0.5, Re=9.

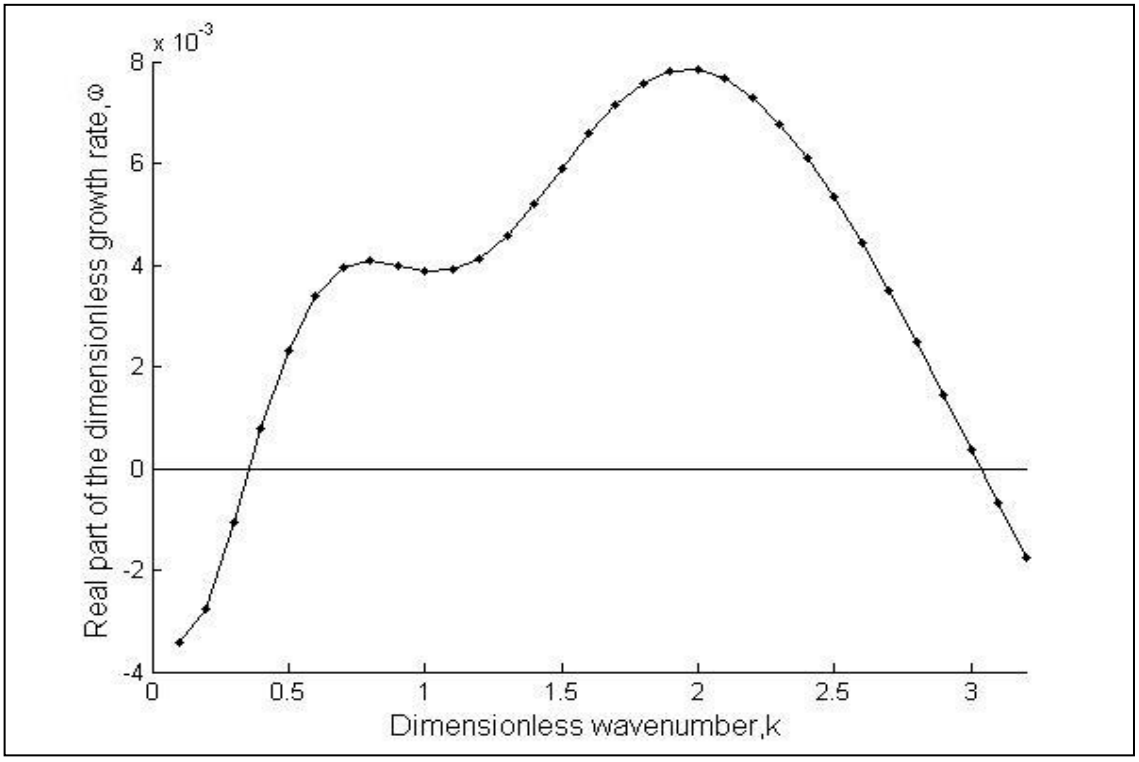

Figure E.36. Dispersion curve for We=0.5, Re=10.

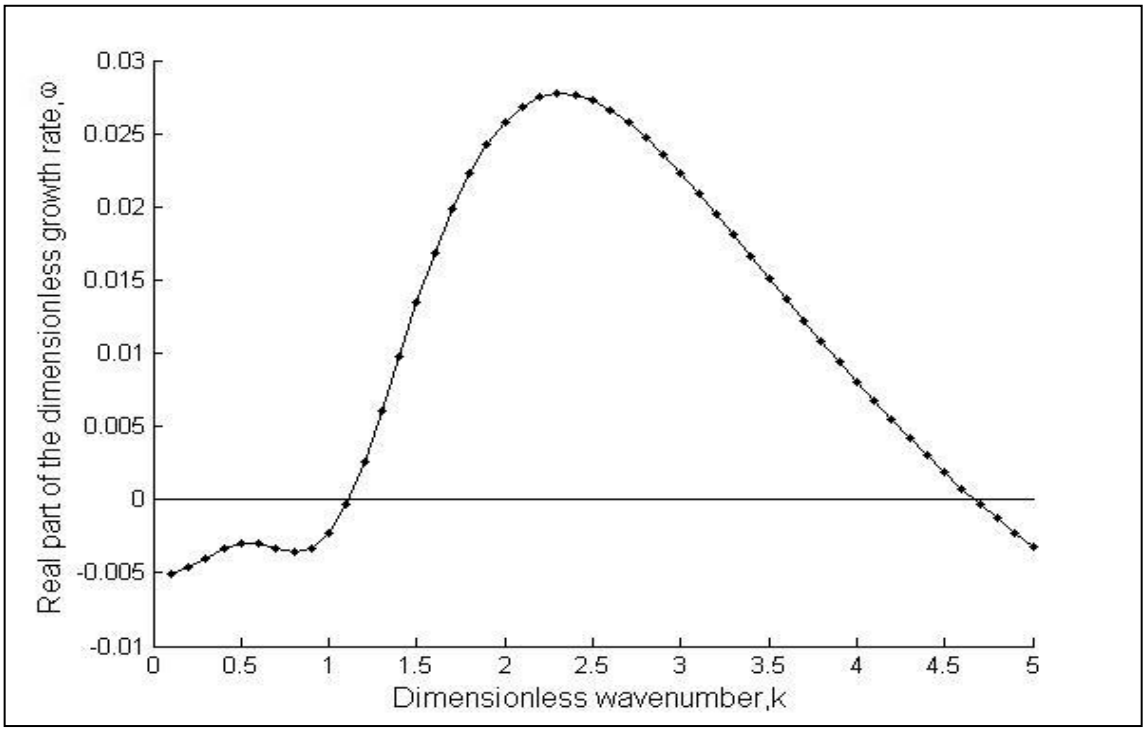

Figure E.37. Dispersion curve for We=0.5, Re=20.

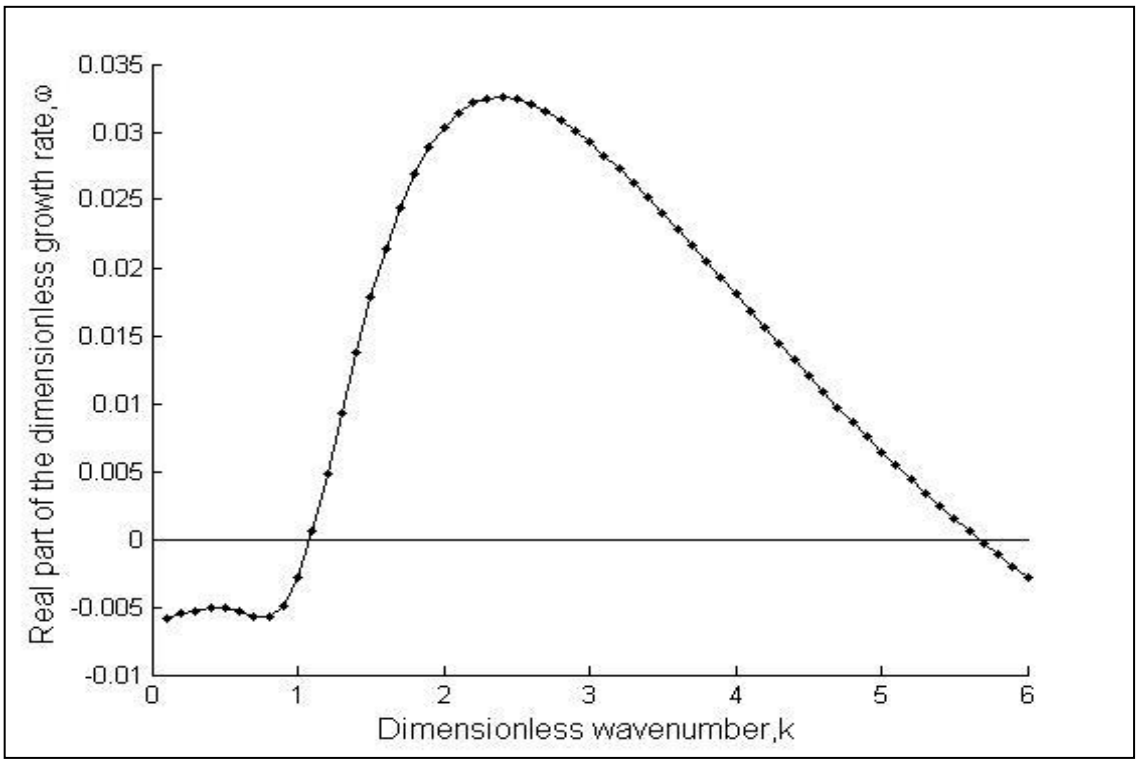

Figure E.38. Dispersion curve for We=0.5, Re=30.

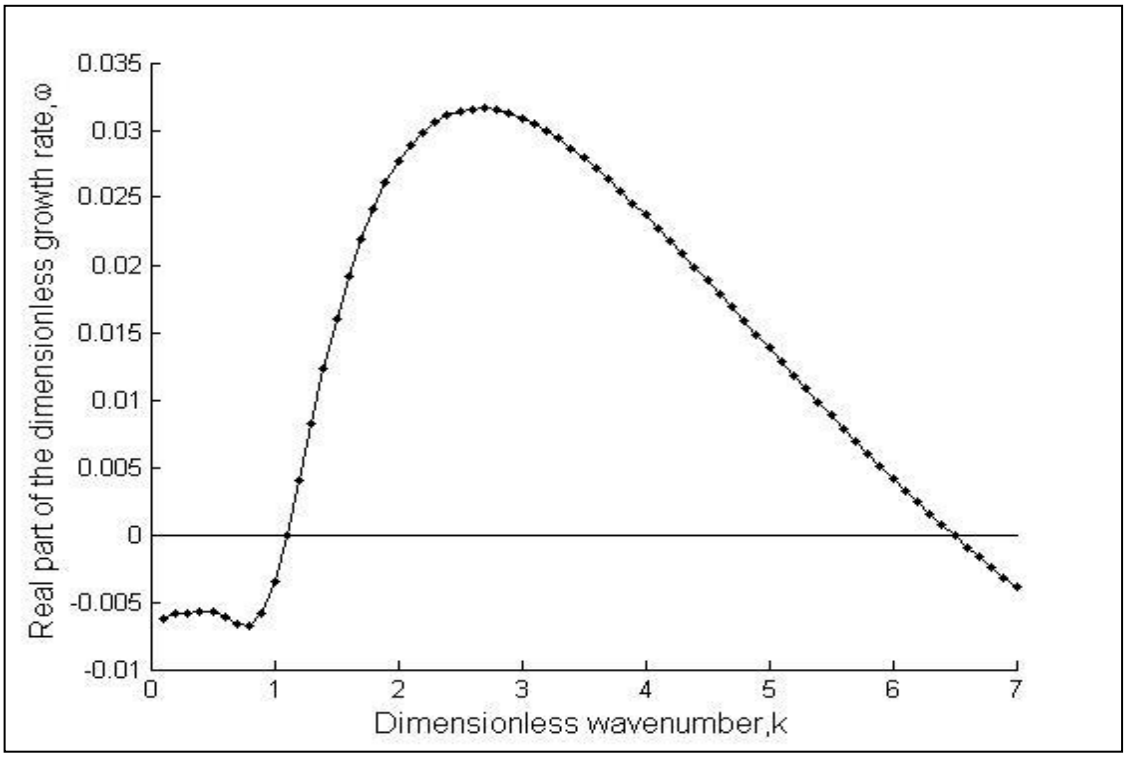

Figure E.39. Dispersion curve for We=0.5, Re=40.

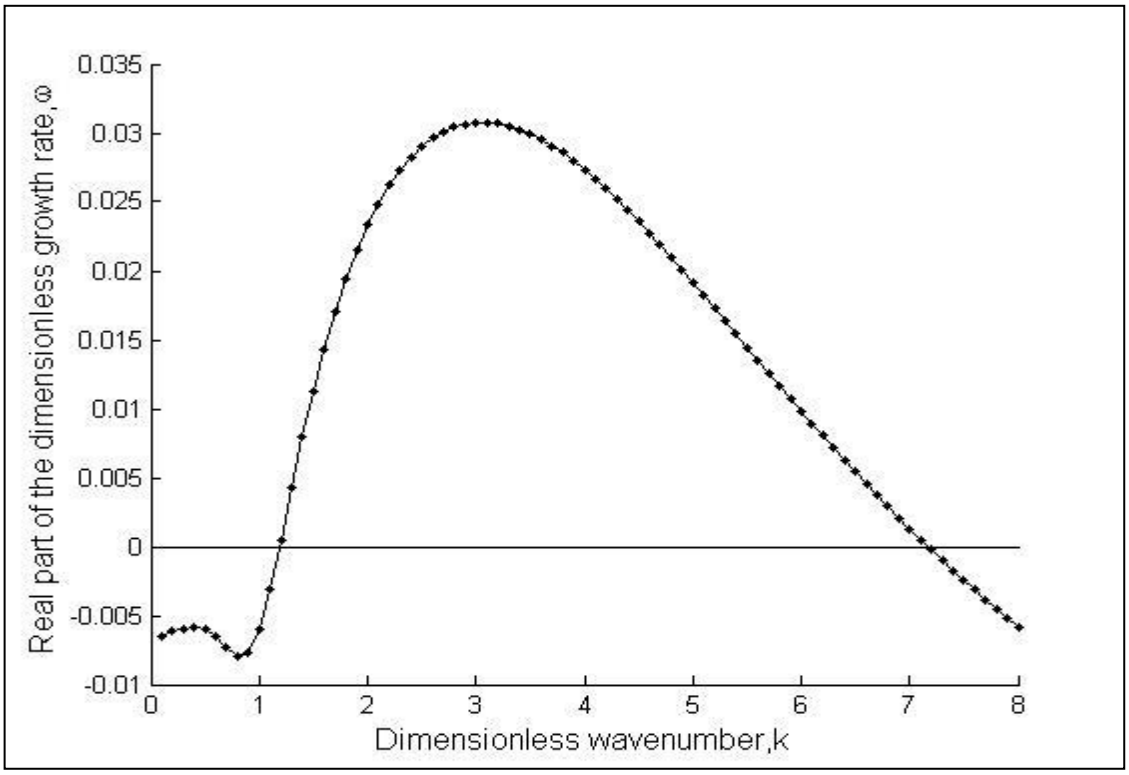

Figure E.40. Dispersion curve for We=0.5, Re=50.

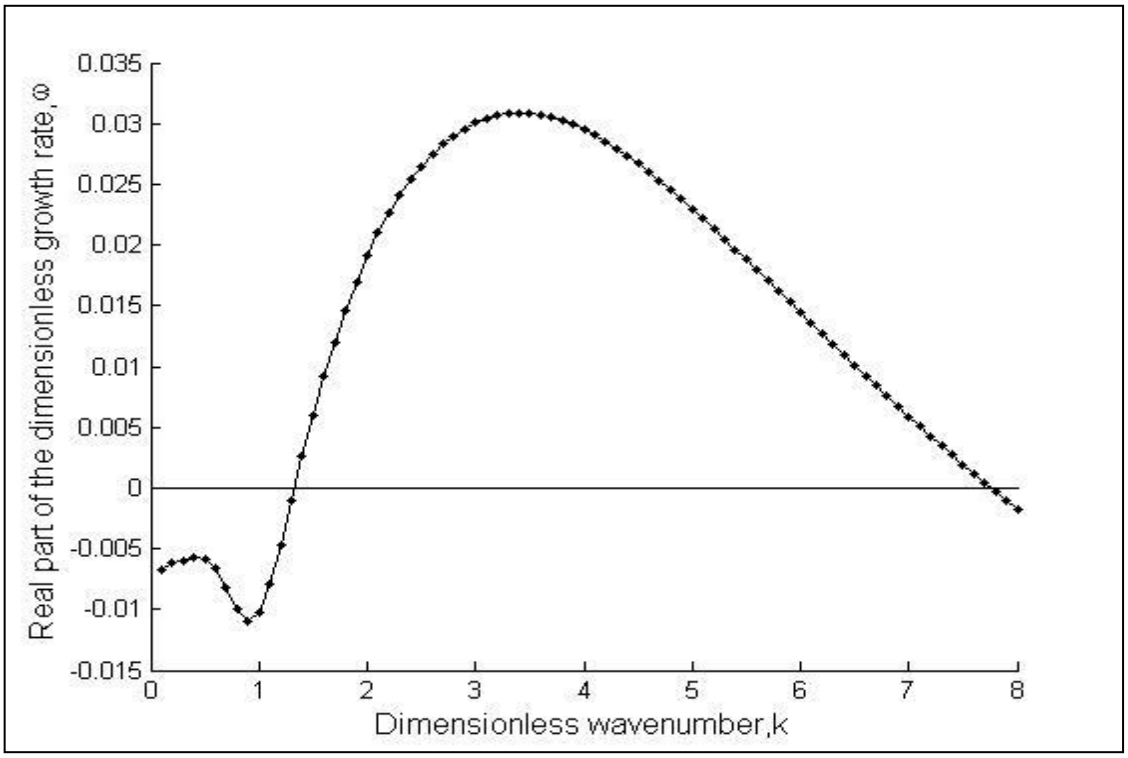

Figure E.41. Dispersion curve for We=0.5, Re=60.

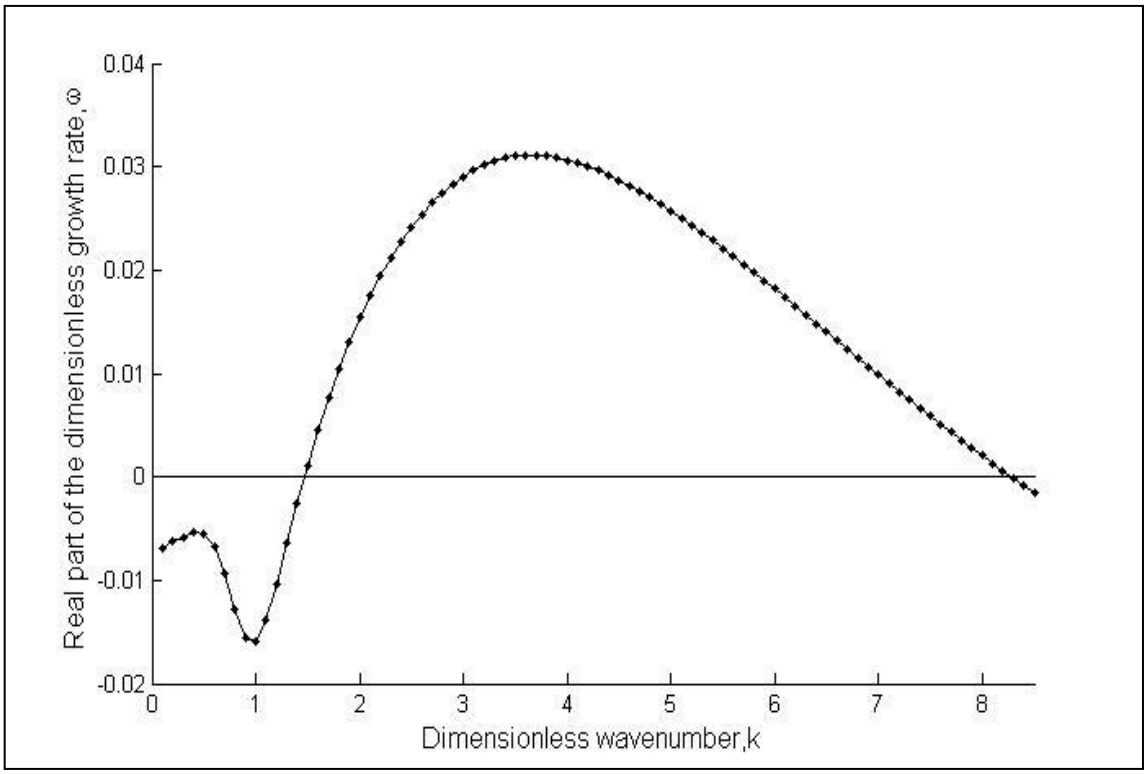

Figure E.42. Dispersion curve for We=0.5, Re=70.

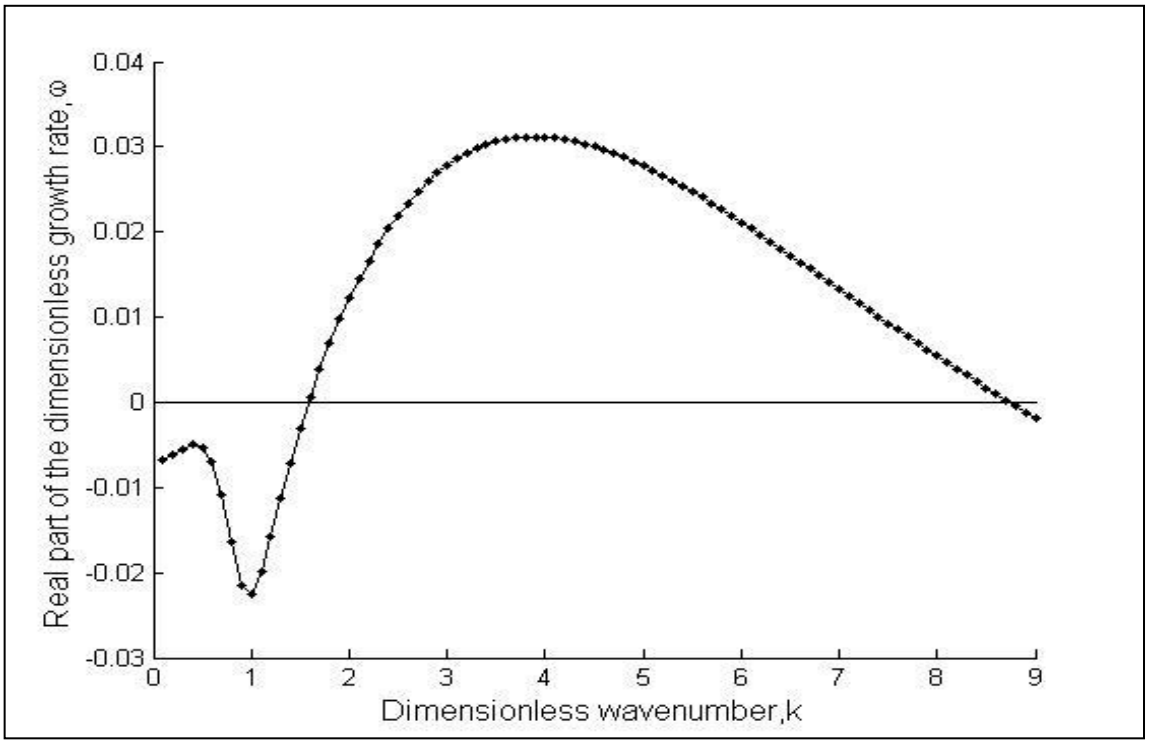

Figure E.43. Dispersion curve for We=0.5, Re=80.

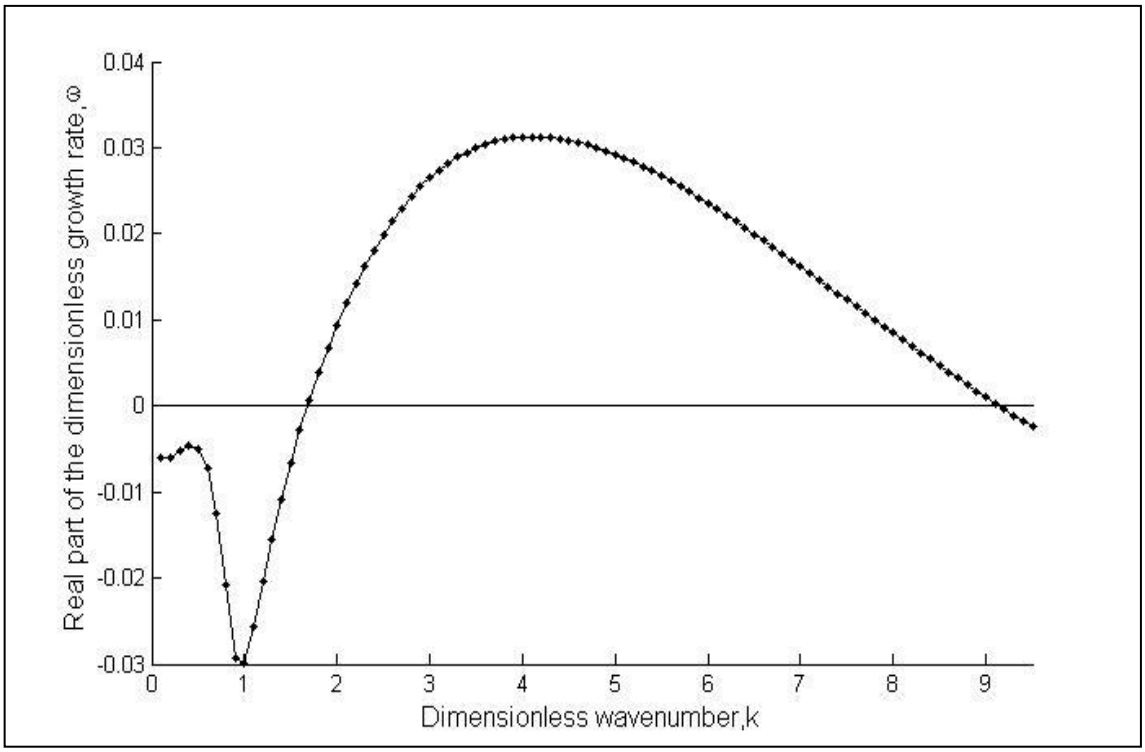

Figure E.44. Dispersion curve for We=0.5, Re=90.

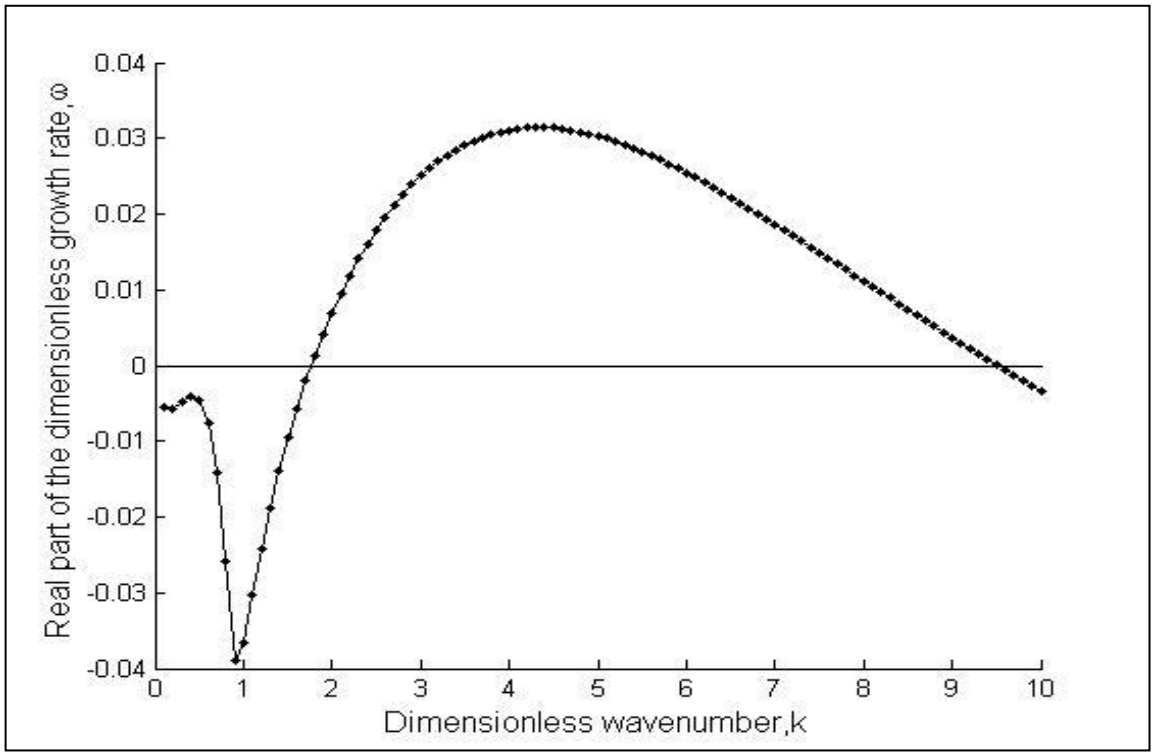

Figure E.45. Dispersion curve for We=0.5, Re=100.

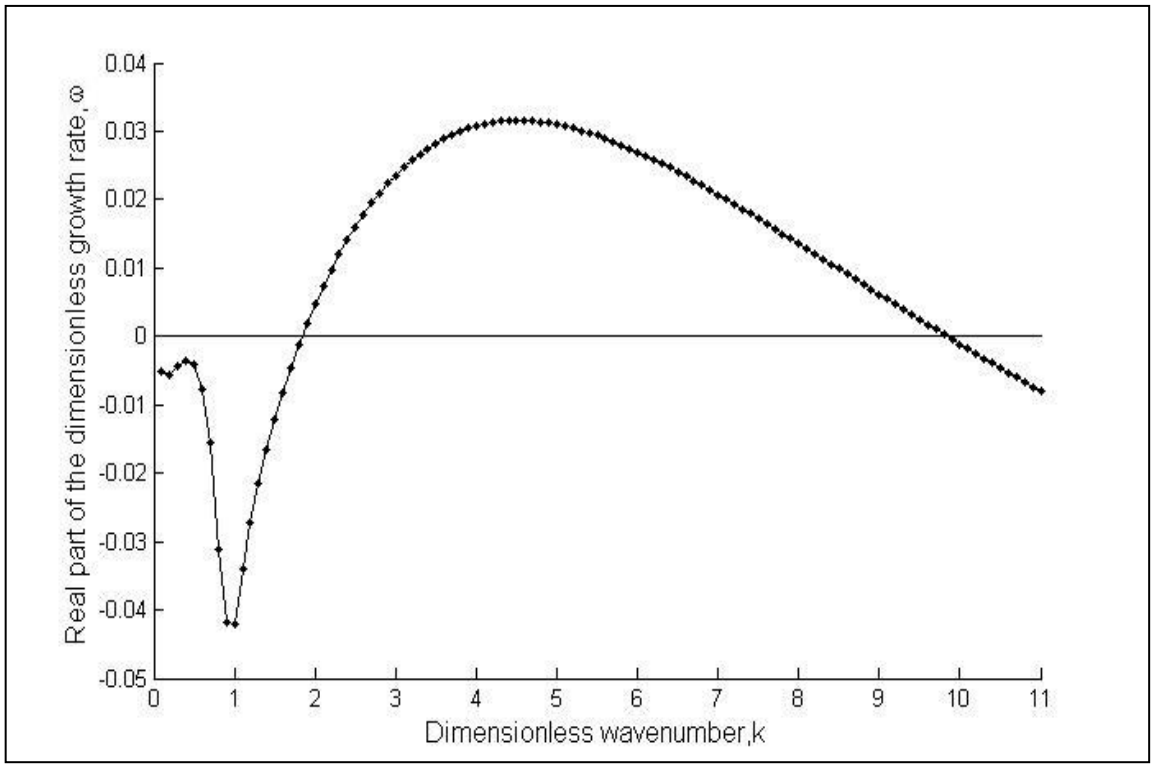

Figure E.46. Dispersion curve for We=0.5, Re=110.

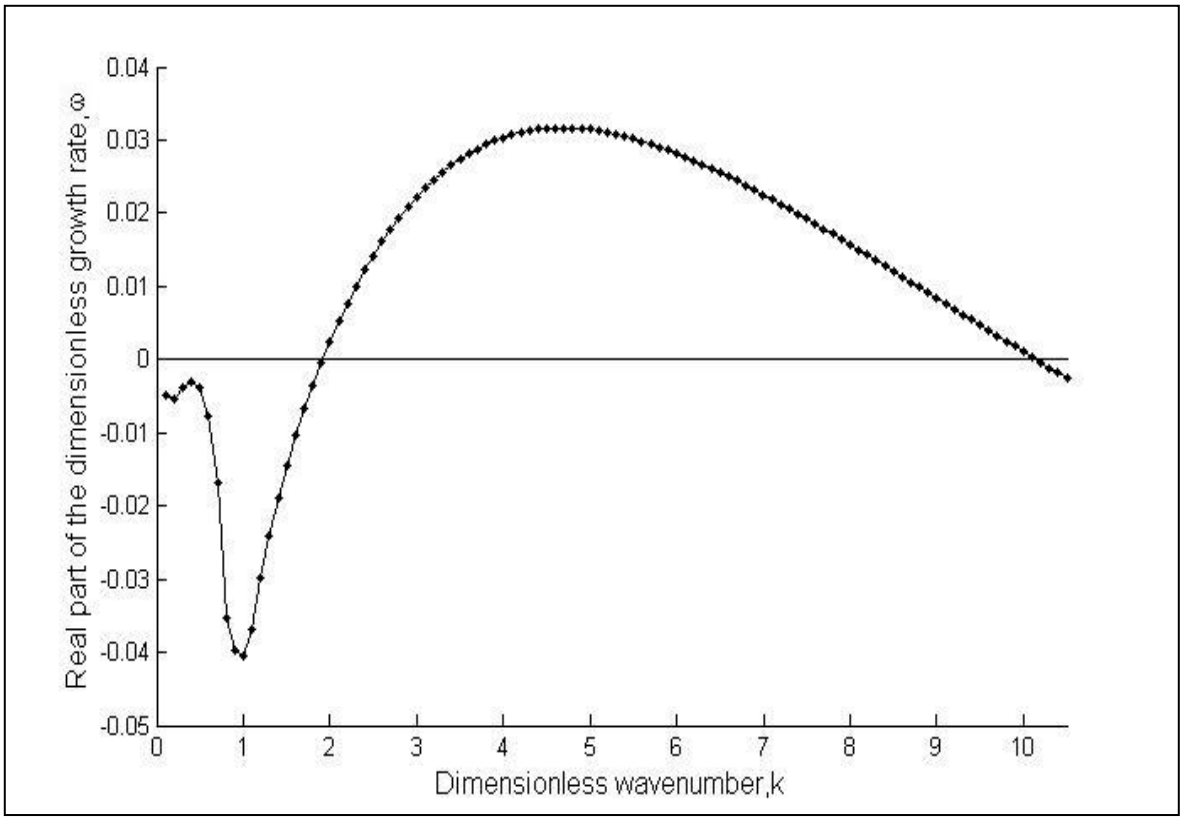

Figure E.47. Dispersion curve for We=0.5, Re=120.

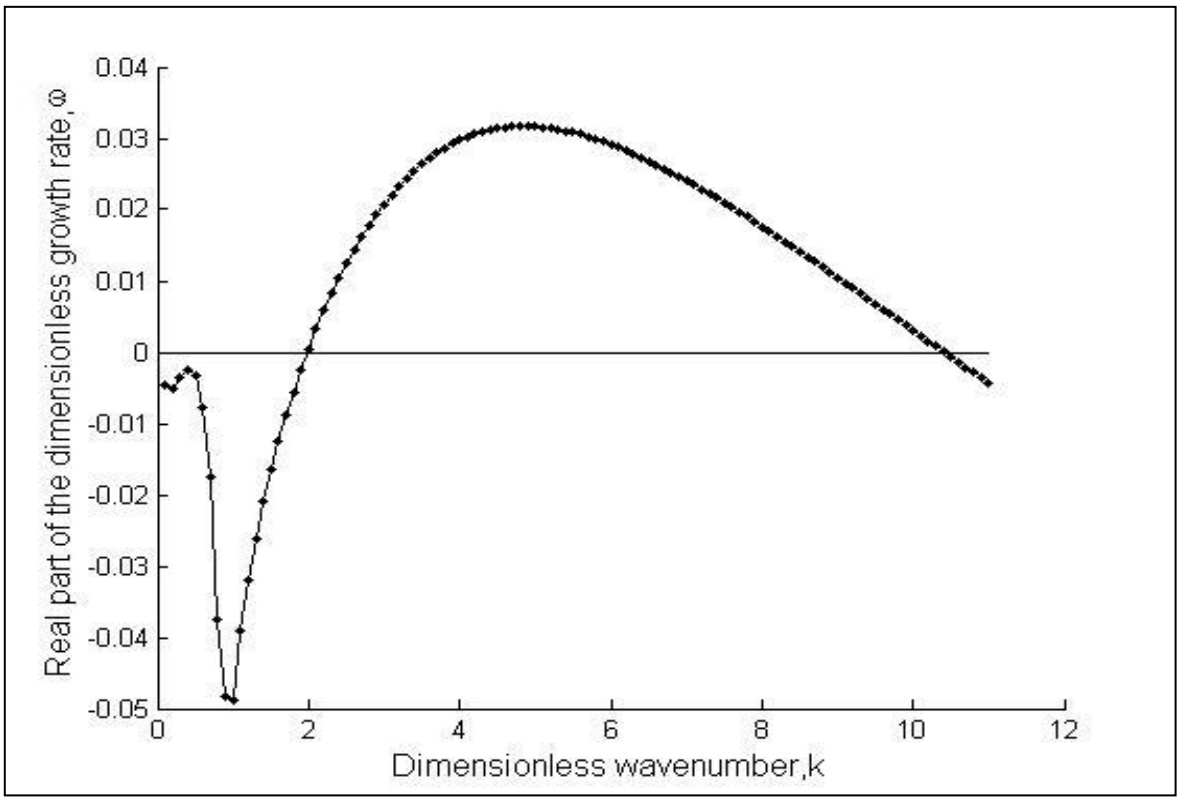

Figure E.48. Dispersion curve for We=0.5, Re=130.

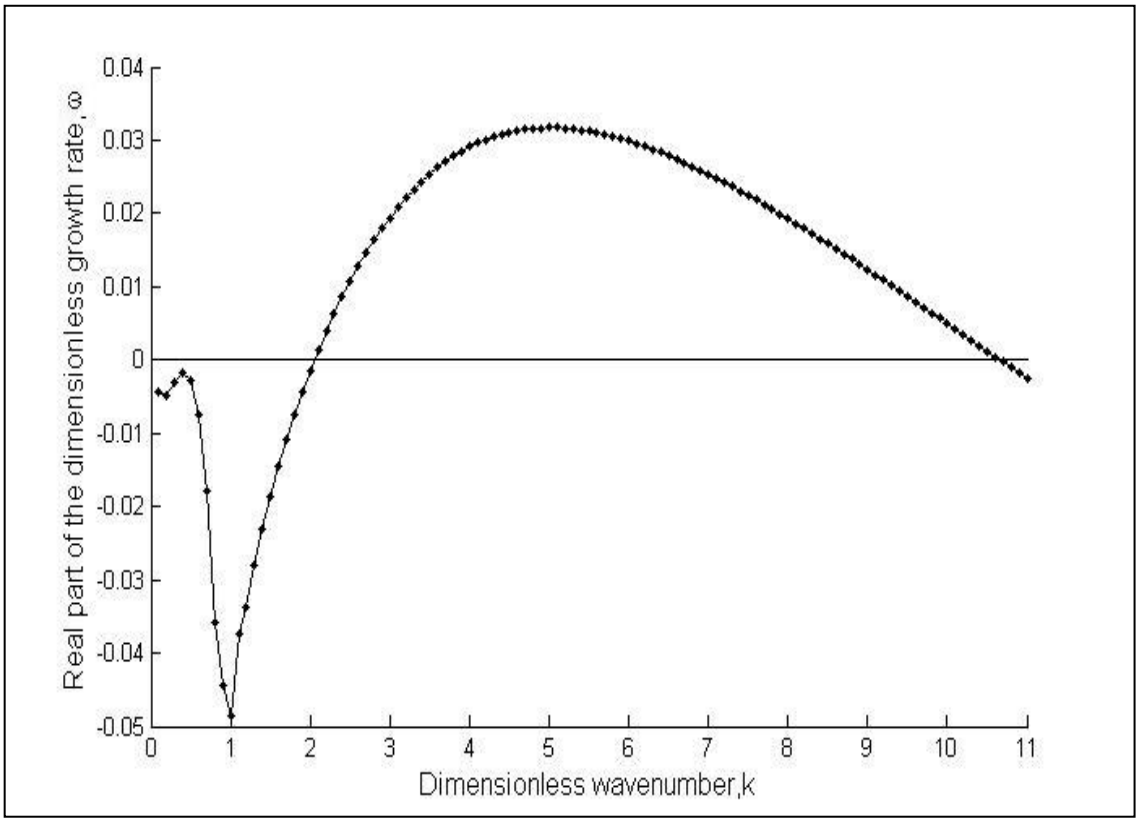

Figure E.49. Dispersion curve for We=0.5, Re=140.

REFERENCES

Abdella, K., and H. Rasmussen, 1997, "Electrohydrodynamic Instability of Two Superposed Fluids in Normal Electric Fields", *Journal of Computational and Applied Mathematics*, Vol. 78, pp. 33-61.

Bandyopadhyay, D. and A. Sharma, 2007, "Electric Field Induced Instabilities in Thin Confined Bilayers", *Journal of Colloid and Interface Science*, Vol. 311, pp. 595-608.

Baygents, J. C., and F. Baldessari, 1998, "Electrohydrodynamic Instability in a Thin Fluid Layer with an Electrical Conductivity Gradient", *Physics of Fluids*, Vol. 10, pp. 301-311.

Bird, R. B., R. C. Armstrong, and O. Hassager, 1987, *Dynamics of Polymeric Liquids*, Vol.1, John Wiley, New York, USA.

Briskman, V. A., and G. F. Shaidurov, 1968, "Parametric Instability of a Fluid Surface in an Alternating Field", *Soviet Physics-Doklady*, Vol. 13, pp. 540-542.

Castellanos, A. and A. González, 1998, "Nonlinear Electrohydrodynamics of Free Surfaces", *IEEE Dielectrics and Electrical Insulation Society*, Vol. 5, pp. 334-343.

Chang, S., and Y. H. Cho, 2003, "Static Chaos Microfluid Mixers Using Microblock-Induced Alternating Whirl and Microchannel-Induced Lamination", *Proceedings of International Mechanical Engineering Congress and R&D expo ASME, Washington, D.C., USA-41230.*

Chang, C. C., and R. J. Yang, 2007, "Electrokinetic Mixing in Microfluidic Systems", *Microfluidics and Nanofluidics*, Vol. 3, pp. 501-525.

Chen, C. H., H. Lin, S. K. Lele, and J. G. Santiago, 2005a, "Convective and Absolute Electrokinetic Instability with Conductivity Gradients", *Journal of Fluid Mechanics*, Vol. 524, pp. 263-303.

Chen, L., L. Zhuang, P. Deshpande, and S. Chou, 2005b, "Novel Polymer Patterns Formed by Lithographically Induced Self-Assembly (LISA)", *Langmuir*, Vol. 21, pp. 818-821.

Chhabra, R. P., and J. F. Richardson, 2008, *Non-Newtonian Flow and Applied Rheology*, 2nd ed., Butterworth-Heinemann, Oxford, U.K..

Chou, S. Y., and L. Zhuang, 1999, "Lithographically Induced Self-Assembly of Periodic Polymer Micropillar Arrays", *Journal of Vacuum Science and Technology*, Vol.17, pp. 3197-3202.

Chou, S. Y., L. Zhuang, and L. Guo, 1999, "Lithographically Induced Self-Construction of Polymer Microstructures for Resistless Patterning", *Applied Physics Letters*, Vol. 75, pp. 1004-1006.

Craster, R. V., and O. K. Matar, 2005, "Electrically Induced Pattern Formation in Thin Leaky Dielectric Films", *Physics of Fluids*, Vol. 17, 032104.

Denn, M. M. , 1990, "Isues in Viscoelastic Mechanics", *Annual Review of Fluid Mechanics*, Vol. 22, pp. 13-34.

Deshpande, P., L. F. Pease III, L. Chen, S. Chou, and W. B. Russel, 2004, "Cylindrically Symmetric Electrohydrodynamic Patterning", *Physical Review E*, Vol. 70, 041601.

Eldabe, N. T., 1987, "Electrohydrodynamic Stability of Two Stratified Power Law Liquids in Couette Flow", *Journal of Mathematical* Physics, Vol. 28, pp. 2791-2800.

El Moctar, A. O., N. Aubry, and J. Batton, 2003, "Electro-hydrodynamic Micro-Fluidic Mixer", *Lab on a Chip*, Vol. 3, pp. 273-280.

El-Sayed, M. F., and M. I. Syam, 2007, "Numerical Study for the Electrified Instability of Viscoelastic Cylindrical Dielectric Fluid Film Surrounded by a Conducting Gas", *Physica A*, Vol. 377, pp. 381-400.

Fujii, T., Y. Sando, K. Higashino, and Y. Fujii, 2003, "A Plug and Play Microfluidic Device", *Lab on a Chip,* Vol. 3, pp. 193-197.

Gambhire, P., and R. M. Thaokar, 2010, "Electrohydrodynamic Instabilities at Interfaces Subjected to Alternating Electric Field", *Physics of Fluids*, Vol. 22, 064103.

Glasgow, I., J. Batton, and N. Aubry, 2004, "Electroosmotic Mixing in Microchannels", *Lab on a Chip,* Vol. 4, pp. 558-562.

Glasgow, I., and N. Aubry, 2003, "Enhancement of Microfluidic Mixing Using Time Pulsing", *Lab on a Chip,* Vol. 3, pp. 114-120.

Harkema, S., E. Schäffer, M. D. Morariu, and U. Steiner, 2003, "Pattern Replication by Confined Dewetting", *Langmuir,* Vol. 19, pp. 9714-9718.

Hoburg, J. F., and J. R. Melcher, 1976, "Internal Electrohydrodynamic Instability and Mixing of Fluids with Orthogonal Field and Conductivity Gradients", *Journal of Fluid Mechanics*, Vol. 73, pp. 333-351.

Hoburg, J. F. and J. R. Melcher, 1977, "Electrohydrodynamic Mixing and Instability Induced by Colinear Fields and Conductivity Gradients", *Physics of Fluids*, Vol. 20, pp. 903-911.

Hooper, A. P. , 1989, "The Stability of Two Superposed Viscous Fluids in a Channel", *Physics of Fluids A*, Vol. 1 (7), pp. 1133-1142.

Hsiung, S. K., C. T. Chen, and G. B. Lee, 2006, "Micro-droplet Formation Utilizing Microfluidic Flow Focusing and Controllable Moving-wall Chopping Techniques", *Journal of Micromechanics and Microengineering*, Vol. 16, pp. 2403-2410.

Huang, M. Z., R. J. Yang, C. H. Tai, C. H. Tsai, and L. M. Fu, 2006, "Application of Electrokinetic Instability Flow for Enhanced Micromixing in Cross-shaped Microchannel", *Biomedical Microdevices*, Vol. 8, pp. 309-315.

Ismagilov, R. F., H. Song, and D. L. Chen, 2006, "Reactions in Droplets in Microfluidic Channels", *Angewandte Chemie International Edition*, Vol. 45, pp. 7336-7356.

Jensen, K. F. , 2001, "Microreaction Engineering - Is Small Better?", *Chemical Engineering Science*, Vol. 56, pp. 293-303.

Joanicot, M., and A. Ajdari, 2005, "Droplet Control for Microfluidics", *Science*, Vol. 309, pp. 887-888.

Johns, L. E., and R. Narayanan, 2002, *Interfacial Instability*, Springer-Verlag, New York.

Kopaç, M., A. Topuz, and M. Arıkol, 1998, "Viskoelastik Akıskanların İvmeli Akışında Malzeme Parametrelerinin Türev Tipli Bünye Denklemlerine Etkisi", *Turkish Journal of Engineering and Environmental Science*, Vol. 22, pp. 495-502.

Larson, R. G., S. G. E. Shaqfeh, and S. J. Muller, 1990, "A Purely Elastic Instability in Taylor-Couette Flow", *Journal of Fluid Mechanics*, Vol. 218, pp. 573-800.

Leach, K. A., S. Gupta, M. D. Dickey, C. G. Wilson, and T. P. Russell, 2005, "Electric Field and Dewetting Induced Hierarchical Structure Formation in Polymer/Polymer/Air Trilayers", *Chaos*, Vol. 15, 047506.

Li, F., O. Ozen, N. Aubry, D. T. Papageorgiou, and P. G. Petropoulos, 2007, "Linear Stability of a Two-Fluid Interface for Electrohydrodynamic Mixing in a Channel", *Journal of Fluid Mechanics*, Vol. 583, pp. 347-377.

Lin, H. , 2009, "Electrokinetic Instability in Microchannel Flows: A Review", *Mechanics Research Communications*, Vol. 36, pp. 33-38.

Lin, H., B. D. Storey, M. H. Oddy, C. H. Chen, and J. G. Santiago, 2004, “Instability of Electrokinetic Microchannel Flows with Conductivity Gradients”, *Physics of Fluids*, Vol. 16, pp. 1922-1935.

Lin, Z., T. Kerle, S. M. Baker, D. A. Hoagland, E. Schäffer, U. Steiner, and T. P. Russel, 2001, “Electric Field Induced Instabilities at Liquid/Liquid Interfaces”, *Journal of Chemical Physics*, Vol. 114, pp. 2377-2381.

Lin, Z., T. Kerle, T. P. Russel, E. Schäffer, and U. Steiner, 2002a, “Structure Formation at the Interface of Liquid/Liquid Bilayer in Electric Field”, *Macromolecules*, Vol. 35, pp. 3971-3976.

Lin, Z., T. Kerle, T. P. Russell, E. Schäffer, and U. Steiner, 2002b, “Electric Field Induced Dewetting at Polymer-Polymer Interfaces”, *Macromolecules*, Vol. 35, pp. 6255-6262.

Liu, R. H., K. V. Sharp, M. G. Olsen, M. Stremler, J. G. Santiago, R. J. Adrian, H. Aref, and D. J. Beebe, 2000, "A Passive Three-dimensional 'C-shape' Helical Micromixer", *Journal of Microelectromechanical Systems*, Vol. 9, pp. 190-198.

Manz, A., N. Graber, and H. Widmer, 1990, “Miniaturized Total Chemical Analysis Systems: A Novel Concept for Chemical Sensing”, *Sensors and Actuators*, Vol. B1, pp. 244-248.

Melcher, J. R. and W. J. Schwarz, 1968, “Interfacial Relaxation Overstability in a Tangential Electric-Field”, *Physics of Fluids*, Vol. 11, pp. 2604-2616.

Melcher, J. R., and C.V. Smith, 1969, “Electrohydrodynamic Charge Relaxation and Interfacial Perpendicular Field Instability”, *Physics of Fluids*, Vol. 12, pp. 778-790.

Melcher, J. R., and G. I. Taylor, 1969, “Electrohydrodynamics: A Review of Role of Interfacial Shear Stresses”, *Annual Review of Fluid Mechanics*, Vol. 1, pp. 111-146.

Mengeaud, V., J. Josserand, and H. H. Girault, 2002, "Mixing Processes in a Zigzag Microchannel: Finite Element Simulations and Optical Study", *Analytical Chemistry*, Vol. 74, pp. 4279-4286.

Morariu, M. D., N. E. Voicu, E. Schäffer, Z. Lin, T. P. Russell, and U. Steiner, 2003, "Hierarchical Structure Formation and Pattern Replication Induced by an Electric Field", *Nature Materials*, Vol. 2, pp. 48-52.

Munson, M. S., and P. Yager, 2003, "A Novel Microfluidic Mixer Based on Successive Lamination", *The 7th lnternational Conference on Miniaturized Chemical and Biochemical Analysis Systems, Squaw Valley, California USA*, pp. 495-498.

Oddy, M. H., J. G. Santiago, and J. C. Mikkelsen, 2001, "Electrokinetic Instability Micromixing", *Analytical Chemistry*, Vol. 73, pp. 5822-5832.

Ozen, O., N. Aubry, D. Papageorgiou, and P. Petropoulos, 2006a, "Monodisperse Drop Formation in Square Microchannels", *Physical Review Letters*, Vol. 96, 144501.

Ozen, O., D. T. Papageorgiou, and P. G. Petropoulos, 2006b, "Nonlinear Stability of a Charged Electrified Viscous Liquid Sheet under the Action of a Horizontal Electric Field", *Physics of Fluids*, Vol. 18, 042102.

Ozen, O., N. Aubry, D. Papageorgiou, and P. Petropoulos, 2006c, "Electrohydrodynamic Linear Stability of Two Immiscible Fluids in Channel Flow", *Electrochimica Acta*, Vol. 51, pp. 5316-5323.

Park, J., S. M. Shin, K. Y. Hun, and I. S. Kang, 2005, "Application of Electrokinetic Instability for Enhanced Mixing in Various Micro-T-Channel Geometries", *Physics of Fluids*, Vol. 17, 118101.

Pease III, L. F., and W. B. Russel, 2002, "Linear Stability Analysis of Thin Leaky Dielectric Films Subjected to Electric Fields", *Journal of Non-Newtonian Fluid Mechanics*, Vol. 102, pp. 233-250.

Posner, J. D. and J. G. Santiago, 2006, "Convective Instability of Electrokinetic Flows in a Cross-Shaped Microchannel", *Journal of Fluid Mechanics*, Vol. 555, pp. 1-42.

Roberts, S. A. and S. Kumar, 2009, "AC Electrohydrodynamic Instabilities in Thin Liquid Films", *Journal of Fluid Mechanics*, Vol. 631, pp. 255-279.

Robinson, J. A., M. A. Bergougnou, G. S. Peter Castle, and I. I. Inculet, 2001, "The Electric Field at a Water Surface Stressed by an AC Voltage", *IEEE Transactions on Industry Applications*, Vol. 37, pp. 735-742.

Saville, D. A., 1997, "Electrohydrodynamics: The Taylor-Melcher Leaky Dielectric Model", *Annual Review of Fluid Mechanics*, Vol. 29, pp. 27-64.

Schäffer, E., T. Thurn-Albrecht, T. P. Russell, and U. Steiner, 2000, "Electrically Induced Structure Formation and Pattern Transfer", *Nature*, Vol. 403, pp. 874-877.

Schäffer, E., T. Thurn-Albrecht, T. P. Russel, and U. Steiner, 2001, "Electrohydrodynamic Instabilities in Polymer Films", *Europhysics Letters*, Vol. 53, pp. 518-523.

Shankar, V., and A. Sharma, 2004, "Instability of the Interface Between Thin Fluid Films Subjected to Electric Field", *Journal of Colloid Interface Science*, Vol. 274, pp. 294-308.

Shaqfeh, E. S. G., R.G. Larson, and G.H. Fredrickson, 1989, "The Stability of Gravity Driven Viscoelastic Film Flow at Low to Moderate Reynolds Number", *Journal of Non-Newtonian Fluid Mechanics*, Vol. 31, pp. 87-113.

Sharma, R. C., and P. Kumar, 1997, "On the Stability of Two Superposed Walters-B' Viscoelastic Liquids", *Czeck Journal of Physics*, Vol. 47, pp. 197-204.

Shin, S. M., I.S. Kang, and Y.K. Cho, 2005, "Mixing Enhancement by Using Electrokinetic Instability Under Time-periodic Electric Field", *Journal of Micromechanics and Microengineering*, Vol. 15, pp. 455-462.

Squires, T. M., and S. R. Quake, 2005, "Microfluidics: Fluid physics at the Nanoliter Scale", *Reviews of Modern Physics*, Vol. 77, pp. 977-1026.

Stone, H. A., A. D. Stroock, and A. Ajdari, 2004, "Engineering Flows in Small Devices: Microfluidics Toward a Lab-on-a-chip", *Annual Review of Fluid Mechanics*, Vol. 36, pp. 381-411.

Storey, B. D., B. S. Tilley, H. Lin, and J. G. Santiago, 2005, "Electrokinetic Instability in Thin Microchannels", *Physics of Fluids*, Vol. 17, 018103.

Stroock, A. D., S. K. W. Dertinger, A. Ajdari, I. Mezic, H. A. Stone, and G. M. Whitesides, 2002a, "Chaotic Mixer for Microchannels", *Science*, Vol. 295, pp. 647-651.

Stroock, A. D., S. K. Dertinger, G. M. Whitesides, and A. Ajdari, 2002b, "Patterning Flows Using Grooved Surfaces", *Analytical Chemistry*, Vol. 74, pp. 5306-5312.

Tanner, R. I., 2000, *Engineering Rheology*, 2nd ed., Oxford University Press, Oxford.

Thaokar, R. M., and V. Kumaran, 2005, "Electrohydrodynamic Instability of the Interface Between Two Fluids Confined in a Channel", *Physics of Fluids*, Vol. 17, 084104.

Thorsen, T., R. W. Roberts, F. H. Arnold, and S. R. Quake, 2001, "Dynamic Pattern Formation in a Vesicle-Generating Microfluidic Device", *Physical Review Letters*, Vol. 86, pp. 4163-4166.

Tomar, G., V. Shankar, A. Sharma, and G. Biswas, 2007, "Electrohydrodynamic Instability of a Confined Viscoelastic Liquid Film", *Journal of Non-Newtonian Fluid Mechanics*, Vol. 143, pp. 120-130.

Trefethen, L. N., 2000, *Spectral methods in MATLAB*, SIAM, Philadelphia.

Tsouris, C., C. T. Culbertson, D. W. DePaoli, S. C. Jacobson, V. F. de Almeida, and J. M. Ramsey, 2003, "Electrohydrodynamic Mixing in Microchannels", *AIChE Journal*, Vol. 49, pp. 2181-2186.

Uguz, A. K., and N. Aubry, 2008, "Quantifying the Linear Stability of a Flowing Electrified Two-Fluid Layer in a Channel for Fast Electric Times for Normal and Parallel Electric Fields", *Physics of Fluids*, Vol. 20, 092103.

Uguz, A. K., O. Ozen, and N. Aubry, 2008, "Electric Field Effect on a Two-Fluid Interface Instability in Channel Flow for Fast Electric Times", *Physics of Fluids*, Vol. 20, 031702.

Wang, H., P. Iovenitti, E. Harvey, and S. Masood, 2002, "Optimizing Layout of Obstacles for Enhanced Mixing in Microchannels", *Smart Materials and Structures*, Vol. 11, pp. 662-667.

Wilkinson, W. L., 1960, *Non-Newtonian Fluids*, Pergamon Press, New York, USA.

Wu, L., and S.Y. Chou, 2005, "Electrohydrodynamic Instability of a Thin Film of Viscoelastic Polymer Underneath a Lithographically Manufactured Mask", *Journal of Non-Newtonian Fluid Mechanics*, Vol. 125, pp. 91-99.

Wu, N., L. F. Pease III, and W. B. Russel, 2005, "Electric-Field-Induced Patterns in Thin Polymer Films: Weakly Nonlinear and Fully Nonlinear Evolution", *Langmuir*, Vol. 21, 12290.

Yiantsios, S. G., B.G. Higgins, 1988, "Linear Stability of Plane Poiseuille Flow of Two Superposed Fluids", *Physics of Fluids* Vol. 31 (11), pp. 3225-3238.

Zahn, J. D., and V. Reddy, 2006, "Two Phase Micromixing and Analysis Using Electrohydrodynamic Instabilities", *Microfluidics and Nanofluidics*, Vol. 2, pp. 399-415.